TECHNISCHE UNIVERSITÄT MÜNCHEN

Wacker-Lehrstuhl für Makromolekulare Chemie

Molecular Brushes of Poly(2-oxazoline)s

Ning Zhang

Vollständiger Abdruck der von der Fakultät für Chemie der Technischen Universität München zur Erlangung des akademischen Grades eines

Doktors der Naturwissenschaften

genehmigten Dissertation.

Vorsitzender:	Univ.- Prof. Dr. Ulrich K. Heiz
Prüfer der Dissertation:	1. Univ.- Prof. Dr. Rainer Jordan, Technische Universität Dresden
	2. Univ.- Prof. Dr. Sevil Weinkauf

Die Dissertation wurde am 24.08.2010 bei der Technischen Universität München eingereicht und durch die Fakultät für Chemie am 19.10.2010 angenommen

Die vorliegende Arbeit wurde in der Zeit von November 2006 bis März 2010 unter der Leitung von Prof. Dr. Rainer Jordan am Wacker-Lehrstuhl für Makromolekulare Chemie von Prof. Dr. Dr. h.c. Bernhard Rieger der Technischen Universität München angefertigt.

Acknowledgements

First and foremost, I would like to gratefully and sincerely thank my supervisor, Prof. Dr. Rainer Jordan, for giving me the opportunity to work on such an exciting project. He introduced me to the field of polymer and interface science, broadened my perspective and knowledge, and gave me confidence to apply myself in my graduate study. I am deeply impressed by his wide knowledge, patient guidance as well as the professional attitude towards scientific work. When I made the decision to stay in Munich for the last few months of my Ph.D. study, he also showed his kind understanding of it which has been of great importance to me. Without his constant support, guidance and encouragement this dissertation would not have been possible.

I would also like to express my deep gratitude to Prof. Dr. Dr. h. c. Bernhard Rieger for giving me the opportunity to work at the Wacker-Lehrstuhl für Makromolekulare Chemie. His constructive comments and scientific work style continually impressed me and have been of great value for my work. I wish to sincerely thank Prof. Dr. -Ing. Oskar Nuyken, whose generous supports and encouragement always inspired me and became a large driving force for the present study. I gratefully thank Dr. Carsten Troll and Dr. -Ing. Heidi Samarian for their supports both technically and scientifically.

A warm and heartfelt thank goes to Dr. Marin Steenackers and Dr. Robert Luxenhofer for their fruitful cooperation, enlightening discussion and most importantly their warm friendship throughout my Ph.D. study. Marin taught me the valuable laboratory techniques, and put time and energy into correcting this dissertation. 'Luxi' always helped me with suggestion on both my work and my life, and offered me the "warmest hotel" in Dresden. Words are not sufficient enough to express all my appreciation for their countless help.

I am grateful to Dr. Tilo Pompe from Leibniz Institute of Polymer Research Dresden for performing the protein adsorption and cell adhesion experiments, and Dr. Schilp Sören from Universität Heidelberg for offering the surfaces. Without these excellent cooperations, this dissertation would not have been completed.

Many thanks to Naïma Aurelia Hutter for her precise English-German translation, as well as her kind help during my graduate study. At the same time, I would like to thank Anita Schulz and Hans Koss for their kind assistance in the lab work.

I would like to give my special thank to my labmates Dr. Stephan Huber, Dr. Tianzhu Zhang, Amir Doroodian, and Khalifah Salmeia for the harmonious lab atmosphere.

Thanks go to all the other Makros, Dr. Martin Schneider, Andreas Feigl, Dr. Liyi Chen, Gerhard Richter, Dr. Carola Gantner, Ulrike Will, Dr. Michael Reif, Dr. Sergei Vagin, Uwe Seemann, Alexander Schöbel, Timo Korfmann, Udo Schmidt, Paul Heinz, Monika Kellner, Anastasia Golosova, Sabine Martinetz-Große, Timo Anselment, Pierre Göppert, Dr. Julia Müller, Felix Schulz, Frank Deubel, Stephan Klaus, Christian Hanisch, Joachim Dengler, Dr. Carly Anderson, Manuel Winkenstette, Philip Zehetmaier, Sanna Zimmer, Sandra Hochwarter, Robert Reichardt, Maximilian Lehenmeier, Konrad Hindelang, Meifang Yin, Tobias Diesner, Abdussalam Qaroush, Manfred Gunesch, Anna Lennartson, as well as other new comers for making my stay such a pleasant and great experience. I sincerely appreciate all the advices and skills that I have picked up in this period of time.

I would like to thank my parents and my friends for their love and help.

Finally, I would like to give my last but unique thank to my wife Hang for her endless love, termless sacrifice and patience.

To my wife Hang

Table of Contents

Abbreviation and Symbols

ACN	acetonitrile
AFM	atomic force microscopy
AIBN	N,N-azobisisobutyronitrile
ATR-FTIR	attenuated total reflection Fourier transform infrared
ATRP	atom transfer radical polymerization
a.u.	arbitrary units
-b-	-block-
BBB	bottle-brush brush
BDE	bond dissociation energy
b.p.	boiling point
BT	4-mercapto-1,1'-biphenyl thiol
Boc	N-tert-butyloxycarbonylpiperazine
BuOx	2-butyl-2-oxazoline
-co-	copolymerize
DMAc	dimethyl acetamide
DNA	deoxyribonucleic acid
DP	degree of polymerization
DRIFT	diffusion reflectance Fourier transformed infrared
EBCD	electron beam induced carbon deposition
EBCL	electron beam chemical lithography
EtOx	2-ethyl-2-oxazoline
equiv.	equivalence
-g-	-graft-
GC	gas chromatography
GPC	gel permeation chromatography
*i*PrOx	2-iso-propyl-2-oxazoline
IPOx	2-isopropenyl-2-oxazoline
IR	infrared
LCROP	living cationic ring-opening polymerization
LCST	lower critical solution temperature

MDR	multiple drug resistance
MeOTf	methyl trifluoromethane sulfonate
MeOx	2-methyl-2-oxazoline
MTT	3-(4,5-dimethylthiazol-2-yl)-2,5-diphenyltetrazolium bromide
n-BuLi	n-buthyl lithium
NonOx	2-*n*-nonyl-2-oxazoline
*n*PrOx	2-*n*-propyl-2-oxazoline
OTf	Triflate (trifluoromethanesulfonate)
P	poly
PBS	phosphate buffered saline
PDI	poly dispersity index
PEG	poly(ethylene glycol)
PEO	poly(ethylene oxide)
pipd	piperidine
PIPOx	poly(2-isopropenyl-2-oxazoline)
$PIPOx^{A}$	poly(2-isopropenyl-2-oxazoline) prepared by anionic polymerization
$PIPOx^{R}$	poly(2-isopropenyl-2-oxazoline) prepared by free radical polymerization
PMMA	poly(methyl methacrylate)
PNAAm	poly(N-alkyl acrylamide)
PNIPAAm	poly(N-isopropyl acrylamide)
POMA	poly(octadecene-*alt*-maleic anhydride)
POx	poly(2-oxazoline)s
PS	poly(styrene)
RBITC	rhodamine B isothiocyanate
SAM	self-assembled monolayer
SEM	scanning electron microscopy
SIP	surface-initiated polymerization
SIPGP	self-initiated photografting and photopolymerization
SIPP	surface-initiated photopolymerization
SPM	scanning probe microscopy
St	styrene
THF	tetrahydrofuran
TFA	trifluoroacetic acid
UCST	upper critical solution temperature

UV	ultraviolet

cm	centimeter
℃	degree Celsius
eV	electron volt
g	gram
h	hour
H	heterotactic
h_d	dry polymer layer thickness
$[I]_0$	initial concentration of the initiating group
I	isotactic
k_p^{app}	apparent propagation rate
kDa	kilo Dalton (1000g/mol)
L	liter
m	meter
$[M]_0$	initial monomer concentration
$[M]_t$	monomer concentration of the time
mbar	millibar
min	minute
mmol	millimole
mol %	molar percent
M_n	number average molar mass
M_w	weight average molar mass
N_{Av}	avogadro constant
ng	10^{-9} gram
nm	10^{-9} meter
R_g	radius of gyration
S	syndiotactic
t_p	polymerization time
T	temperature
v/v	volume ratio
w/w	weight ratio
wt %	weight percent

λ	wavelength
μm	micrometer
ρ	bulk density
σ	grafting density

Chapter 1 Introduction

Driven by the desire to produce novel materials for new applications, polymer science as an interdisciplinary field came into being in 17th century. Since then, polymer has been used in a wide range of applications, such as coatings, adhesives, plastics, elastomers, and natural biopolymers e.g. DNA and proteins that are essential for life. A key feature of successful and versatile polymer materials is that it is possible to build in properties by control, including the control of the molecular architecture, and chemical functionality. For example, the progress in living/controlled polymerization techniques has enabled the preparation of polymers with well defined molecular architecture. **Figure 1** shows different possible polymer architectures.

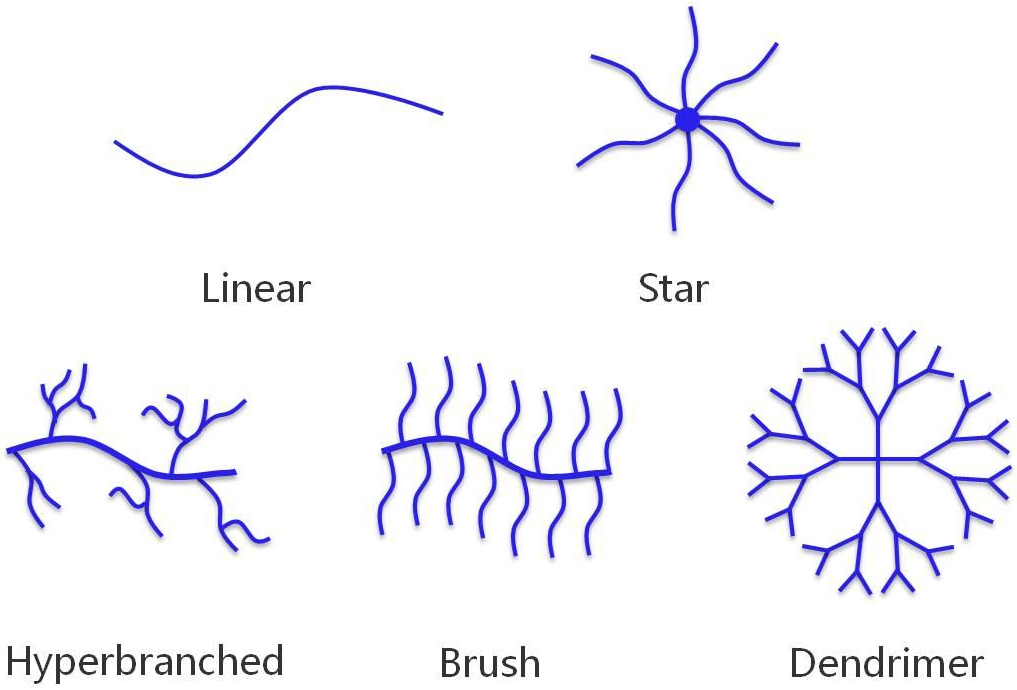

Figure 1. Different possible polymer architectures, linear, star, hyperbranched, brush polymer and dendrimer.

A linear polymer is a macromolecule in which the monomers are linked in one continuous string. A branched polymer may be a star polymer, graft/brush polymer and hyperbranched/dendritic polymer. A star polymer is defined as a macromolecule containing one single branch point from which linear chains (arms) emanate. A dendritic polymer, being a perfectly hyperbranched polymer, is monodisperse macromolecule and has a completely regular branching structure leading to a further branching. A brush polymer, also called

molecular brush is copolymer containing a high density of side chains, which leads to significant congestion and stretching of the backbone. Recently, branched polymer has gained much attention due to its interesting and sometimes unexpected properties opening new areas of applications.

1.1 Molecular brushes

Molecular brushes[1,9] are unique polymeric molecules. They are also referred to as bottle brush macromolecules because of their appearance. The conformation and physical properties of molecular brushes are mainly controlled by the steric repulsion between grafted side chains because of high crowding. Molecular brushes of different conformations have been prepared in the past decade. **Figure 2** presents the conformational change of molecular brushes with the increasing grafting densities. **Figure 5** shows some other factors that can also determine the conformations, e.g. flexible or stiff side chains and backbone, homopolymers or copolymers side chains, linear or branched in side chains and backbone. All these variables affect the conformation and properties, but it is believed that the dense grafting of pendant chains has the greatest effect. Dense grafting enables a formation of entropically unfavorable elongated backbone chain, and at the same time, ensures the high density of functional groups on the side chain along the backbone. The unique structure endows molecular brushes with novel properties, facilitating its potential applications as sensors,[2] elastomers[3,4] and template for nanowires.[5]

Bottle brush structures can also be found in nature. Proteoglycans,[6] for instance, are polyelectrolyte brush-like macromolecules that consist of a protein backbone with carbohydrate side chains (**Figure 3**). These bottle brush molecules widely exist in the connective tissue and function from cell signaling and cell surface protection to joint lubrication and lung clearance. In addition, enlarged ‘molecular brush’ such as callistemon,[7] also known as bottlebrush is a genus of shrubs and trees found in Australia.

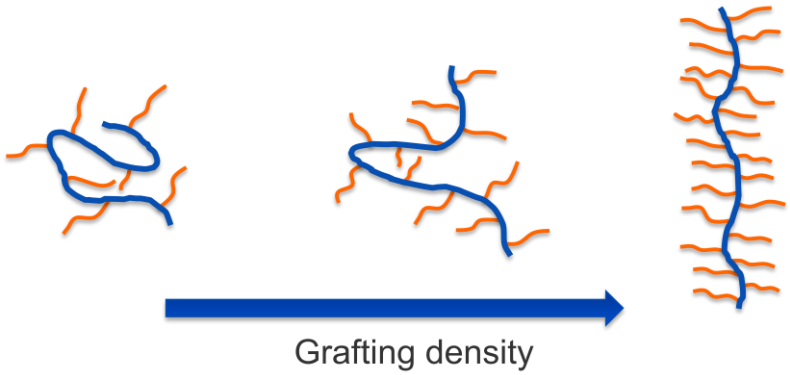

Figure 2. Conformational change of molecular brush as a function of grafting density.

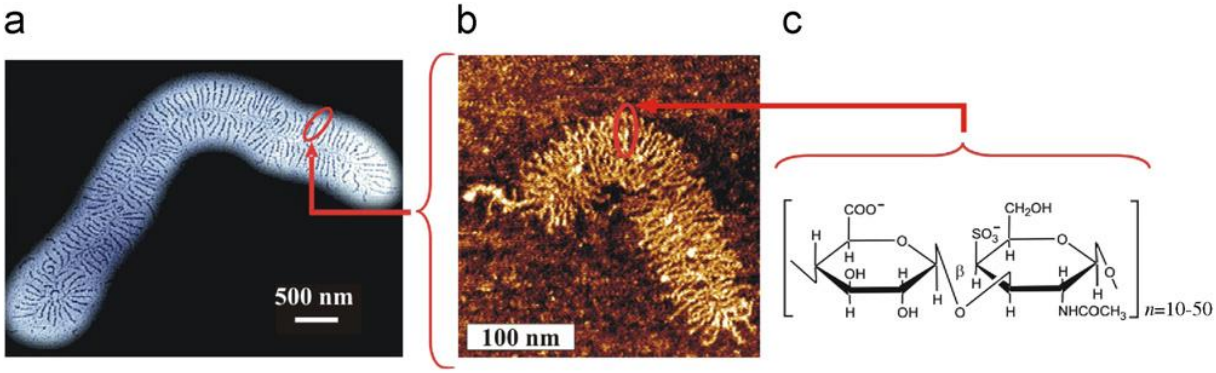

Figure 3. Structural hierarchy of proteoglycan aggregate in cartilage.[8] (a) Transmission electron microscopy (TEM) micrograph of the aggregate, (b) enlarged TEM micrograph of protein backbone with glucosaminoglycan side chains, (c) chemical structure of the disaccharide repeating unit of the side chains (From Ref. [9]).

1.1.1 Synthesis of molecular brushes

As comb copolymers, molecular brushes can be prepared by the *grafting through* approach (polymerization of macromonomers), *grafting onto* approach (polymer analogue coupling of polymers onto a backbone with pendant attachment groups), or the *grafting from* approach (polymerization from a macroinitiator backbone). All the three strategies have been successfully employed for the synthesis of defined molecular brushes. However, depending on the functionality and polarity of the monomers, each approach has its advantages and limitations.[9] For example, the *grafting through* approach ensures side chain attachment to every backbone unit, thus leads to the formation of molecular brush of high grafting density (**Figure 4**). However, the synthesis of macromonomer is inevitable in this method and has been proved to be very difficult. Moreover, the macromonomers are difficult to polymerize to

a high degree and difficult to separate from molecular brushes. The g*rafting onto* approach involves the separate synthesis of the backbone and side chain by different living polymerization techniques (**Figure 4**). Therefore, the resulting molecular brushes are structurally well defined with respect to their backbones and side chains. However, a limited grafting density could be easily found out due to the steric interaction between the grafted side chain and the approaching side chains. The g*rafting from* approach involves the synthesis of a backbone polymer (macroinitiator) with initiation sites along the backbone, which is subsequently used to initiate polymerization of the side chains (**Figure 4**). The macroinitiator can be synthesized directly by the polymerization of monomers with initiating moieties or by synthesis and conversion of a precursor to macroinitiator with initiating moieties. The gradual growth of the side chains impairs the steric concerns which are often the limiting factors in the *grafting through* and *grafting onto* methods. Therefore, the *grafting from* approach allows for the preparation of molecular brushes with a high grafting density and a narrow molecular weight distribution. However, compared to the *grafting through* approach, *grafting from* has relatively less control of side chain length and grafting density.

All of the above mentioned methods aim at controlling different structural parameters, including chemical composition, grafting density, degree of polymerization (DP) of side chains and the backbone. Even though each of these strategies demonstrates distinct advantages with respect to the molecular design, the *grafting from* strategy is the most broadly applied method for the synthesis of densely grafted polymers.[35]

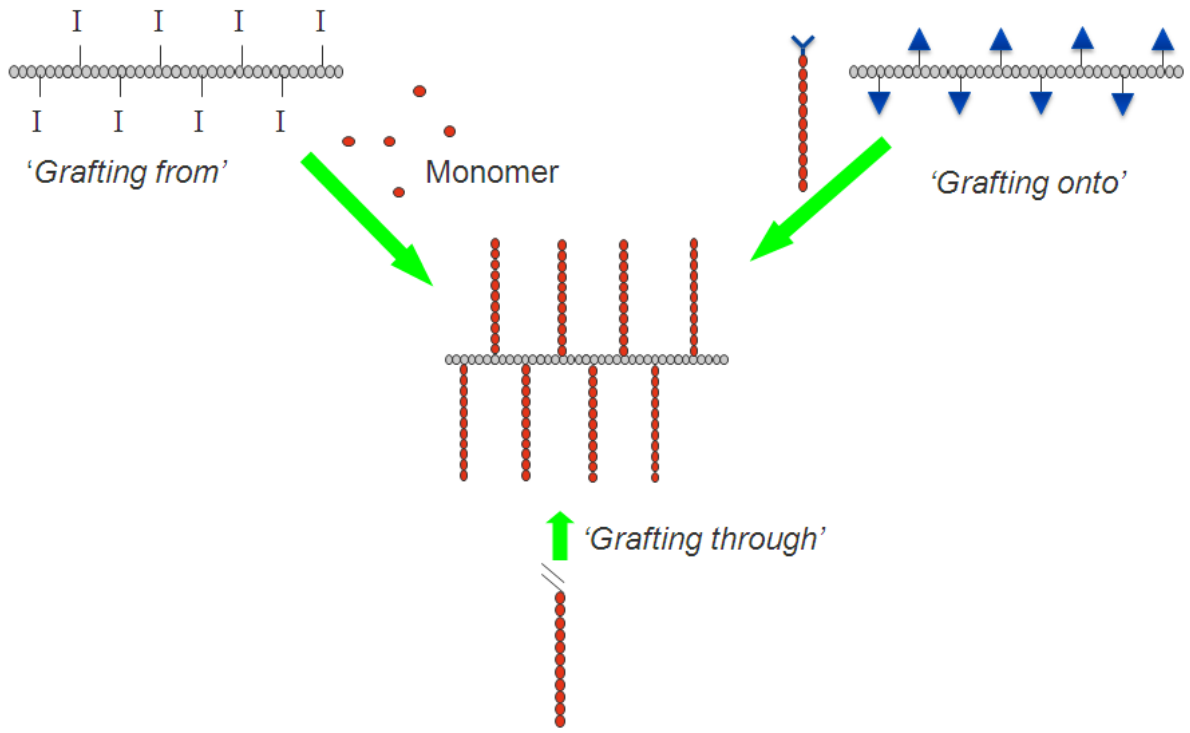

Figure 4. Pathways for synthesis of molecular brushes: '*grafting through*', '*grafting onto*' and '*grafting from*' ('I' is an initiating group).

Within each strategy, various polymerization techniques such as anionic polymerization, ring-opening (metathesis) polymerization, conventional and controlled radical polymerizations, and various coupling reactions (for example 'click chemistry') have been employed. Therefore, brush molecules with different architectures as well as different backbone and side chain compositions have been successfully prepared (**Figure 5**). In the past decade, particular attention has been paid to develop living ionic as well as controlled radical polymerization techniques, which have been proven particularly useful and effective for the preparation of well-defined, functional molecular brushes. It is worth mentioning that controlled radical polymerization techniques are suitable for the synthesis of molecular brushes due to the employed low radical concentration, thereby intermolecular and intramolecular termination reactions are suppressed. This is especially important for brush polymerizations because of the high local concentration of side chains that exist in the vicinity of the backbone polymer.

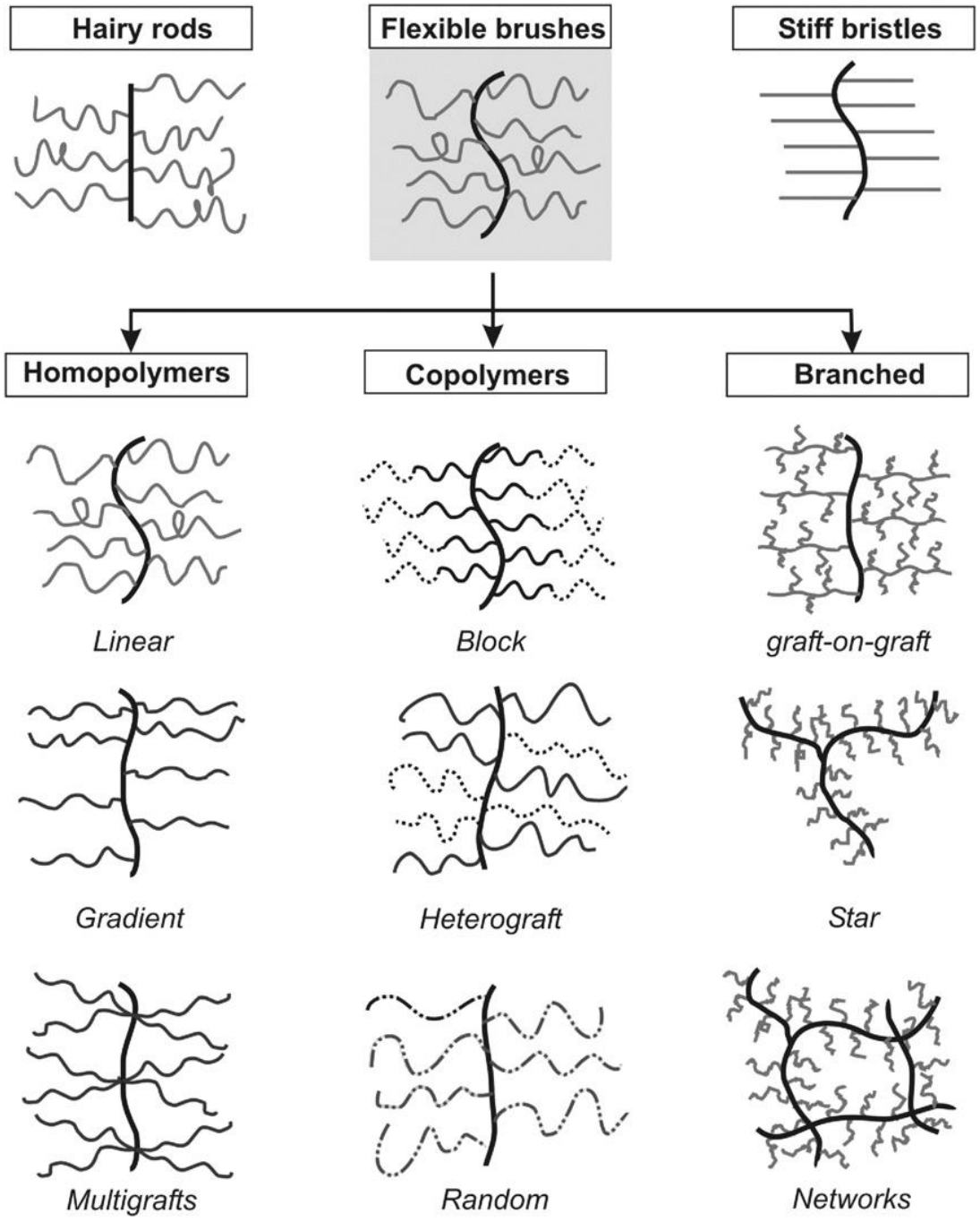

Figure 5. Various branching topologies and architectures of molecular brushes (From Ref. [9]).

So far, such brush-like molecules have mainly been prepared via atom transfer radical polymerization (ATRP).[10,11] ATRP is an example of a controlled/living radical polymerization where carbon-carbon bond is formed through transition metal catalyst. ATRP reactions are tolerant to many functional groups like allyl, amino, epoxy, hydroxyl and vinyl groups.[12] This method prevails in many aspects, such as the ease of preparation, the commercial availability of the reactant, including catalyst (usually copper complexes), pyridine based ligands, and initiators (alkyl halides). In addition, the ease of forming pendant α-bromoester groups on a

polymer backbone and grafting side chains from the multifunctional initiator also make ATRP a suitable method for molecular brush synthesis. However, the steric interactions between the initiation sites and the rather bulky ligands used in ATRP will inevitably affect the grafting efficiency.[13] Matyjaszewski and co-workers prepared molecular brushes using the *grafting from* method via ATRP, and compared the initiation efficiency of brush molecules with that of linear polymers (**Figure 6**).[13] They found a significantly reduced initiation efficiency for the molecular brushes which was attributed to the congested environment and high local concentration of initiation sites. However, it should be noted, for a defined synthesis of molecular brushes, a high initiation efficiency is needed.

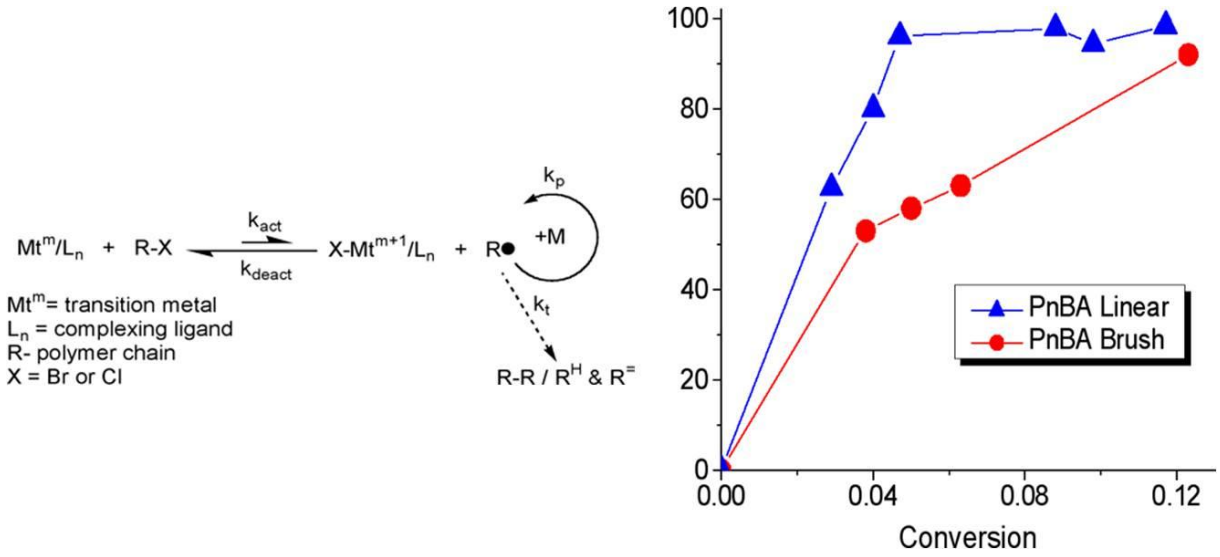

Figure 6. ATRP for the synthesis of molecular brushes. Left: Mechanism of metal complex-mediated ATRP; Right: Initiation efficiency as a function of monomer conversion for the brush and linear polymerizations (From Ref. [13,14]).

Up to now, molecular brushes based on poly(methacrylate)s or poly(styrene) (PS) backbones and various side chains such as poly(acrylate), poly(methacrylate), PS, poly(N-isopropyl acrylamide) (PNIPAAm) and sugar have been prepared via ATRP. Meanwhile, molecular brushes carrying different functionalities as well as different block copolymer side chains to form core-shell structures have been synthesized. The topologies of these molecular brushes are shown in **Figure 5**.

1.1.2 Stimuli-responsive molecular brushes

1.1.2.1 Stimuli-responsive polymers

Stimuli-responsive polymers[15] are defined as polymers that undergo large and abrupt physical or chemical changes in response to the external environment changes. These so called 'responsive-polymers' have been given as stimuli-sensitive,[16] intelligent,[17] smart[18,19] or environmentally sensitive polymers.[20] The stimuli could be either chemical or physical nature. Chemical stimuli such as pH, ionic strength or another chemical will change the interactions between polymer chains or between polymer chains and solvent molecules. Whereas, physical stimuli refers to the alteration of molecular interactions at critical onset points with temperature, electric or magnetic fields, and mechanical stress. These responses of polymer systems are very useful in bio-related applications such as drug delivery[21,22,23,24,25] and biotechnology. Some systems have been developed to combine two or more responsive mechanisms into one polymer system. For instance, temperature-sensitive polymers may also respond to pH changes.[26,27,28,29]

Temperature is the most widely used stimulus for responsive polymer systems. One unique property of temperature-responsive polymers is the presence of a critical solution temperature. Therefore, hydrophilic polymers with a lower critical solution temperature (LCST) have gained much attention. These polymers are soluble in water through hydrogen bond with water molecules below their LCST. Increasing the temperature impairs the formation of hydrogen bond. When temperature is above the LCST, polymers dehydrate and become insoluble in water as the hydrophobic interactions become entropically favorable (**Figure 8**). For example, poly(N-isopropylacrylamide) (PNIPAAm) has a cloud point of around 32 ℃, across which it undergoes a reversible volume phase transition caused by the coil-to-globule transition. However, the mixture of polymer and solution is miscible when the temperature is below the LCST. The phase transition is favored by the entropic gain as water molecules associated with the side chain (isopropyl moieties) are released into the bulk aqueous phase.

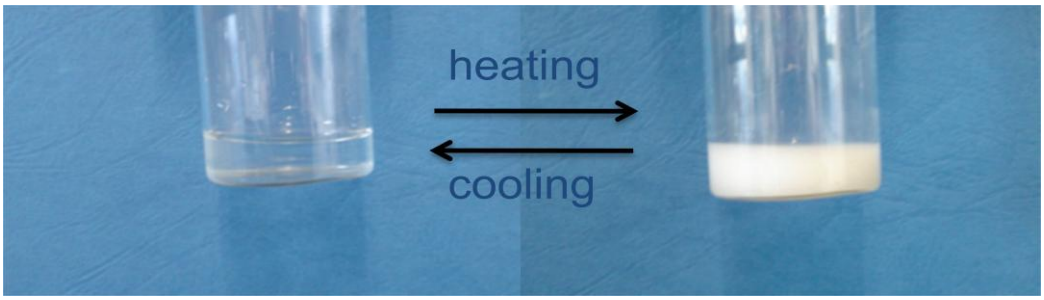

Figure 7. Thermo-responsive polymer below and above its LCST in water (From Ref.[30]).

The phase transition temperature can be adjusted by changing structural parameters such as molecular weight,[31,32] end groups,[32,33] and molecular structure.[34] According to previous studies, the LCST usually decreases with the increased molecular weight due to an attenuated polymer-solvent interaction. The incorporation of hydrophobic groups in the polymer causes a decrease of the LCST. The hydrophilic/hydrophobic balance can be additionally changed by the end groups.

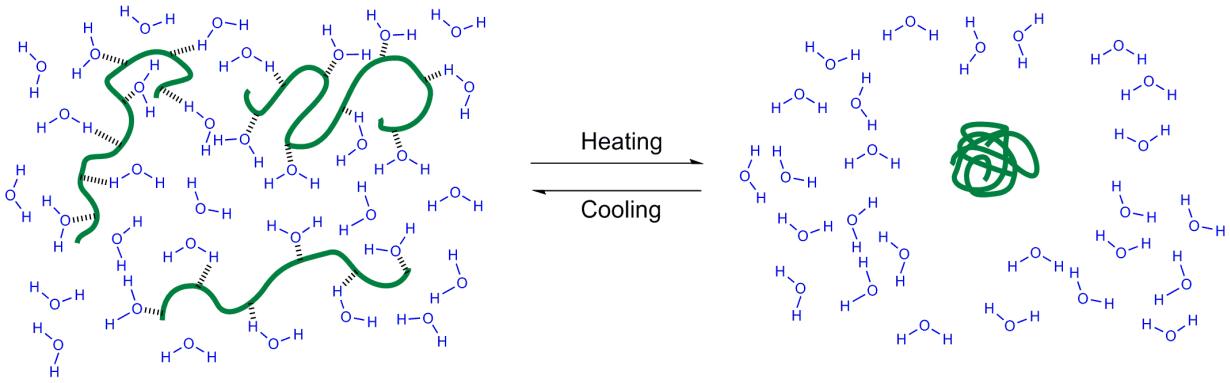

Figure 8. Illustration of reversible temperature-responsive solubility of linear polymers at their lower critical solution temperature (LCST). Left: hydrated polymer below its LCST and right: single chain collapse and intermolecular aggregate due to loss of water above the LCST.

1.1.2.2 Thermo-responsive molecular brushes

In solution, the length and flexibility of the molecular brush is mainly controlled by the solvent quality, temperature, pH, light and ionic strength. The ability to trigger these conformational changes using various stimuli will greatly enhance the significance and practical value of these molecules. Actually, one focus of the related research of molecular brushes is the development of stimuli-responsive adaptive systems,[35] especially hydrophilic molecular brushes with a lower critical solution temperature (LCST) in aqueous environments

for biomedical applications such as biosensors and drug delivery systems. [36,37,38,39,40,41,42,43,44,45]

The extended conformation of molecular brushes in solution can be adjusted by incorporation of stimuli-responsive segments. At the transition temperature, the polymer brushes not only show the change of the contour length, they also show a transition from rod-like to globular conformation. It is known that linear polymers become insoluble and aggregate at their LCST due to hydrophobic interactions. Unlike linear polymers, it is very interesting that after collapsing, the brush molecules do not aggregate and remains in solution as single molecules.[36]

These thermo-responsive molecular brushes have been widely investigated in the past decade. The first example was reported by Schmidt and coworkers in 2004.[36] Molecular brushes with thermo-responsive polymer side chains were prepared by ATRP of 2-hydroxyethyl methacrylate (HEMA) followed by subsequent reaction with bromoisobutyric acid bromide to form a poly-2-bromoisobutyryloxyethyl methacrylate macroinitiator followed by a second ATRP of (N-isopropylacrylamide) (NIPAAm) to form the side chain. The resulting molecular brushes collapsed in aqueous solution at LCST of the PNIPAAm side chains. The conformation of the brush molecular showed a transition from a single macromolecule cylinder to a globule within a small temperature range (collapse from a radius of gyration from 61nm at 20 ℃ to 25 nm at 32 ℃).

Like linear thermo-responsive polymers, the LCST of molecular brushes can be tuned by varying the hydrophilicity of the backbone and/or side chains. The simplest way to achieve this fine tuning is a copolymerization of hydrophilic and hydrophobic monomers of the side chain of the molecular brushes. For instance, molecular brushes with statistical or block copolymers of di(ethylene glycol) methyl ether methacrylate (MEO_2MA) (hydrophobic) and tri(ethylene glycol) methyl ether methacrylate (MEO_3MA) (hydrophilic) in the side chain have been prepared by grafting from a poly-2-bromoisobutyryloxyethyl methacrylate macroinitiator by ATRP.[40] In the case of brushes with statistical copolymer side chains, the LCST increased with the mole fraction of MEO_3MA in the side chain. However, very interestingly, for the molecular brushes with block copolymer side chains, the LCST curve of the block brushes showed two stages during heating, exhibiting both intermolecular and intramolecular aggregation (**Figure 9**). This behavior was strongly dependent on the sequence of the side chain segments. As the temperature increased, molecules consisting of collapsed $PMEO_2MA$ (core) and $PMEO_3MA$ (shell) segments aggregated to precipitate as larger

aggregates. However, brush molecules with $PMEO_3MA$-b-$PMEO_2MA$ side chains formed vesicles consisting of aggregated $PMEO_2MA$ shell segments and soluble $PMEO_3MA$ core segments.

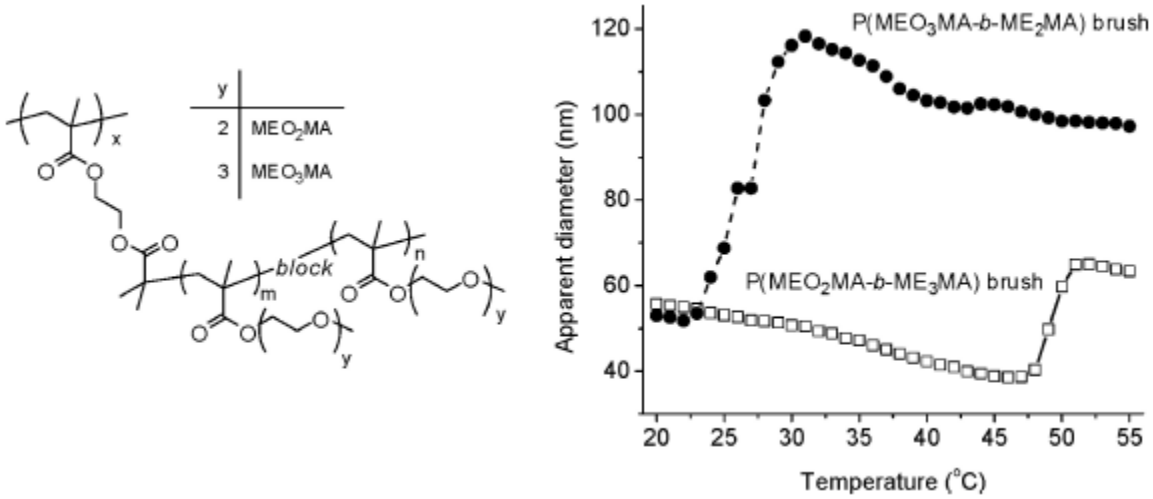

Figure 9. Temperature dependence of the hydrodynamic diameter change for 0.3 wt % aqueous solution of block molecular brushes. Solid curve: P($PMEO_3MA$-*b*-$PMEO_2MA$) brush. Dashed curve: P($PMEO_2MA$-*b*-$PMEO_3MA$) (From Ref. [40]).

Another interesting phenomenon is the unusual dependence between aggregation and concentration. Matyjaszewski and co-workers[38] prepared two thermosensitive molecular brushes with thermo-responsive side chains. As shown in **Figure 10**, dynamic light scattering (DLS) studies were performed for aqueous solutions of molecular brushes below and above the LCST, and found an unusual concentration-dependent LCST. Due to the compact structure of molecular brushes, intramolecular collapse occurred when the average distance between brush molecules was much larger compared to the hydrodynamic dimensions of the individual macromolecules. However, when the concentration of the solution of molecular brushes was increased to a level where the separation distance was comparable to the brush hydrodynamic dimensions, intermolecular aggregation occurred, which is typically observed for solutions of linear polymers.

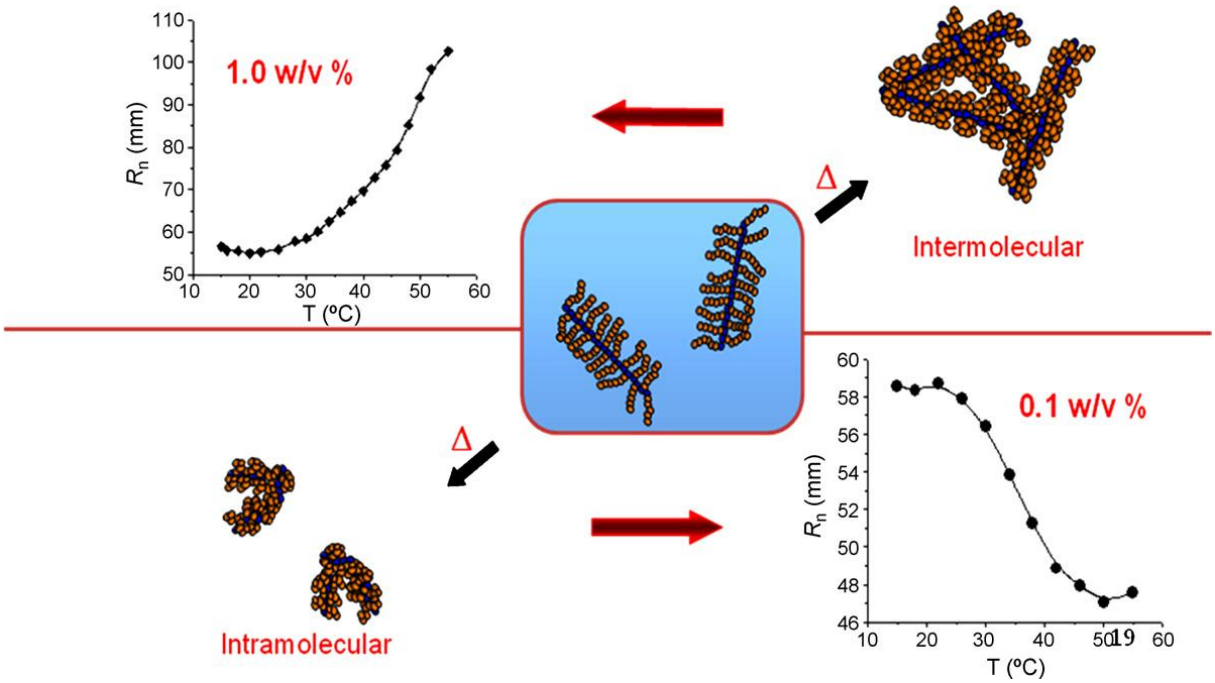

Figure 10. Illustration of conformation for temperature-responsive molecular brushes at the lower critical solution temperature (LCST). Below: intramolecular collapse of molecular brush above LCST in dilute solution. Above: intermolecular aggregation above LCST in relatively higher concentration (From Ref. [35,38]).

1.1.3 Molecular brushes on surfaces

When adsorbed on surfaces, brush molecules may undergo both association and dissociation depending on the strength of adsorption and the molecular architecture (**Figure 11**).[9] Atomic force microscopy (AFM) techniques allow the in-situ visualization of single molecular brush adsorbed on surfaces. Therefore, this technique triggered numerous contributions to synthesize defined molecular brushes and use the macromolecules as an individual device or as single molecule templates.[36, 46 , 47] Analysis by AFM gives not only dimensions and conformations of molecular brushes, but also molecular weight by combination with Langmuir-Blodgett (LB) techniques. Sheiko and coworkers[48] calculated the molecular weight distribution of molecular brushes using AFM and LB techniques. The LB technique provided the mass density (mass/area), while visualization of molecular brush layer by AFM allowed the measurement of molecule number per area. The number average molecular weight was determined as the ratio of the above two parameters. The obtained molecular weight was in good agreement with the one from conventional measurements by gel permeation chromatography (GPC).

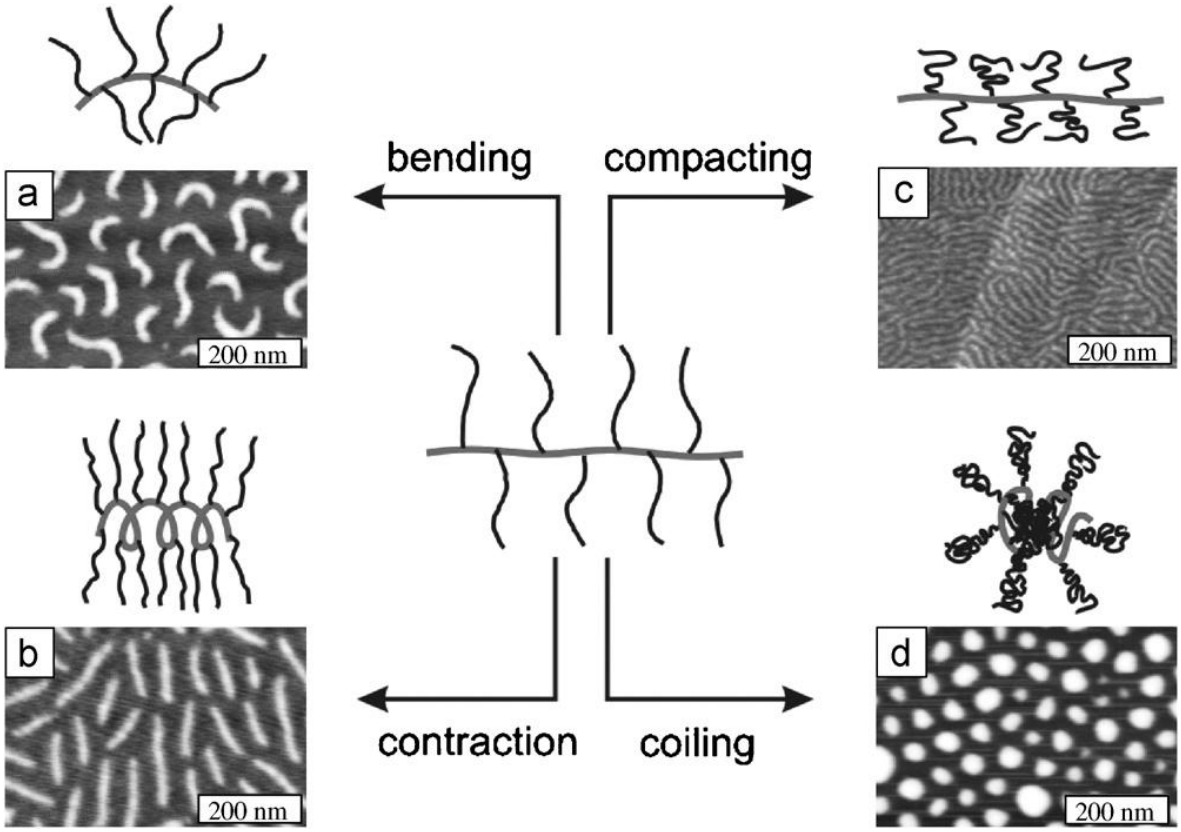

Figure 11. AFM height images along with schematics demonstrate four distinct conformations observed for molecular brushes adsorbed on different surfaces. The conformational transformations occur due to variations in the fraction of adsorbed side chains (From Ref. [9]).

The unusual properties of brush macromolecules on surfaces arise from their ability to change conformation in response to the substrate of varied surface energy as well as the lateral compression. Recently, Sheiko and co-workers[49] used ATRP to prepare the polymer backbone with more than 2000 2-hydroxyethyl methacrylate units and side chains containing 140 *n*-butyl acrylate units. They successively deposited the brush-like molecules on the surfaces of various liquid and solid substrates. As the densely grafted side chains adsorbed, they underwent steric repulsion which created tension in the backbone. This tension, was controlled by the grafting density, the side chain length, and the extent of substrate attraction. After adsorption of molecular brushes, the side chain adsorption-induced tension may overcome the covalent bond strength and cause molecular fracture via C-C bond scission (**Figure 12**).[49,50] The scission of the backbone was verified by the observation of shortened brush molecules.

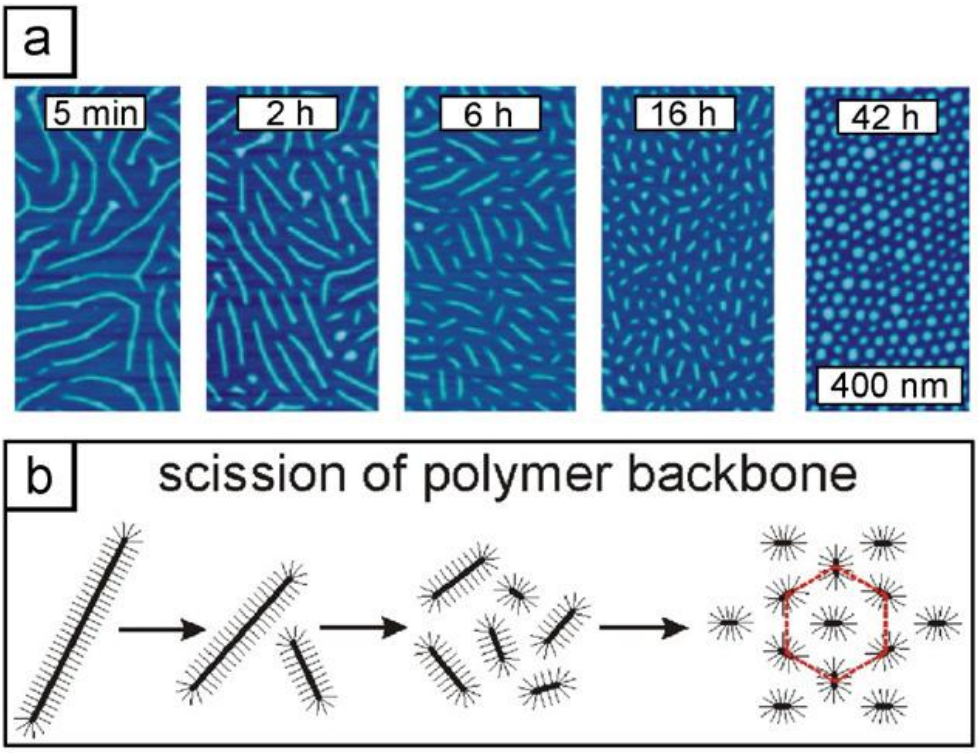

Figure 12. (a) AFM height images of the molecular brush with long side chains (n = 140) were measured at different exposure times to the water/propanol (99.8/0.2 wt/wt) substrate. (b) The molecules became shorter with greater exposure time to the substrate, which was attributed to spontaneous scission of the polymer backbone (From Ref. [49]).

1.2 Polymer Brushes

Polymer brushes are ensembles of polymer molecules that are terminally attached to an interface. Polymers can be anchored to a surface either by physical e.g. electrostatic adsorption or chemical linkage. As one of the coating techniques, application of polymer brushes has extended much beyond the conventional decoration and protection aspects and becomes a popular technology in diverse high-tech areas ranging from computer chips[51] to biomedical surfaces.[76] Investigation in polymer brushes is driven by the desire to control the interfacial properties of the polymer layer and its compatibility with the environment.

Polymer chains of the polymer brushes exhibit different conformations on surfaces. If the distance between two anchoring points is larger than the size of the surface-attached polymers, the segments of the individual chains can not interact with each other and as a result polymer chain will adopt a mushroom or pancake conformation (**Figure 13**). A completely different situation is obtained if the polymer chains are attached to the surface at a short distance

between the anchor points, and the polymer chains overlap. In this case, the segments of the chains try to avoid each other. At high grafting density, adsorbed polymers change their conformation from a random coil to an extended chain (**Figure 13**).

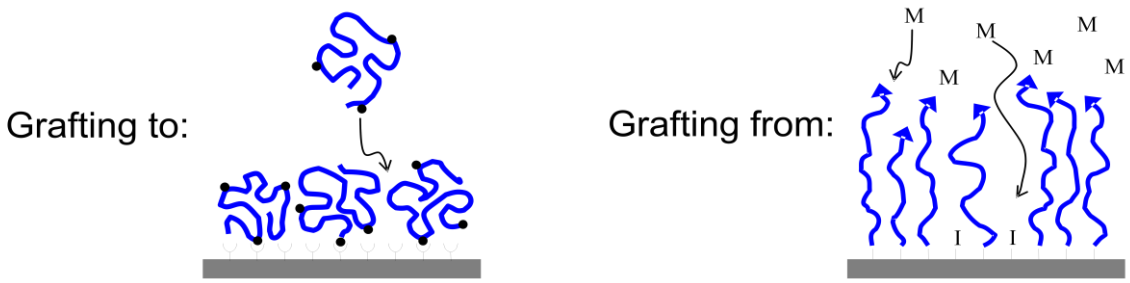

Figure 13. Schematic illustration of polymer brushes with different grafting densities prepared by 'grafting to' and 'grafting from' methods (From Ref. [66**]).**

As shown in **Figure 13**, polymer brushes can be prepared by the *grafting to* or *grafting from* method (mostly referred to as surface-initiated polymerization (SIP)). In the first method, one or more anchor groups of polymer chain can attach to the substrate. The *grafting to* method is difficult to achieve high grafting densities because of the screening of reactive surface sites by already anchored polymers. Therefore, films generated by this method are limited to thicknesses between 1 and 20 nm. The SIP from surface-bound initiators is a powerful alternative to control the density of polymer brushes (**Figure 14**). Since the diffusing species during the SIP are small monomer molecules (instead of macromolecules in the *grafting to* method), a high grafting density can be achieved. Up to now, almost all the developed polymerization techniques in solution have been successfully adapted for the SIP, such as free, controlled and living radical polymerization, living anionic and cationic polymerization, and ring-opening metathesis polymerization.[76]

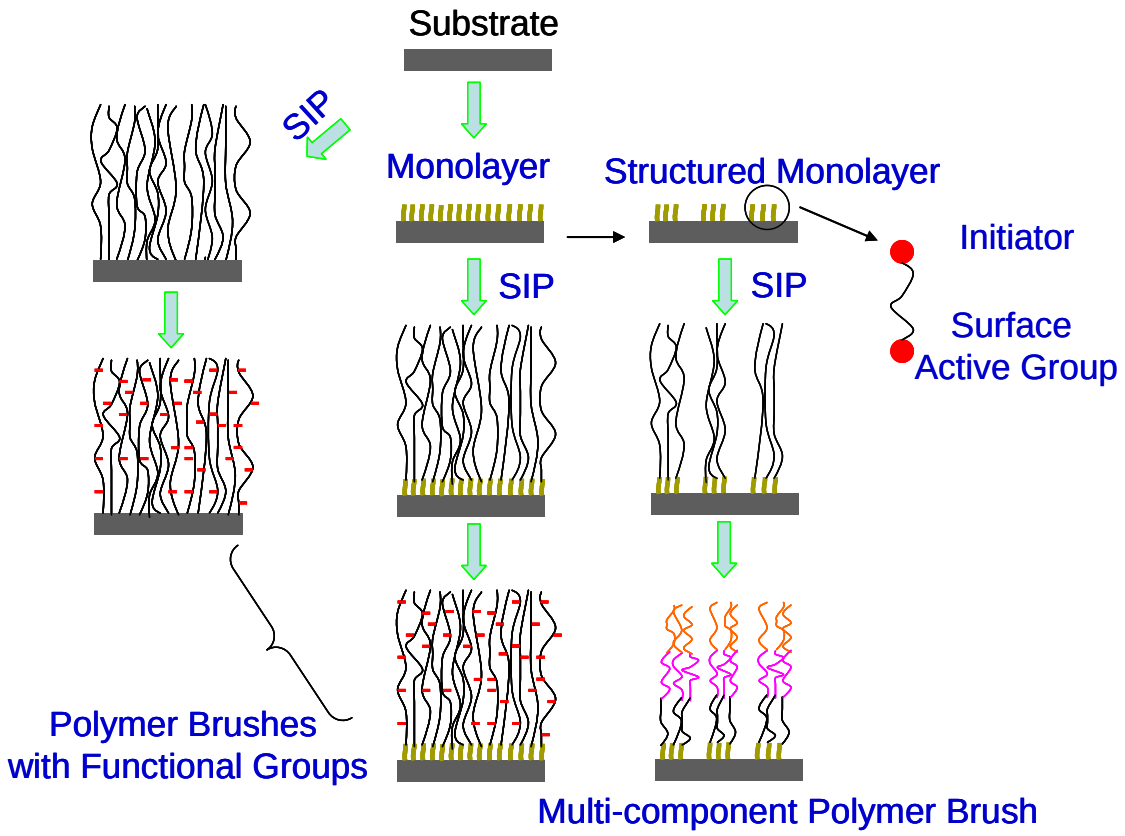

Figure 14. Scheme for the preparation of (structured) polymer brushes by surface initiated polymerization (SIP). Polymer brushes can be prepared on either initiator-anchored surface (e.g. self assembled monolayer (SAM)) or initiator-free surfaces. Functionalities can be introduced by analogue reactions. Furthermore, structured polymer brushes can be obtained on structured SAM by chemical lithography and microcontact printing. Multi-block copolymer brushes can be realized by a variety of polymerization methods.

Within various strategies developed for the preparation of polymer brushes, the most popular way is to grow monomers from or attach a polymer chain to a surface-bonded initiator system. Defined initiator systems can be prepared by the modification of the substrate with a self-assembled monolayers (SAMs) of bi-functional molecules bearing a surface grafting function and an initiator function for the SIP (**Figure 14**). SAMs can be formed on almost any surface, as long as the anchor group is correctly chosen.[52] Due to the versatility of such system, various surface coupling strategies have been developed during the last decades. One way is that polymer brushes were bonded to gold substrate by thiols[53,54] or to silica by silane functions.[55,56] However, these SAM systems have a limited chemical/thermal/UV stability and make them inappropriate for long-term applications. For instance, silane-based systems on oxides are prone to hydrolyze and have a poor stability in saline solutions at 37 ℃, thus impairing their use for many biomedical applications.[57,58] Thiol-based coatings are mainly

limited to coinage metal substrates, and their limited thermal[59] and UV stability[60] are well-known. Therefore, more effective and stable systems are demanded for the preparation of polymer brushes.

1.2.1 Self-initiated photografting and photopolymerization (SIPGP)

In the 1990s, Rånby and coworkers[61] developed a photografting polymerization procedure to prepare polymer grafts. A crosslinked polymer substrate such as poly(ethylene) (PE), poly(ethylene terephthalate) (PET), nylon, poly(propylene) (PP) and poly(vinylchloride) (PVC) were submerged in a solution of benzophenone in bulk vinyl monomer. Benzophenone here acts as a photosensitizer. After irradiation by UV light of a spectral distribution between 200 and 400 nm, 2-5 μm thick polymer layers were formed on the substrates. This one-step procedure has the advantage of e.g. formation of thick and dense polymer grafts directly on polymer substrates without the immobilization of initiators. Later, it was shown that a broad variety of vinyl monomers can be directly grafted onto organic substrates such as polyolefines in the absence of benzophenone by self-initiated photografting and photopolymerization (SIPGP).[62,63] In this case, the substrate was immerged only in bulk monomer and then irradiated with UV-light, resulting in the formation of polymer brush on the organic substrates. Here, the presence of benzophenone was no more necessary and a mechanism of SIPGP of vinyl monomer (e.g. styrene)[64] was proposed and described as follows. As shown in **Figure 15**, styrene absorbs a photon and reaches its excited state. This excited single state can transform through intersystem crossing (ISC) to its excited triplet state, which is in equilibrium with a biradical form. The biradical can subsequently initiate a free radical polymerization in solution. Besides, it can also abstract a hydrogen from the substrate. As a consequence, the radical formed on the substrate initiates the free radical surface-initiated polymerization. Therefore, defined, stable, and homogeneous polymer brush layers can be prepared directly onto surface containing abstractable groups. From the above mentioned procedure, it was found that the formation of defined, reactive interlayer such as a SAMs is not necessary, and surface-initiated polymerization of vinyl monomers can be performed and directly graft polymer onto surfaces. However, it should be noted that hydrogen can only be abstracted from surfaces when the triplet state of monomer possess enough energy. Brown[63] and Fang[65] calculated the excited states of acrylic acid, revealing a potential energy of 112.5 $kcal \cdot mol^{-1}$ for the T_3 triplet state of acrylic acid (T_1: 71.4 $kcal \cdot mol^{-1}$; T_2: 86.9 $kcal \cdot mol^{-1}$). In this case, the hydrogen could be abstracted from the PE substrate due to the T_3-state potential

energy of acrylic acid is higher than the C-H bond dissociated energy (BDE) on PE substrates (the BDE of primary, secondary and tertiary hydrogen atoms for PE is 100, 96 and 93 kcal·mol^{-1}).

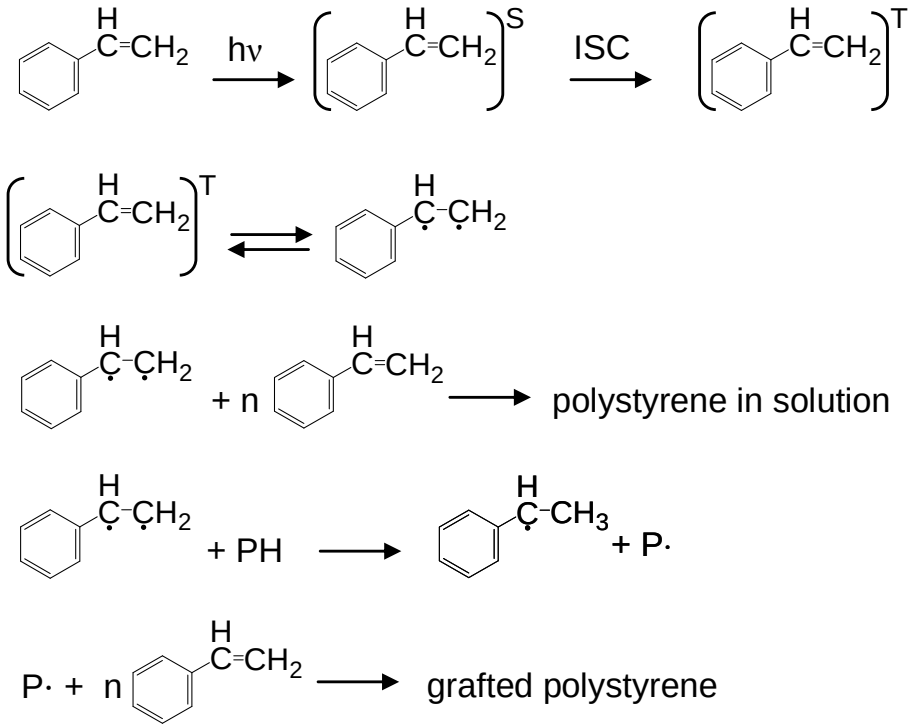

Figure 15. Principle of the self-initiated photografting and photopolymerization of styrene on a polymer substrate (From Ref. [66]).

Recently, Jordan and co-workers found that structured, extremely stable and homogenous polymer brush of controlled morphology can be prepared directly onto carbonaceous materials by the SIPGP of vinyl monomers.[67,68,69] First, a stable ultrathin (around 1 nm) template layer of carbonaceous material was locally deposited on an inorganic substrate by means of a focused electron beam. Amplification of the template by surface-initiated polymerization resulted in polymer brush layers of a controlled three dimensional shape. The dependence between the polymer layer thickness and the amount of locally deposited carbon allowed the preparation of complex 3D polymer architectures on surfaces. Taking advantage of the high thermal and chemical stability of the grafting, polymer brushes were further modified by polymer analogue reactions under drastic conditions such as nitration or sulfonation of poly(styrene) (PS) brushes. By this general approach, stable polymer brushes having all kinds of dimensions, architectures and chemical functionalities can be prepared on various substrates (**Figure 16**).

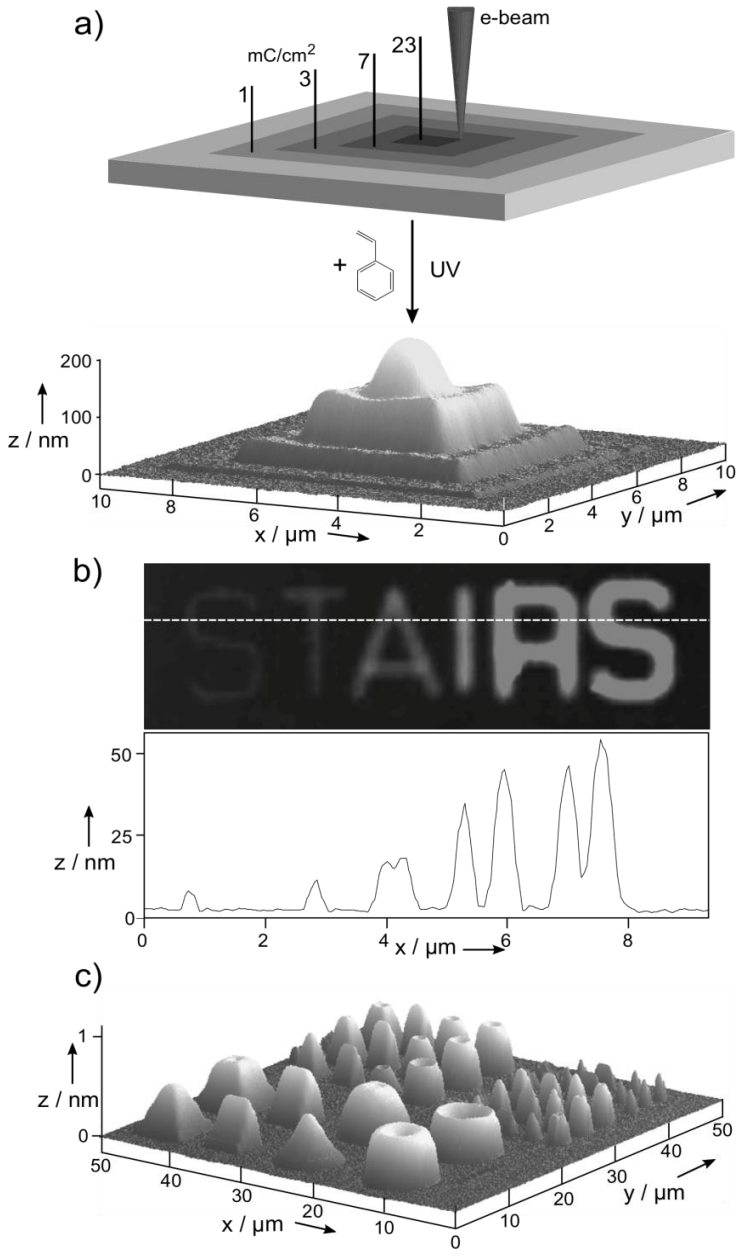

Figure 16. Structured polymer brushes by carbon templating on various substrates. a) A step pyramid of polystyrene (PS) brushes on silicon nitride created from a carbon template of concentric squares written with different electron doses (top: irradiation scheme, below: AFM image); b) AFM and height analysis of 'STAIRS' templated on a silicon substrate with lines of 100 nm width and increasing electron dose for each letter (1, 2, 4, 8, 12, 16 mC/cm^2). PS brush lines of 6, 10, 16, 35, 44 and 53 nm height, and widths were characterized between 200 and 350 nm; c) AFM image of PS brush objects of different sizes and shapes on a bare gallium arsenide substrate (maximum structure height: 0.5 µm). The variation of the polymer brush thickness is due to the change of the polymer grafting density, which is caused by the different applied electron beam dosage (From Ref. [68]).

1.2.2 Bottle-brush brushes (BBBs)

Using atom transfer radical polymerization (ATRP), Baker and co-workers [70] prepared polymer brushes of poly(methyl methacrylate) (PMMA) through the polymerization of MMA from a surface-bound initiator on gold. It was found that only 10 % of the surface-bound initiators actually initiated the polymerization, so that many initiator sites remained on the surface and the produced polymer brushes only exhibited a low grafting density. The insufficient initiation could be explained by the partial screening of initiators by the grafted polymer chains, or the loss of initiator through termination and chain transfer reactions.[71,72] This indicates that it is difficult to obtain polymer brushes with extended polymer chains using ATRP or free radical polymerizations.

An effective strategy to generate polymer brushes with extended polymer chains is the preparation of branched i.e. so called 'bottle-brush brushes' (BBBs) structures from surfaces. For instance, as shown in **Figure 17**, 176 nm-thick poly(hydroxyethyl methacrylate) (PHEMA) brush was created on gold. After functionalization of the pendant hydroxyl groups, a 358 nm-thick polymer film was obtained. The drastic increase in thickness was due to the mass increase of repeating unit and the subsequent stretching of the main chain.

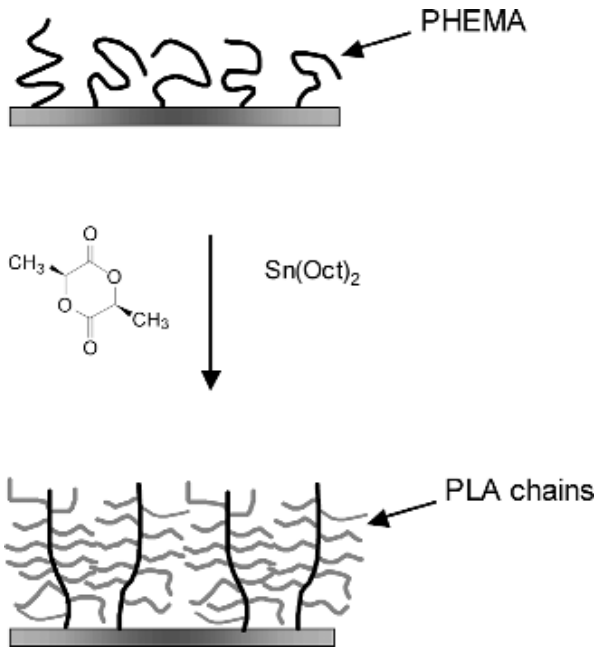

Figure 17. Extension of PHEMA brushes by functionalization of side chains to form bottle-brush brush structures (From Ref. [76]).

Until now, only very few research groups have reported on BBB systems.[73,74,75,76] However, it is of certain importance to study on this topic in depth since it has a promising future in

biological applications. The complex polymer architectures intriguingly resemble the structure of various polyglycans that is found on nearly every living cell. It has been shown that carbohydrates in the form of polysaccharides, glycoproteins, glycolipids and other glycoconjugates play essential roles in many biological processes. They serve as recognition sites for the cell and contribute to the steric repulsion which prevents undesirable nonspecific adhesion.[77] Actually, highly aggregated surface-tethered carbohydrate ligands e.g. the glycocalyx are dominated by glycosylated molecules on the cell surface, resulting in not only the enhancement of binding strength in specific recognition of proteins but also the minimization of nonspecific protein adsorption.[73] Non-toxic BBBs structures as biomimetic functional soft interfaces between solid semiconductors and biological systems may find direct applications for designing advanced biomedical devices.

1.3 Bioactive surfaces

Protein adsorption[78,79] at interfaces widely exists in nature ranging from food processing to biomedical science. Preventing adsorption of proteins[80,81] is a key for the performance of medical devices and all applications including biosensors,[82] cell culture,[83] biomedical implants from hip replacement to contact lenses,[84] etc. As a macro fouling (attachment of larger organisms), marine fouling (**Figure 18**) is a constant problem for boats, ports and anything kept in the sea for a period of time. Marine organisms are prone to adhere to almost any type of surface. Modern method for preventing fouling is to use paints containing metals such as copper or tin, as well as herbicides. However, these metals are toxic and cause severe environmental problems. Alternatives for reducing the unwanted bio fouling is to graft self-assembled monolayer (SAM) or antifouling polymers onto surfaces.[85,86,88]

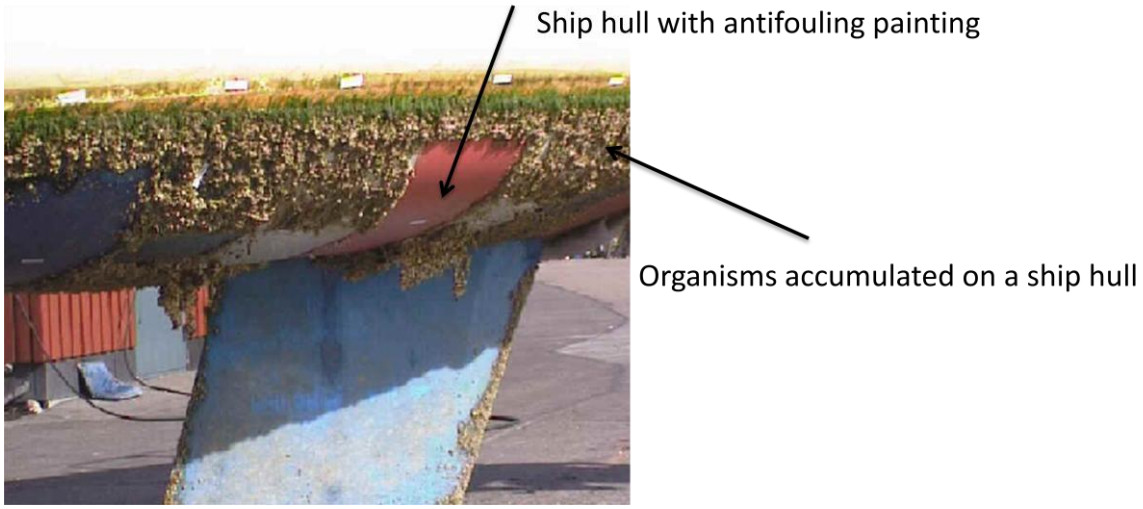

Figure 18. Macro fouling i.e. organisms accumulated on a ship hull, however, no significant adsorption was observed on antifouling painting area (From Ref. [87]).

So far oligoethylene glycol monolayers on gold[79, 88] or SiO_2 [89] have been the mostly investigated SAMs for resisting non specific protein adsorption. The protein-resistant efficiency of these short monodisperse molecular layers was reported to increase with the length of the oligoethylene glycol. A minimum of two ethylene glycol units is necessary for negligible protein adsorption.[78] However, the limited chemical, thermal and UV stability of these SAMs make them inappropriate for long-term applications under tough conditions.

Polymer brushes via surface-initiated polymerization (SIP) have triggered numerous investigations of synthetic surface-bound polymers as non-fouling coatings. Up to now, the SIP to prepare the protein-resistant surface is regarded as one of the best methods due to the versatility of monomers and stability.

In spite of the various reported criteria for the design of antifouling polymers, some common parameters i.e. the presence of flexible hydrophilic groups and highly branched architecture can lead to effective protein resistance. So far, a variety of polymers including nonionic,[90] zwitterionic,[91, 92] peptidomimetic[93] and polysaccharides[94,95,96] polymers have been developed to resist nonspecific protein adsorption and have gained some success in *in vitro* and *in vivo*. However, to date, very few effective non fouling surfaces meet the practical demands of a daily application. In the following part, some promising polymers for non-fouling surfaces are introduced.

Poly(ethylene glycol) (PEG) and PEG-based polymers are widely studied polymers to prevent the adsorption of proteins and cells.[97] However, current PEG technology has major limitations

for long-term applications. PEG coatings can undergo oxidative degradation and lose their function when placed in *in vivo*.[98,99,100] Moreover, PEG system is short of functional groups for ligand immobilization which is required for many applications. The introduction of additional functional groups into PEG may, however, alter its properties.[101] In a word, there is continuous need to develop new and effective system to overcome such problems.

Zwitterionic polymers are macromolecules with oppositely charged groups located at the chain ends. Polymers incorporating zwitterionic molecules such as phosphatidylcholines[102] and carboxybetaine methacrylate[103] are promising for anti-biofouling surfaces. It is believed that zwitterionic polymers resist nonspecific protein adsorption with either a mixture of anionic and cationic terminal groups based charge interactions or a strong hydration of the polymer through ionic salvation.

Surfaces coated with oligosaccharide grafted polymers mimic the antifouling glycocalyx,[94] which directs the specific interactions such as cell-cell recognition and prevents the undesirable non-specific adhesion of other molecules and cells. In addition, dendritic saccharide surfactant polymers were prepared by Marchant[95] as antifouling interface materials to reduce platelet adhesion. In this case, the hexyl side chains facilitate the adsorption of the surfactant polymers onto hydrophobic substrates, while the maltose dendron side chains provide a dense canopy of protective glycocalyx-like layer as an antifouling interface that suppresses platelet adhesion.

Poly(2-methyl-2-oxazoline), a peptide-like hydrophilic polymer, has showed very promising properties in biological application since the first demonstration of its biocompatibility by Goddard.[124] Recently, Konradi and co-workers investigated a comb polymer consisting of poly(2-oxazoline) side chains and a polycationic backbone as the protein-repellent polymer. The comb polymer adsorbed on the negatively charged surface through static charge interaction forming a polymer coating. Such coatings with an optimal side chain grafting density restrict a protein adsorption as low as $2 ng/cm^2$, which is quantitatively equal to the protein-repellent property of PEG coatings. However, it should be noted that the electro-static adsorbed coating is prone to desorption at certain conditions i.e. in salt water, and thus covalent attachment is preferred.

1.4 Poly(2-oxazoline)s

1.4.1 2-Oxazoline

Oxazolines are five-membered heterocyclic compounds. Depending on the location of the double bond, three different oxazolines can be classified. Among them, 2-oxazoline is the most investigated and widely used compound (**Figure 19**).

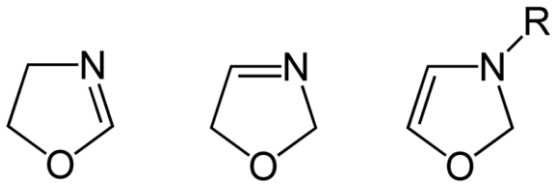

Figure 19. 2-Oxazoline, 3-oxazoline and 4-oxazoline (from left to right).

1.4.2 Living cationic ring-opening polymerization (LCROP)

The 2-oxazoline ring can be opened and polymerized to form a polypeptide-analog polymer, which is known as ring-opening polymerization. In 1966, Kagiya *et al*. reported the first time on the ring-opening polymerization of 2-oxazolines.[104] It was shown that the polymerization reaction of 2-oxazolines was not disturbed by chain transfer and termination under appropriate conditions. In the following decades, many reports showed that depending on the type of initiator, the mechanism of chain growth can be cationic, or covalent. When cationic initiators such as methyl triflate are used, the polymerization is cationic. The cationic propagating species of the oxazolinium salt is stable. Therefore, it was conveniently employed in the synthesis of block copolymers and end-functionalized polymers. The living cationic ring-opening polymerization (LCROP) behavior of 2-oxazolines having a variety of 2-substituents has been extensively investigated by Saegus and Kobayashi et al.[105,106,107] If the monomer reacts with more nucleophilic alkyl halides, e.g. methyl iodide, the polymerization is slow and proceeds via a different mechanism, namely the covalent mechanism.

The general mechanism of cationic polymerization for initiation and propagation of 2-oxazolines is shown in **Figure 20**. The nucleophilic nitrogen of the 2-oxazoline ring can

convert to oxazolinium cation under the attack of electrophiles such as alkylating agents, or Lewis and Brønsted acids. The resulting oxazolinium ring can further react with another 2-oxazoline so that the ring is opened and a linear amide structure is formed. This process can be repeated until a nucleophilic terminating reagent terminates the polymerization.

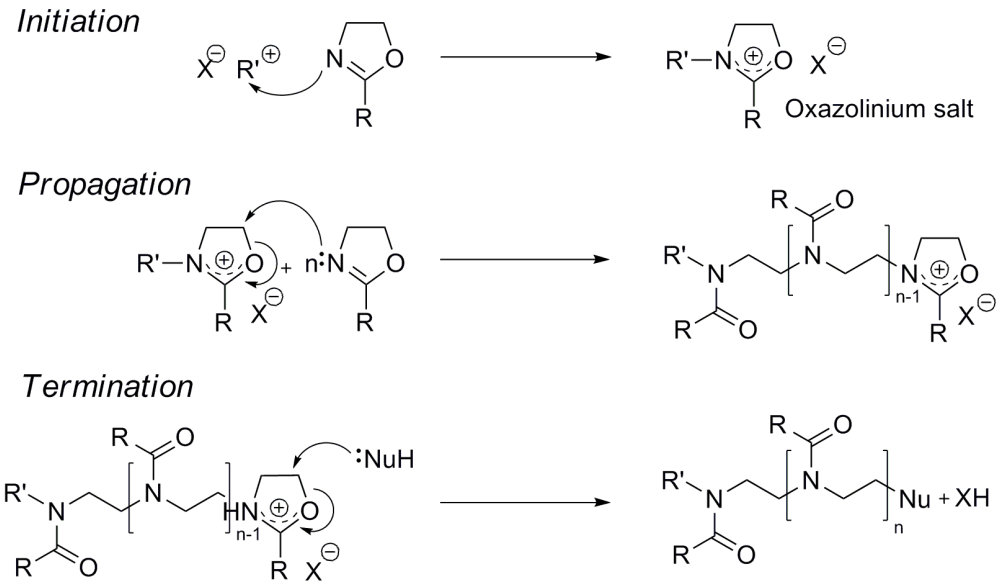

Figure 20. Mechanism of cationic ring-opening polymerization of 2-oxazolines.

It is generally believed that increasing the nucleophilicity of the initiator counter ion and monomer decreases the tendency of the living cationic ring-opening polymerization (LCROP) to be ionic. With the counter ion of non-nucleophilic trifluoromethylsulfonate (triflate, OTf), the propagating species is the cation of any type of 2-oxazoline and the propagation rate increases significantly.[108,109] Methyl trifluoromethylsulfonate (MeOTf) as a commonly used initiator shows many advantages in LCROP of 2-oxazolines. Due to its high reactivity, MeOTf reacts fast with 2-oxazolines even below room temperature and the propagation starts at temperatures above 40 ℃. Fast and quantitative initiation with respect to the propagation of polymerization is crucial when preparing well-defined polymers with narrow molar mass distributions. Since the initiation is nearly instantaneous and the formed oxazolinium triflate salt is sterically and electronically similar to the propagating polymer chain end, poly(2-oxazoline)s (POx) with low polydispersity indices (i.e. M_w/M_n of 1.02~1.20) can be prepared.

However, in spite of the living character of the cationic polymerization, side reaction can occur via chain transfer reactions especially at high temperatures (T>120 ℃) and at very low $[M]_0/[I]_0$ ratios. Hoogenboom and co-workers[110] found a shoulder in the GPC traces at high molar mass region of poly(2-ethyl-2-oxazoline)s (PEtOx). This might be due to the occurrence of chain transfer reactions followed by chain coupling at high monomer

conversions as already reported earlier by Litt and coworkers.[111] Moreover, yellow polymerization mixtures were obtained at low monomer concentrations ([M]<3 M), indicating the occurrence of side reactions. An optimum monomer concentration between 4 M and 7 M was established for the living cationic ring-opening polymerization of 2-ethyl-2-oxazoline initiated with benzyl bromide in *N*,*N*-dimethylacetamide at 100 ℃.

The living character of the polymerization of 2-substituted 2-oxazoline provides synthetic possibilities to tailor macromolecules with a broad variety of architectures, composition, numerous side and end functions as well as the ease of preparation of block, gradient and random copolymers. Therefore, these polypeptide-like polyamides of various architectures have found many early-stage or potential applications as stabilizers, compatibilizers and thermo-settings.[112] In the past decades, the biocompatibility as well as stealth behavior[113,114,115] of POx triggered the application of POx in the biomedical field.[116] Moreover, water soluble POx with a lower critical solution temperature (LCST) broadened the research area for thermo-responsive or so called 'smart' materials. **Figure 21** shows POx of various structures and their biomedical applications.

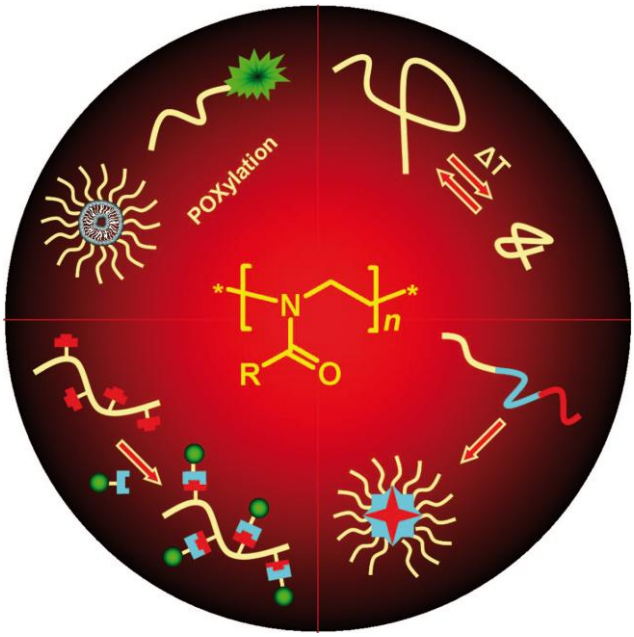

Figure 21. Poly(2-oxazoline)s have potential use as biomaterials and thermo-responsive materials. In addition, the easy access to hydrophilic, hydrophobic, and fluorophilic polymers by simply changing the side chain or by the combination of click chemistry provides the possibility to prepare a range of polymer structures and the self-assembly of copolymers (From Ref. [117]).

1.4.3 Thermo-responsive poly(2-oxazoline)s

Recently, hydrophilic poly(2-oxazoline)s (POx) came into focus as temperature-responsive polymers. Compare to the well-studied PNIPAAm and PEG systems, POx prepared by living cationic ring-opening polymerization (LCROP) of 2-oxazolines have several advantages e.g. ease of access of a broad variety of architectures, composition, and end functionalities. Additionally, the lower critical solution temperature (LCST) of hydrophilic POx can be tailored over a broad temperature range by means of the molar mass and composition adjustment.

In 1988, Kwei and co-workers first investigated the thermo-sensitivity of aqueous solutions of poly(2-ethyl-2-oxazoline) (PEtOx). It was shown that the LCST is dependent on the polymer concentration, and cloud points in a range of 61 ℃-64 ℃ were found for the molar mass of 500 kg/mol to 20 kg/mol.[118] Since the first report of thermo-responsive POx, the LCST of hydrogels, linear, homo- and coPOx were investigated in details as a function of the side chain and/or end-group functionality as well as the molar mass and concentration. In 1992, Uyama and Kobayashi[161] reported that poly(2-isopropyl-2-oxazoline) (P*i*PrOx) exhibited a cloud point in the range of 36-39 ℃, which makes it a suitable candidate for biomedical purposes. Recently, Park and Kataoka[167] reported that poly(2-*n*-propyl-2-oxazoline) (P*n*PrOx) also exhibited thermo-sensitivity in water, with a cloud point of 24 ℃ in a 1 wt% aqueous solution. In addition, Schubert and co-workers[168] finely tuned the LCST of poly(2-oxazoline)s by varying composition and molar mass. The thermal transitions of these copolymers with cloud points of ~34 ℃ showed no hysteresis or concentration dependence, making them superior to PNIPAAm.

Besides homopolymers, the copolymerization of different 2-oxazoline monomers allows accurate control over the LCST. Park and Katoaka[171] reported the copolymerization of 2-isopropyl-2-oxazoline (*i*PrOx) with the hydrophilic 2-ethyl-2-oxazoline (EtOx), which led to a linear increase of the cloud point up to 67 ℃ as a function of the EtOx content of 75 mol %. Copolymerization of *i*PrOx with the more hydrophobic *n*PrOx also resulted in a linear dependence between cloud points and the composition. Recently, Jordan and co-workers further decreased the cloud point of P*i*PrOx down to 9 ℃ by gradient copolymerization of *i*PrOx with hydrophobic 2-*n*-butyl-2-oxazoline (BuOx) and 2-*n*-nonyl-2-oxazoline (NonOx).[119]

Furthermore, Jordan and co-workers investigated the effect of end groups with different polarity on the cloud point of P*i*PrOx.[33] It was found the LCST strongly depends on the polarity of the terminal moiety especially for low molecular weight polymer. For instance, the introduction of a hydrophobic unit e.g. *n*-nonyl decreased the cloud point to 28 ℃ as compared to a terminal methyl group (cloud point = 47 ℃). In addition, the location of the amide groups in the POx and poly(N-alkyl acrylamide)s (PAAm) resulted in different LCSTs, e.g. POx pendant group modification caused a stronger shift of LCST as compared to PAAm.

In addition, Schlaad's group tuned the LCST of copolymers of *i*PrOx and 2-(3-butenyl)-2-oxazoline in a range of 5-90 ℃ by introducing various side chain functionalities through the 'click' reaction.[120] Kim and co-workers[121] investigated thermo-responsive micellar gels formed by diblock PEtOx-b-Poly(ε-caprolactone) at low temperature. As temperature increases, gel-sol transition and subsequent precipitation occured due to the collapse of PEtOx.

Another interesting phenomenon of POx is that some of them show an upper critical solution temperature (UCST), above which a mixture is miscible in all proportions. The UCST is in general dependent on pressure, degree of polymerization as well as the polydispersity in polymer mixtures. The phase separation at the UCST is in general driven by an unfavorable entropy, in particular, interactions between components favor a partially demixed state. Schubert and co-workers reported that poly(2-phenyl-2oxazoline) (PPhOx) showed an UCST in ethanol.[122] With addition of water to the ethanol solution, the solubility of PPhOx increased, leading to a solubility maximum in the range 6-25 wt% of water in ethanol. This maximum solubility was due to the presence of monomeric water molecules in these solvent mixtures. These water molecules formed hydrogen bonds with the polymeric amide groups, and resulted in a compatibilizing hydration shell around the polymer.

1.4.4 Biomedical applications of poly(2-oxazoline)s

In the past decade, poly(2-oxazoline)s (POx) were found nontoxic/biocompatible[123] and, similar to the well established poly(ethylene oxide) (PEO). Besides, it exhibited the so-called 'stealth' effect. In 1989, Goddard demonstrated poly(2-ethyl-2-oxazoline) (PEtOx) as a biocompatible polymer.[124] Afterwards, ^{125}I-labeled POx was found to be excreted from mice without significant accumulation in organs. Recent studies by Jordan and co-workers on the biodistribution and excretion of radiolabeled poly(2-methyl-2-oxazoline) (PMeOx) and PEtOx took this research to a new level.[113] No accumulation in tissue and rapid clearance

from blood were found. Chung and co-workers[125] also investigated blood compatibility of PEtOx in *in vitro*. PEtOx was attached to a polyurethane film and reduced platelet adsorption was observed.

Another interesting aspect of POx is their high chemical functionality e.g. they can be used as drug and protein conjugates. Polymer-drug conjugation is a versatile method to increase the circulation time and improve the solubility, moreover, the targeting group on the polymer can deliver the drug to expected places. Since the first report of PMeOx as peptide conjugates by Saegusa,[126] a number of studies have been carried out to investigate POx in the polymer-drug system. For example, Jordan and co-workers investigated the PMeOx and PEtOx conjugates with ^{111}In radiolabel.[113] In addition, Hoogenboom and co-workers demonstrated PEtOx as a potential alternative to poly(ethylene oxide) (PEO) for protein/drug conjugates. [127] Comparable results were obtained for PEtOx in regard to PEO, e.g., protein-rejecting properties, drug-release profile, and *in vitro* cytotoxicity. Up to now, there have been some polymer-drug conjugates on the market for the treatment of different diseases. However, there are continuous demands for new polymer-drug conjugates regarding a diversity of requirements.

Chapter 2 Objective of this work

In this work, molecular brushes based on poly(2-oxazoline)s are to be synthesized for the first time and characterized with respect to their defined architecture. Key compound of the work is the 2-isopropenyl-2-oxazoline with two polymerizable groups: First, the vinyl group in the 2-position for living anionic or radical polymerization forming the molecular brush back bone, second, the 2-oxazoline ring for the living cationic ring-opening polymerization forming the pendant polymer chains of the molecular brush. Synthetic routes are to be investigated and optimized to allow a direct synthetic access to well-defined molecular brushes in solution as well as to well-defined bottle-brush brushes on solid surfaces. As the living cationic ring-opening polymerization (LCROP) of 2-oxazolines allows a precise variation of the side chain length and composition and end group functionality, the impact of such structural variations upon the final polymer properties such as solubility, aggregation, thermo-responsiveness, properties of bottle-brush brush coatings such as layer morphology, wetting behavior, adsorption and adhesion characteristics are main aspects of this work.

Chapter 3 Results and discussion

3.1 Monomer synthesis

Oxazolines are five-membered heterocyclic compounds with a double bond in the ring (shown in **Figure 22**). The double bond can be located in three different positions resulting in oxazolines of different types.[128] 2-oxazolines are the most common and investigated compounds. There are many ways in which 2-oxazoline can be synthesized e.g. from amino alcohols, amides, haloamides, aziridines, epoxides, grignard reagents and reaction of $SOCl_2$ on hydroxy amides.[129,130,131,132,133,134]

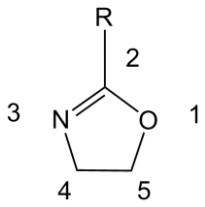

Figure 22. Structure of 2-substituted oxazoline.

2-oxazoline monomers are directly accessible in high yields via different synthetic routes. One of the common used one-step synthesis is thought the addition of amino ethanol to nitriles,[132] which was developed by Seeliger and co-workers. As shown in **Figure 23**, through a one-step synthesis from the corresponding nitrile compound, 2-*n*-propryl-, 2-isopropyl- and 2-butyl- 2-oxazoline can be prepared by a reaction with amino ethanol in the presence of cadmium or zinc acetate in high yield. Thus, broad choices of 2-oxazolines are accessible by changing the substituted group in nitriles.

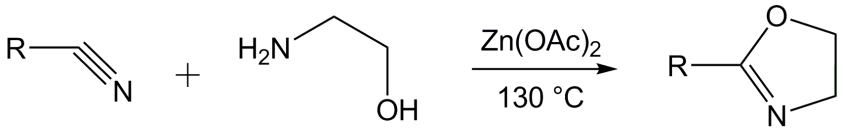

R = $CH_2CH_2CH_3$, $CH(CH_3)_2$, $(CH_2)_3CH_3$

Figure 23. Synthesis of 2-oxazolines by a reaction between amino ethanol and nitriles.

As shown in **Figure 24**, 2-isopropenyl-2-oxazoline (IPOx) was synthesized according to the procedure published previously by Seeliger.[135] Specifically, 2-ethyl-2-oxazoline (EtOx)

reacted with paraformaldehyde in the presence of catalytic amounts of strong bases (e.g. triethylamine) to form 2-[1-(hydroxymethyl)ethyl]-oxazoline. Water was eliminated from the hydroxymethyl derivatives at elevated temperatures in the presence of alkali metal alkoxides or other strong alkaline substances. However, it should be noted that the reaction with EtOx proceeds differently when formaldehyde is present in excess: the reaction of IPOx with formaldehyde leads to hydroxyethyl oxazoline derivatives as shown in **Figure 24**. Therefore, a stochiometric amount of paraformaldehyde was used in the reaction with EtOx.

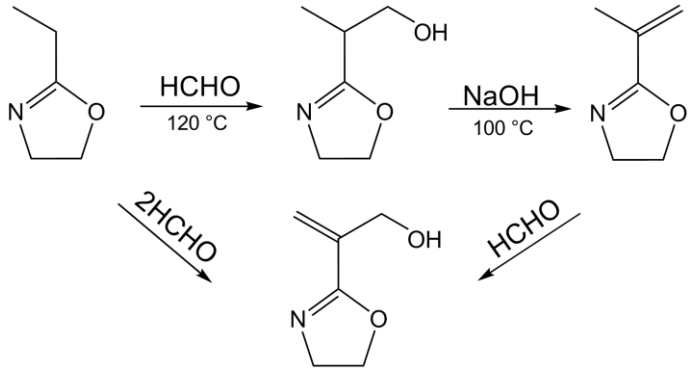

Figure 24. Synthesis of 2-isopropenyl-2-oxazoline and spontaneous side reactions.

3.2 Molecular brushes via free radical and cationic polymerization of 2-oxazolines

3.2.1 Reaction of 2-isopropenyl-2-oxazoline

2-Isopropenyl-2-oxazoline (IPOx) allows four ways of polymerization as shown in **Figure 25**: (1) olefinic polymerization via radical or anionic polymerization to produce poly((2-oxazoline-2-yl)propylene), (2) living cationic ring-opening polymerization (LCROP) to poly((N-methacryloyl imino)-ethylenes)), (3) cationic polymerization to give ring-preserved polymer, and (4) spontaneous polymerization of IPOx by the N-alkylation of the 2-oxazoline moiety with strong alkylating agents to poly[1-(3-alkyl-2-oxazolinium-2-yl)ethylene.[136]

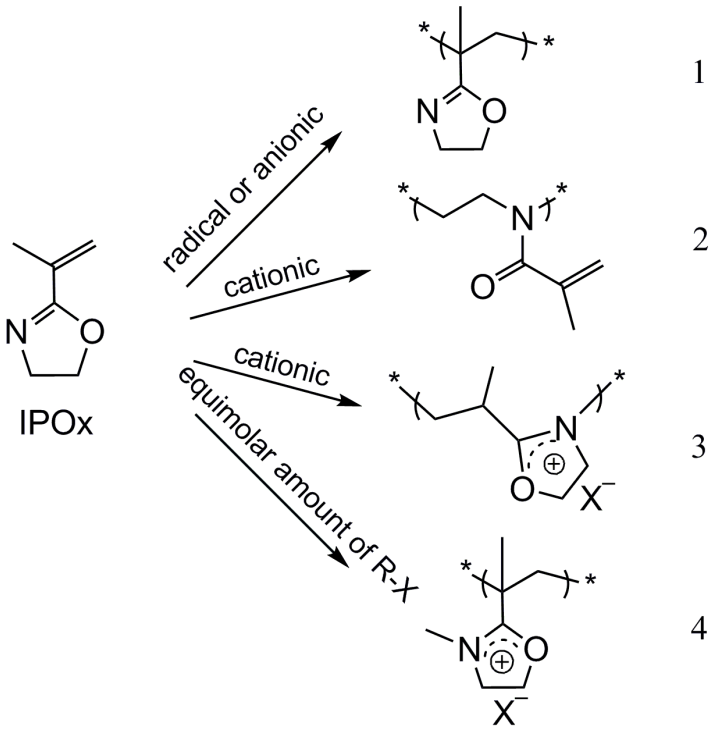

Figure 25. Possible ways to polymerize IPOx. 1) Radical or anionic polymerization to produce poly((2-oxazoline-2-yl)propylene), 2) LCROP to poly((N-methacryloyl imino)-ethylenes)), 3) cationic polymerization to give ring-preserved polymer, and 4) spontaneous polymerization of IPOx by the N-alkylation of the 2-oxazoline moiety with strong alkylating agents to poly(1-(3-alkyl-2-oxazolinium-2-yl)ethylene).

We became interested in the preparation of molecular brushes of 2-oxazolines. On the one hand, 2-oxazolines can be polymerized by living cationic ring-opening polymerization. This

allows for the incorporation of initiators with functional groups, terminal groups, and especially broad choice of monomers, which facilitates design and construct polymers with multifunctional architectures. On the other hand, the non-toxic peptide-like poly(2-oxazoline)s have shown potential applications as responsive materials and biomaterials. We choose IPOx as starting molecule for the preparation of molecular brushes i.e. free radical polymerization of IPOx forming backbone with pendant 2-oxazoline ring. Subsequently, as shown in **Figure 26**, LCROP of 2-oxazolines from the charged PIPOx backbone form side chains.

For the preparation of POx cylindrical molecular brushes all three routes (*grafting from*, *grafting through* or *grafting onto*) are possible. For example, the *grafting through* of POx macromonomers were employed with comonomers to realize sufficient degrees of polymerization.[137,138,139,140] Since POx is prepared by LCROP, it is of advantage to use the *grafting from* approach, analogue to the surface-initiated polymerization of 2-oxazolines on surfaces or nanoparticles.[54,141] For the *grafting from* approach, several synthetic strategies are possible. Kobayashi et al.[142] used hydroxyl groups of saponified poly(ethylene-co-(vinyl acetate)) to create pendant tosylate moieties for the grafting of POx side chains and Nuyken et al.[143 , 144 , 145 , 146] used linear as well as (hyper-) branched macroinitiators containing benzylchloride functions for the grafting of 2-oxazolines. Both approaches lead to comb polymers with POx side chains of medium grafting density. Though some reports have been published in the past for comb like poly(2-oxazoline)s, they are either showing low grafting density or lacking reactivity for the LCROP of 2-oxazlines.

3.2.2 Polymerizations

The monomer IPOx has two orthogonal polymerizable groups, a vinyl group for the free radical or living anionic polymerization and the 2-oxazoline ring for the living cationic ring-opening polymerization (LCROP). It has been shown that the conversion of the vinyl group to poly(2-isopropenyl-2-oxazoline) (PIPOx) by radical[147 , 148 , 149 ,215] as well as anionic[216] polymerization does not affect the 2-oxazoline ring. Since the oxazoline ring can be well preserved during the vinyl polymerization, it is possible to prepare molecular brushes from POx.

Firstly, IPOx was initiated by N,N-azobisisobutyronitrile (AIBN) and polymerized by free radical polymerization to form the molecular brush backbone; Successively, 2-oxazolines i.e.

2-methyl-2-oxazoline (MeOx), 2-ethyl-2-oxazoline (EtOx), 2-isopropyl-2-oxazoline (*i*PrOx), 2-*n*-propyl-2-oxazoline (*n*PrOx) and 2-*n*-butyl-2-oxazoline (BuOx) were polymerized by LCROP to form the side chains. For the latter, the PIPOx backbone has to be converted to a macroinitiator salt with pendant oxazolinium rings by the reaction with a stochiometric amount of methyl triflate (MeOTf). This approach has the advantage that a robust and very effective macroinitiator [150] is formed with equal reactivities as compared to e.g. triflates or tosylates.[151] Moreover, the charge at each monomer unit, thus a polyelectrolyte induces significant chain stretching due to the coulomb repulsion. This improves the accessibility of the initiation sites for the monomers along the main chain, as shown in **Figure 27**. A fast initiation reaction is crucial to obtain side chains of low polydispersities, especially for grafting by the ionic living polymerization. Both aspects, macroinitiator chain stretching and the formation of the oxazolinium salt, work in favor for a fast initiation reaction of the LCROP for a defined side chain grafting. As outlined in the reaction pathway (**Figure 26**) molecular brushes with five types of poly(2-oxazoline) homopolymer side chains were synthesized. MeOx gives very hydrophilic brushes, BuOx gives very hydrophobic brushes, EtOx, *n*PrOx and iPrOx result in slightly amphiphilic molecular brushes which are known to show a sharp LCST.[167] The results of the radical polymerization of IPOx and the grafting from polymerization of 2-alkyl-2-oxazoliness by LCROP using the macroinitiator salt are summarized in **Table 1.**

As outlined in **Figure 26**, the molecular brush backbone prepared by free radical polymerization is facile but not well controlled, thus not suitable for preparation of defined polymers. An alternative would be to use controlled radical polymerization. However, previous studies showed it is difficult to convert IPOx by widely used atom transfer radical polymerization (ATRP) to PIPOx. Only oligomeric products were obtained probably due to a strong complexation of the copper by the pendant 2-oxazoline units of oligomers.

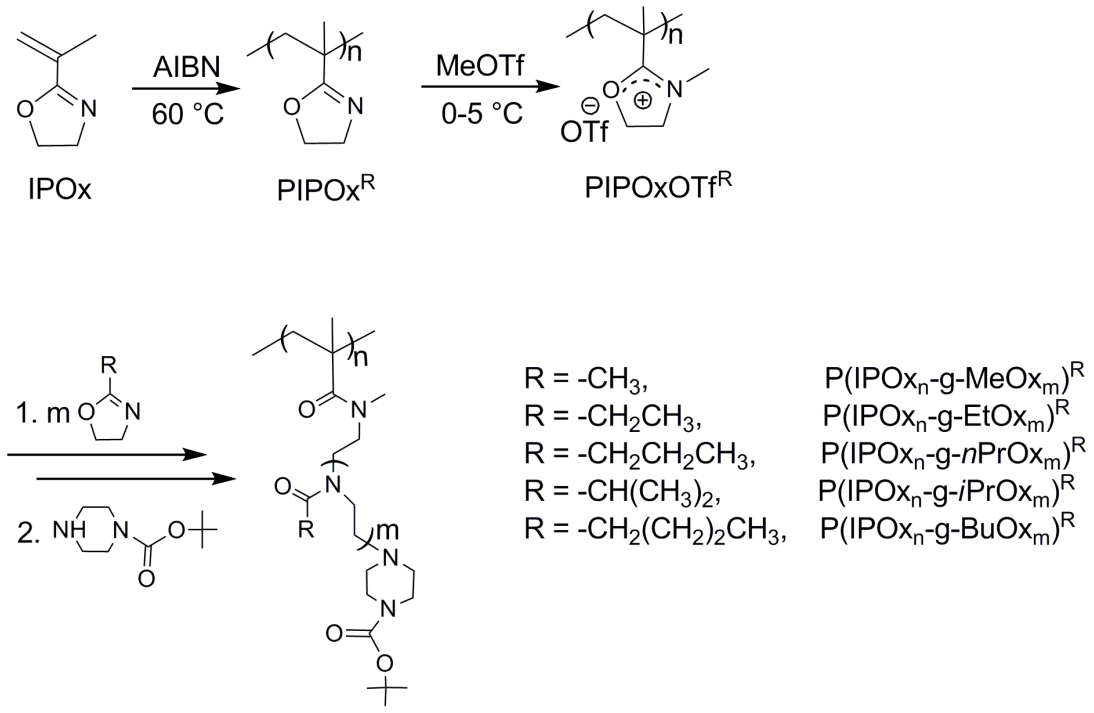

Figure 26. Synthesis of molecular brushes of 2-oxazolines via combination of radical polymerization of 2-isopropenyl-2-oxazoline and subsequent cationic ring-opening polymerization of 2-alkyl-2-oxazolines (‘R’ = prepared by radical polymerization).

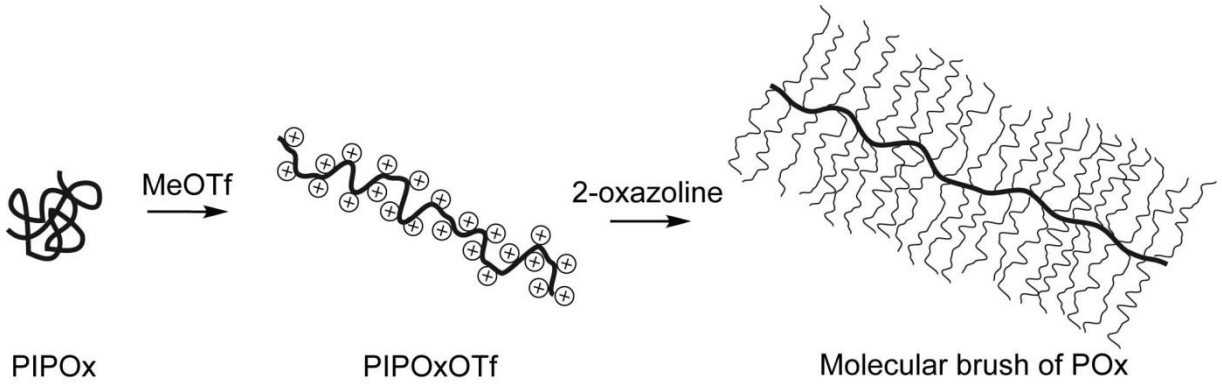

Figure 27. Schematic illustration of the formation of stretched macroinitiator (PIPOxOTf) by methylation of methyl triflate (MeOTf) and successive cationic ring-opening polymerization of 2-oxazlines to form side chains.

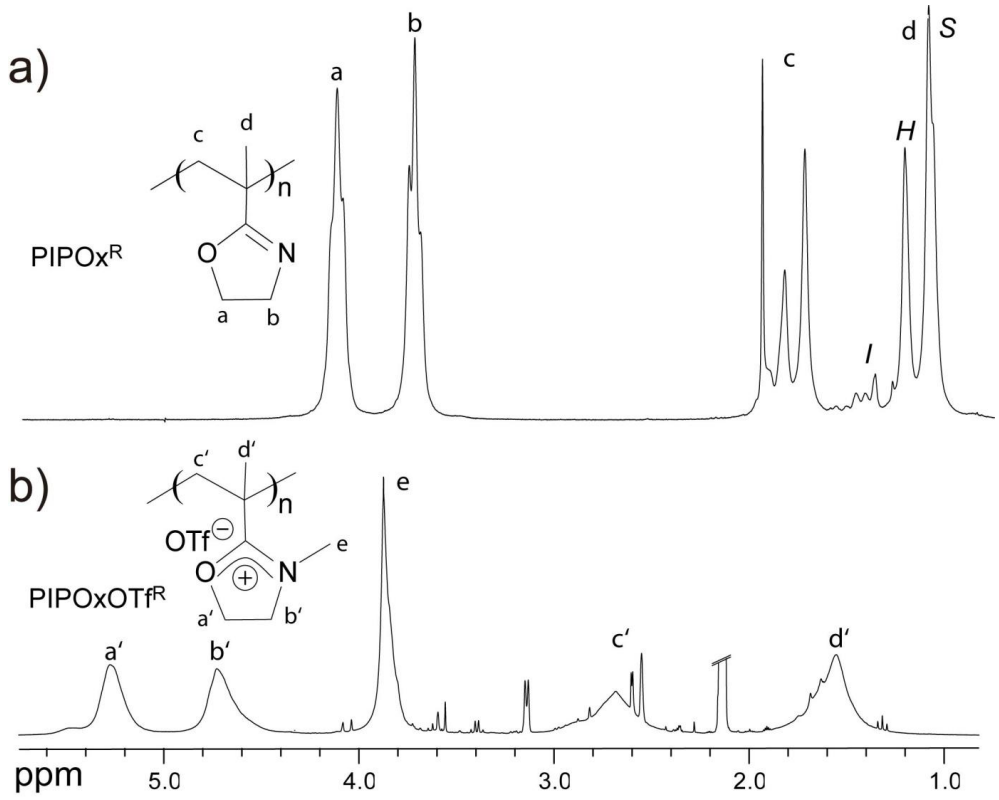

Figure 28. ^{1}H NMR spectra of a) PIPOx^{R} and b) PIPOxOTf^{R} along with the chemical structures and assignments. The free radical polymerization did not affect the integrity of the pendant 2-oxazoline ring. The new signal at 3.7 ppm and the quantitative shift of the two triplets from the pendant 2-oxazoline ring as well as the backbone signals (c,d to c',d') indicate a quantitative conversion to the polycationic macroinitiator PIPOxOTf. The intensity ratio of the α-methyl signals (d) at 1.12 (syndiotactic, *S*), 1.24 (heterotactic, *H*) and 1.39 (isotactic, *I*) ppm was used to determine the polymer tacticity.

Similar to earlier reports,[148,215] the free radical polymerization of IPOx using AIBN resulted in hydrophilic PIPOx^{R} with a molar mass distribution of 2.12. The analysis by ^{1}H NMR confirmed that the pendant 2-oxazoline rings were preserved (**Figure 28**). The integral ratio of the ring methylene groups (a, 2H and b, 2H) and the corresponding signal integrals of the polymer backbone (c, 2H; d 3H) is in excellent agreement and confirms the depicted polymer structure. Closer inspection of the proton backbone signals (c, d) in **Figure 28** also reveals a fine structure due to the tacticity of PIPOx.[147] Similar to PMMA,[152] the tacticity of PIPOx can be estimated from the relative intensity of the characteristic α-methyl signals for syndio (*S*) - (1.12 ppm), hetero (*H*) - (1.24 ppm) and isotactic (*I*) (1.39 ppm) polymer sequences. For PIPOx, an *S:H:I* ratio of 57:37:6 was found. The determined *S:H:I* ratio for PIPOx is in agreement with earlier findings by Kagiya et al.[147]

The polycationic macroinitiator salts, PIPOxOTf^{R}, were prepared from PIPOx^{R} and methyl triflate (MeOTf). The ^{1}H NMR spectrum of PIPOxOTf^{R} is shown in **Figure 28**. Upon methylation, a new signal of the N-methyl group at 3.7 ppm appears and the characteristic two triplet signals of the 2-oxazoline methylene protons at 3.76 and 4.16 ppm are quantitatively shifted to 4.54 and 5.08 ppm. The intensity ratio of the new N-methyl oxazolinium ring and the methyl signals is again in excellent agreement with signal intensities originating from the backbone protons. Based on ^{1}H NMR spectral analysis, the conversion of PIPOx^{R} to the macroinitiator salt, PIPOxOTf^{R}, was quantitative.

However, in the spectrum of the macroinitiator some low molar mass impurities are noticeable. First attempts to remove these impurities resulted in minor but noticeable decomposition of the oxazolinium rings (by e.g. hydrolysis). Thus, we used PIPOxOTf^{R} as obtained after a single precipitation and washing step to initiate the side chain grafting from polymerization of 2-methyl-, 2-ethyl-, 2-*n*-propyl-, 2-iso-propyl- and 2-butyl- 2-oxazolines by LCROP. The targeted length of the side chains was set to m = 25 by the initial $[M]_0/[I]_0$ ratio.

According to our previous accounts on functionalized POx,[151] N-Boc-piperazine (Boc) was used as the terminating reagent. This terminal group is useful for ^{1}H NMR end group analysis and moreover, after deprotection of the secondary amine group, it allows an additional functionalization of each side chain end.[151,153,154,155,156]

The obtained molecular brushes were analyzed by gel permeation chromatography (GPC). For all five graft copolymers a significant increase of the molar mass was observed and no remaining macroinitiator could be detected. In all cases a monomodal distribution was obtained and no fraction of polymers having lower molar masses was observed. Because of the side chain grafting, the number average molar mass (characterized by GPC) increased from 9.8×10^{3} g/mol to $M_n = 7\times10^{4}$ g/mol, 8×10^{4} g/mol, 5×10^{4} g/mol, 5×10^{4} g/mol, 6×10^{4} g/mol for MeOx, EtOx, *i*PrOx, *n*PrOx, and BuOx, respectively. In **Figure 29**, the GPC trace of PIPOx^{R} (1) is compared with the traces of the resulting molecular brushes (2-4).

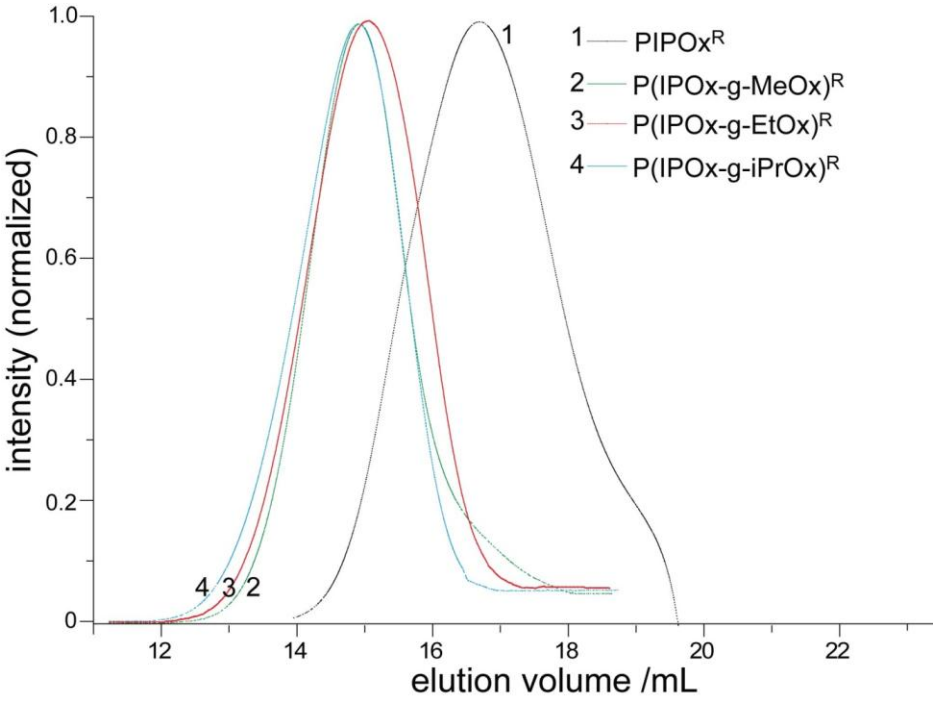

Figure 29. GPC traces of $PIPOx^R$ and molecular brushes $P(IPOx\text{-}g\text{-}MeOx)^R$, $P(IPOx\text{-}g\text{-}EtOx)^R$ and $P(IPOx\text{-}g\text{-}iPrOx)^R$.

The successful side chain formation from the macroinitiators by the grafting from approach was further confirmed by ^{1}H NMR spectroscopy (**Figure 30**). For all grafting polymerization, the signals corresponding to the oxazolinium pendant group disappeared completely. Instead, characteristic signals for the respective side chain polymers could be unambiguously assigned. Furthermore, a successful end functionalization with N-boc-piperazine is confirmed by the presence of a strong signal around 1.45 ppm originating from the tert. butyl group (overlapping with the α-methyl signals of the brush backbone). Estimation of the average degree of polymerization, m, of the POx side chains was performed by comparing the signal integral of the tert. butyl group and the α-methyl signals at 1.45 ppm of the brush backbone versus the methylene signal of the POx side chain at 3.45 ppm. Although a degree of polymerization of m = 25 for the side chains was targeted, in all cases slightly shorter chains with m = 20 were determined (**Table 1**).

An incomplete grafting from or termination reaction would calculate to longer side chains. Thus, this result indicates a very high grafting density (within experimental error, 100%) and efficient end group functionalization via the termination reaction. The resulting shorter side chains may be caused by chain transfer reactions or, more likely, residual MeOTf in the macroinitiator salt. In fact, for the grafting of 2-oxazolines minor amounts of homopolymer was observed that we attribute to traces of MeOTf in the macroinitiator. However, to ensure a

homogeneous and high grafting density along the polymer backbone, we decided to avoid elaborate cleaning procedures of the macroinitiator.

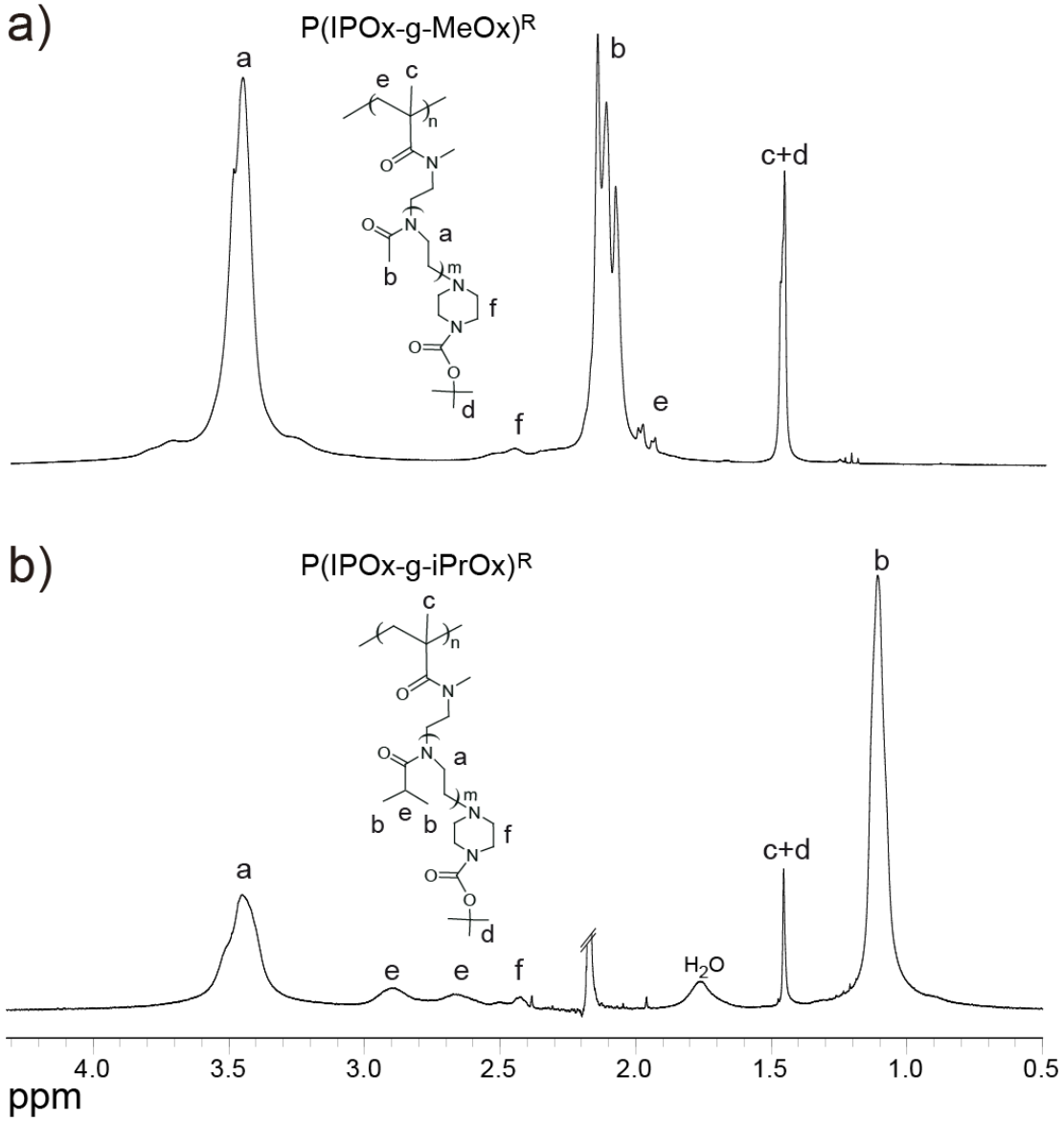

Figure 30. ^{1}H NMR spectra of the molecular brushes a) P(IPOx-g-MeOx)^{R} and b) P(IPOx-g-iPrOx)^{R} with their assignments. Besides the characteristic backbone and POx monomer unit signals (a, b), end group signals (d, f) are detectable.

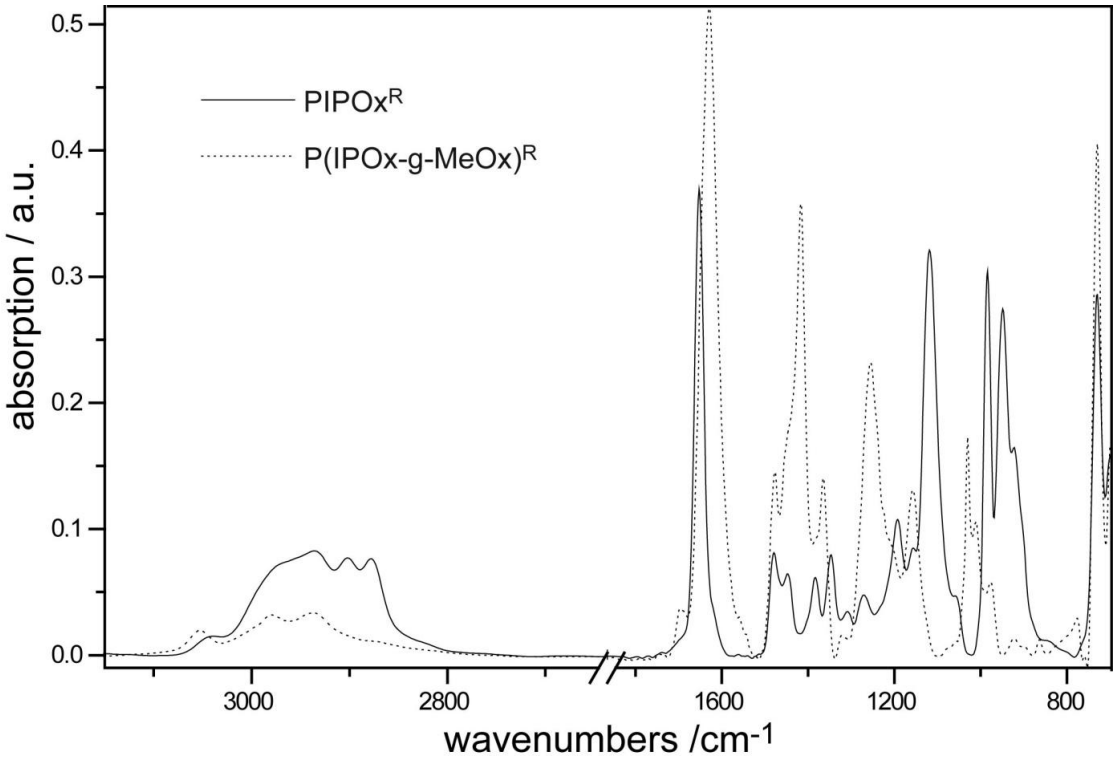

Figure 31. FTIR spectra of $PIPOx^R$ (solid line) and the molecular brush $P(IPOx\text{-}g\text{-}MeOx)^R$ (grey dashed line).

Further confirmation for the successful grafting of POx from the macroinitiator salts was obtained by FTIR spectroscopy. In **Figure 31**, the IR spectra of $PIPOx^R$ and $P(IPOx\text{-}g\text{-}MeOx)^R$ are compared. The strong bands at 1654 and 1118 cm^{-1} are assigned to the (C=N) and (C-O) moieties and the bands at 986 and 951 cm^{-1} originate from the ring skeletal vibration of the pendant 2-oxazoline rings in $PIPOx^R$. After ring-opening polymerization, these bands disappeared completely, and a new sharp and intensive band appeared around 1630 cm^{-1} which is characteristic for the carbonyl stretching mode of the amide function (amide I)[151,212] and confirms the successful grafting by LCROP to $P(IPOx\text{-}g\text{-}MeOx)^R$. Moreover, the characteristic CH_x stretching pattern between 2800 and 3200 cm^{-1} and the CH_x deformation modes for POx observed between 1365 and 1477 cm^{-1} as well as the carbonyl stretching vibration of the Boc group are found in the spectrum.

Table 1. Poly(2-oxazoline) macroinitiators prepared from the PIPOx backbone by free radical polymerization and corresponding molecular brushes of homopoly(2-oxazoline) side chains.

Polymer	Yield (%)	M_n (kg/mol)[b]	PDI[b] (M_w/M_n)	n[b]	m[c]	$m^{theor.}$	$M_n^{theor.}$ (kg/mol)[d]
$PIPOx_n^R$	50[a]	9.8	2.12	88	-	-	-
$PIPOx_nOTf^R$	96	-	-	-	-	-	-
$P(IPOx_n\text{-g-}MeOx_m)^R$	80	70.0	1.69	88	19	25	168
$P(IPOx_n\text{-g-}EtOx_m)^R$	76	78.0	1.75	88	23	25	227
$P(IPOx_n\text{-g-}i\text{PrOx}_m)^R$	50	53.0	1.58	88	18	25	205
$P(IPOx_n\text{-g-}n\text{PrOx}_m)^R$	79	56.0	1.61	88	20	25	205
$P(IPOx_n\text{-g-}BuOx_m)^R$	77	61.0	1.65	88	21	25	236

a) calculated against initial initiator feed.
b) as calculated from GPC traces.
c) average degree of polymerization, (m) calculated from end group analysis using ^{1}H NMR spectral data.
d) calculated using GPC determined molar mass of precursor polymer and ^{1}H NMR determined degree of side chain polymerization.

3.2.3 Thermo-responsiveness of poly(2-oxazoline)s molecular brushes

The hydrophilicity of poly(2-alkyl-2-oxazoline)s is determined by the length of the pendant alkyl group. Longer alkyl chains of the monomer unit results in an increasingly stronger amphiphilic character of the monomer unit and the polymer becomes a non-ionic polysoap.[55,153,157] As most of the water-soluble polymers,[158] hydrophilic POx have a lower critical solution temperature (LCST) above which the polymer becomes water-insoluble. Taking advantage of the flexibility of the 2-oxazoline chemistry and the LCROP giving access to defined (co-) polymers having various side and end groups, recent studies by Kataoka[167] and our group[33,119] demonstrated the fine-tuning of the LCST of POx over a broad temperature range. Until now, the LCST of hydrogels and linear POx homo- and copolymers were investigated in detail as a function of the side chain and/or end group functionality as well as the molar mass and concentration.[159,118] Here, the temperature-dependant water solubility of the obtained POx molecular brushes were determined. The LCST was measured analogue to previous accounts[33,146] by turbidity measurements of a 1.0 wt % aqueous solution of $P(IPOx\text{-g-}EtOx)^R$, $P(IPOx\text{-g-}i\text{PrOx})^R$, and $P(IPOx\text{-g-}n\text{PrOx})^R$. The cloud point was defined

at 10 % optical transmittance decrease of an aqueous polymer solution. The results are summarized in **Figure 32**. P(IPOx-g-MeOx)^{R} was too hydrophilic and remained soluble in water at a temperature above 95 °C. Whereas, P(IPOx-g-BuOx)^{R} was not water soluble in the accessible temperature range.

For all three thermo-responsive molecular brush solutions, the LCST transition was found to be very sharp (the complete transition occurred within a temperature range of 0.5 - 1.5 °C) and fully reversible, with no remaining insoluble polymer fraction below the respective LCST. The LCST of P(IPOx-g-EtOx)^{R} was found to be about 53 °C, which is significantly lower than the LCST between 73 °C and 69 °C found for linear PEtOx with a comparable high molar mass as reported by Du Prez.[160] For molecular brushes with P*i*PrOx side chains, a transition temperature of 30 °C was determined. Also in this case, the LCST is significantly lower than the earlier reported values for linear P*i*PrOx (35-45 °C)[161,167] as well as crosslinked P*i*PrOx hydrogels (shown in **Table 2**). For the molecular brush with P*n*PrOx side chains, a transition temperature of 19 °C was determined. Again, the LCST is significantly lower than the earlier reported values for linear P*n*PrOx (23.8 °C ~). It was reported that linear P*n*PrOx homopolymer show independent sharp LCST at around 24 °C almost regardless of the molar mass and concentration. The present findings suggest that the compact structure of a molecular brush slightly affects the LCST, which is consistent to the previous report i.e. the unique molecular architecture has minor effects upon the value of the LCST.[36,38,40]

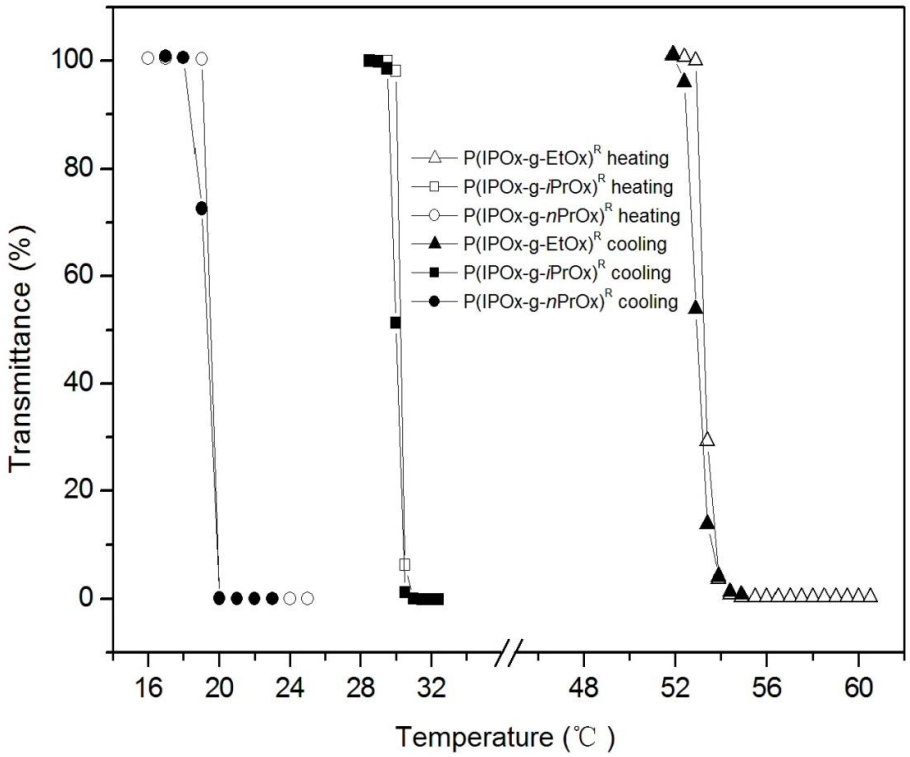

Figure 32. LCST of P(IPOx-g-EtOx)^{R}, P(IPOx-g-*i*PrOx)^{R}, and P(IPOx-g-*n*PrOx)^{R} determined by turbidity measurements of a 1.0 wt % aqueous polymer solution. Upon heating and cooling, the same transition point was found with no noticeable hysteresis.

After deprotection of P(IPOx-g-*i*PrOx)^{R} using trifluoroacetic acid (TFA) resulting in terminal secondary amide end groups of each polymer side chain, the LCST of the POx brush was increased by 23 ℃ to 53 ℃. This indicates a high end group functionality of the polymer pendant chains and further corroborates the high grafting density of the molecular brush side chains. The observed differences can be explained by the replacement of hydrophobic tert. butyl group by hydrophilic second amine group in the POx pendant chains. As recently reported, the impact of the polarity of the POx end group upon the LCST modulation was found to be significantly stronger as compared to e.g. the well-studied poly(N-isopropyl acryl amide) (PNIPAAm).[33]

The results show that composition as well as end groups have pronounced effects on the LCST of molecular brushes. In such a compact molecular condition, the LCST is very sensitive to end groups. However, the compact structure of molecular brushes has a effect on the LCST, but relatively weak compared to side chain composition and end group.

Table 2. Summary of the LCST measurements of polymers and comparison of thermal behavior with corresponding linear polymers.

	$P(IPOx_n\text{-}g\text{-}EtOx_m)^R$	$P(IPOx_n\text{-}g\text{-}iPrOx_m)^R$	$P(IPOx_n\text{-}g\text{-}nPrOx_m)^R$
LCST (°C)	53	30	19
Width of transition[a] (°C)	1.5	1	1.0
LCST of linear polymer[b] (°C)	69[160]	36[c] ($M_n \approx 16.7$ kg/mol) [161]	24[c] ($M_n \approx 347$kg/mol)[168]

[a] temperature range between 100 % and ~ 0 % transmittance.
[b] of comparable molar mass.
[c] no references were found which studied 2-iso-propyl-2-oxazoline and 2-n-propyl-2-oxazoline based polymers of comparable molar mass.

3.2.4 Morphology of adsorbed molecular brushes on surfaces

The visualization of molecular brushes by e.g. AFM allows for the direct determination of their molecular dimensions, such as contour length, brush width, backbone curvature, and persistence length, and the overall dimensions, such as radius of gyration and end-to-end distance in real space. The ^{1}H NMR spectroscopy data indicate that the *grafting from* reactions from the macroinitiator salts are quantitative and a molecular brushes with very high grafting densities were formed. This will result in cylindrical molecular brushes with a strongly stretched polymer brush backbone.[9,46,162] To investigate the molecular shape of the synthesized molecular brushes, AFM was used to visualize the individual molecules deposited on naturally oxidized silicon substrates from a dilute chloroform solution. Molecular brushes adsorb onto silicon substrate due to the interaction between molecular side chains and the substrate. In **Figure 33** the AFM measurement of the adsorbed $P(IPOx\text{-}g\text{-}EtOx)^R$ is shown. The individual molecular brushes could be successfully visualized and display the expected and characteristic shape of strongly stretched chains. Clearly, the length of the polymer brushes varies considerably because of the synthesis of the PIPOx backbone via free radical polymerization and their broad dispersity. This, of course, is not surprising. With a polydispersity index of 2.12 for the polymer backbone a wide variety of polymers with short and long backbones is observed. However, as the polymer side chains were prepared by LCROP, the width of the polymer appears to be uniform.

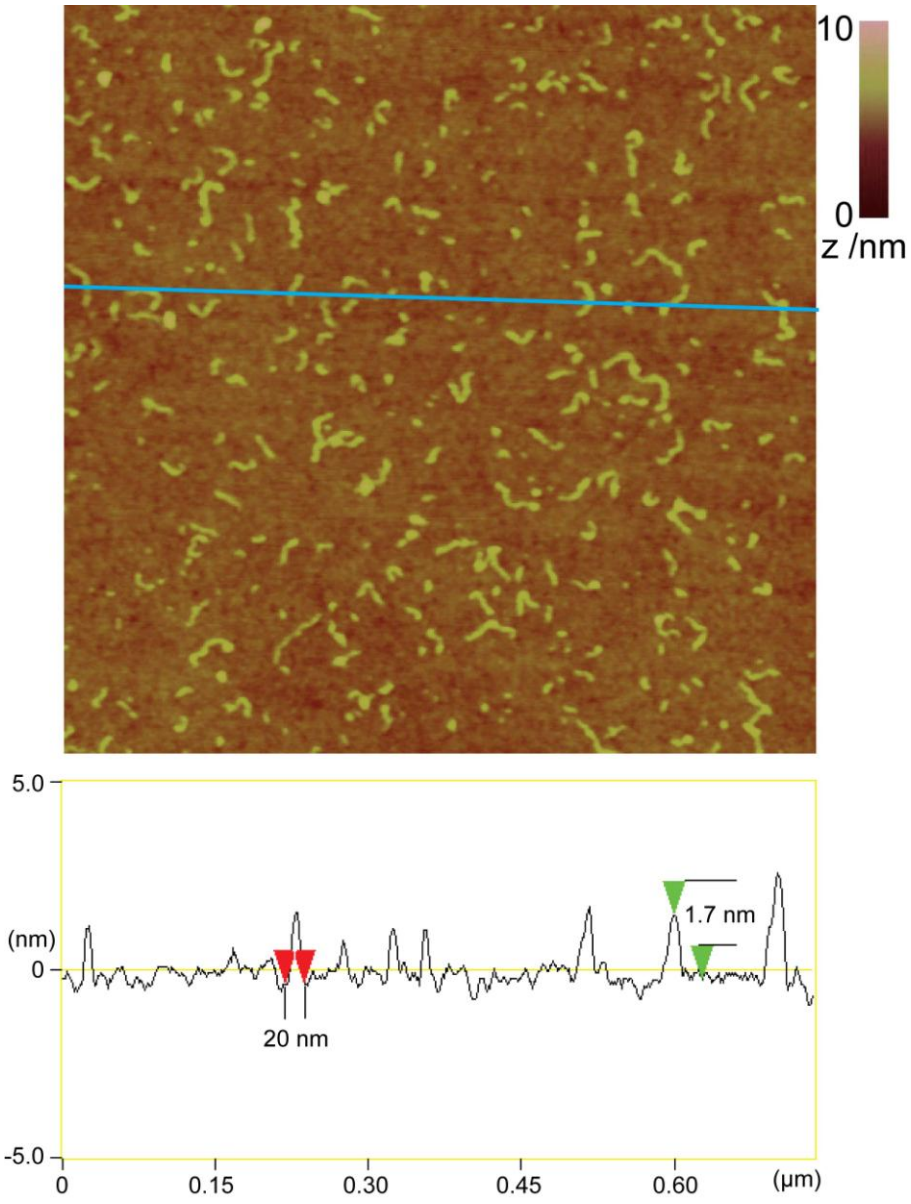

Figure 33. AFM (tapping mode) scan (above) and section view (below) of the molecular brush P(IPOx-g-EtOx)^{R}. The polymer was deposited by dip-coating from a dilute chloroform solution onto an oxidized silicon wafer.

The height of the brushes was found to be uniform and on average around 1.7±0.2 nm with a constant width of 18±2 nm. As expected, this indicates strong adsorption of the POx side chains onto the silicon dioxide surface and no major defects in terms of side chain heterogeneities is noticeable.[55] Due to the free radical polymerization route for the P(IPOx-g-EtOx)^{R} backbone, the distribution of the chain length is broad. With statistical analysis of the determined chain length (from 30 randomly selected chains in **Figure 33**), the number-average length of the molecules calculates to be 20 nm. GPC revealed an average degree of polymerization of 88 for the backbone. The contour length of a fully extended chain

calculates to be 22 nm, which further corroborates the assumption of a strongly stretched cylindrical brush due to the high crowding of the POx side chains.[49]

3.2.5 Cytotoxicity assay, MTT

Toxicity test of the obtained molecular brushes was performed by Dr. Robert Luxenhofer from the research group of Prof. Sasha Kabanov at University of Nebraska Medical Center, Omaha. Polymers which are suitable for uses in living organisms have to fulfill requirements concerning their biocompatibility, cytotoxicity, possibly biodegradability, and/or immunocompatibility.[163] The biocompatibility of poly(2-oxazoline)s have been known for a period of time.[110,120] Here, the toxicity test of the prepared molecular brushes were performed according to a 3-(4,5-Dimethylthiazol-2-yl)-2,5-diphenyltetrazolium bromide (MTT) assay.

MTT assay is a standard colorimetric assay for measuring cellular proliferation (cell growth). It can also be used to determine cytotoxicity of a given compound.[164] Yellow MTT is reduced to purple formazan in the mitochondria of living cells. This reduction takes place only when reductase enzymes are active, and therefore conversion is often used as a measurement for viable (living) cells.[165]

MCF-7/ADR cells, a human breast multiple drug resistance (MDR) cancer cell line, were incubated with P(IPOx-g-MeOx)^{R} for 72 h. As shown in **Figure 34**, P(IPOx-g-MeOx)^{R} showed 100 % viability when the concentration was below 2 mg/mL. The cell viability kept above 80 % even if the polymer concentration was increased to 10 mg/mL. This indicated that the P(IPOx-g-MeOx)^{R} caused no harm to cells under the conditions used and seemed to be suitable as a non-toxic material in living organisms.

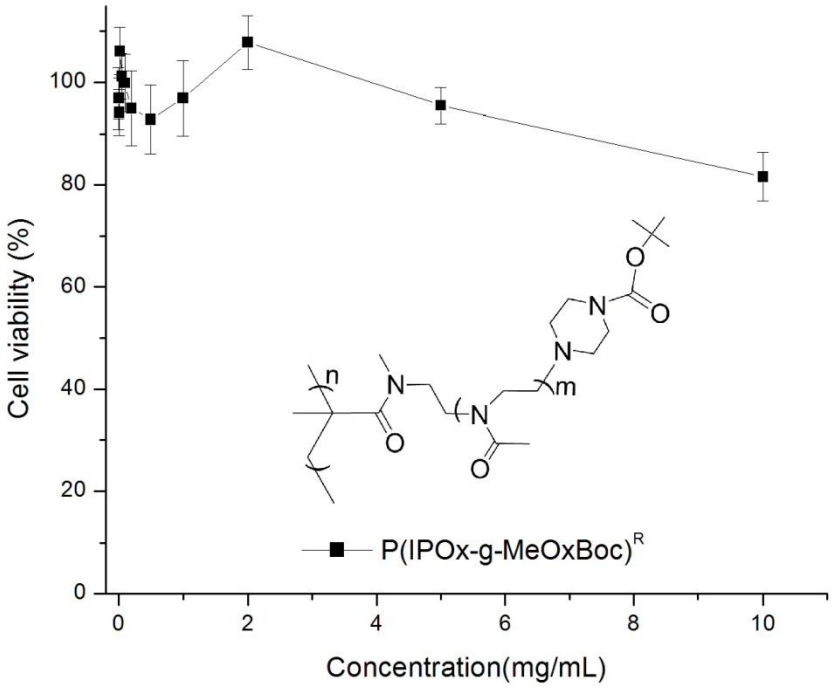

Figure 34. Cell viability determined by the MTT assay as a function of the P(IPOx-g-MeOxBoc)^{R} concentration. The data are presented as mean ± SEM (standard error of the mean).

3.3 Molecular brushes via anionic and cationic ring-opening polymerization

In this part of work, we prepared molecular brushes by a combination of anionic vinyl polymerization of 2-isopropenyl-2-oxazoline (IPOx) for the backbone and the living cationic ring-opening polymerization (LCROP) of 2-oxazoline moiety for the side chain synthesis. Two macroinitiators with different degree of polymerizations (DP) were prepared to polymerize *n*PrOx or *i*PrOx with variable side chain DP. The kinetics of the LCROP of 2-oxazolines in the presence of short and long macroinitiators were investigated. The results were compared with the polymerization of 2-oxazoline initiated by methyl triflate (MeOTf) under the same reaction condition. The thermo-responsive properties of the resulting molecular brushes were studied to examine the effect of side chain length on the LCST values. Furthermore, various parameters such as concentration and molar mass in determining the LCST of brush molecules were also investigated.

3.3.1 Anionic polymerization of 2-isopropenyl-2-oxazoline

It was shown in the previous chapter that the conversion of the 2-isopropenyl-2-oxazoline (IPOx) to poly(2-isopropenyl-2-oxazoline) (PIPOx) by free radical polymerization did not affect the 2-oxazoline ring. However, the molar mass distribution of the PIPOx backbone was relatively broad due to the used synthetic route. In order to synthesize a more defined molecular brush, the anionic polymerization was adopted to prepare PIPOx backbone. It was reported that the conversion of IPOx to PIPOx by living anionic polymerization did not affect the 2-oxazoline ring.[216] Moreover, the it gave narrow molar mass distributions of PIPOx. Therefore, a better overall control of the resulting molecular brushes is expected. However, early reports on anionic polymerization of IPOx showed the formation of polymers with low molar mass and poor PDI e.g. M_n = 1447 g/mol, PDI = 1.55.[216]

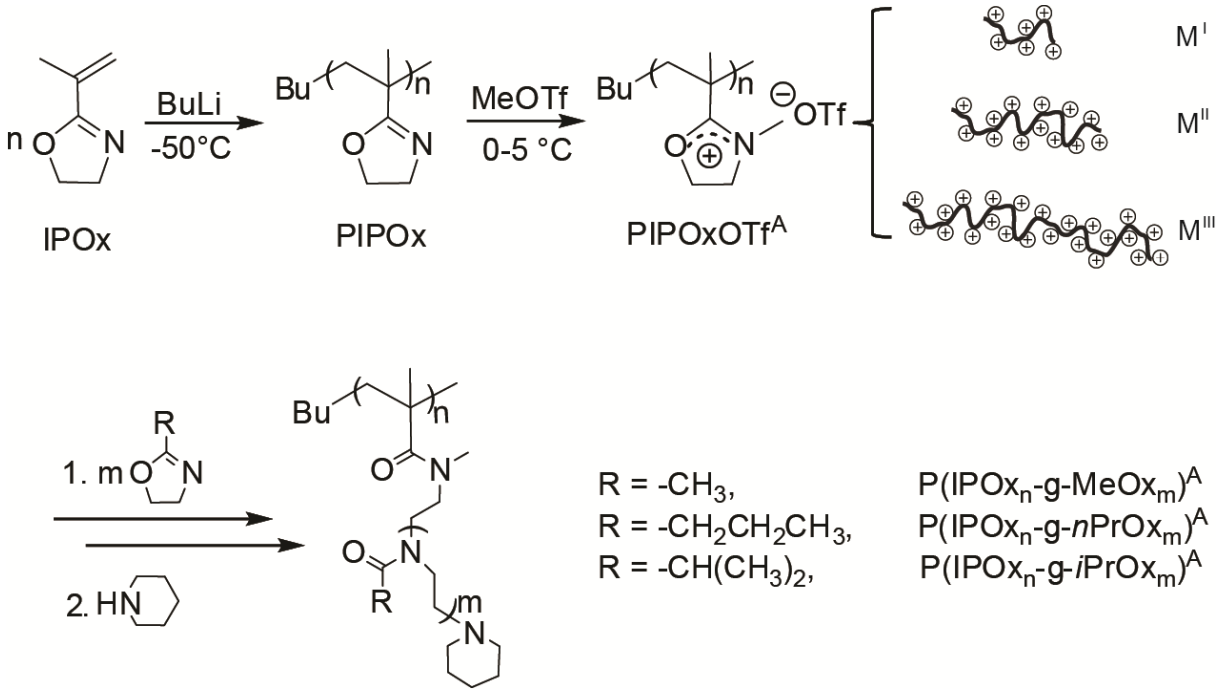

Figure 35. Molecular brushes prepared by anionic polymerization of IPOx initiated by butyl lithium and LCROP of 2-oxazolines to form the side chains. ('^{A}' = prepared by anionic polymerization)

Table 3. PIPOx backbones prepared by living anionic polymerization.

Entry	M_n(kg/mol)	PDI	DP[a]	DP[b]
PIPOx^{AI}	5.8	1.15	52	58
PIPOx^{AII}	14.6	1.21	131	146
PIPOx^{AIII}	24.0	1.20	216	225

a) degree of polymerization calculated from apparent molecular weight from GPC traces
b) degree of polymerization calculated from end group analysis from ^{1}H NMR

In this part of work, PIPOx backbone was prepared through the anionic polymerization of IPOx with butyl lithium (BuLi) as the initiator (**Figure 35**). Briefly, IPOx monomer was added dropwise into a BuLi containting THF solution at -50 ℃. Three PIPOx^{A} polymers with different molar mass were obtained by varying the $[M]_0/[I]_0$ ratio. There, the molar mass weight average (M_w), polydispersity (PDI = M_w/M_n), degree of polymerization (DP) and end-group analysis by ^{1}H NMR are summarized in **Table 3**. The anionic polymerization of IPOx resulted in PIPOx^{A} with a PDI between 1.15 and 1.21 depending on the targeted chain length. Compared to an early report fro Tomalia et al.,[216] higher degrees of polymerization and lower

molar mass distributions are obtained here. However, the PDI of 1.21 indicates that the anionic polymerization is accompanied, at least to some extent, by termination and chain transfer reactions via proton abstraction.[166] The estimation of the average DP, based on gel permeation chromatography data (with PMMA standards for calibration), appears to be accurate since it nicely fits the results calculated from ^{1}H NMR end-group analysis. As shown in **Figure 36**, the complementary end-group analysis of PIPOx^A based on ^{1}H NMR data using the signals at 0.9 ppm (9H) of the terminal butyl group versus the signals of the monomer units resulted in a DP which is similar to the value calculated from GPC, i.e. a DP of 52 calculated from GPC and a DP of 58 found from ^{1}H NMR. The tacticity i.e. the *S:H:I* ratio of 73:25:2 for PIPOx^A was calculated from ^{1}H NMR. The living anionic polymerization of IPOx resulted in PIPOx^A which showed a significant larger syndiotactic and lower isotactic fraction compared to results from PIPOx^R. This can be explained by the steric demand of the pendant 2-oxazoline ring during the slower anionic reaction.

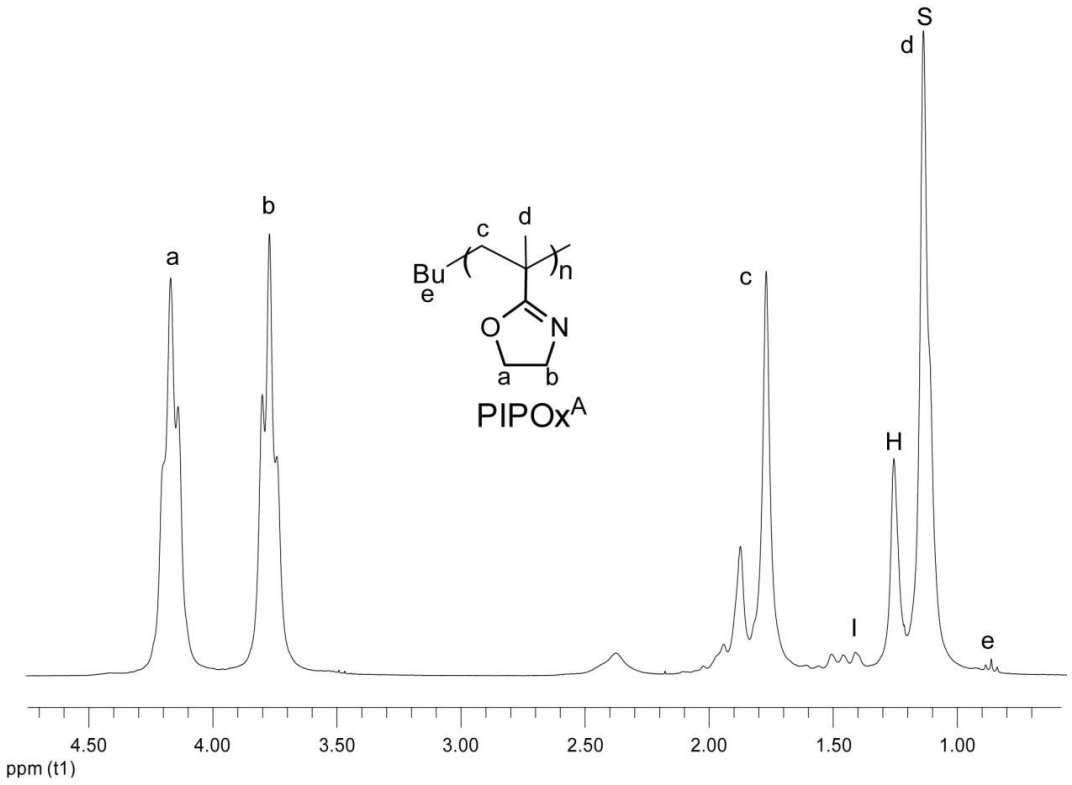

Figure 36. ^{1}H NMR spectrum of PIPOx^A along with the chemical structure and assignment. The spectrum indicates that the anionic polymerization did not affect the pendant 2-oxazoline ring. The intensity ratio of the α-methyl signals (d) at 1.12 (syndiotactic, *S*), 1.24 (heterotactic, *H*) and 1.39 (isotactic, *I*) ppm was used to determine the polymer tacticity.

3.3.2 Kinetic studies of the living cationic ring-opening polymerization of 2-oxazolines

The moderate propagation rate for the polymerization of 2-oxazoline allows for kinetic investigations.[211] Recently, our group performed kinetic measurements through gas chromatography, revealing that multiple initiating groups (2, 3 and 4) are of equal reactivity for initiating the polymerization of 2-oxazolines and uniform poly(2-oxazoline)s with 2, 3 and 4 arms were achieved (**Figure 37**).[211] Analogue to these studies, gas chromatography (GC) was used for kinetic investigations of the cationic polymerization of 2-oxazolines with defined macroinitiator salts of different length and the obtained kinetic behavior was compared with the one initiated by MeOTf. It should be noted that the polymerization was carried out in a glass vial sealed with a septum, and the GC automatically collected samples at the set time intervals.

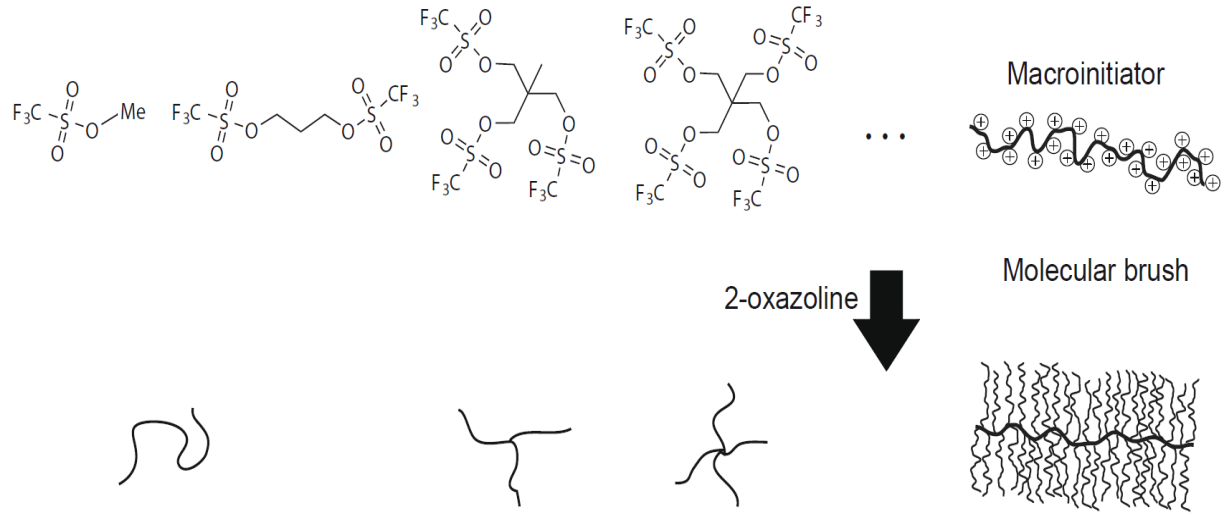

Figure 37. Preparation of linear, multi-armed and brush-like poly(2-oxazoline)s.

To compare the kinetics of polymerization using mono- and multifunctional initiators, one would compare the apparent polymerization rate. However, the apparent polymerization rate for macroinitiators is inaccurate because of the intrinsic error in determining the molar mass of the macroinitiator. Therefore, we compared the apparent polymerization rate per initiating group i.e. single oxazolinium triflate. In the equation below, k_p^{app} denotes the apparent propagation rate for the polymerization, [M] is the monomer concentration, $[I]_0$ is concentration of the initiating group and t is the reaction time.

$$\ln\left(\frac{[M]_0}{[M]_t}\right) = k_p^{app}[I]_0 t$$

Since k_p^{app} and $[I]_0$ are constant, a linear plot of $\ln\left(\frac{[M]_0}{[M]_t}\right)$ vs. t is expected in case of a living polymerization mechanism.

To investigate the effect of the macroinitiator length on the kinetics of polymerization, two macroinitiators of different length were prepared. First, the PIPOx backbones were synthesized by living anionic polymerization of IPOx. By controlling the feed ratio of IPOx (monomer) and BuLi (initiator), two backbone polymers ($PIPOx^{AI}$ and $PIPOx^{AII}$) with different molecular weight were obtained. $PIPOx^{AI}$ had a DP of 52 and a relatively narrow PDI (M_w/M_n=1.15). $PIPOx^{AII}$ had a DP of 132 and a slightly higher PDI (M_w/M_n= 1.21). The macroinitiators (M^I and M^{II}) were obtained subsequently by reactions of $PIPOx^{AI}$ and $PIPOx^{AII}$ with a stochiometric amount of MeOTf as described in the previous chapter.

As outlined in the reaction pathway (**Figure 38**), kinetic experiments with varied 2-oxazoline monomers i.e. MeOx, *n*PrOx and *i*PrOx in the presence of the macroinitiators were investigated, and for comparison, MeOTf intitiated reaction was also carried out. Before the polymerization of monomers, the conversion from the PIPOx backbone into the macroinitiator was determined by ^{1}H NMR spectroscopy to be greater than 98.5%. (we compared the signal from the oxazolinium triflate with that from the uncharged oxazoline). The high conversion from PIPOx to macroinitiator provides the possibility to prepare molecular brushes with a high grafting density. It should be noted that the determination of the molar mass of the macroinitiator salts was not performed due to its hydroscopic and unstable properties.

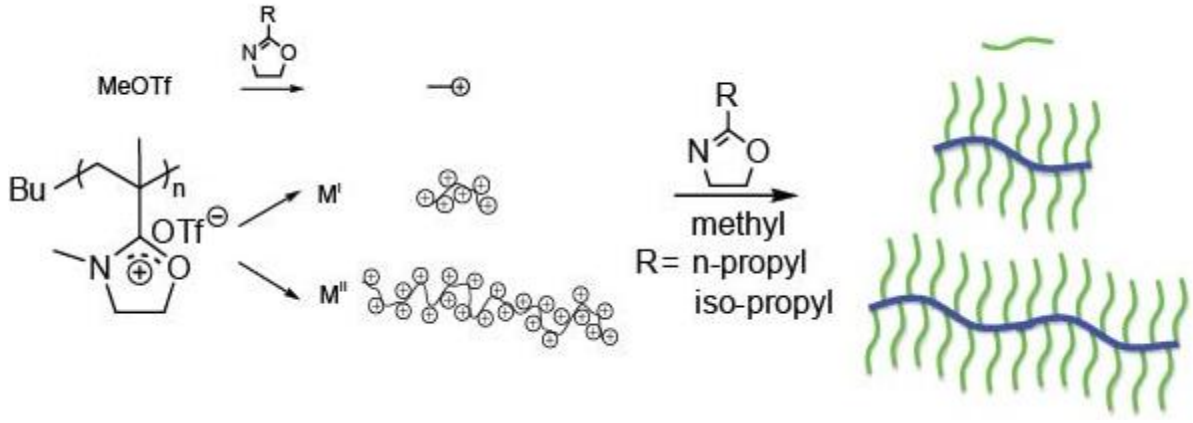

Figure 38. Living cationic ring-opening polymerization (LCROP) of 2-oxazolines in the presence of short and long macroinitiators (M^I, M^{II}), as well as methyltrifluoro-methansulfonate (MeOTf) initiator.

In the first set of experiments, *n*PrOx was polymerized with the initiators M^{I}, M^{II} and MeOTf respectively. **Figure 39** shows the first order kinetic plots of the polymerizations of *n*PrOx initiated by M^{I}, M^{II} and MeOTf at 80 ℃ (an initial concentration of $[n\text{PrOx}]_0$ = 1.0 mol/L). For all experiments, the oxazolinium triflate concentration was kept constant ($[I]_0$ = 0.04 mol/L).

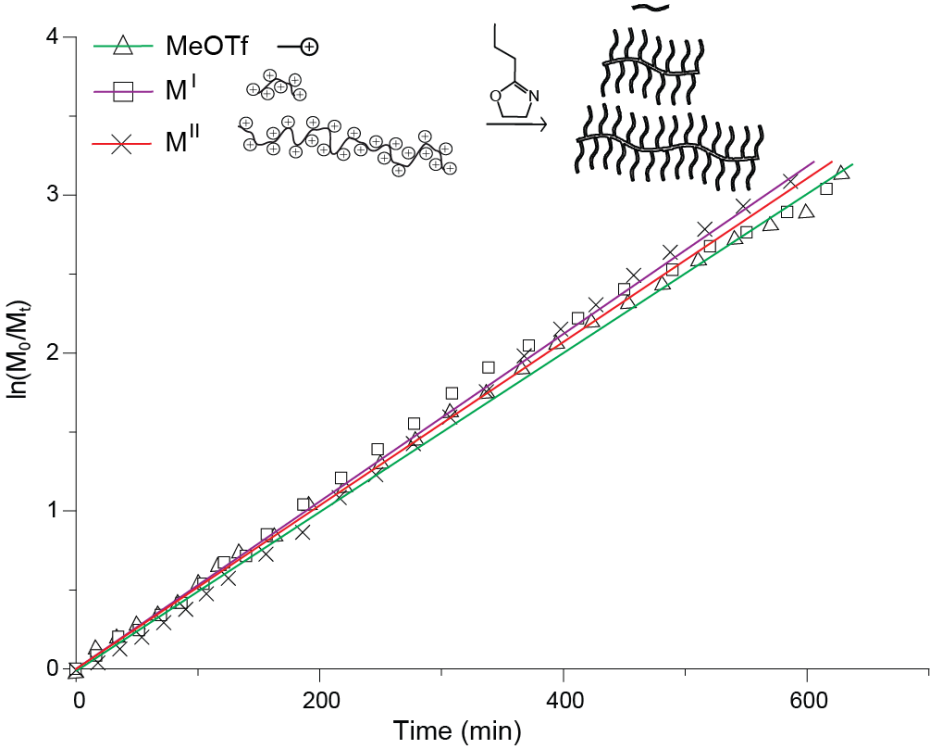

Figure 39. First order kinetic plots for the polymerization of *n*PrOx using MeOTf, M^{I} and M^{II} initiators.

As apparent from **Figure 39**, all three plots are strictly linear, indicating the living character of the cationic polymerization, without noticeable termination reaction. For all three reactions, polymerization proceeded to quantitative monomer conversions (**Figure 41**). Furthermore, the slopes of the first order kinetic plots are almost constant regardless of the length of macroinitiator. The apparent polymerization rates per initiating group were calculated to be 2.18, 2.12 and 2.08 ml S^{-1} mol^{-1} for polymerizations of *n*PrOx with M^{I}, M^{II} and MeOTf respectively. The slight differences are within the experimental error. For comparison, the calculated apparent polymerization rates are listed in **Table 4**. These results suggest that compared to MeOTf, every initiating site of the macroinitiator has equal reactivity and accordingly the polymerization rate of 2-oxazolines is identical. The present results show that it is possible to obtain molecular brushes of different backbone length with uniformly equal pendant POx side chains.

Table 4. Calculation of apparent rate constants per initiating group for the polymerization of 2-oxazolines using MeOTf and different macroinitiators.

Initiator	Degree of functionalization[a]	Monomer	$[M]_0/[I]_0$	k_p(ml S^{-1} mol^{-1})
MeOTf	100 %	*n*PrOx	25/1	2.08
M^I	98 %	*n*PrOx	25/1	2.18
M^{II}	98.5 %	*n*PrOx	25/1	2.12
MeOTf	100%	*i*PrOx	25/1	1.25
M^{II}	98.5 %	*i*PrOx	25/1	1.28
MeOTf	100%	MeOx	25/1	2.90
M^{II}	98.5 %	MeOx	25/1	2.95

[a] Determined by ^{1}H NMR.

To further confirm the above results, using more steric monomer *i*PrOx, the kinetic behavior of the polymerization initiated by M^{II} was studied and compared with that initiated by MeOTf under identical reaction conditions. The apparent polymerization rate per initiating group was calculated to be 1.28 and 1.25 ml S^{-1} mol^{-1} for M^{II} and MeOTf, respectively. Even for steric demanding 2-oxazoline monomers such as *i*PrOx, the apparent polymerization rate per initiator function is the same as MeOTf. Likewise, using MeOx as the monomer, the kinetics of polymerizations initiated by M^{II} and MeOTf were studied, revealing the apparent polymerization rate per initiating group to be 2.95 and 2.90 ml S^{-1} mol^{-1} respectively. The results of kinetic studies are summarized in **Table 4**. These results indicate that initiating sites (oxazolinium triflate) along the macroinitiator have equal reactivity in the polymerization of 2-oxazolines, and can form side chains of equal length regardless of the type of monomer and the length of macroinitiator. Moreover, every oxazolinium triflate in the macroinitiator has the same reactivity as MeOTf.

For the *grafting from* polymerization, PIPOx has to be first converted to a macroinitiator salt with pendant oxazolinium rings. The formed oxazolinium triflate is a very effective initiator for polymerization of 2-oxazolines. [150] As shown in the previous chapter, the charging of each monomer unit along the PIPOx chain to a polyelectrolyte induces significant chain stretching which improves the accessibility of each initiation site for 2-oxazoline monomers. Both aspects, the formation of the oxazolinium salt and macroinitiator chain stretching, work in favor for a fast initiation reaction of the living cationic ring-opening polymerization for a defined side chain grafting. Therefore, molecular brushes with defined side chains can be prepared using this method.

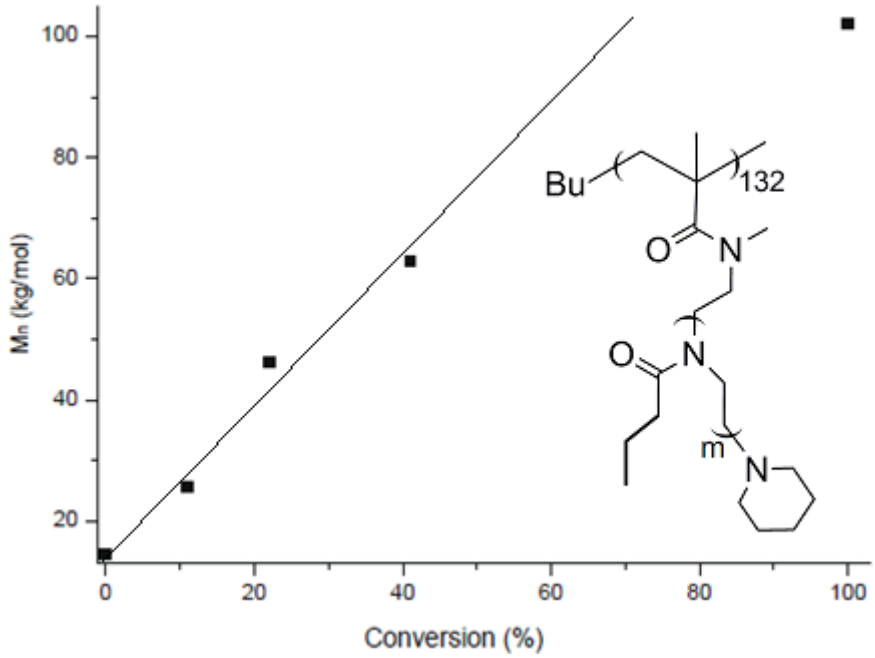

Figure 40. Increase of the number average molar mass (M_n) of P(IPOx-g-*n*PrOx) versus the conversion of *n*PrOx with M^{II} as the macroinitiator.

Another evidence for the living character of the polymerizations of 2-oxazolines from the macroinitiator was obtained from GPC measurements. **Figure 40** shows that the number-average molecular weight (M_n) of the molecular brushes increased linearly with the increasing conversion of monomer with P*n*PrOx as the side chain (from M^{II}). It should be noted that, the M_n determined by GPC is lower than the theoretical values calculated from conversion of *n*PrOx, which is consistent with a previous report by Matyjaszewski.[13] This is due to the relatively compact structure of molecular brushes compared to linear polymers, and different hydrodynamic volumes of brush molecules as compared to the linear PMMA used for GPC calibration. It was found at 100% conversion that the characterized molar mass is significant lower than expected. This deviation is because of the highly compact structure of molecular brushes and the possible termination reaction at high conversion.

The kinetics of polymerizations of MeOx, *n*PrOx and *i*PrOx in the presence of M^{II} were also compared. **Figure 41** shows the correlation between monomer consumption and reaction time for the polymerizations of different 2-oxazolines using M^{II}. It was observed in each experiment that the monomer consumption proceeded to 100%. The polymerizations of MeOx, *n*PrOx and *i*PrOx were complete in approx. 10h, 15h and 24h, respectively. Moreover, the first order kinetic plots were found to be strictly linear as shown in **Figure 42**, indicating the living character of polymerization of 2-oxazolines.

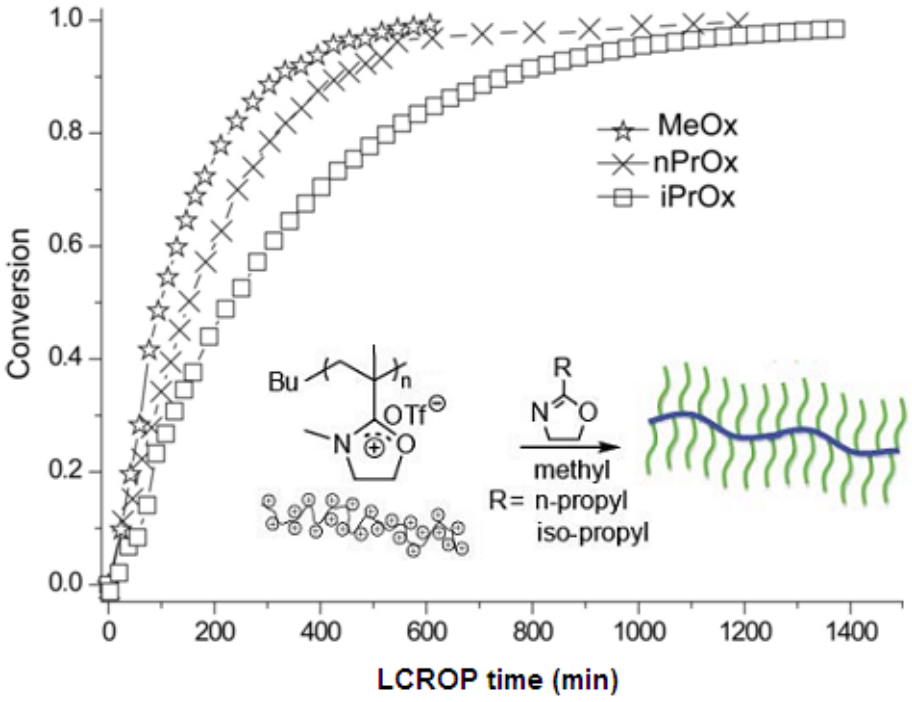

Figure 41. Plots of MeOx, *n*PrOx and *i*PrOx consumption vs. LCROP time for the polymerization in the presence of M^{II}.

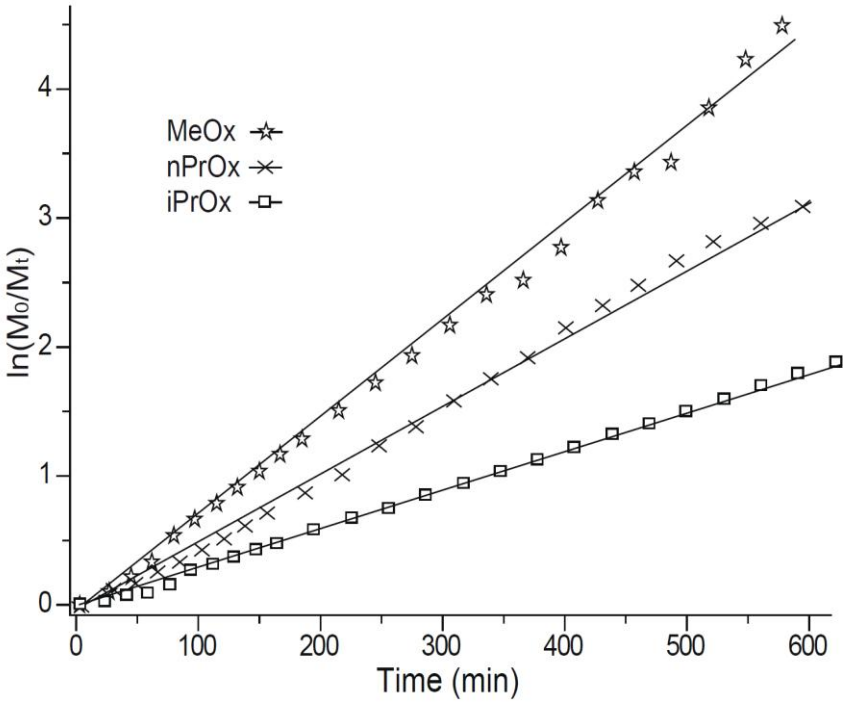

Figure 42. First order kinetic plots for the polymerization of MeOx, EtOx and *n*PrOx in the presence of M^{II}.

3.3.3 Thermo-responsive properties - impact of different parameters on the LCST

The LCST of linear thermo responsive polymers, including POx, is a function of molar mass and concentration.[33,118,159] Besides, it also can be affected by the structure and polarity of side chain and end groups.[119,161,162,163,167,168] Hence, it is expected that these parameters also have a certain influence on the LCST of molecular brushes. The influence of the side chain composition and end group functionalities on the LCST were discussed in the previous chapter. Here we investigated the effect of other possible factors e.g. side chain length, concentration and backbone length on the LCST of molecular brushes of POx.

3.3.3.1 Side chain length effect

It was shown in the previous chapter that the unique molecular architecture has only minor effects upon the LCST. Here, to examine the effect of side chain length, molecular brushes with P*n*PrOx or P*i*PrOx pendant chains of different length were prepared with the macroinitiators (M^I, M^{II}). The side chain length was controlled by terminating the side chain polymerizations after a given time, and afterwards determined from the kinetic plot of monomer conversion *vs* LCROP time (**Figure 41**). Characterizations of macroinitiators M^I, M^{II} and molecular brushes prepared by LCROP of *n*PrOx/*i*PrOx from macroinitiators are summarized in **Table 5**. M^I 1 - M^I 3 are molecular brushes prepared from macroinitiator M^I with different P*n*PrOx side chain length, i.e. LCROP of *n*PrOx for 1, 2 and 8 h, respectively. M^{II} 1 - M^{II} 4 are brushes from macroinitiator M^{II} with different P*n*PrOx side chain length, i.e. LCROP of *n*PrOx for 0.5, 1, 2 and 8 h, respectively. M^{II} 5 - M^{II} 7 are brushes from M^{II} with different P*i*PrOx length, i.e. LCROP of *i*PrOx for 1.3, 3 and 24 h, respectively.

Table 5. Synthesis of macroinitiators and molecular brushes with P*n*PrOx/ P*i*PrOx side chains.

	Initiator	Polymerization time (h)[a]	Side chain	Conversion (%)[b]	DP[c]	M_n (kg/mol)[d]	M_w/M_n[d]	LCST (℃)[e]
$PIPOx^{I}$	-	0	-	0	-	5.8	1.15	-
M^{I} 1	M^{I}	1	P*n*PrOx	22	6	16.4	1.18	19.5
M^{I} 2		2		42	11	27.3	1.17	18.1
M^{I} 3		8		98	24	40.7	1.14	19.2
$PIPOx^{II}$	-	0	-	0	-	14.6	1.21	-
M^{II} 1	M^{II}	0.5	P*n*PrOx	11	3	25.8	1.26	24
M^{II} 2		1		22	6	46.2	1.23	19.2
M^{II} 3		2		42	11	63	1.28	18.2
M^{II} 4		8		97	24	102	1.30	19.2
M^{II} 5		1.3	P*i*PrOx	19	4	35.1	1.24	29
M^{II} 6		3		40	10	48.5	1.24	28.1
M^{II} 7		24		99	25	86.9	1.24	29.1

a. 2^{nd} cationic grafting polymerization time
b. as calculated by GC measurement
c. degree of polymerization of side chain calculated from GC measurements
d. as calculated from GPC traces
e. determination of the cloud point by turbidity measurements of a 1.0 wt % aqueous polymer solution (upon heating curves)

The thermo-responsive properties of the resulting brushes containing side chains with different length were investigated by turbidity measurements. The cloud point was defined analogue to previous reports[146] at 10 % transmittance decrease of a 1.0 wt % aqueous polymer solution. The results are summarized in **Table 5**. For molecular brushes with P*n*PrOx side chains initiated by M^{II} (**Figure 43**), the transmittance of the aqueous polymer solution decreased sharply when the temperature reached the cloud point. In addition, the cloud point of the resulted brush molecules with P*n*PrOx side chains from M^{II} versus their side chain length were plotted to analyze the side chain length effect upon the cloud point (**Figure 44**). The cloud point for M^{II} 1 (DP of side chain = 3) was found to be 24 ℃ which is identical with the value of linear P*n*PrOx with comparable molar mass (23.8 ℃). When the length of side chain increased (3<DP<10), the cloud point continuously decreased to 18.2 ℃ for M^{II} 3 at a side chain DP of 10, which nicely demonstrates the increased crowding as the side chain is growing from the macroinitiator.

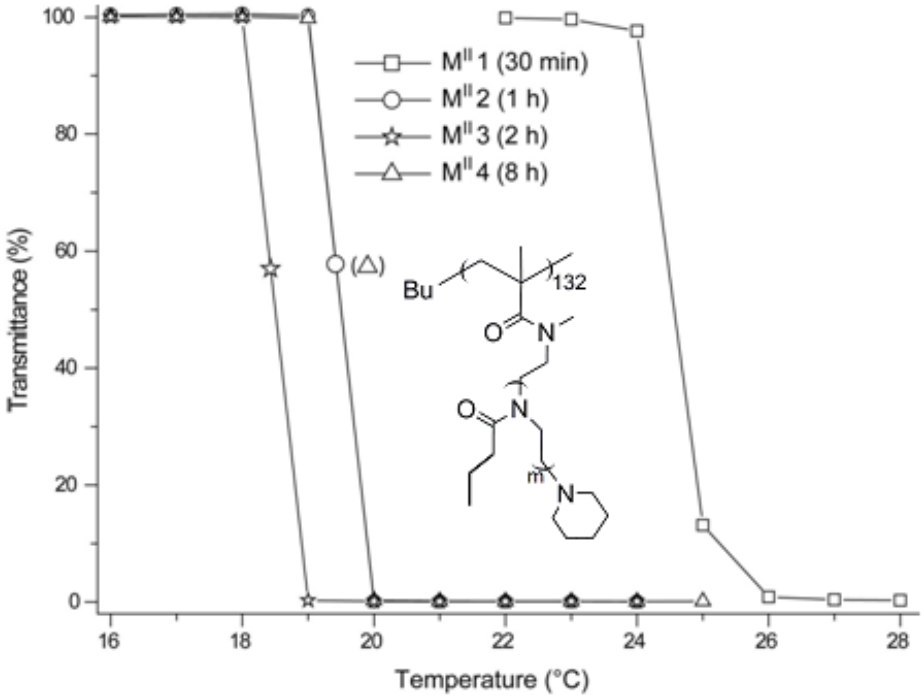

Figure 43. Determination of the cloud points of molecular brushes with different lengths of P*n*PrOx side chains by turbidity measurements. The transition temperatures were determined by 10% transmittance decrease for brush molecules in 1.0 wt % of aqueous solution (only heating curves are shown).

More interestingly, the further increase of side chain length (10<DP<25) resulted in a slight increase of the LCST to 19.2 ℃ (M^{II} 4). This subtle, but distinct dependency between the LCST and the side chain length was reproducible and could not be neglected. As shown in **Figure 45**, like linear polymer, the molecular brush with short side chains adopts a coiled conformation. Successively, the molecular brush becomes stretched as the side chain length increases, which results in a decrease of cloud point as discussed in the previous chapter. However, the terminal part of side chain becomes loose as the side chain length further increases. Given the same grafting density, the free volume per side chain is proportional to d^2 (d is the apparent diameter of a molecular brush as shown in **Figure 45**). Therefore, the local concentration of the side chain terminal part significantly decreases when the side chain length increases. It is known for POx that the cloud point increases with the decrease of concentration. As a result, the cloud point increased.

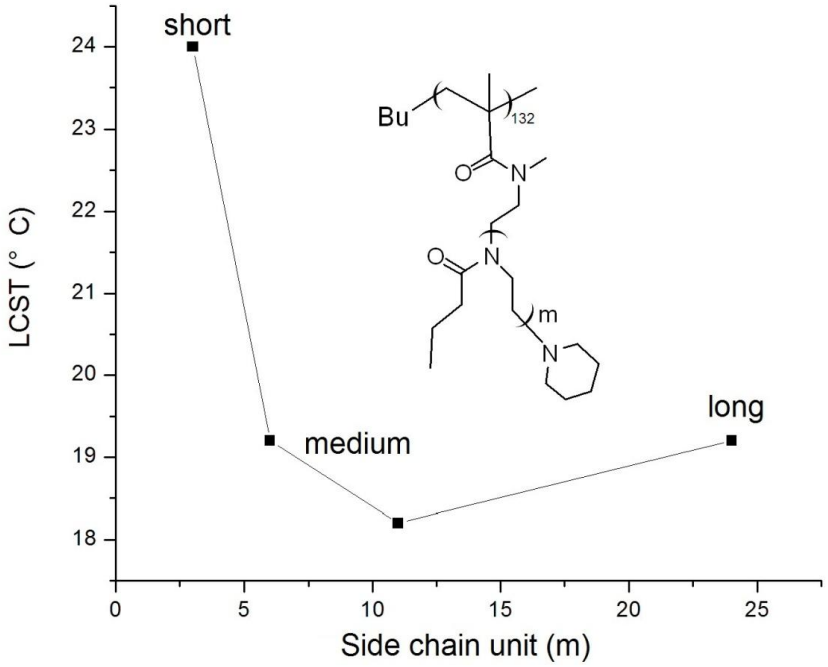

Figure 44. LCST of molecular brushes with P*n*PrOx side chains of different length along with the structure of the molecular brush.

To summarize the effect of side chain length on the LCST of molecular brushes, at very short side chain length (DP = 3) the side chain oligomers do not yet induce a steric crowding, and the LCST is virtually identical with linear polymer.[169,170] However, as the side chains grow the crowding of side chains results in a decrease of LCST by several degrees. Furthermore, as the side chain length increases further, the segments of side chain end experience the increased volume/side chain i.e. a decrease of local concentration. Thus, the LCST values increase again, albeit only slightly.

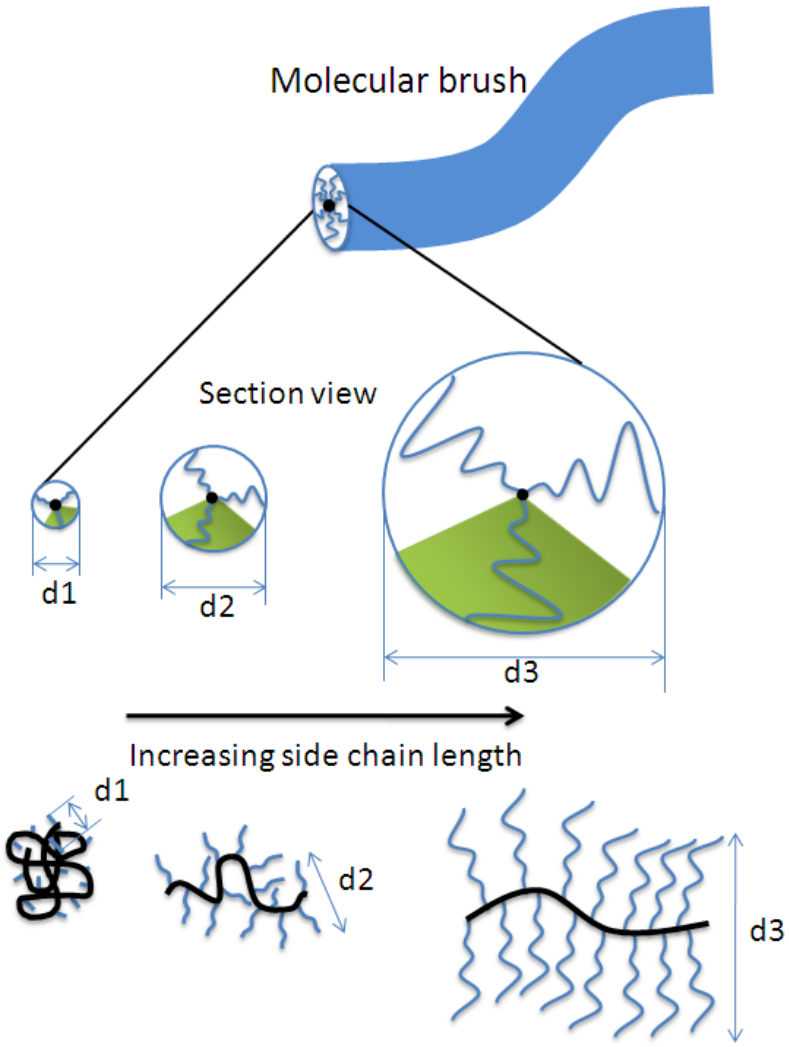

Figure 45. Illustration for the side chain length effect on the conformation of the molecular brushes. Top: profile of a molecular brush, middle: section view of molecular brushes and volume/side chain at different side chain length, bottom: conformation of molecular brushes with different side chain length.

To further certify this subtle side chain length effect on the LCST, molecular brush with P*n*PrOx side chain in different length from a shorter macroinitiator (M^{I}) and brush with poly(2-iso-propyl-2-oxazoline) (P*i*PrOx) side chain in different length from M^{II} were also compared. Similar results were found out. The LCST value of M^{II} 5 (DP = 4) was found to be 29 ℃ and decreased to 28 ℃ for M^{II} 6 (DP = 10) as P*i*PrOx side chain grew. The further increase of the side chain length resulted in a slight increase of LCST to 29.1 ℃ for M^{II} 7 (DP = 24). On the other hand, the LCST value of M^{I} 1 (DP = 6) decreased from 19.5 to 18.1 ℃ for M^{I} 2 (DP = 11) and increased to 19.2 ℃ for M^{I} 3 (DP = 24) as the P*n*PrOx side chain grew.

It was reported by Schmidt[36] and Matyjaszewski[40] that molecular brushes tend to aggregate intramolecularly in dilute brush solutions as shown in **Figure 46**. However, linear polymers

tend to aggregate intermolecularly upon heating. In order to better understand the observed LCST behavior, dynamic light scattering (DLS) studies were performed to investigate the side chain length effect on aggregation behaviors of the brush molecules. The apparent diameters of M^{II} 1and M^{II} 2 were measured at different temperatures in dilute aqueous solutions. As shown in **Figure 47**, the diameter of M^{II} 2 continuously decreased to a minimum (with a diameter decrease of 11 %) at 22 ℃ and suddenly increased upon further increasing of the temperature. However, in the case of M^{II}1, the apparent diameter kept constant below 30 ℃, and drastically increased upon further increasing of the temperature. These observations corroborate the formation of dense brush like structure of M^{II} 2 and the linear polymer resemblance of M^{II} 1, which confirms our postulation of side chain length effect on the conformation of molecular brush. The postulated side chain length effect on the conformation is shown in **Figure 45**.

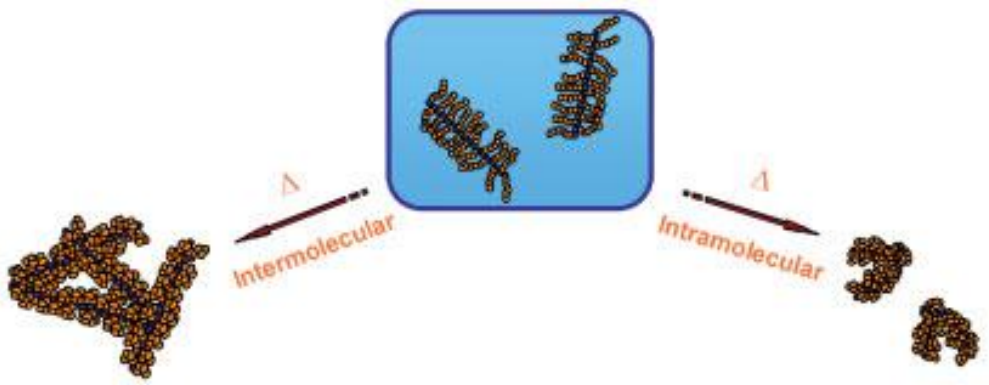

Figure 46. Molecular brushes tend to aggregate intermolecularly at high concentration, whereas intramolecular collapse is preferred at dilute solution (From Ref. [38]).

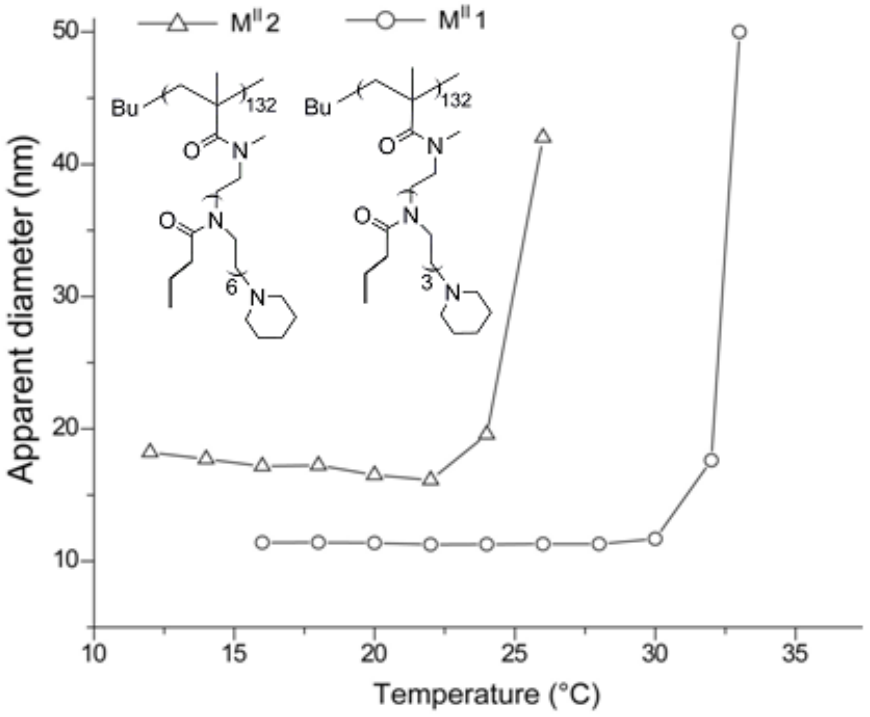

Figure 47. Temperature dependence of apparent diameters of M^{II} 1 and M^{II} 2 in 0.3 wt % aqueous solutions.

3.3.3.2 Concentration effect

The concentration effects on the LCST of the homoPOx and coPOx have been investigated previously. For the hydrophilic PEtOx,[118] a strong decrease of the cloud point temperature was observed with increasing concentration, while the cloud point temperature of amphiphilic P*n*PrOx almost kept constant regardless of the increasing concentration.[167] However, the exact nature of the dependence of polymer hydration on variations e.g. chain length and concentration for the POx is not yet understood.

Here, the cloud point of amphiphilic P(IPOx-g-*n*PrOx)^{A} at various concentrations was investigated. As shown in **Figure 48**, the LCST continuously dropped from 24 ℃ at 0.1 wt % to 19 ℃ at 1.0 wt %. However, a further increase of concentration did not affect the LCST significantly (not shown in the picture). The significant decrease of LCST observed here is in contrast to the results of linear P*n*PrOx reported before.[167] Some previous reports revealed that the unique and compact structure of molecular brushes facilitate intramolecular collapse above the LCST when the average distance between molecules is much larger than their hydrodynamic dimensions i.e. in dilute solution.[38] However, like most thermo-responsive linear polymers in solution, intermolecular aggregation is preferred when the intermolecular

distance was comparable to the individual molecular dimensions i.e. at high concentration. The abnormal LCST dependence on the concentration observed here most likely ascribes to the compact structure of molecular brushes. **Figure 48** depicts the concentration effect on the LCST of P(IPOx-g-*n*PrOx)^{A}.

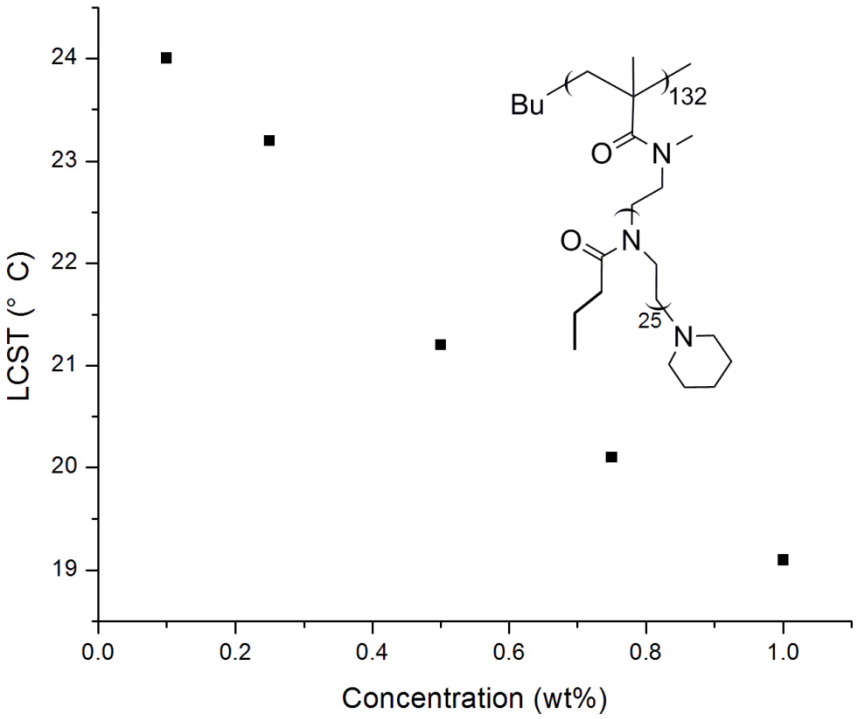

Figure 48. LCST of molecular brush P(IPOx-g-*n*PrOx)^{A} at various concentrations (side chain DP = 25, determined from heating curves).

3.3.3.3 Backbone length effect

In a recent report, the effect of molar mass on the cloud point of linear homoPOx has been investigated,[118] revealing a stronger influence to the more hydrophilic POx in comparison with the more hydrophobic POx. For example, Schubert and co-workers reported that PEtOx only exhibited a LCST when DP was larger than 100. Specifically, the LCST decreased from 94 ℃ at DP = 100 to 66 ℃ at DP > 500. In contrast, P*n*PrOx exhibited LCST ranging from 30 ℃ to 43 ℃ at the DP of 50-150. Only minor changes in LCST could be observed at DP > 150.

Table 6. Characterizations of molecular brushes with different backbones containing homo-poly(2-iso-propyl-2-oxazoline) side chains.

Polymer	Yield (%)	M_n (kg/mol)[a]	PDI[a] (M_w/M_n)	n[a]	m[b]	$m^{theor.}$	$M_n^{theor.}$ (kg/mol)[c]
$PIPOx_n^{AI}$	90	5.8	1.15	52	-	-	-
$P(IPOx_n\text{-g-}i\text{PrOx}_m)^{AI}$	48	42	1.18	52	19	25	122
$PIPOx_n^{AII}$	96	14.6	1.21	131	-	-	-
$P(IPOx_n\text{-g-}i\text{PrOx}_m)^{AII}$	50	64	1.22	131	20	25	273
$PIPOx_n^{AIII}$	95	24.0	1.20	216	-	-	-
$P(IPOx_n\text{-g-}i\text{PrOx}_m)^{AIII}$	49	125	1.33	216	18	25	480

a) as calculated from GPC traces.
b) average degree of polymerization, m was calculated from end group analysis using ^{1}H NMR spectral data.
c) calculated using GPC determined molar mass of precursor polymer and ^{1}H NMR determined degree of side chain polymerization.

Here, the effect of backbone length on the cloud point of POx molecular brushes was investigated. Molecular brushes containing identical length of P*i*PrOx pendant chains (M_0/I_0 = 25/1) but different lengths of backbone were prepared. Characterizations of the different backbones and the resulting molecular brushes are listed in

Table 6. After the side chain LCROP of *i*PrOx, all the number molecular weights of the polymers shifted to higher molar values. For example, after the LCROP of *i*PrOx, the number average molecular weight shifted from 24 kg/mol for $PIPOx^{AIII}$ to 125 kg/mol for P(IPOx-g-*i*PrOx)^{AIII} (**Figure 49**). The LCST of the resulting molecular brushes were investigated. As shown in **Figure 50**, P(IPOx-*g*-*i*PrOx)^{A1}(M_n = 42 KDa) exhibited a transition temperatures of 33 ℃, P(IPOx-*g*-*i*PrOx)^{R} (M_n = 53 KDa) of 30 ℃ , P(IPOx-*g*-*i*PrOx)^{AII} (M_n = 64 KDa) of 29 ℃, and P(IPOx-*g*-*i*PrOx)^{AIII}(M_n = 125 KDa) of 27 ℃. Interestingly, the less structurally defined P(IPOx-*g*-*i*PrOx)^{R} showed a LCST transition as sharp as that for the defined P(IPOx-*g*-iPrOx)^{A}. These results indicate that the LCST of molecular brushes decreases with the increase of backbone length. These results are consistent with previous reports for linear POx.[118]

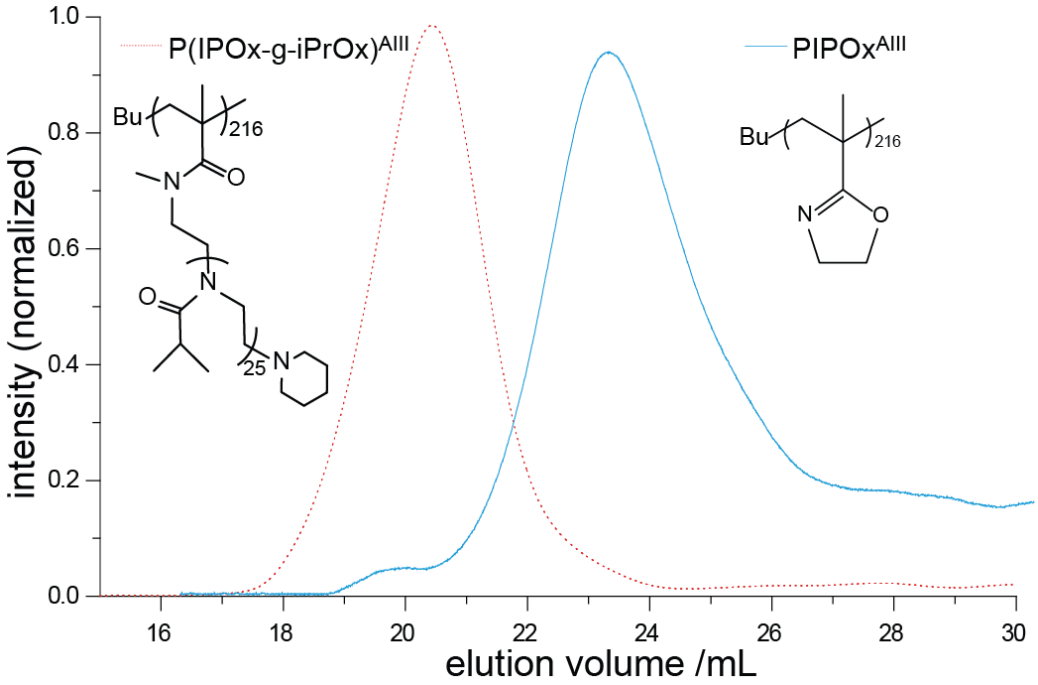

Figure 49. GPC traces of PIPOx^{AIII} backbone and molecular brush P(IPOx-g-*i*PrOx)^{AIII}.

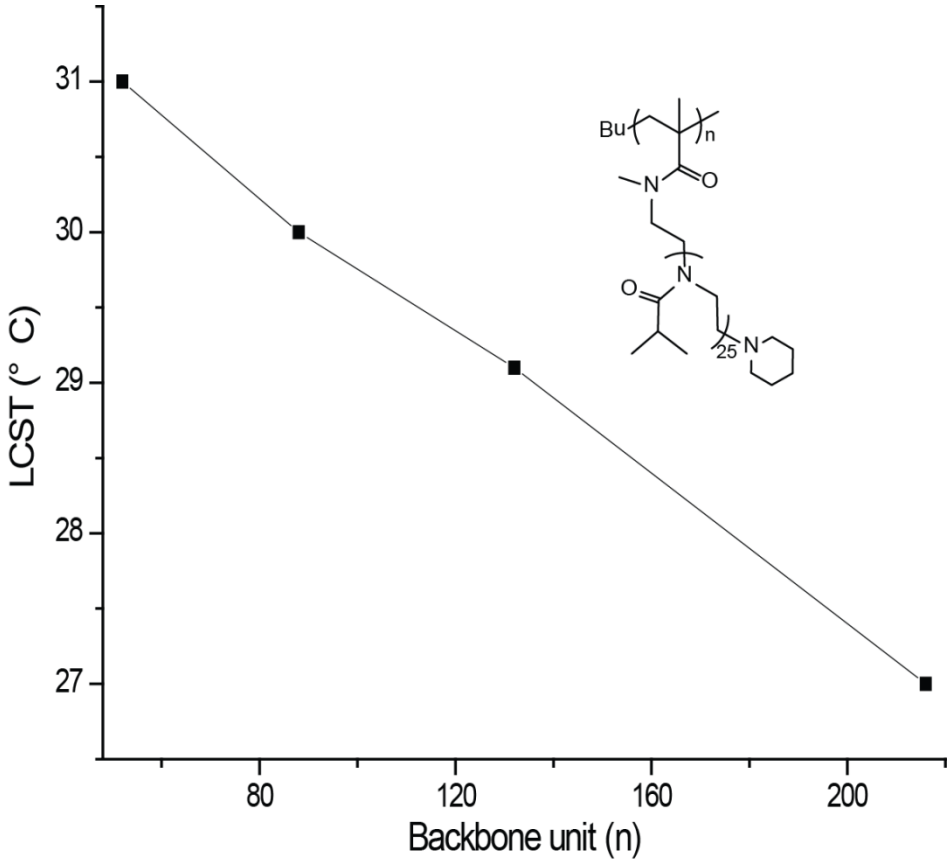

Figure 50. LCST of molecular brushes with identical P*i*PrOx side chains but different backbone length in 1.0 wt % aqueous solution (side chain DP = 25, determined from heating curves).

3.4 Molecular brushes with copoly(2-oxazoline) side chains

3.4.1 Background

A large number of reports investigated structure and composition property relationships for POx, mainly by varying the monomer composition or end groups. For linear poly(2-oxazoline)s (POx), changing the length of alkyl chain in the 2-position, the nature of the POx can be changed from hydrophilic (2-methyl and 2-ethyl as substituents) to hydrophobic POx with longer alkyl or phenyl 2-substituents. For example, Schubert and co-workers finely tuned the LCST of poly(2-oxazoline)s by varying composition and molar mass.[168] In addition, the amphiphilicity can be adjusted by the combination of hydrophilic and hydrophobic monomers in different degree of polymerization ratio. For instance, Kataoka[171,167] and Jordan[33,119] systematically investigated the accurate control of the thermo-sensitivity of linear POx by copolymerization of 2-alkyl-2-oxazolines. The LCST of the copolymers decreased with an increase of the content of hydrophobic monomer i.e. 2-*n*-propyl-2-oxazoline (*n*PrOx). Parameters influencing the thermo sensitivity of linear POx are expected to have similar effect on the LCST of molecular brushes of POx. Here, molecular brushes of copoly(2-oxazoline) side chains were prepared. The thermo-responsive properties of the resulting molecular brushes were investigated.

3.4.2 Molecular brushes with statistical copolymer side chains

The *grafting from* approach and living cationic ring-opening polymerization (LCROP) of 2-oxazoline allow the efficient and accurate control of the chemical composition of the polymer chains. In addition to molecular brushes with homopolymer side chains, here the synthesis of molecular brushes with both, statistical- and block- copolymer side chains is described and their thermo-responsive properties are investigated. The kinetics of the polymerization of 2-methyl-2-oxazoline (MeOx) and *n*PrOx in the presence of macroinitiator M^{II} were investigated before the preparation of molecular brushes. The apparent polymerization rates per initiating group were calculated to be 2.12 and 2.95 mL S^{-1} mol^{-1} for *n*PrOx and MeOx, respectively. As shown in **Figure 51**, the two first order kinetic plots are strictly linear, indicating a living character of the polymerization. Furthermore, the minor difference in the

polymerization rates for both monomers allows for the formation of almost random side chains.

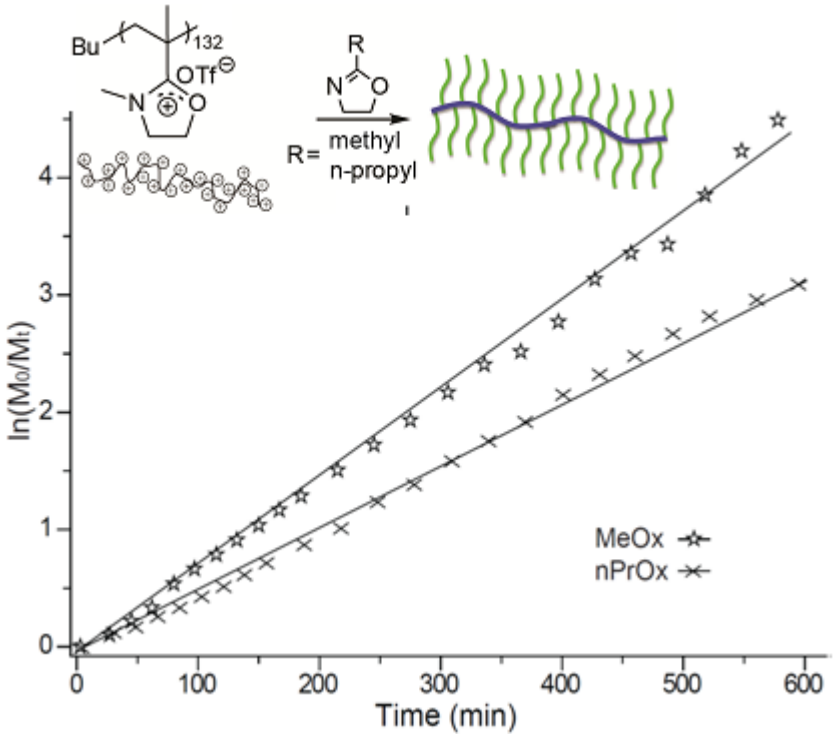

Figure 51. First order kinetic plots for the polymerization of 2-methyl- and 2-*n*-propyl- 2-oxazoline with the macroinitiator (M^{II}).

3.4.2.1 Synthesis

First, molecular brushes comprising statistical copolymer side chains of PMeOx and P*n*PrOx were synthesized by LCROP of MeOx and *n*PrOx from the macroinitiator M^{II} (DP = 132). The total length of the side chains was set to m = 25 by the initial $[M]_0/[I]_0$ ratio. The LCROP reactions were conducted at different monomer feed ratios under otherwise identical conditions. The reactions and conditions for the synthesis of each compound are summarized in **Figure 52**.

The copolymerization of the two monomers resulted in molecular brushes with relatively low PDI. The compositions of the side chains and molar ratio of the monomers presented in the side chains estimated by ^{1}H NMR was found to be close to the feed ratio of the monomers. The results of polymerizations and properties of the resulted polymers are summarized in **Table 7**.

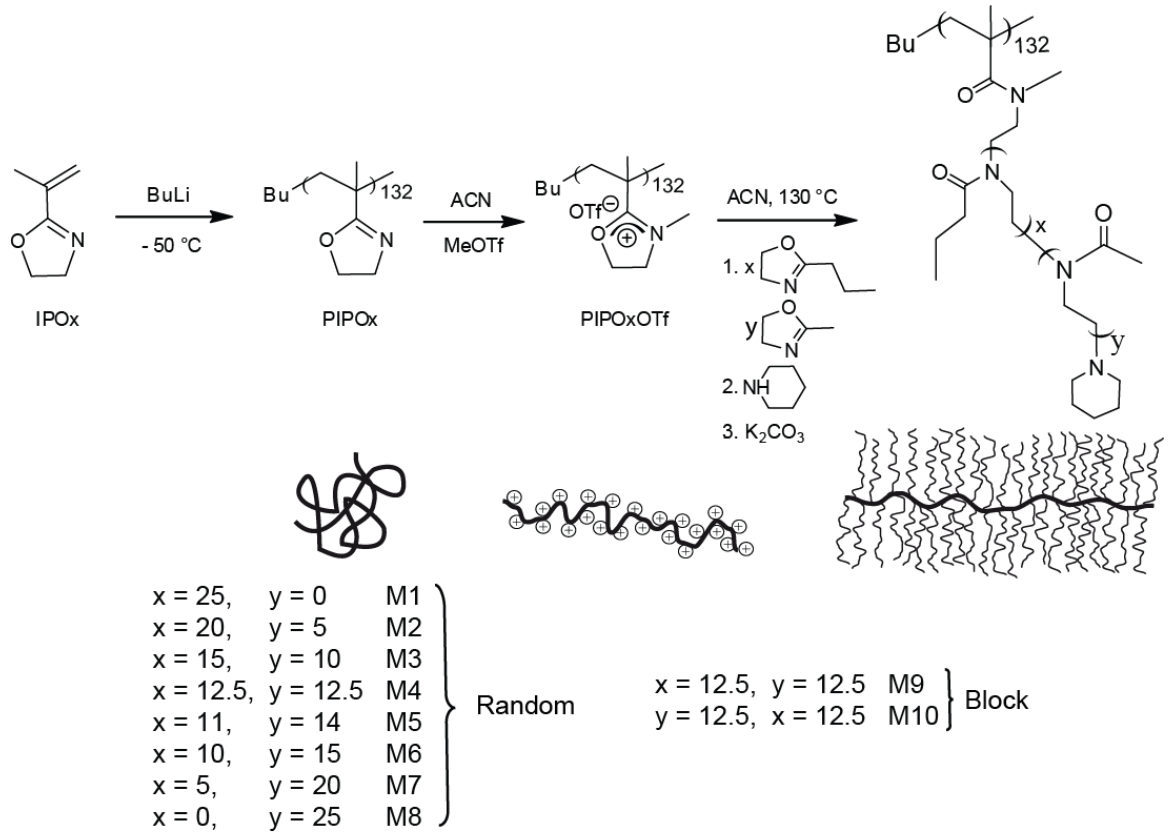

Figure 52. Reaction scheme of the synthesis of molecular brushes with statistical and block copoly(2-oxazoline) side chains. The backbone was synthesized by anionic polymerization of IPOx.

3.4.2.2 LCST of molecular brushes with random copolymer side chains

Some of the resulting molecular brushes (M1-M5) with statistical coPOx side chains exhibited thermo-responsive properties i.e having LCST. The LCST was determined by measuring transmittance of light through aqueous solutions of polymers using a UV spectrometer. The transmittance of 1.0 wt % aqueous solution of brush molecules was monitored at 500 nm at a heating and cooling rate of 1.0 ℃ $5min^{-1}$. The results are summarized in **Table 7**.

The linear homoP*n*PrOx and homoPMeOx have LCST at around 23.8 ℃ and above 100 ℃ respectively, and molecular brushes composed of these polymers are expected to have similar value of LCST. **Figure 53** shows the transmittance of the aqueous solution of molecular brushes. It is seen the transmittance of the polymer solution decreased sharply when the temperature reaches their LCST. In addition, the dependence of LCST value on MeOx

content was plotted and shown in **Figure 54**. The LCST values increased from 19 ℃ (MeOx mol % = 0) to 79 ℃ (MeOx mol % = 70 %), suggesting the balance shifted towards higher hydrophilicity due to the higher content of MeOx. Moreover, LCST values were found to increase linearly with the increasing molar content of MeOx (**Figure 54**) which is consistent with linear POx. No change in the transmittance was observed in case of MeOx content above 80 %, which is due to the too high hydrophilicity of the side chains.

Table 7. Molecular brushes with copolymer side chains from MeOx and *n*PrOx.

entry	Feed (x:y) (*n*PrOx:MeOx)	M_n (KDa)[a]	PDI[a]	LCST[b]	Composition (x:y)[c]
M1	25:0	84	1.20	19	25:0
M2	20:5	92	1.21	33	19:6
M3	15:10	95	1.2	51	14:11
M4	12.5:12.5	98	1.22	57	12:13
M5	11:14	99	1.28	79	9:16
M6	10:15	102	1.26	-	8:17
M7	5:20	113	1.4	-	5:20
M8	0:25	121	1.21	-	0:25
M9	12.5:12.5	96	1.21	32	13:12
M10	12.5:12.5	121	1.6	81	14:11

a) as calculated from GPC traces

b) determined by measuring 10% transmittance decrease of light at $\lambda = 500$ nm through aqueous solutions of the corresponding polymer using a UV spectrometer

c) calculated from ^{1}H NMR spectroscopy

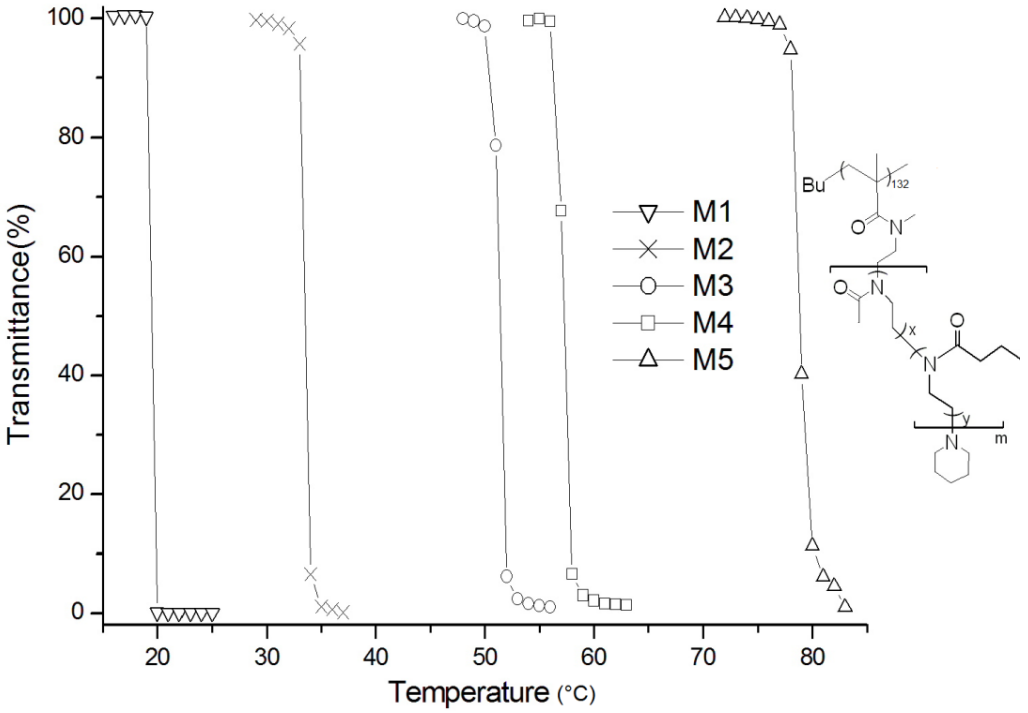

Figure 53. Determination of cloud points of molecular brushes with different MeOx content. Only heating curves are shown here (the same transition point was found with no noticeable hysteresis upon cooling).

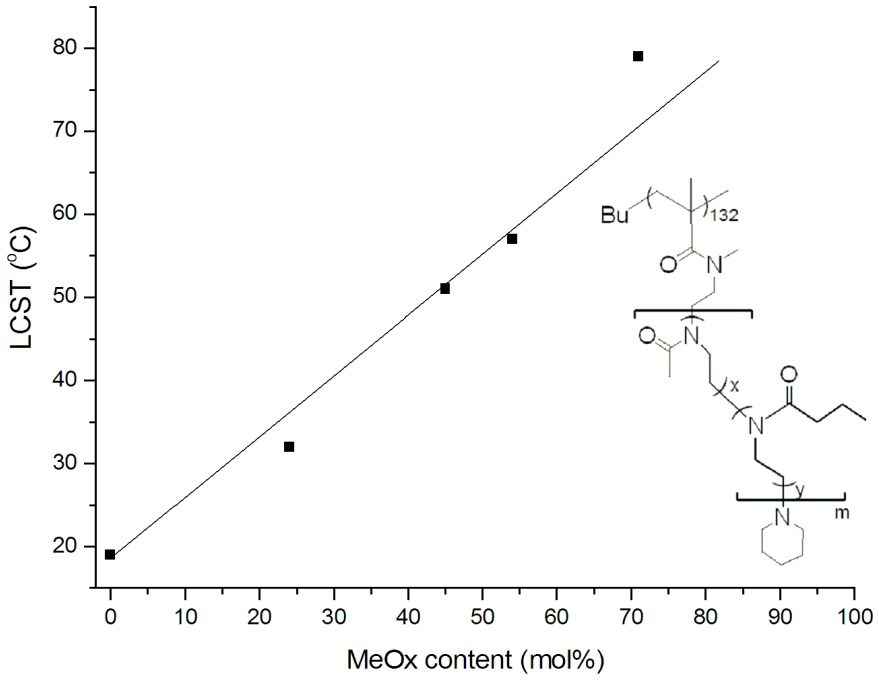

Figure 54. LCST values versus MeOx molar content of the side chain of molecular brushes.

3.4.3 Molecular brushes with block copolymer side chains

Molecular brush with P*n*PrOx-block-PMeOx (M9) and PMeOx-block-P*n*PrOx (M10) block sequences in the side chain were prepared to examine the segment sequences effect on the LCST. M9 and M10 are molecular brushes with opposite block sequences i.e. M9 has a P*n*PrOx core and a PMeOx shell, while M10 has a PMeOx core and a P*n*PrOx shell. The side chain length of the molecular brushes was set to *n*PrOx:MeOx = 12.5:12.5. Molecular structures of M9 and M10 are shown in **Figure 55**. The composition of side chain and molar ratio of comonomers presented in the side chain were estimated by ^{1}H NMR. The final composition of side chains was found close to the feed ratio of the comonomers. In addition, the GPC trace of the molecular brushes shifted to higher molecular weight after a second LCROP of 2-oxazoline, indicating the successful introduction of the second block, however with slightly increased PDI. The characterization of M9 and M10 with respect to ^{1}H NMR and GPC is listed in **Table 7**.

3.4.3.1 LCST of molecular brushes with block copolymer side chains

LCST values of M9 and M10 were measured and compared with the value of M4, which consists of statistical copolymer side chain of identical *n*PrOx/MeOx ratio and side chain length. The LCST were determined at 10% transmittance decrease of a 1.0 wt % aqueous polymer solution as shown in **Figure 56**. The sequence of blocks in the side chain of molecular brushes was found to have a pronounced impact on the LCST value. For M9, with a sequence P*n*PrOx-b-PMeOx, the LCST was found to be 32 ℃ in contrast to a transition temperature of 81 ℃ for M10 with a sequence of PMeOx-b-P*n*PrOx. A hydrophilic brush core with a hydrophobic shell resulted in a higher LCST than a hydrophobic brush core with a hydrophilic shell. This observation suggests that the more hydrophobic P*n*PrOx block inside the molecular brush firstly aggregates at its intrinsic LCST and then drive the brush molecule to precipitate. However, in the case of PMeOx as the inside block, the *n*PrOx shell starts to aggregate forming small aggregates around the brush molecule while the inside PMeOx block is still soluble. Due to the driving force is not strong enough, brush molecule remains soluble. In the recent report by Matyjaszewski, [40] the impact of the block sequence in molecular brush side chains of oligo(ethylene oxide) on the LCST value was investigated. Molecular brush

with a hydrophilic core (MEO_3MA) and a hydrophobic shell (MEO_2MA) has a lower LCST as compared to molecular brushes with a hydrophobic core and a hydrophilic shell.

The results observed here seem contradict to Matyjaszewski's findings. However, it should be noted the side chain length as well as the hydrophilic/ hydrophobic ratio in the side chain in this experiment differ significantly from the ones in literature. They are not comparable virtually. Additionally, it was discussed in the previous section that the LCST of M4, with statistical copolymer side chains, is 57 ℃, which is just in between the LCST of M9 and M10. This also corroborates the formation of random or slightly gradient copoly(2-oxazoline) side chains as illustrated in **Figure 55**.

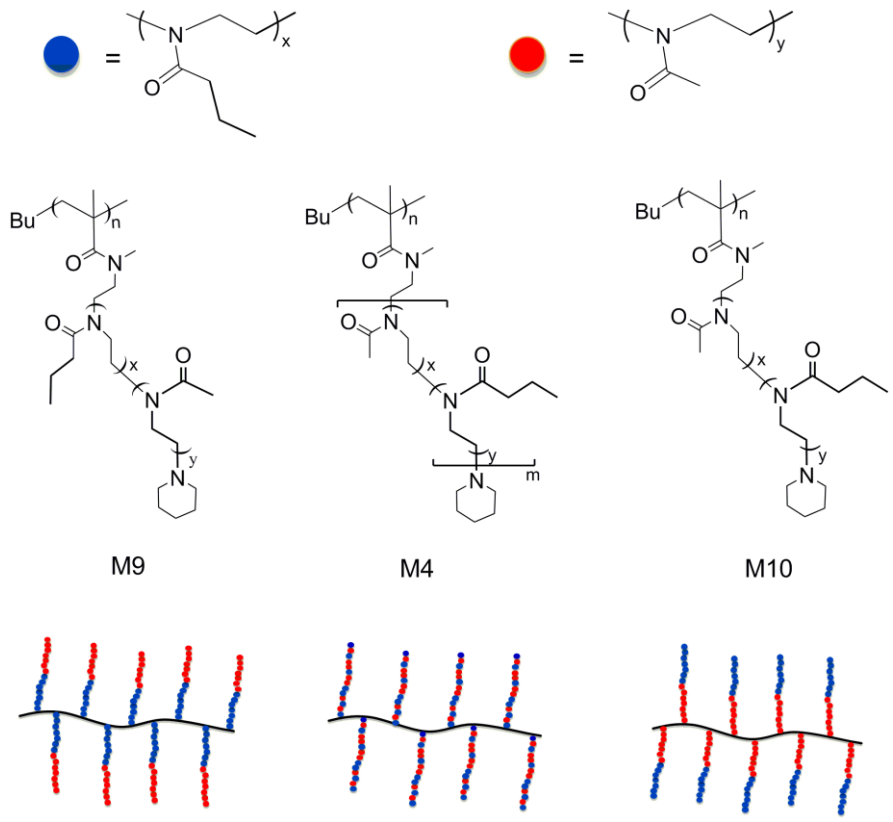

Figure 55. Illustration of the formation of molecular brushes with statistical and block copoly(2-oxazoline) side chains.

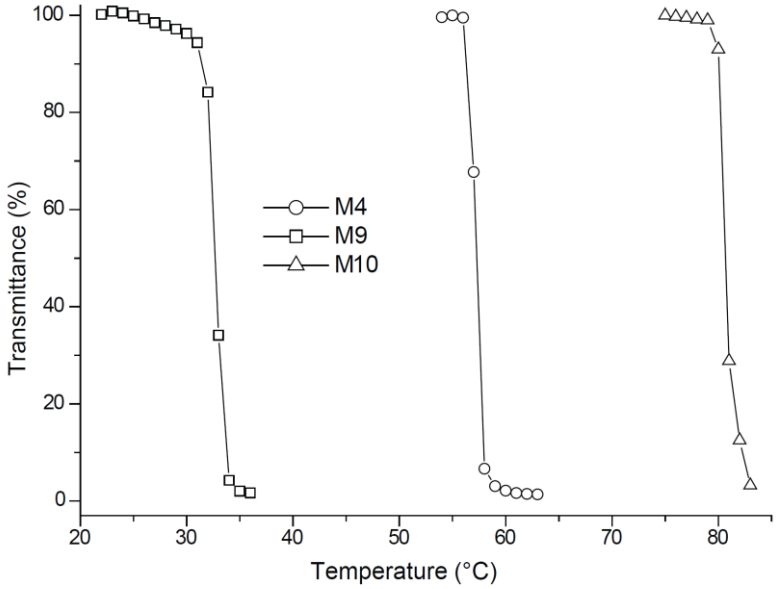

Figure 56. Determination of LCST values of molecular brushes with statistical and block copolymer side chains (MeOx:*n*PrOx = 12.5:12.5, molar ratio) by turbidity measurements of 1.0 wt% aqueous solutions. (only heating curves are shown)

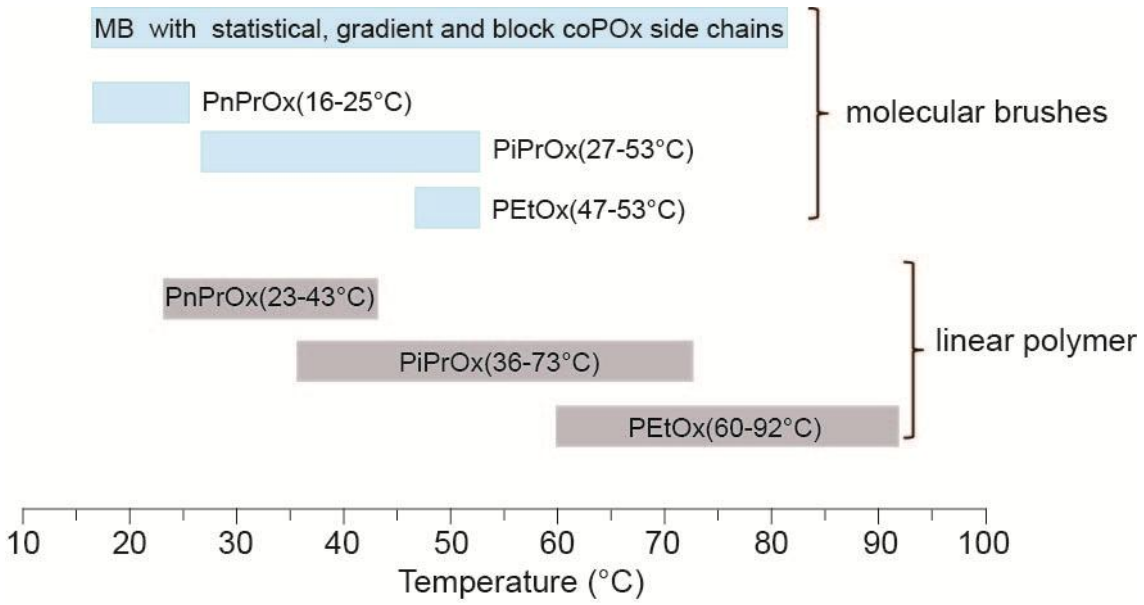

Figure 57. LCST of linear POx and molecular brushes of POx.

To sum up, the LCST of POx molecular brushes can be adjusted in a broad range from 16 to 81 ℃ by copolymerizing 2-oxazolines, varying end groups, molar mass, side chain length and composition (**Figure 57**). In addition, molecular brushes of block coPOx side chains have been prepared forming core-shell structures.

3.5 Bottle-brush brushes of poly(2-oxazoline)s

3.5.1 Background

The preparation of polymer brushes[172] on solid substrates, to tune the interfacial properties, has been of great interest due to the potential application of polymer brushes as sensing layers, anti-corrosion layers, protein resistant surfaces and nanostructured surfaces.[76,173,174,175]

Recently, our group developed the preparation of nano/micro structured polymer brushes on a variety of surfaces by electron beam chemical lithography (EBCL)/electron beam carbon deposition (EBCD) and successive self-initiated photografting and photopolymerization (SIPGP).[66,67,68,69] SIPGP, compared to other methods for the preparation of polymer brushes, has gained much interest. It allows the preparation of polymer brushes on various surfaces simply by irradiation of the substrate by UV light in the presence of bulk monomer. The only requirement is the presence of surface functionalities on the substrate possessing abstractable groups that can be abstracted by a photoactivated monomer. The formed surface-bound radicals initiate a free radical polymerization. This method allows for the formation of polymer grafts on relatively undefined organic surfaces. Specific pretreatment and modification of surfaces with special initiator functions is strongly facilated.

In this part of work, poly(2-isopropenyl-2-oxazoline) (PIPOx) brushes were prepared by the SIPGP of 2-isopropenyl-2-oxazoline (IPOx) on various substrates such as bare polished glassy carbon, amino silane modified glass slide/silicon wafer and biphenylthiol self-assembled monolayers (SAMs) modified gold. Subsequently, by following the synthetic route for the preparation of molecular brushes of poly(2-oxazoline)s in the previous chapter, PIPOx brushes were converted to macroinitiator brushes by the reaction with MeOTf. This macroinitiator was then used to prepare brushes of bottle-brushes of poly(2-oxazoline)s (POx) by the LCROP of different 2-oxazoline monomers. In the following, these structures are referred to ‘bottle-brush brushes’ (BBBs).

Molecular brushes of PMeOx side chains have been found non-toxic in the previous chapter. In this part of work, polymer brushes of POx were introduced between solid substrates and biosystems. Micro/nano structured polymer brushes have been realized by stencil mask or electron beam chemical lithography. The discussion of first biomedical test i.e. non-specific

protein adsorption and cell adhesion using these BBB coatings will be shown in the last chapter of the thesis.

3.5.2 Bottle-brush brushes of poly(2-oxazoline)s on glassy carbon

3.5.2.1 Glassy carbon

Glassy carbon,[176] also called vitreous carbon, is a non-graphitizing carbon that combines glassy and ceramic properties. Remarkable properties of glassy carbon include high temperature and chemical resistance, and impermeability to gases and liquids.[177] Therefore, glassy carbon is widely used as electrode materials in electrochemistry, as well as for high temperature crucibles and as a component of some prosthetic devices. Glassy carbon is prepared by a series of heat treatments of organic precursors, such as polymeric resins at temperatures up to 3000 ^{o}C. The structure of glassy carbon has long been a subject of debate. Early structural models assumed that both sp^2 and sp^3 -bonded atoms were present, but it is now known that glassy carbon is composed of 100% sp^2 material. Recent research suggests that glassy carbon has a fullerene-related structure (**Figure 58**).[178]

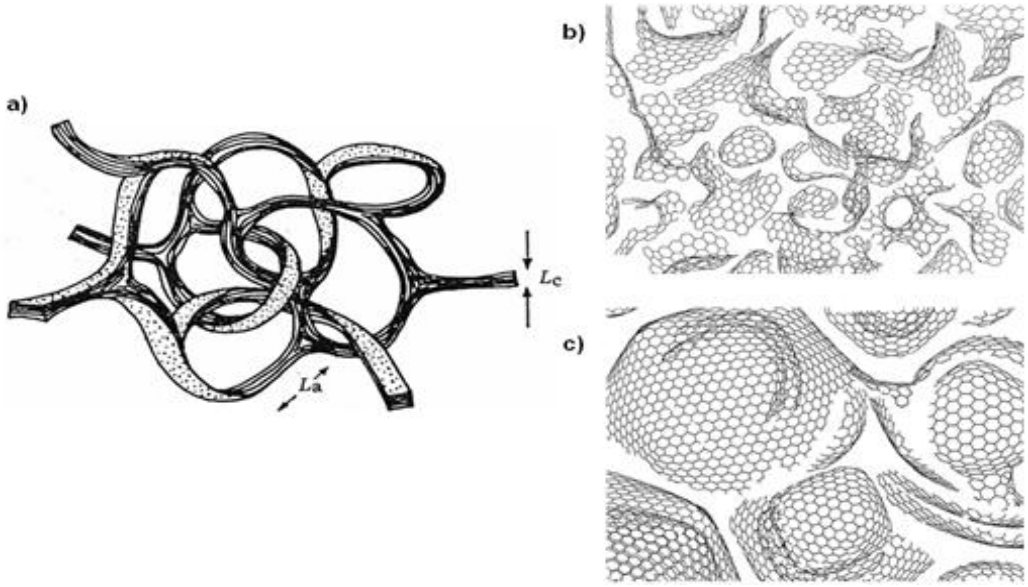

Figure 58. Models for the structure of glassy carbon: a) The Jenkins-Kawamura model of glassy carbon, La and Lc are the lengths of the graphitic domains perpendicular and parallel to the graphite axis; b) at low-temperature and c) at high-temperature glassy carbon made from the Harris-Tsang model (From Ref. [178]).

3.5.2.2 Self-initiated photografting and photopolymerization

The monomer 2-isopropenyl-2-oxazoline (IPOx) has two orthogonal polymerizable groups, namely a vinyl group for living anionic or radical polymerization (here used for the SIPGP) and the 2-oxazoline ring for the living cationic ring-opening polymerization (LCROP). After thorough cleaning with ultrasound in different organic solvents, a polished glassy carbon substrate was submerged in bulk IPOx and irradiated with UV-light of a spectral distribution between 300 and 400 nm (λ_{max} = 350 nm) for 40 h. In order to structure the substrate, the UV-irradiation was performed through a stencil mask (TEM grid) with rectangular openings of 50×50 µm^2. After the polymerization, the substrate was rigorously cleaned by ultrasound in several solvents of different polarity to ensure that only chemically grafted polymer remains on the substrate. The preparation of structured PIPOx brushes on glassy carbon is schematically outlined in **Figure 59** (for structuring) and **Figure 60**.

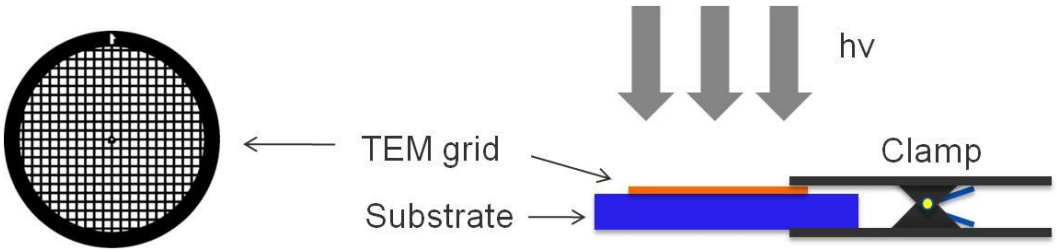

Figure 59. Scheme of the setup for SIPGP of IPOx, structures can be introduced by UV light through a transmission electron microscopy (TEM) grid (opening: 50×50 µm^2).

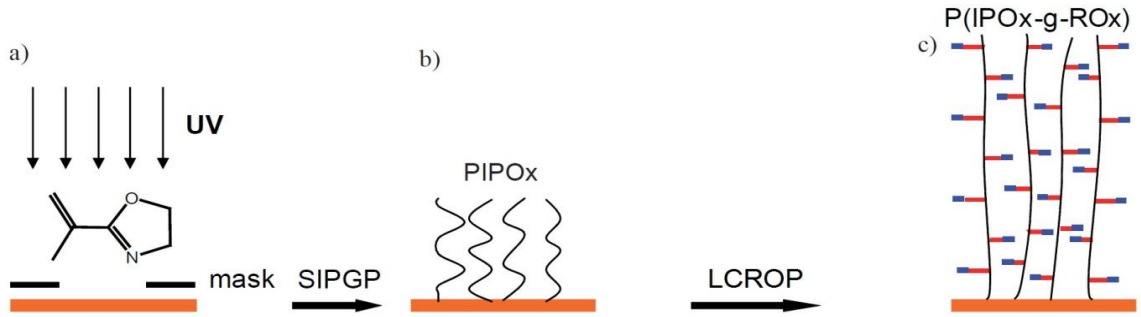

Figure 60. Preparation of structured P(IPOx-g-2-alkyl-2-oxazoline) bottle-brush brushes on glassy carbon. a)-b) Structured PIPOx brush was created on glassy carbon by UV-induced SIPGP of IPOx, structures were from a stencil mask. b)-c) Living cationic ring-opening polymerization of 2-oxazolines from the grafted PIPOx macroinitiators to form bottle-brush brushes.

AFM measurements revealed that a polymer brush layer with a thickness of 76 ± 9 nm was selectively formed on the irradiated surface area after 16h UV irradiation (**Figure 61**). Moreover, the surface roughness of the native glassy carbon substrate (rms 4.6 nm) was rendered by the additional polymer layer, showing a lower average roughness value of 3.0 nm (rms).

The successful modification of the glassy carbon substrate by PIPOx brushes was further confirmed by infrared (IR) spectroscopy. In **Figure 66**, the characteristic absorption bands of PIPOx are observed. The strong bands at 1648 cm^{-1} and 1128 cm^{-1} are assigned to the (C=N) and (C-O) stretching modes. The two bands at 987 and 951 cm^{-1} originate from the ring skeletal vibration of the 2-oxazoline rings. These assignments are in agreement with bulk PIPOx as discussed previously.

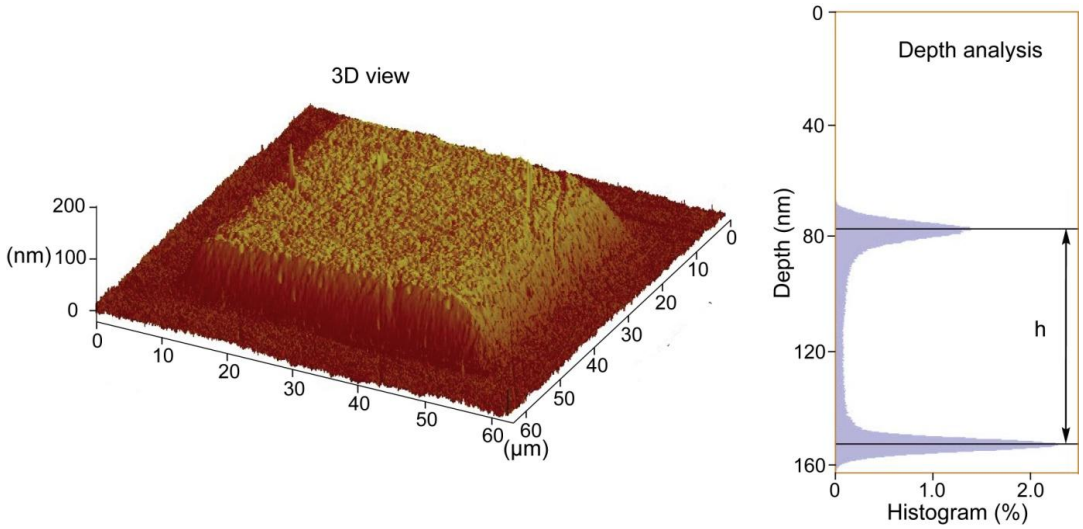

Figure 61. AFM 3D view and depth analysis of structured PIPOx brush (irradiation time = 16h). The average height was determined by depth analysis to be h = 76nm.

As shown in previous studies, using different substrates such as polyethylene,[62] aromatic SAMs on gold[69] and oxidized diamond,[67] the grafting reaction and the formation of polymer brushes occurs via the SIPGP mechanism in which the monomer acts as a photosensitizer to activate a surface functional group by hydrogen abstraction to start a free radical surface-initiated polymerization. The only requirement for the photografting reaction is the possibility for hydrogen abstraction by a radical mechanism. The SIPGP of IPOx also follows this mechanism as shown in **Figure 63**. All the presented SIPGP experiments in the thesis were performed at room temperature using a UV-light of a spectral distribution between 300 and 400 nm (λ_{max} = 350) from Rayonet.

Various studies have investigated the surface functionalities of polished glassy carbon substrates. Raman spectroscopy has shown that polishing severely disrupts the substrate structure.[179] Polishing does not only affect the upper monolayer but dramatically changes the substrate microstructure within a region of 10-20 nm. Polished glassy carbon surfaces are composed of smaller microcrystallites (compared to bulk glassy carbon) with many graphitic edges.[179] The formation of PIPOx brushes on polished glassy carbon can be explained by the low C-H bond dissociation energy (BDE) on such graphitic edges.[180] Furthermore, polishing causes a partial oxidation of the glassy carbon substrate resulting in C-OH and C=O surface functionalities (**Figure 62**).[181] Collier *et al.* reported that polished glassy carbon substrates are covered with up to 10 % of aromatic OH groups.[182] Due to the low BDE of aromatic alcohol groups,[183] it is most likely that hydrogen atoms are also abstracted radically from surface OH functionalities during the SIPGP process.

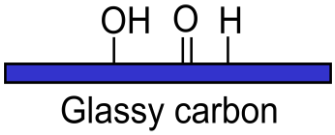

Figure 62. Representative surface functionalities on glassy carbon surface.

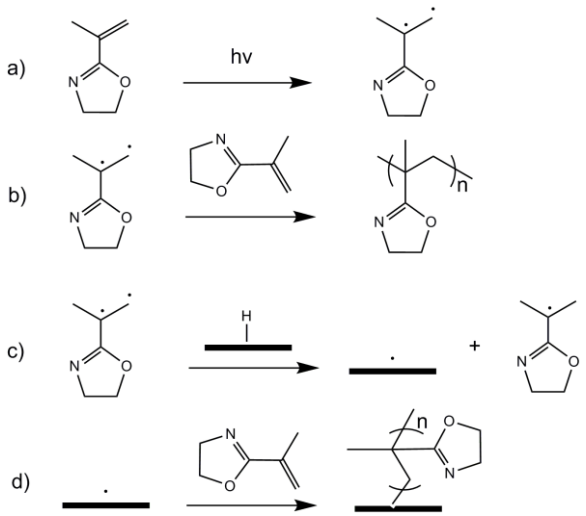

Figure 63. SIPGP reaction mechanism for the formation of PIPOx brush on polished glassy carbon.

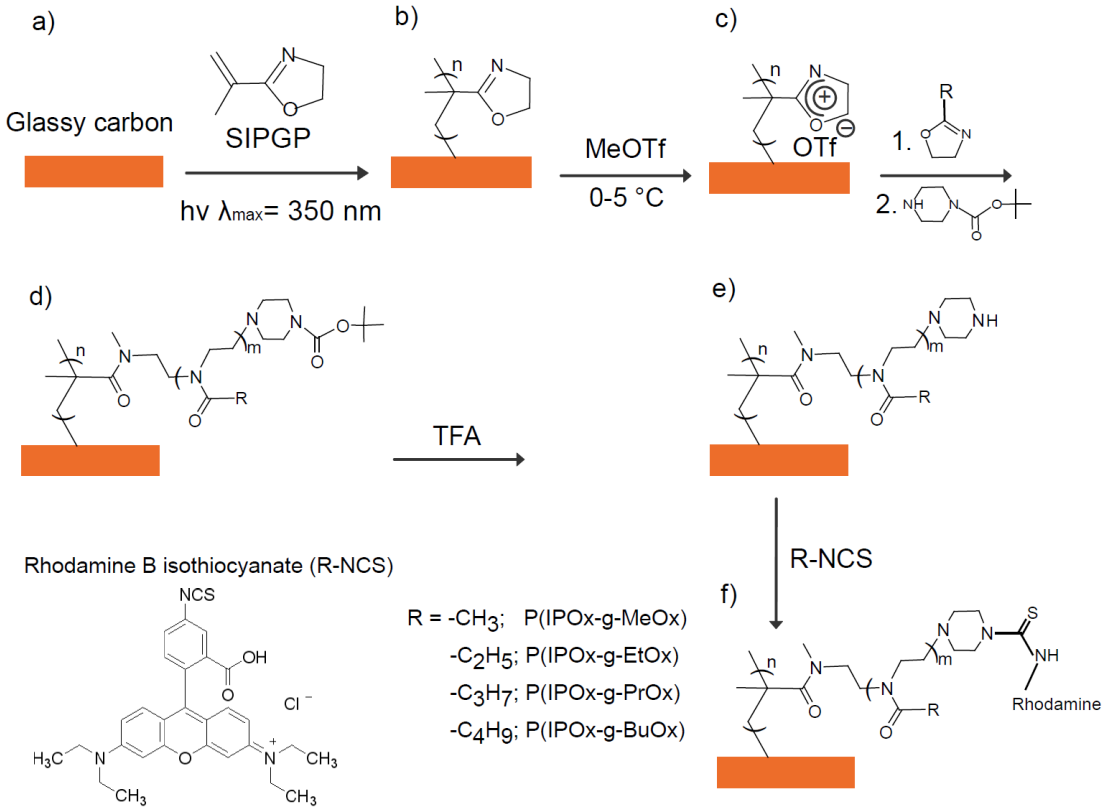

Figure 64. Preparation of P(IPOx-g-2-alkyl-2-oxazoline) bottle-brush brushes on glassy carbon. a)-b) PIPOx brushes were created on the substrate by the SIPGP of IPOx. c) Conversion of the PIPOx brush backbone to the surface bound macroinitiator PIPOxOTf. d) LCROP of 2-alkyl-2-oxazoline from the macroinitiator. e) Termination of the side chain polymerization with *N*-Boc-piperazine and deprotection of the Boc groups allows the further functionalization of the side chain end groups with rhodamine B isothiocyanate.

Ex situ kinetic studies of the SIPGP of IPOx monomer were performed on individual glassy carbon samples at different UV irradiation times (2 - 40 h) using the same stencil mask. In **Figure 65**, the thickness of the polymer brush layer as measured by AFM under ambient conditions is plotted as a function of the UV irradiation time. For polymerization times below 10 h, an almost constant growth rate of 6.1 $nm.h^{-1}$ is observed. However, the layer thickness growth rate decreases significantly for longer polymerization times. We observed that the bulk monomer phase became highly viscous with longer irradiation times due to self-initiated photopolymerization of the IPOx monomer in solution. The limited film growth can therefore be explained by either the monomer concentration decrease and/or the limited mass transport of the remaining monomer molecules. This kinetic behavior is in agreement with previous reports for SIPGP for other vinyl monomers.[184]

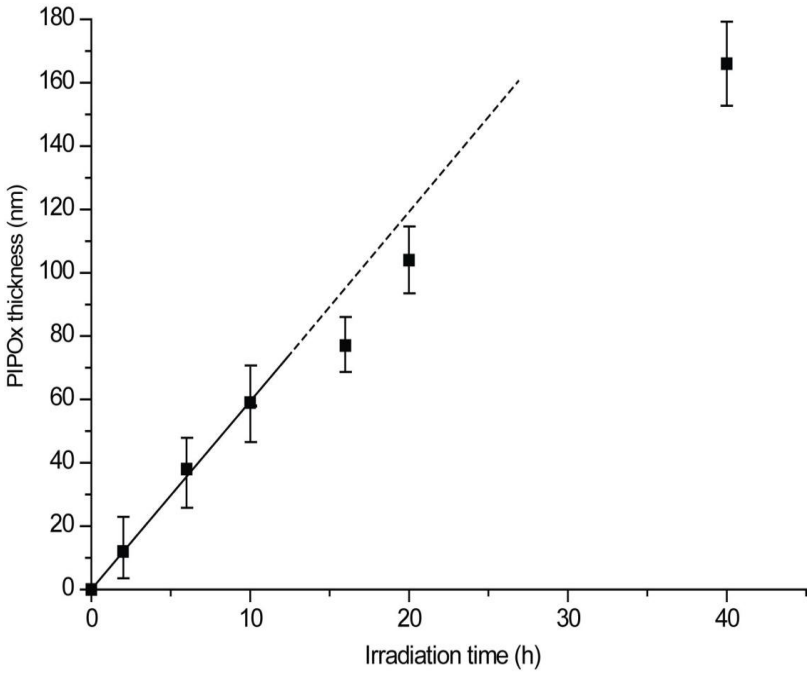

Figure 65. PIPOx brush layer thickness on polished glassy carbon as a function of the irradiation time as measured by AFM on structured polymer layer ($50 \times 50\ \mu m^2$).

3.5.2.3 Surface-initiated living cationic ring-opening polymerization

We have discussed the preparation of molecular brushes from the dual-functional IPOx monomer in the previous chapter. The PIPOx backbone was converted quantitatively with methyl triflate to a polycationic macroinitiator for living cationic polymerization of different 2-alkyl-2-oxazolines. Here, we have adapted this synthetic route to prepare bottle-brush brushes on glassy carbon as shown **Figure 64**. PIPOx brushes were converted into the polycationic macroinitiator salt (PIPOxOTf) by submerging the PIPOx modified glassy carbon substrate in a solution of methyl trifluoromethanesulfonate (MeOTf). Successively, the LCROP of 2-ethyl-2-oxazoline (EtOx) was performed for 20 min at 130 ℃. *N*-Boc-piperazine was used as terminating reagent. This terminal group allows an additional functionalization of each side chain end after deprotection of the secondary amine in trifluoroacetic acid (TFA). After the LCROP and deprotection of the Boc group, the substrate was intensively cleaned by ultrasound in different solvent to remove physisorbed material.

The successful conversion of PIPOx brushes to P(IPOx-g-EtOx) bottle-brush brushes was confirmed by IR spectroscopy (**Figure 66**). The (C=N) and (C-O) stretching bands at 1648, 1128 and 987cm^{-1} as well as the two ring skeletal vibration bands from the pendant 2-oxazoline ring in PIPOx brushes disappeared. A new intensive band appeared around 1627

cm^{-1} which is characteristic for the carbonyl stretching mode of the amide function. Moreover, the characteristic CH_x deformation modes for EtOx are observed around 1421 cm^{-1}. The complete disappearance of the oxazoline ring IR bands indicates a high side chain grafting density and quantitative reaction.

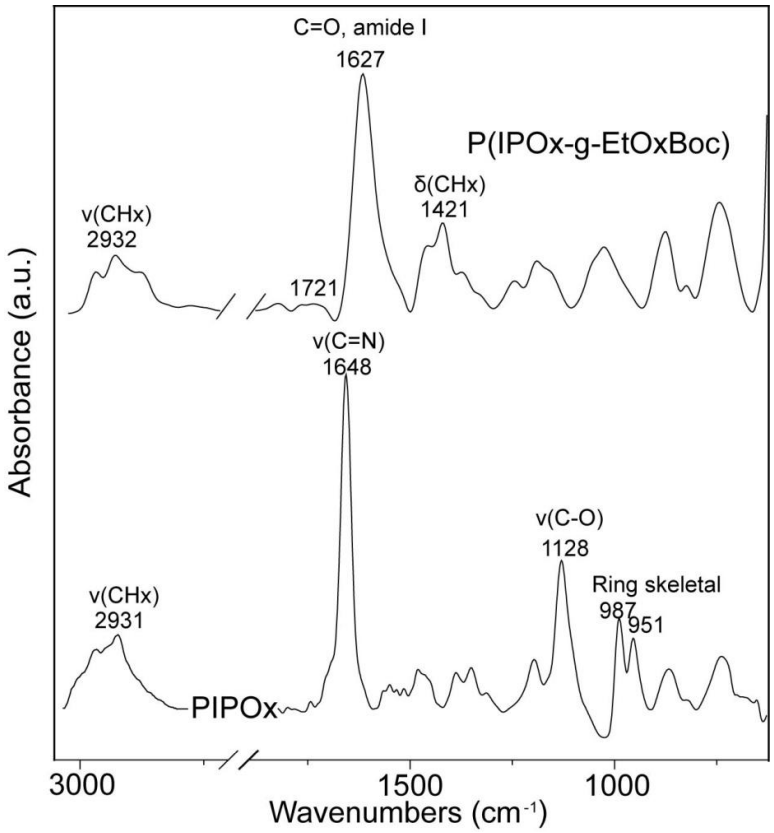

Figure 66. IR spectra of PIPOx and P(IPOx-g-EtOxBoc) brushes on glassy carbon.

AFM analysis of the resulting polymer layer revealed that the polymer brushes did not desorb during the successive reaction steps. This demonstrates that besides the ultrasound stability, the polymer grafts created on glassy carbon are thermally (the LCROP was performed at 130 ℃) as well as chemically stable under various reaction conditions. Furthermore, as shown in **Figure 67**, AFM measurements showed a significant thickness increase of the polymer structures from 159 ± 8 nm to 330 ± 10 nm after the LCROP. The layer thickness increase of approximately 108 % is attributed to the increase of the molecular mass of the grafted chains and the additional stretching of the backbone due to the crowding of the side chains. We also found that the deprotection of the Boc group results in a slight thickness decrease of approximately 5 % due to material loss.

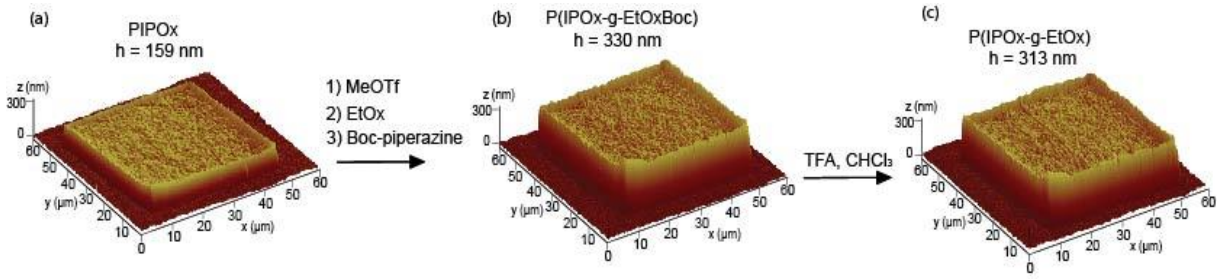

Figure 67. AFM 3D view of polymer brushes structure on glassy carbon. a) The SIPGP of IPOx for 40h through a stencil mask gives structured PIPOx brushes with a thickness of 159 ± 8 nm. b) The LCROP of EtOx and termination with N-Boc-piperazine results in 330 ± 10 nm thick P(IPOx-g-EtOxBoc) bottle-brush brushes. c) Same structure after deprotection of the side chain terminal Boc group.

Also for the second surface-initiated living cationic ring-opening polymerization (SI-LCROP), the thickness increase was investigated as a function of the polymerization time. For this, a PIPOx brush was prepared by SIPGP and then divided into three pieces. With each sample, SI-LCROP was performed using MeOx as the monomer for 60, 120, and 240 minutes (**Figure 68**) at 80 °C. The percentage of the respective thickness increase due to the formation of bottle-brush brushes with PMeOx side chains was found to be linear as shown in **Figure 69**. The systematic thickness increase demonstrates that the sensitive SI-LCROP can be performed in reproducible and consistent manner and individual SI-LCROP reactions can be compared. However, these experiments do not give a detailed picture about the grafting efficiency and the resulting polymer architecture. On the other hand, based on our experience with SI-LCROP using initiator functionalized self-assembled monolayers on planar substrates[54] and especially on nanoparticles,[141] this route to coat and functionalize a broad variety of surfaces[68] with the versatile POx has a high potential for the development of functional surfaces for the control of protein adsorption and cell adhesion which will be discussed in chapter 3.7.[204]

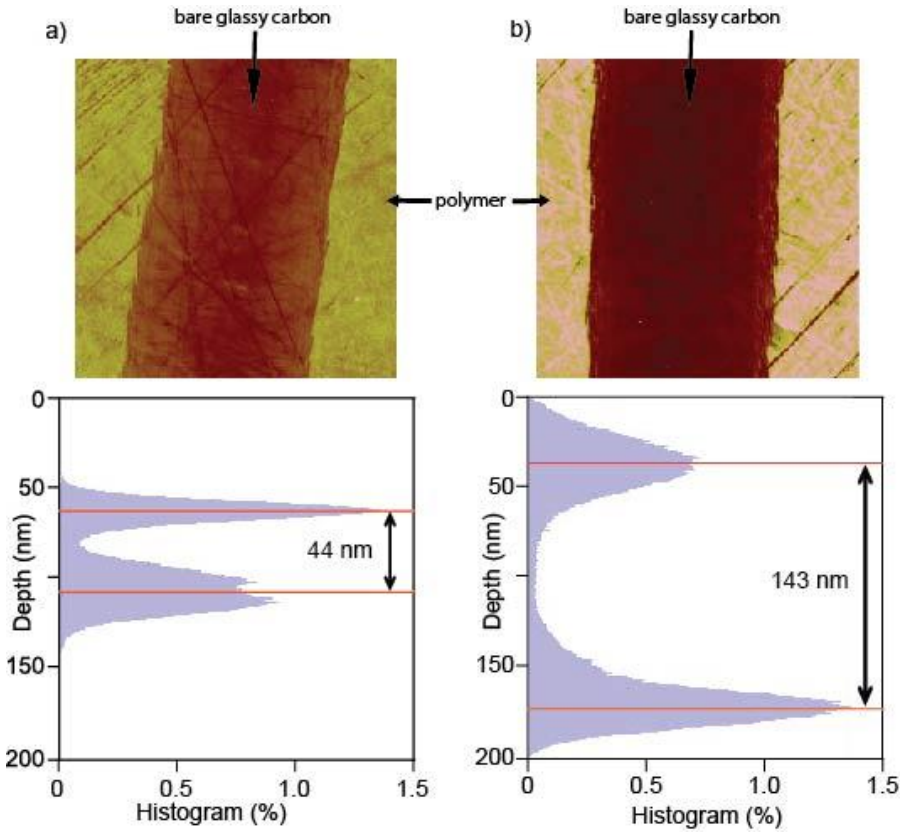

Figure 68. AFM scans of PIPOx and P(IPOx-g-MeOx) brush layer on polished glassy carbon a) PIPOx brush and depth analysis; b) P(IPOx-g-MeOx) brush after LCROP of MeOx for 4h and depth analysis.

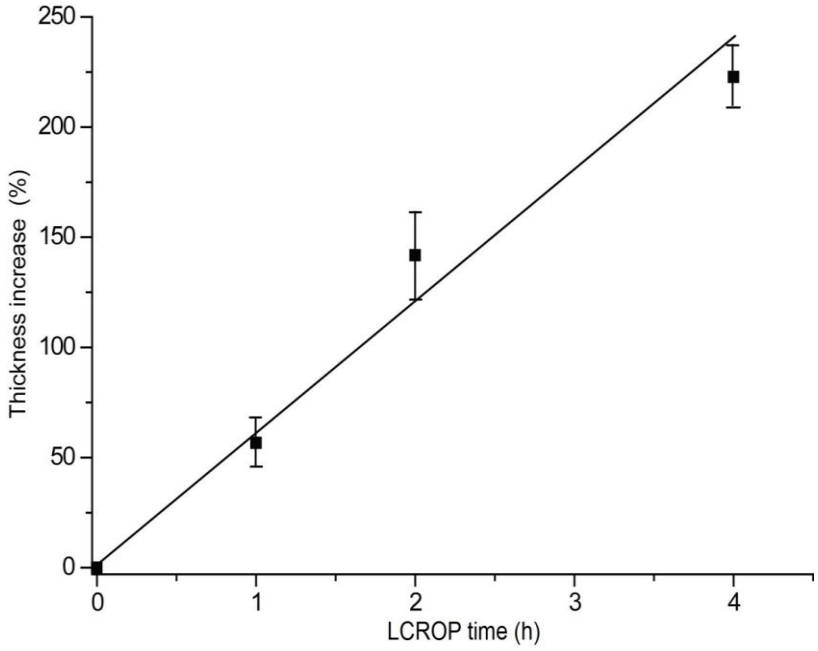

Figure 69. P(IPOx-g-MeOx) brush layer thickness on polished glassy carbon as a function of the cationic polymerization time as measured by AFM on structured polymer grafts (50×50 μm^2).

3.5.2.4 Wettability of the bottle-brush brushes

The projected use of polymer brushes in the biomedical field will require a broader choice of functional and biocompatible/bioresponsive surfaces. We have prepared molecular brushes in solution, the LCROP from the PIPOxOTf macroinitiator could be performed with different 2-alkyl-2-oxazolines. By changing the side chain composition, it is possible to change the hydrophobicity of the molecular brushes and to fine-tune the LCST temperature.

In order to demonstrate that bottle-brush brushes with a variety of side chains are accessible by an analogue approach, we have performed the LCROP from PIPOxOTf macroinitiator brush with different 2-alkyl-2-oxazolines under identical reaction conditions. We have tested 2-methyl-, 2-ethyl, 2-n-propyl- and 2-butyl-2-oxazoline (MeOx, EtOx, *n*PrOx and BuOx respectively). The influence of the bottle-brush brushes side chains on the hydrophilic/ hydrophobic character of the polymer coating was investigated by contact angle measurements (**Table 8**). The LCROP of the different 2-alkyl-2-oxazolines was performed under identical reaction conditions from homogeneous and unstructured PIPOxOTf brushes on glassy carbon. **Figure 70** shows that the hydrophilicity of the bottle-brush-brushes can be adjusted by the side chain composition.

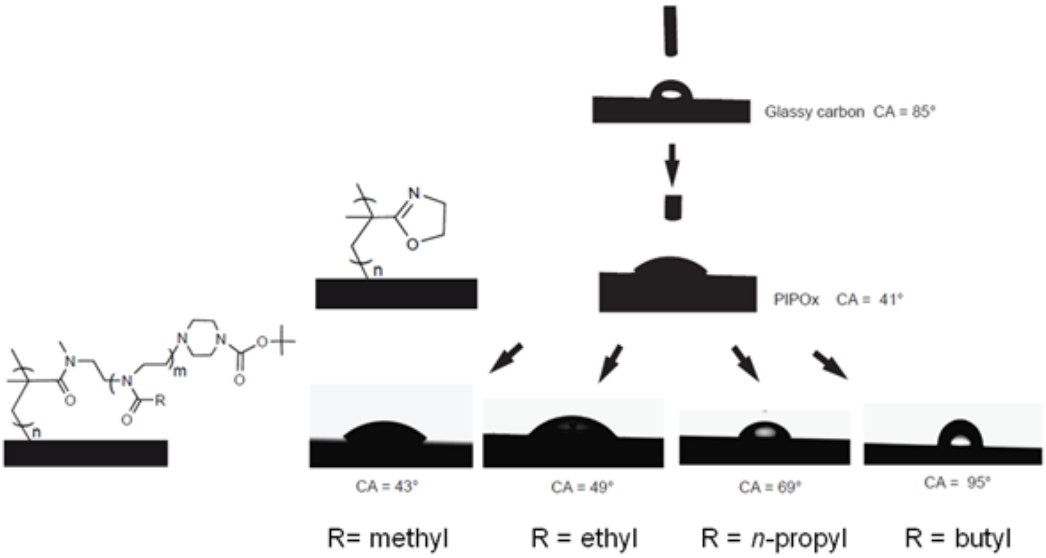

Figure 70. Static water contact angles of PIPOx and P(IPOx-g-2-alkyl-2-oxazoline) on glassy carbon.

Table 8. Static water contact angles of on different homogeneous polymer brush coatings on polished glassy carbon substrates. The PIPOx brushes were performed by the SIPGP of IPOx over night. The LCROP was performed at 130 ℃ by microwave heating for 20 minutes.

Substrate	Static contact angle (°)
Polished glassy carbon	85 ± 2
PIPOx	41 ± 3
P(IPOx-g-MeOxBoc)	43 ± 2
P(IPOx-g-EtOxBoc)	49 ± 2
P(IPOx-g-PrOxBoc)	69 ± 3
P(IPOx-g-BuOxBoc)	95 ± 2

It is noteworthy that part of LCROP reactions in this chapter were performed at 130 ℃ by microwave heating. This technique is an efficient method for performing the LCROP of 2-oxazoline, overcoming the long reaction times when carried out under conventional heating. Furthermore, the living character of the polymerization is retained under microwave irradiation.[185] In order to estimate the influence of the microwave irradiation, the LCROP of EtOx was performed from structured PIPOxOTf brushes on glassy carbon at 130 ℃ by conventional oil bath heating and in identical reaction conditions. AFM measurements revealed a thickness increase of approximately 97 % (from 150 nm for the PIPOx brushes to 293 nm for the P(IPOx-g-EtOxBoc)). Taking the experimental error into account, this result shows that the microwave irradiation do not accelerate significantly the surface initiated LCROP reaction.

3.5.2.5 Further functionalization of bottle-brush brushes

In order to demonstrate that the side chain terminal amino group (after deprotection of the Boc group) can be further functionalized, P(IPOx-g-EtOx) bottle-brush brushes were labeled with rhodamine B isothiocyanate (**Figure 64**). After intensive cleaning with ultrasound in ethanol in order to remove all physisorbed material, a strong fluorescence signal was detected selectively at the polymer modified surface (**Figure 71**), indicating that the fluorescent dye was covalently bonded to the polymer brushes. This experiment shows that despite the high crowding of polymer chains in such bottle-brush brushes, the side chain terminal amino group is still accessible for further functionalization, even with steric demanding organic molecules.

The functionalization of the terminal amino group of bottle-brush brushes with biomolecules (polysaccharides, proteins, etc.) will be the subject of future experiment.

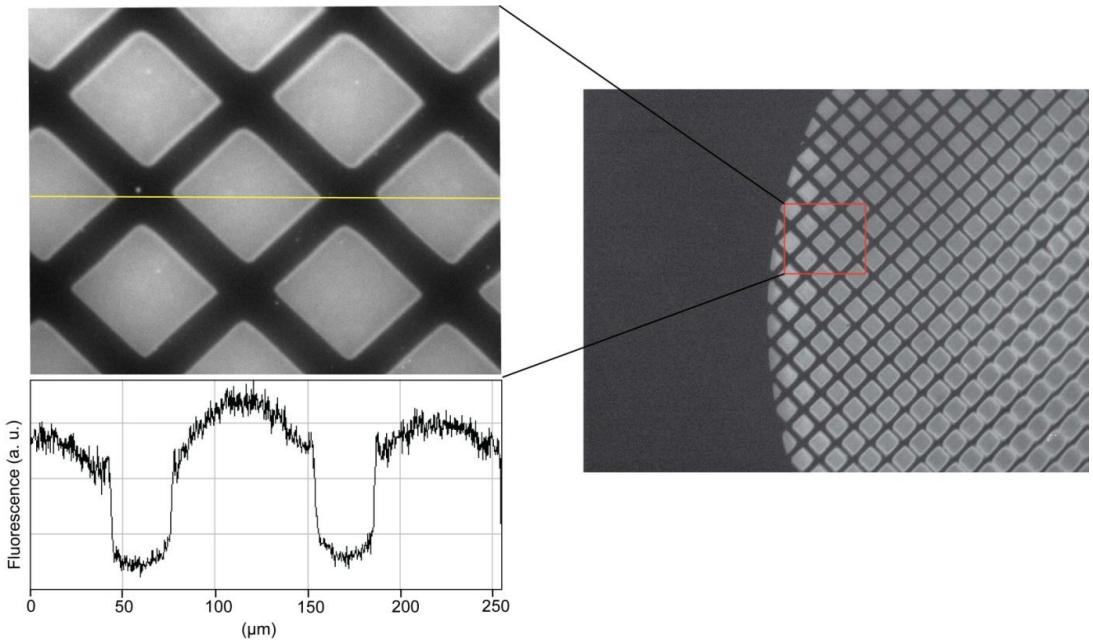

Figure 71. Fluorescence image and section analysis of a patterned P(IPOx-g-EtOx) bottle brushes labeled with rhodamine B isothiocyanate on glassy carbon. The bright regions are polymer brushes coated glassy carbon.

3.5.2.6 Stability test

To test the stability of the BBB coating, prolonged ultrasonication in toluene, acetate, ethanol and water 5minutes each was performed. These unusual drastic treatments had no significant effect on thickness as well as morphology as confirmed by IR and AFM analysis. Therefore, we used these cleaning procedures to remove the physisorbed polymer and clean the substrate.

In addition, BBBs coated substrates were boiled in solvents such as water, chloroform and toluene over night. Again, no influence can be found. Moreover, the polymer brush also showed very good stability in chemical harsh conditions such as strong acid (HCl, 1M) and base (NaOH, 1M) at 100 ℃ over night. These stability tests showed that the polymer layer was covalently attached to the glassy carbon substrate.

3.6 Bottle-brush brushes on self-assembled monolayers

3.6.1 Self-assembled monolayers

Self-assembled monolayers (SAMs) allow a defined modification of inorganic substrates such as gold, and oxidized surfaces.[186] For the preparation of SAMs, the inorganic substrate is immersed into a dilute organic solution of reactive molecules. The molecules (covalently) bind to the substrate and assemble into a monolayer. Typically, these reactive molecules are composed of a reactive anchor group which binds to the substrate and a mesogen in order to induce local order into the monomolecular layer. For example, n-alkyl thiols form S-Au bonds on gold substrate, yielding densely packed monolayers when the n-alkyl chains are longer than ten carbon atoms. Similarly, glass and silicon substrates can be modified with chloro- or alkoxy silanes.

Silicon wafers are ideal substrates for the study of surface initiated polymerizations (SIP) as they are relatively smooth (for AFM investigation), reflective (for spectroscopic investigations) and readily available. The surface of silicon consists of a thin layer of silicon oxide with silane functionalities. Thus, the treatment of silicon substrate with chlorosilanes or alkoxysilanes results in a polysiloxane network that is covalently linked to the native SiO_2 surface via siloxane bonds (**Figure 73**). Chlorosilanes are very sensitive to water, and generally form less-ordered SAMs than alkoxysilanes. Alkoxysilanes are utilized widely since they are less reactive and easier to handle. The preparation of SAMs on glass is identical to that of silicon substrates. Glass is optically transparent and can be thus characterized by UV-vis spectroscopy in the transmittance mode.

In the previous chapter, the self-initiated photografting and photopolymerization (SIPGP) of 2-isopropenyl-2-oxazoline (IPOx) on glassy carbon was described. Here, adapting this procedure, poly(2-isopropenyl-2-oxazoline) (PIPOx) brushes and bottle-brush brushes (BBBs) were created on aminosilane modified glass/ oxidized silicon and biphenylthiol modified gold substrates. Before the grafting of PIPOx brush on SAM modified substrate, attempts were made to grow PIPOx brush directly on silicon/ glass and gold substrates by SIPGP. However, no PIPOx brushes were found after SIPGP of IPOx due to the higher bond-dissociation energy of SiO-H bond on silicon/ glass and the absence of abstractable hydrogen on gold.

3.6.1.1 3-Aminopropyltrimethoxysilane monolayers

Silicon substrates and glass slides were first cleaned by a piranha solution (H_2SO_4/H_2O_2 (30 % aqueous solution) (v/v) = 3/1) and successively rinsed with deionized water. The water contact angles on oxidized silicon and glass substrates were nearly 10 °, revealing the high cleanness and uniformity of the surfaces. SAMs of 3-aminopropyltrimethoxysilane were prepared on these substrates according to a synthetic procedure shown in **Figure 73**. The water contact angle of SAM-modified substrates was found to be 55 ± 3 °. It has been reported previously that the contact angle of aminoalkoxysilane SAMs ranges from 40 ° to 63 °.[187,188,189,190] It has also been found that a 100% amino-terminated monolayer exhibit a contact angle of approximately 60 °.[191] Here, the contact angle of SAM modified samples is in good agreement previous studies.

3.6.2 Bottle-brush brushes on 3-aminopropyltrimethoxysilane modified oxidized silicon and glass substrates

3.6.2.1 Self-initiated photografting and photopolymerization

The 3-aminopropyltrimethoxysilane modified silicon substrate was submerged in 2-isopropenyl-2-oxazoline (IPOx) monomer and the self-initiated photografting and photopolymerization (SIPGP) was performed for 24 h with UV-light of a spectral distribution between 300 and 400 nm (λ_{max} = 350 nm). After 24 h of irradiation and thorough cleaning of the substrate in water, ethanol and ethyl acetate, AFM analysis revealed that a polymer layer with a thickness of 56 ± 4 nm was formed on the silicon substrate. The NH-H bond dissociation energy (BDE) of 3-aminopropyltrimethoxysilane was calculated to be approx. 97 kcal·mol^{-1}.[192] The formation of PIPOx brush on aminosilane functionalized substrate can be explained by the SIPGP mechanism in which surface hydrogen atoms from amino groups can be abstracted radically by excited IPOx molecules.

Structured PIPOx brushes with dimension of 50×50 µm^2 were created on aminosilane modified glass by SIPGP of IPOx with UV irradiation through a stencil mask (TEM grid) as shown in **Figure 72**. After 24 h UV irradiation, a 130 nm-thick polymer layer was formed on the glass substrate, which is around two times the thickness of PIPOx brush on silicon

substrate (56 nm after identical SIPGP time). This might be caused by the optical transparency of the glass substrate between 300 and 400 nm. The SIPGP experiments were performed by placing the substrate in between two identical UV lamps. For the transparent glass substrate, the UV intensity in the vicinity of surface is approximately two times of that on silicon substrate. Therefore, the PIPOx brush on glass substrate is twice as thick as on silicon substrate. This is in agreement with the results of Steenackers' PhD thesis.[66]

The successful modification of the silicon substrate by PIPOx brushes was further confirmed by infrared (IR) spectroscopy (**Figure 75**). The strong adsorption bands at 1648 cm^{-1} and 1128 cm^{-1} were assigned to the (C=N) and (C-O) stretching modes of the 2-oxazoline ring. Besides, the two bands at 987 cm^{-1} and 951 cm^{-1} originated from the ring skeletal vibration of the 2-oxazoline rings.

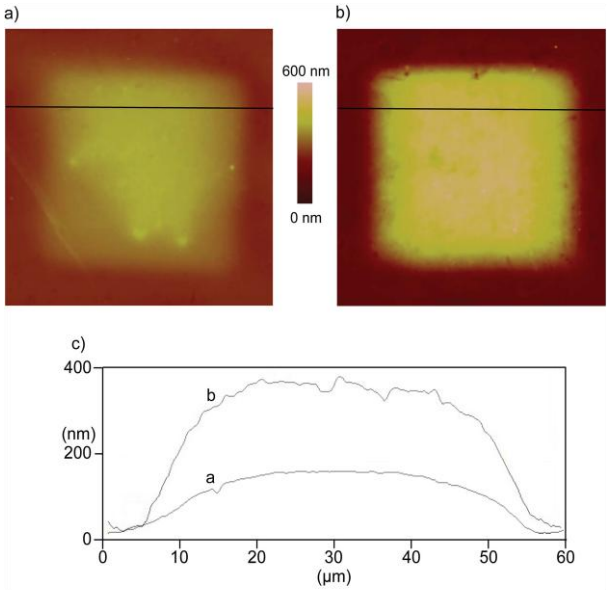

a) Structured PIPOx brush on glass slice (50µm× 50µm).
b) P(IPOx-g-MeOx) bottle-brush.
c) Section view of a and b.

Figure 72. AFM scans (60 × 60 μm^2) and section analysis of the structured polymer brush on glass. a) The SIPGP of IPOx for 24 h (λ_{max} = 350 nm) through a stencil mask results in structured PIPOx brushes with a thickness of 130 ± 15 nm on 3-aminopropyltrimethoxysilane modified glass substrate. b) The LCROP of 2-methyl-2-oxazoline (MeOx) from the surface bound macroinitiator results in bottle-brush brushes with a layer thickness of 340 ± 10 nm.

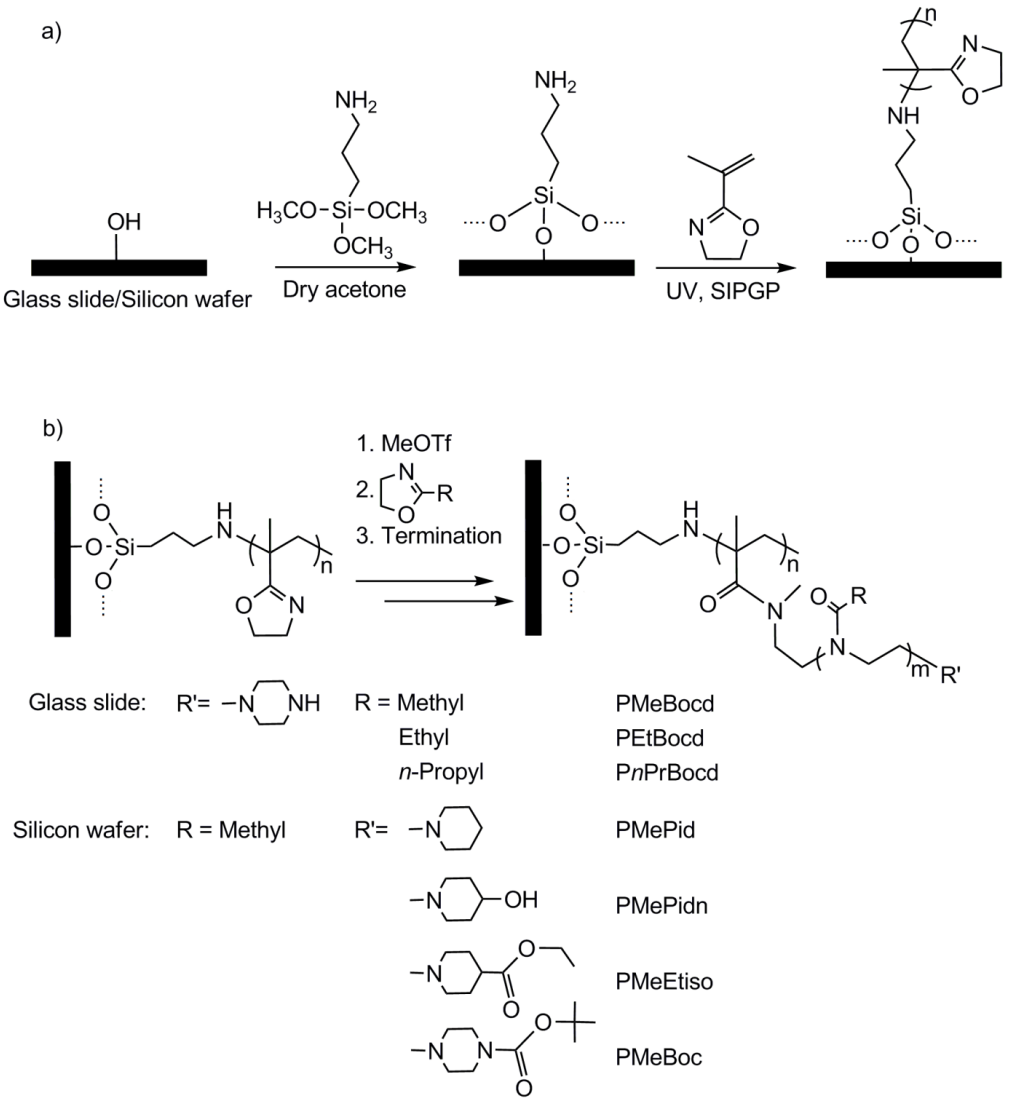

Figure 73. Preparation of bottle-brush brushes of poly(2-oxazoline)s on oxidized silicon or glass. a) Formation of aminopropyltrimethoxysilane monolayer on oxidized silicon /glass and successive creation of PIPOx brushes by SIPGP of IPOx on the formed monolayer. b) Conversion of the PIPOx brush to the surface bound macroinitiator by reaction with MeOTf and LCROP of 2-alkyl-2-oxazolines from the macroinitiator brush, followed by the termination of the side chain end with different terminal groups.

3.6.2.2 Surface-initiated living cationic ring-opening polymerization

Adapting the procedure for preparation of BBBs on glassy carbon, BBBs with PMeOx, poly(2-ethyl-2-oxazoline) (PEtOx) and poly(2-*n*-propyl-2-oxazoline) (P*n*PrOx) side chains were created on silicon/ glass substrates. In addition, in a series of experiments, various end groups i.e. piperidine, N-boc-piperazine, 4-piperidinol, and ethyl isonipecotate were

introduced into the BBBs. Here, different end groups provide a broad choice of functionalities for further functionalization and i.e. protein immobilization. The preparation of 3-aminopropyltrimethoxysilane self-assembled monolayer on oxidized silicon or glass substrates, SIPGP of IPOx and the LCROP of 2-oxazoines are summarized in **Figure 73**.

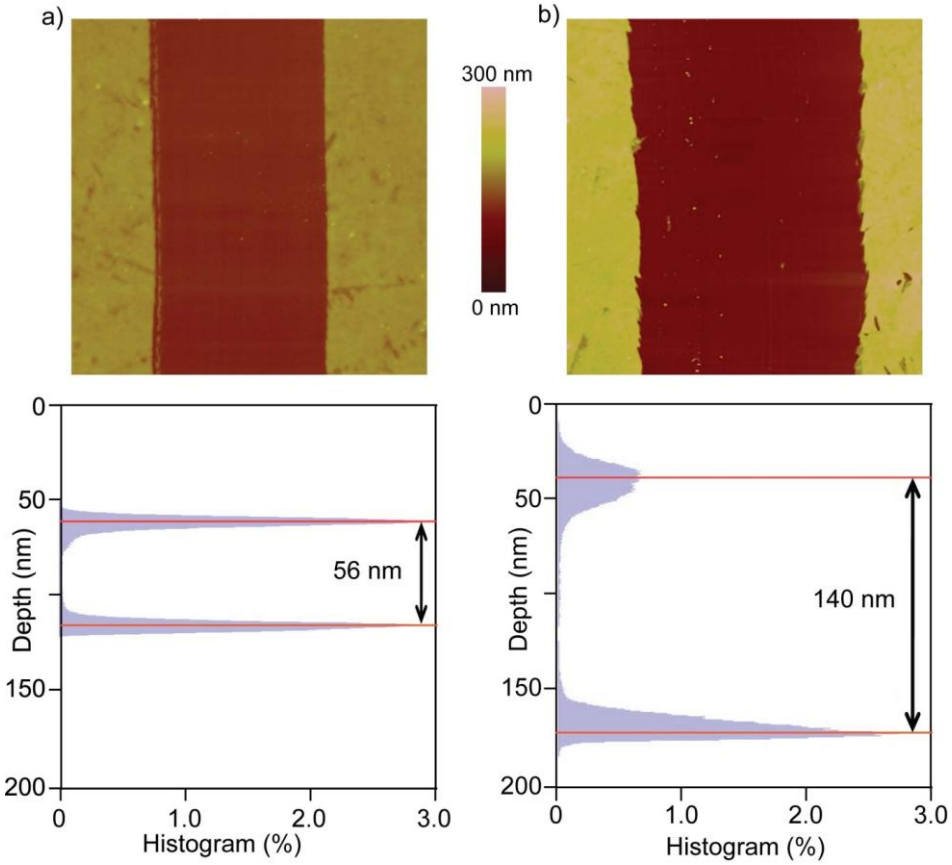

Figure 74. AFM scans (50 × 50 μm^2) and depth analysis of the polymer brush on oxidized silicon. a) The SIPGP of IPOx for 24 h (λ_{max} = 350 nm) results in 56 ± 3 nm thick PIPOx brushes on 3-aminopropyltrimethoxysilane modified silicon substrate. b) The LCROP of MeOx from the surface-bound macroinitiator results in a 140 ± 10 nm thick bottle-brush brush (the dark region is the bare substrate, the bright area is covered by BBB).

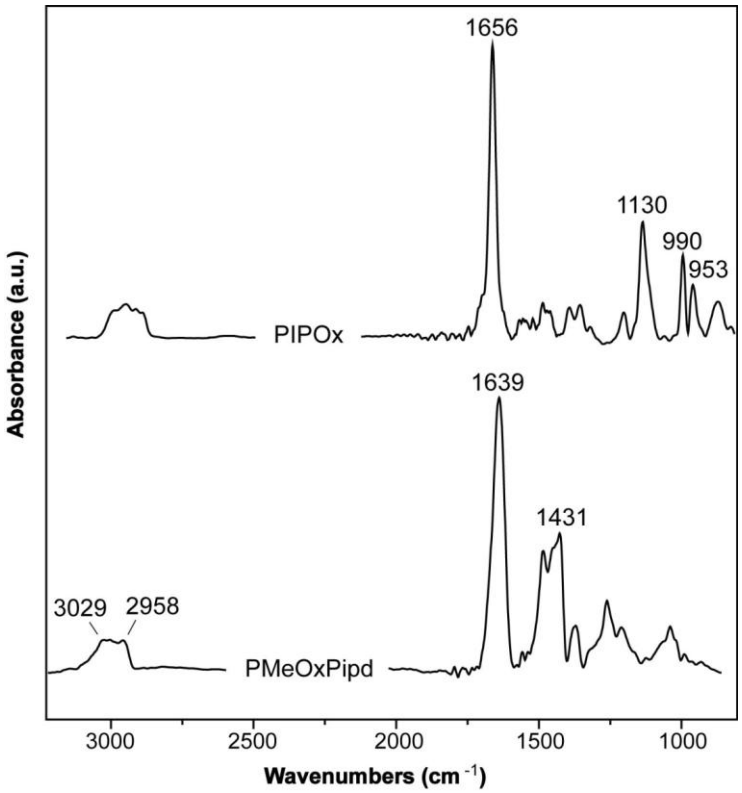

Figure 75. FT-IR spectra of PIPOx and PMeOxPipd brushes on oxidized silicon substate.

The successful conversion of PIPOx brushes to P(IPOx-g-MeOx) BBBs on oxidized silicon was confirmed by FT-IR spectroscopy (**Figure 75**). The (C=N) and (C-O) stretching bands (1656, 1130 cm^{-1}) and the two ring skeletal vibration bands (990, 953 cm^{-1}) from the 2-oxazoline ring disappeared and a new intensive band appeared around 1627 cm^{-1} which is characteristic for the carbonyl stretching mode of the amide function (amide I band). Moreover, the characteristic CH_x deformation modes for PMeOx were found at 1421 cm^{-1}. The complete disappearance of the bands from oxazoline ring indicates the full conversion from the pendant 2-oxazoline ring to poly(2-oxazoline)s.

Furthermore, AFM measurements showed a significant increase of the polymer layer thickness after the LCROP of MeOx for 4h, from 56 ±4nm to140 ±6 nm (**Figure 74**).

In summary, the presented method allows the formation of bottle-brush brushes of POx on silicon or glass substrates. The ease of chemical modification (by e.g. side chain variation and end group functionalization) allows a defined synthesis of a variety of functional surfaces for the design of soft interlayer between a semiconductor material and e.g. biological systems. These surfaces will be used in the last chapter of this work to investigate the protein adsorption and cell adhesion on BBB modified surfaces.

3.6.3 Bottle-brush brushes on self-assembled monolayers of biphenylthiol on gold

It has been reported that the electron beam irradiation of ω-functionalized biphenylthiol self-assembled monolayers (SAMs) causes lateral cross-linking of the biphenyl species.[69,193,194] The successive self-initiated photografting and photopolymerization (SIPGP) of vinyl monomers on such SAMs allows the formation of stable nanostructured polymer brushes on gold substrate.[69]

Here, SIPGP of 2-isopropenyl-2-oxazoline (IPOx) on nanostructured ω-functionalized biphenylthiol SAMs on gold which were selectively cross-linked and chemically modified by electron beam chemical lithography (EBCL) was investigated. The increasing extent of cross-linking for the SAMs caused the formation of PIPOx brushes with a gradient grafting density. As a consequence, a PIPOx brush with a gradient polymer layer thickness was obtained. Successive LCROP of 2-*n*-propyl-2-oxazoline (*n*PrOx) resulted in gradient bottle-brush brushes (BBBs).

Sören Schilp from the research group of Prof. Michael Grunze at the Universität Heidelberg prepared biphenylthiol SAMs on gold and irradiated them with a focused electron beam. As shown in **Figure 76**, the 4-mercapto-1,1′-biphenyl SAM on gold was structured and cross-linked by electron irradiation using a focused electron beam of a scanning electron microscope (SEM) coupled to a pattern generator (direct e-beam writing). The pattern generator allows the creation of almost any 2D structure. Furthermore, the applied electron dosage can be controlled within each structure. For a $10 \times 50\ \mu m^2$ gradient, a write field of 100 parallel $10 \times 0.5\ \mu m^2$ lines was created. The lines were written with linearly increasing electron dosage from 0 to 10 mC/cm^2 (corresponding to 0~1 as indicated in **Figure 77**). The electron beam induced lateral cross-linking of biphenylthiol SAMs, and therefore enhanced the stability of the monolayer due to the multiple adhesion sites of the entire SAM layer.

It is known that thiol-gold interaction can be photooxidize[60] and thiols desorbed from the gold surface during UV irradiation. However, the electron induced cross-linking renders the SAM stable at elevated temperature and UV irradiation. Depending on the applied electron dosage, the extent of the electron-induced cross-linking can be varied, which cause the formation of biphenylthiol monolayer with a gradual increase of cross-linking[66], thus resulting in SAM areas of increasing UV stability. On a basis of that, a successive SIPGP reaction occurs on a surface with increasing grafting sites, and therefore results in polymer brushes gradients.

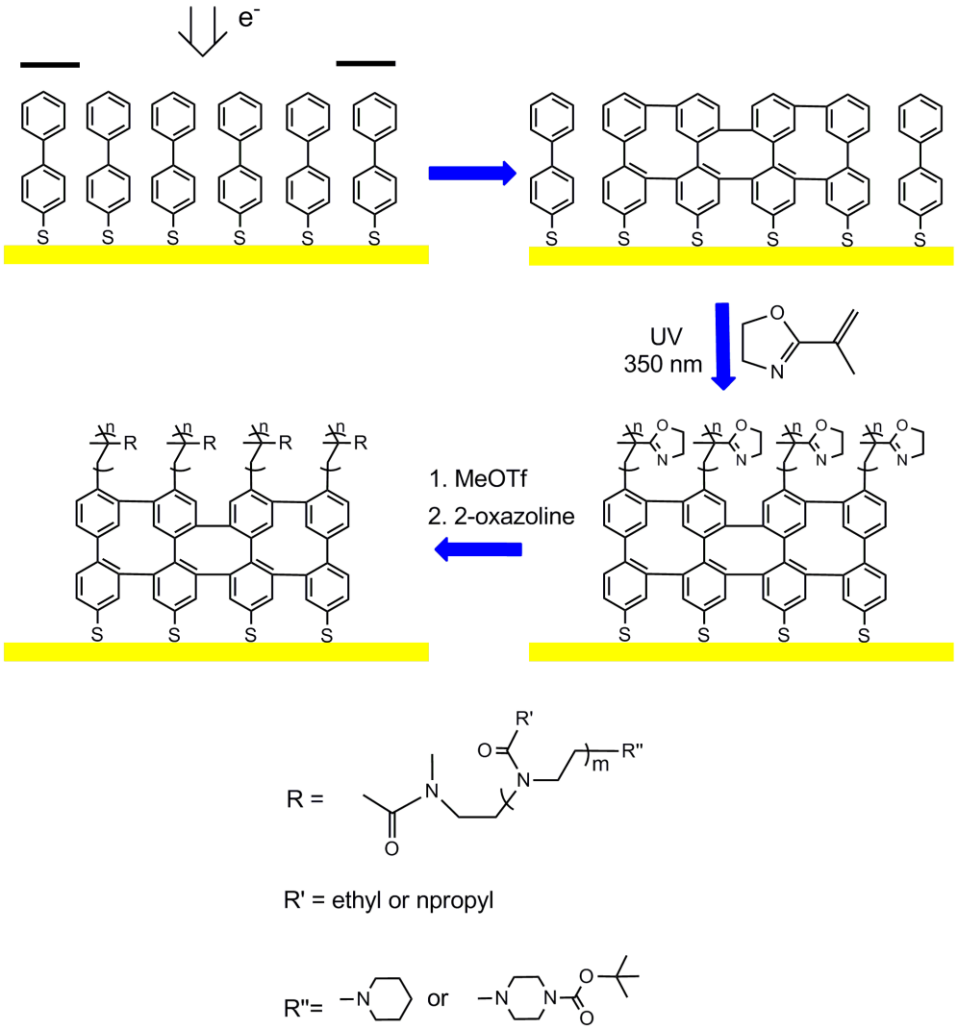

Figure 76. Schematic illustration of bottle-brush brushes (BBBs) formed on Au. (a) Electron beam irradiation of BT SAMs on gold, (b) Cross-linking of the biphenyl mesogen, (c) SIPGP of IPOx monomer with UV-irradiation results in patterned PIPOx brush, (d) LCROP of 2-oxazoline forms the BBBs structures.

Following the previously reported procedure for the SIPGP of styrene and acrylic monomers,[69] we performed photopolymerization of 2-isopropenyl-2-oxazoline (IPOx) on biphenyl thiol SAM as illustrated in **Figure 76**. After 16h UV irradiation, structured and gradient PIPOx brushes were formed on biphenyl thiol monolayer. **Figure 77** (A) shows AFM scans of the resulting polymer structure. Between 0 and 0.2 (corresponding to electron dosage 0 and 2 mC/cm^2), the thickness of PIPOx brush increases steadily and becomes constant between 2 and 10 mC/cm^2. As reported before, layer thickness of polymer brush prepared by SIPGP on EBCL modified SAMs strongly depended on the electron dosage. The polymer layer thickness increased with the applied electron dosage. However, after reaching to a maximum value at about 3-4 mC/cm^2, a further increase of applied electron dosage

resulted in a decrease of polymer layer thickness. In our study, the varying polymer layer thickness is ascribed to the not complete cross-linking of biphenyl molecules. This incomplete cross-linking decreases the number of grafting sites due to the partial desorption of the non-crosslinked molecules during photopolymerization. As a result, the polymer layer thickness varied. Comparing this gradient with our previous results on the morphology control of PS brushes prepared using the same technique,[69] the resulting polymer layer thicknesses of the gradient as a function of the electron beam irradiation dose are slightly different. This may be due to the different electron induced cross-linking of the two SAMs, different electron energy and pressure applied during the EBCL, and different monomers used for SIPGP. Another explanation might be the significantly enhanced stress of the sterical demanding BBB upon the surface attachment sites, namely the thiol-gold bond. Different to linear polymer brushes as in previous work, BBB of increasing grafting density will induce a quite significant stress since the effective grafting density is much higher. It has been reported by Sheiko et al. that C-C bond scission occurs when molecular brushes adsorb on surfaces and strongly interacts with the substrate.[49] The system relaxes by chain scission in the molecular brush backbone as well as side chains. Here, the crowding induced stress of BBB attached to a crosslinked monolayer might cause detachment of larger fractions of the coating which results in a decrease of the total layer thickness as a critical effective grafting density is reached.

The obtained PIPOx brushes were subsequently converted into the polycationic macroinitiator salt by submerging the modified gold substrate in a solution of methyl trifluoromethane-sulfonate (MeOTf). Successively, the LCROP of 2-*n*-propyl-2-oxazoline (*n*PrOx) was performed for 2h at 80 ℃ followed by termination by piperidine. After LCROP of *n*PrOx, the polymer layer thickness increased significantly from 59 nm to 112 nm at electron dosage of 10 mC/cm^2 (**Figure 77**). It should be noted that the shape of the gradient structure was well preserved after the LCROP, and no significant material loss could be observed.

In previous chapter it was discussed that molecular brush of P*n*PrOx side chain exhibited a lower critical solution temperature (LCST) at around 20 ℃. Accordingly, surfaces coated with BBBs of P*n*PrOx side chain are expected to show thermo-responsive properties. Crossing the critical solution temperature, the layer will become hydrophobic and collapse because of the bad solvent conditions. However, in temperature dependant measurements of the static water contact angle no changes of the BBB layer wettability was found within a temperature range from 15 ℃ to 50 ℃. Our finding is in contrast to the switching behavior of well studied thermo-responsive polymer i.e. poly-N-isopropyl acrylamide (PNIPAAm) coated

substrate. PNIPAAm in water undergoes a sharp phase transition at its LCST of 32 ℃. When grafted onto solid substrates, PNIPAAm brushes show a temperature-dependence in the physicochemical surface properties e.g. roughness[195], thickness and contact angle.[196] It was proposed that the rearrangement of the PNIPAAm chain at its critical temperature cause the drastic change of contact angle. However, for the BBBs of poly(2-oxazoline)s, both the SIPGP of IPOx via *grafting from* method and the side chain crowding resulted in the formation of densely packed polymer chains. This will significantly decrease the mobility of the polymer chains for the rearrangement. Therefore, the switching behavior of such dense polymer structure was not observed.

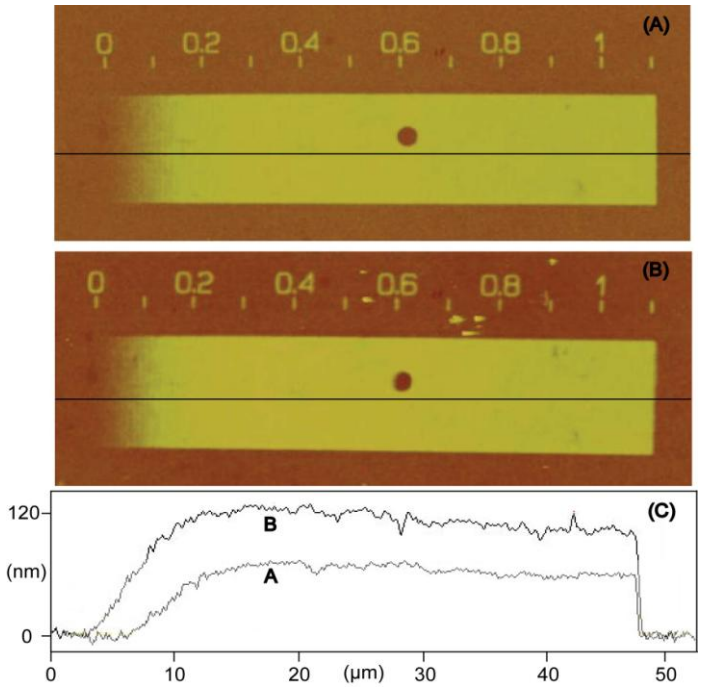

Figure 77. AFM images of bottle-brush brushes of POx on biphenylthiol gradient modified gold (maximum electron dosage = 10 mC/cm^2). (A) after SIPGP of IPOx for 16h, (B) after cationic ring-opening polymerization of *n*PrOx for 2h and terminated by piperidine, and c) section view of (A) and (B).

In summary, in this part of work, the preparation of structured bottle-brush brushes of poly(2-oxazoline)s of micro/nano scale on gold substrates is described. The polymer layer thickness can be directly controlled by the extent of electron-induced cross-linking of the SAM layer.

3.7 Protein adsorption and cell adhesion on bottle-brush brushes of poly(2-oxazoline)s

3.7.1 Background

Protein adsorption and its induced responses including cell adhesion are able to largely influence the biomaterial performance and are key criteria in the fields of biosensing and bioengineering.[82,84,83,197] Proteins tend to adsorb nonspecifically to most surfaces and by this impair the performance of surface based devices.[198] To cope with this problem several strategies to suppress nonspecific protein adsorption, non fouling surfaces have been developed and extensively investigated.[199] Non fouling polymer surfaces are referred to as surfaces which are resistant towards the adsorption of proteins.[90,200] In the past decades, a variety of polymers have been investigated to realize non fouling surfaces.[90,91,92,93,94,95] However, only few were reported to meet the practical applications.

Poly(ethylene glycol) (PEG) is up to now the most studied polymer for the prevention of the protein adsorption and unwanted cells adhesion *in vitro* and *in vivo*.[201] It has good solubility in most solvents, enabling chemical modification on its terminal hydroxyl groups.[202] However, PEG coatings may lose their function in complex biological fluids and can undergo oxidative degradation when used for longer time.[98,99,100] Moreover, the PEG system mainly contains primary hydroxyl terminal group which can be modified. Owing to the deficiency of modifiable functional groups, the possibility for specific end group modifications are not achievable, which is in most cases desirable for various applications. A potential solution is to introduce additional functional groups into PEG system, but this has been reported to alter its properties significantly and probably result in negative coating performance.[101, 203] Consequently, there is a continuous need for the development of alternative polymers to overcome such problems in practical applications.

In search of non fouling polymers, poly(2-oxazoline)s (POx) came into focus as a potential alternative to the well studied PEG systems.[113,116,204] It has been reported that surfaces coated with this type of polymer have quantitatively equal properties as PEG-based coatings and are similarly resistant toward nonspecific protein adsorption.[204, 205] Additionally, the living cationic ring-opening polymerization (LCROP) of 2-substituted-2-oxazoline provides synthetic possibilities to tailor macromolecules with a broad selection of side and end

functions, which enables the polymer with a broad variety of architectures and composition.[206,207,208,209,210,211,212]

For example, Konradi et al. have investigated the protein adsorption on comb polymer consisting of hydrophilic poly(2-methyl-2-oxazoline) (PMeOx) side chains and a polycationic backbone.[204] The positively charged comb polymer adsorbed on negatively charged surface through coulomb interaction. Such coatings with an optimal side chain grafting density strongly reduce protein adsorption to a value of less than 2 ng/cm^2, which is quantitatively equal to the performance of PEG coatings. However, the electrostatic adsorbed coating is prone to desorption at certain conditions and especially in biological environment with higher salt concentration and thus, a covalent attachment is preferable.

In this part of the work, oxidized silicon surfaces were modified with various bottle-brush brushes (BBBs) of neutral POx. As described in previous chapters, the polymer is covalently attached onto the surface, which prevents the desorption of polymer chains. To examine the biocompatibility of POx coatings, protein adsorption and cell adhesion on BBBs modified solids were investigated. Moreover, the influence of the polymer structure e.g. side chain composition, side chain length and terminal groups on its bioadsorption properties is discussed.

3.7.2 Bottle-brush brushes of poly(2-oxazoline)s on oxidized silicon substrate

Bottle-brush brushes (BBBs) of poly(2-oxazoline)s (POx) with different side chains /end groups were prepared on oxidized silicon and characterized with respect to their contact angle and polymer layer thickness. The results are summarized in **Table 9**.

Sample 1-4 are BBBs of POx with a variation of the pendant chain end groups. For sample preparation, the PIPOx coated substrate was first divided into four pieces, and converted to the macroinitiator brush by methyl triflate (MeOTf), and successively LCROP of 2-methly-2-oxazoline (MeOx) was allowed to proceed for 4 h. Finally, the LCROP was terminated with piperidine, N-boc piperazine, 4-piperidinol, and ethyl isonipecotate, respectively, introducing different end groups in the pendant chains of BBBs. Significant increase of polymer layer thickness was observed after the formation of BBBs. For example, the polymer layer thickness increased by 128 % from 57 ± 7nm (PIPOx) to 130 ± 5nm for sample 2 (end group

is piperidine). However, the contact angle after formation of BBBs only showed minor changes. Contact angles of PIPOx changed from 49 ° to 46 °, 49 to 44 °, 49 ° to 33 °, 49 ° to 42 ° for sample 1, 2, 3 and 4, respectively. The minor effect of end groups on the contact angles is expectable and can be interpreted by the surface rearrangement of the flexible polymer brush layer upon change of the solvent quality/ polarity.

Sample 5-7 are BBBs of POx with a variation of the side chain composition. As above, a PIPOx modified substrate was divided into three pieces and LCROP of MeOx, 2-ethyl-2-oxazoline (EtOx) and 2-*n*-propyl-2-oxazoline (*n*PrOx) were performed. All these samples were finally treated with piperidine to terminate the living polymerization. Drastic thickness increase was also observed for these samples. In addition, the surface wettability was found to change significantly after LCROP. Specifically, water contact angles were found to be 38 °, 43 ° and 56 ° for BBBs of PMeOx, PEtOx and P*n*PrOx side chains. These values are consistent with the ones of BBBs on glassy carbon as described in Chapter 3.5.2.

Sample 8-11 are BBBs of POx with a variation of the hydrophilic side chain length. Similarly, a substrate with a PIPOx brush was divided into four pieces. LCROP of MeOx was allowed to proceed at 80 ℃ for 0h, 1h, 2h and 4h respectively. Here, the increase of BBBs thickness was investigated as a function of the LCROP polymerization time. The percentage of the thickness increase due to the formation of BBBs was found to be linear against reaction time. In addition, the contact angle of BBBs varied significantly with the different length of side chains e.g. from 71 ° for sample 8 (LCROP = 0h) to 43 ° for sample 11 (LCROP = 4h). The results indicated that the surface wettability of BBBs increased with increasing length of the hydrophilic side chain. However, the comparison between sample 10 and sample 11 revealed that further increase of the side chain length only showed minor effect on the contact angle value.

Table 9. Preparation of bottle-brush brushes of 2-oxazolines on oxidized silicon and characterization with regard to the water contact angle and the polymer layer thickness.

Sample	Side chain/ CROP time	End groups (R)	CA[a] (PIPOx)	CA[a](after LCROP)	Thickness[b] (PIPOx)	Thickness[b] (after LCROP)
1.PMeBoc	MeOx/4h	N-Boc-piperazine	49 ± 2 °	46 °	49 ± 5nm	101 ± 6nm
2.PMePid		piperidine	49 ± 2 °	44 °	57 ± 7nm	130 ± 5nm
3.PMepidn		4-piperidinol	49 ± 2 °	33 °	54 ± 5nm	117 ± 7nm
4.PMeetiso		ethyl isonipecotate	49 ± 2 °	42 °	51 ± 6nm	110 ± 5nm
5.PMe	MeOx/4h	piperazine	51 ± 2 °	38 ± 3 °	67 ± 8nm	245 ± 7nm
6.PEt	EtOx/4h		51 ± 2 °	43 °	73 ± 9nm	260 ± 11nm
7.P*n*Pr	*n*PrOx/4h		51 ± 2 °	56 ± 3 °	78 ± 9nm	267 ± 10nm
8.PMe0	MeOx/0h	piperidine	50 ± 2 °	71 ± 3 °	43 ± 9nm	54 ± 8nm
9.PMe1	MeOx/1h		50 ± 2 °	51 ± 2 °	42 ± 6nm	62 ± 7nm
10.PMe2	MeOx/2h		50 ± 2 °	45 ± 2 °	51 ± 7nm	82 ± 6nm
11.PMe4	MeOx/4h		50 ± 2 °	43 ± 2 °	50 ± 6nm	116 ± 5nm

a: Static water contact angle (CA) was measured at room temperature (25 °C).

b: Polymer brush thickness was determined by AFM depth analysis.

3.7.3 Protein adsorption

The protein adsorption and cell adhesion measurements were performed by Dr. Tilo Pompe from the research group of Prof. Carsten Werner at the Max Bergmann Center of Biomaterials, TU Dresden/Leibniz Institute of Polymer Research Dresden.

Fibronectin is a high molar mass glycoprotein which is involved in many cellular processes. Here, it serves as a model protein for the investigation of adsorption properties on BBBs. Briefly, BBBs were immersed in 70 % ethanol/water to provide sterile conditions for cell culture. Thereafter, BBBs were immersed in a 50 µg/mL fibronectin (purified from human plasma) solution in phosphate buffered saline (PBS) at pH 7.4 and 37 °C for 1 h. Carboxytetramethylrhodamine was used to label fibronectin prior to the experiments. Non-adsorbed fibronectin was removed by rinsing twice with PBS. Finally, the fluorescence microscopic analysis was performed on the protein adsorbed BBBs surfaces. **Figure 78** shows the fluorescent images of BBBs with a variation of side chain composition i.e. P*n*PrOx, PEtOx and PMeOx after the fibronectin culture. Strong fluorescence could be detected on

BBBs with P*n*PrOx side chain. However, almost no fluorescence signal was found on BBBs with PMeOx and PEtOx side chains. It indicates the protein adsorption is strongly affected by the side chain composition of BBBs. Likewise, the influence of side chain length and end group of BBBs side chains was investigated by fluorescence microscopic analysis as well. Results confirm the significant effects of BBBs structure on the adsorption behavior of fibronectin (Fluorescent images are not shown here).

Additionally, fibronectin adsorption was quantified using fluorescence intensity per unit area. The amount of adsorbed fibronectin on different surfaces was plotted together with that on poly(octadecene-*alt*-maleic anhydride) POMA coated surface, which was used as a reference because it exhibits a large adsorption of fibronectin (～600 ng/cm^2) via stable amide bonds. In the following part, the quantification of protein adsorption on different BBBs surfaces as well as the manipulation of the BBBs will be particularly analyzed and discussed.

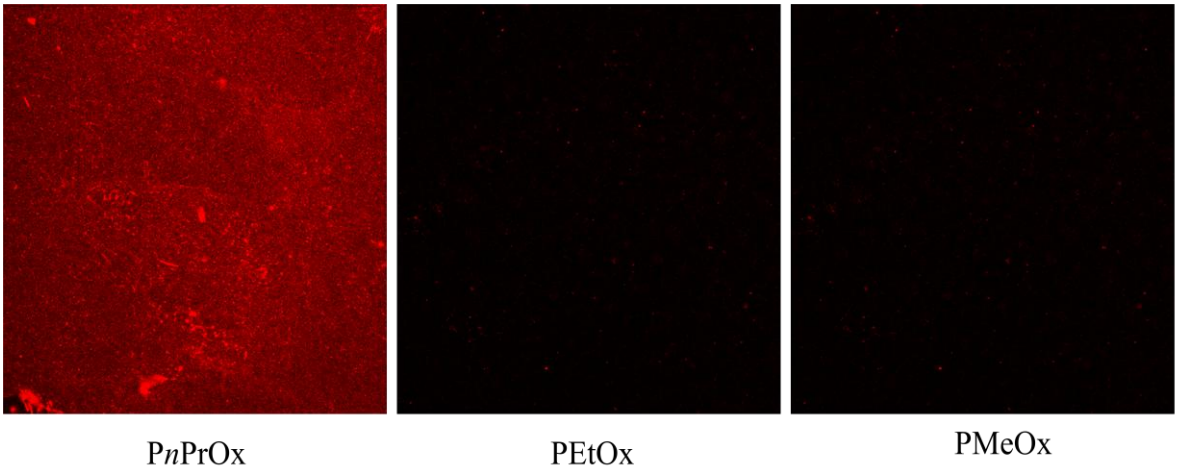

Figure 78. Fluorescent images of BBBs with P*n*PrOx, PEtOx and PMeOx side chains after 1 hour fluorescent-labeled fibronectin culture.

3.7.3.1 Variation of the BBB side chain composition

The amount of adsorbed fibronectin on BBBs with a variation of side chains was investigated and results are shown in **Figure 79**. BBBs with PMeOx and PEtOx pendant chains (Sample 5 and 6) efficiently suppressed protein adsorption down to a value of 6 ng/cm^2, demonstrating an excellent non fouling property of BBB surface. However, a different result was obtained

for protein adsorption on BBB with P*n*PrOx pendant chains (Sample 7), where a high amount of adsorbed fibronection (90 ng/cm^2) was observed. This significant difference may be ascribed to the altered hydrophilicity of POx coatings. In general, hydrophobic interaction is expected to play an important role in the protein adsorption. A hydrophobic surface renders a higher adsorption of proteins, whereas a hydrophilic surface repels the approaching proteins, resulting in a sharply reduced adsorption. In this study, the BBBs surfaces are believed to be manipulated markedly hydrophilic with PMeOx and PEtOx pendant chains (Sample 5 and 6), which greatly impeded the adsorption of fibronectin. However, the BBB modified with P*n*PrOx pendant chains (Sample 7) is slightly hydrophobic, therefore, the amount of adsorbed fibronectin on the surface is higher.

Approving above assumption, the water contact angles of BBBs with variable side chain composition were investigated and the results are listed in **Table 9**. BBBs with PMeOx and PEtOx side chains showed water contact angles of 38 ° and 43 ° at both room temperature and 37 ℃ (the temperature that the protein adsorption experiments were performed). This indicates a pronounced hydrophilic property of the surfaces. However, BBB with P*n*PrOx side chains exhibited water contact angles of 56 ° at room temperature and 60 ° at 37 ℃, thus a more hydrophobic surface. These results are consistent with the protein adsorption behavior. Additionally, the observation corroborates the criteria for designing non fouling polymers i.e. manipulation of surface hydrophilicity is a key factor for the prevention of nonspecific protein adsorption.

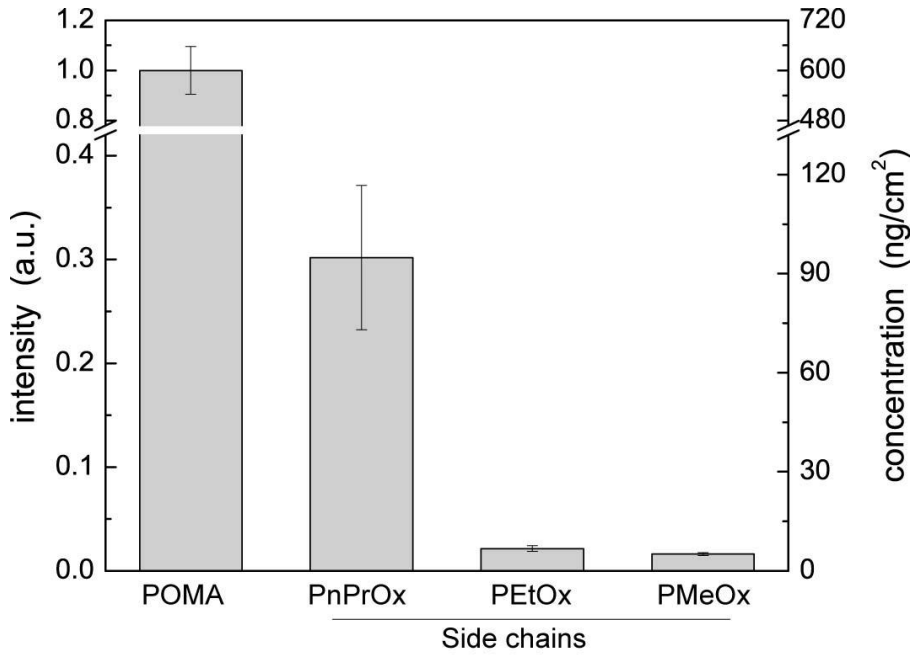

Figure 79. The amount of adsorbed fibronectin as a function of BBBs side chains i.e. P*n*PrOx, PEtOx and PMeOx side chains.

3.7.3.2 Variation of the BBB side chain length

As a second parameter, side chain length of the BBBs was varied and its influence on the protein adsorption was investigated. Briefly, PMe1 (Sample 9) which was prepared from 1 h LCROP of MeOx, represents BBBs with short side chains; PMe2 (Sample 10) from 2 h LCROP of MeOx represents BBBs with middle side chains; and PMe4 (Sample 11) from 4 h LCROP of MeOx represents BBBs with long side chains. It should be noted that PMeOx is very hydrophilic, therefore, the prepared BBBs are expected to reduce the adsorption of proteins greatly.

Figure 80 shows the amount of adsorbed fibronectin on BBBs with a variation of side chain length. For short side chain BBBs, a protein adsorption concentration of 45 ng/cm^2 was observed. As the side chain length increases, a significant decrease in protein adsorption was revealed. Protein adsorption concentration of 11 ng/cm^2 was observed for BBBs with both middle side chains and long side chains. Evidenced by the above results, it seems reasonable to conclude that protein adsorption can be influenced by side chain length of BBBs. However, it is worth noted that the polymer layer thickness of these three BBBs surface is in fact not comparable. As shown in **Table 9**, the polymer layer thicknesses were found to increase by 48 %, 61% and 132 % after LCROP of MeOx for 1 h, 2h and 4h, respectively. It suggests a

large difference in polymer layer thickness between BBBs of PMe1, PMe2 and PMe4. To determine whether the polymer layer thickness of BBBs in this case plays a key role in the protein adsorption, the following experiments were performed.

Protein adsorption on BBBs possessing the same PMeOx side chain length but different polymer layer thickness was compared. Here, BBBs with layer thicknesses of 130 nm (Sample 2), 116 nm (Sample 11) and 51 nm (no shown in this study) are used as the model BBBs for comparison. The protein adsorption on these BBBs surfaces was quantified, revealing the adsorbed protein concentration of 12, 11 and 8 ng/cm^2 for BBBs with layer thicknesses of 130 nm, 116 nm and 51 nm, respectively. Compared with BBBs of different side chain length, results here produced a somewhat opposite correlation between protein adsorption and polymer thickness. However, the difference in the protein adsorption concentration is in fact too small (within 4 ng/cm^2), which is most likely caused by the experimental error. By all means, the decreased polymer layer thickness does not show a significant effect on protein adsorption.

Based on the discussion above, it is more reasonable to conclude that the side chain length played the key role in the protein adsorption properties of BBBs. As the hydrophilic side chain length increases, the surface wettablity increases accordingly. As a result, a reduced amount of adsorbed protein was observed. Actually, water contact angles for the BBBs with short, middle and long PMeOx side chains were found to be 51 °, 45 ° and 43 ° respectively, which was in a good agreement with the above explanation. Again, this result corroborates the criteria for designing non fouling surfaces i.e. hydrophilic surfaces impede the nonspecific protein adsorption.

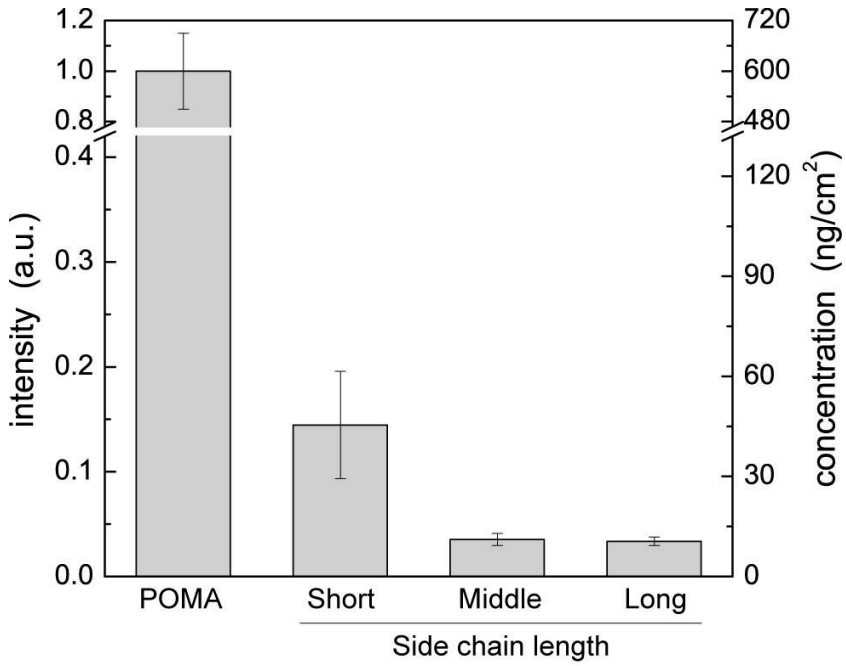

Figure 80. The amount of adsorbed fibronectin on BBBs with PMeOx side chain as a function of side chain length.

3.7.3.3 Variation of the BBB pendant chain end groups

In addition to the variation of side chain composition and side chain length, the biocompatibility of BBBs can also be influenced by the pendant chain end groups. Various chain termini (piperidine, N-boc piperazine, 4-piperidinol, and ethyl isonipecotate) were introduced to the BBBs side chain end to examine the effect of the end groups upon the protein adsorption behavior. Small changes in protein adsorption on the BBBs could be observed (**Figure 81**) after the introduction of different end groups, which is probably because, a) very little amount of adsorbed proteins limit the accuracy of measurement and, b) a small portion of end groups contained in the entire polymer layer contributes little to the protein adsorption. However, the successful introduction of different end groups provides the possibility for further functionalization e.g. protein immobilization.

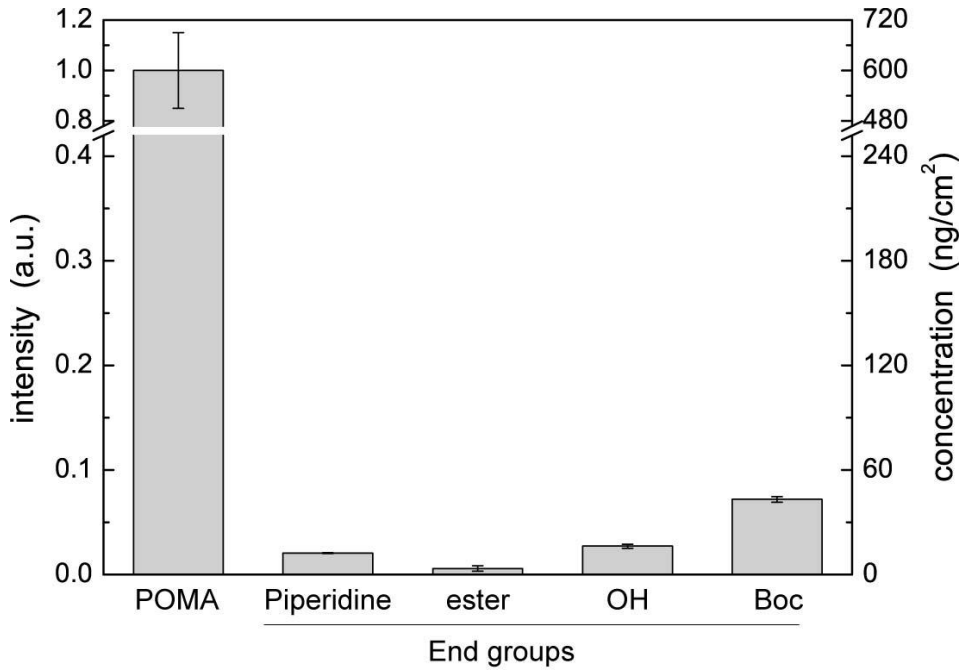

Figure 81. The amount of adsorbed fibronectin on BBBs with PMeOx side chain as a function of end groups.

3.7.4 Cell Adhesion

The control of cell adhesion onto biomaterials is one of the key points in tissue engineering. Under physiological conditions, it is generally accepted that the adhesion of cells to a solid surface is mainly mediated by the presence of a protein layer, which promotes the attachment and determine the final cellular response. In this part of work, cell adhesion experiments were performed in conjunction with the protein adsorption studies. Specifically, human endothelial cells were seeded on the fibronectin adsorbed BBBs. After 1h cell culture, the cell cultured samples were fixed and stained and the density and spreading state of human endothelial cells were evaluated by fluorescence microscopy. As shown in **Figure 82a-5c**, an increase in the amount of adsorbed fibronectin caused an increased cell adhesion which was evidenced by the increased density of attached cells and enlarged area of cell spreading. In **Figure 82d**, no adherent cells were observed, where BBB with PMeOx side chains of medium length and piperidine end group was used as testing surface. It indicates the POx BBBs not only efficiently prevent the protein adsorption, but successively inhibit cell adhesion onto the protein adsorbed polymer layer.

These cell adhesion studies nicely support the results of the protein adsorption experiments outlined above. Furthermore, they demonstrate the ability of the POx BBBs system to tune the protein adsorption and cell adhesion, and additionally to provide specific chemical end groups for further functionalization strategies.

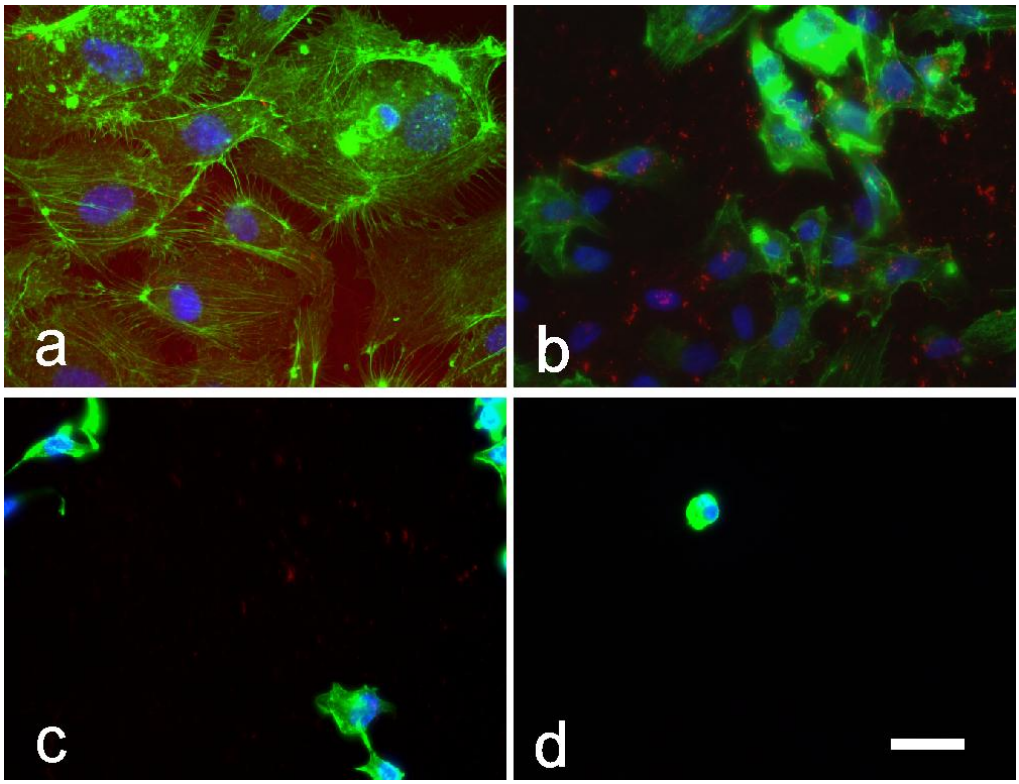

Figure 82. Fluorescence images of cell adhesion on different fibronectin-adsorbed BBBs of POx. In correlation to the amount of adsorbed fibronectin, different degrees of cell adhesion can be observed on POx BBBs surfaces: (a) very good cell adhesion with highly spread cells on BBB with P*n*PrOx side chains of medium length and piperidine end group, (b) good cell adhesion with spread cells on BBB with PMeOx side chains of medium length and Boc end groups, (c) not good cell adhesion with few and almost unspread cells on BBB with PMeOx side chains of medium length and OH end groups, (d) no cell adhesion on BBB with PMeOx side chain of medium length and piperidine end group. [fibronectin (red), actin (green), and nuclei (blue). Scale bar: 50 µm.]

In summary, the protein adsorption and the successive cell adhesion on various BBBs of POx was studied. Quantification of adsorbed protein reveals that, the manipulation of polymer composition and architecture can greatly influence the biocompatibility of the resulting BBBs surfaces. Specifically, (1) BBBs with very hydrophilic PMeOx and PEtOx side chains show no or significantly reduced protein adsorption as compared to more hydrophobic BBBs with P*n*PrOx side chains, (2) Given the same side chain composition, a stronger protein resistance

is observed for BBBs with longer hydrophilic side chains, which is also ascribed to the increased surface wettability of BBBs. (3) Side chain end groups influences the bioadsorption properties as well, however, the influence is minor. The cell adhesion experiments revealed the amount of adhered cells on protein layers, which nicely supported the quantification results of protein adsorption. This study may open up the possibility for broadening the choice of protein resistant surfaces in the future.

Chapter 4 Summary

In this work, the first synthesis of well-defined molecular brushes based on poly(2-oxazoline)s is described. Molecular brushes have been synthesized via the combination of free radical/ as well as anionic polymerization of 2-isopropenyl-2-oxazoline (IPOx) (for the backbone) and living cationic ring-opening polymerization (LCROP) of 2-oxazolines (for the side chains) through the "*grafting from*" method (**Figure 83**). For the brush molecules with a backbone made by free radical polymerization, the polydispersity index (PDI) is relatively broad due to the uncontrolled character of the reaction. However, in the case of the backbone prepared by living anionic polymerization, molecular brushes with relatively narrow PDI in both the backbone and the side chains were achieved.

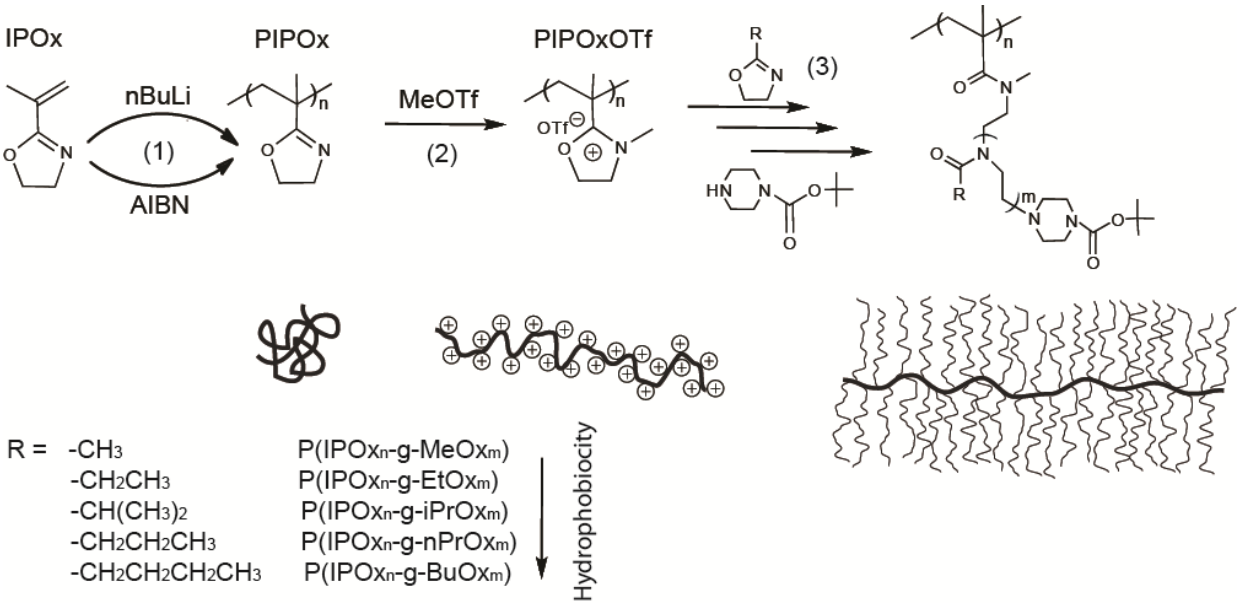

Figure 83. Scheme for the synthesis of molecular brushes of poly(2-oxazoline)s: (1) backbone by free radical as well as anionic polymerization, (2) synthesis of the macroinitiator, (3) Synthesis of pendant chains by living cationic ring-opening polymerization.

The *grafting from* polymerization of 2-oxazoline e.g. 2-*n*-propyl-2-oxazoline (*n*PrOx) and 2-iso-propyl-2-oxazoline (*i*PrOx) from the macroinitiator follows linear first order kinetics and the molar mass of the resulting polymers increases with the monomer conversion. It was shown that the apparent polymerization rate for each intitiation function is independent of the size of the macroinitiators and the initiating sites are of equal reactivity. As consequence, well

defined molecular brushes with high grafting densities of pendant chains of equal length can be realized (**Figure 84**).

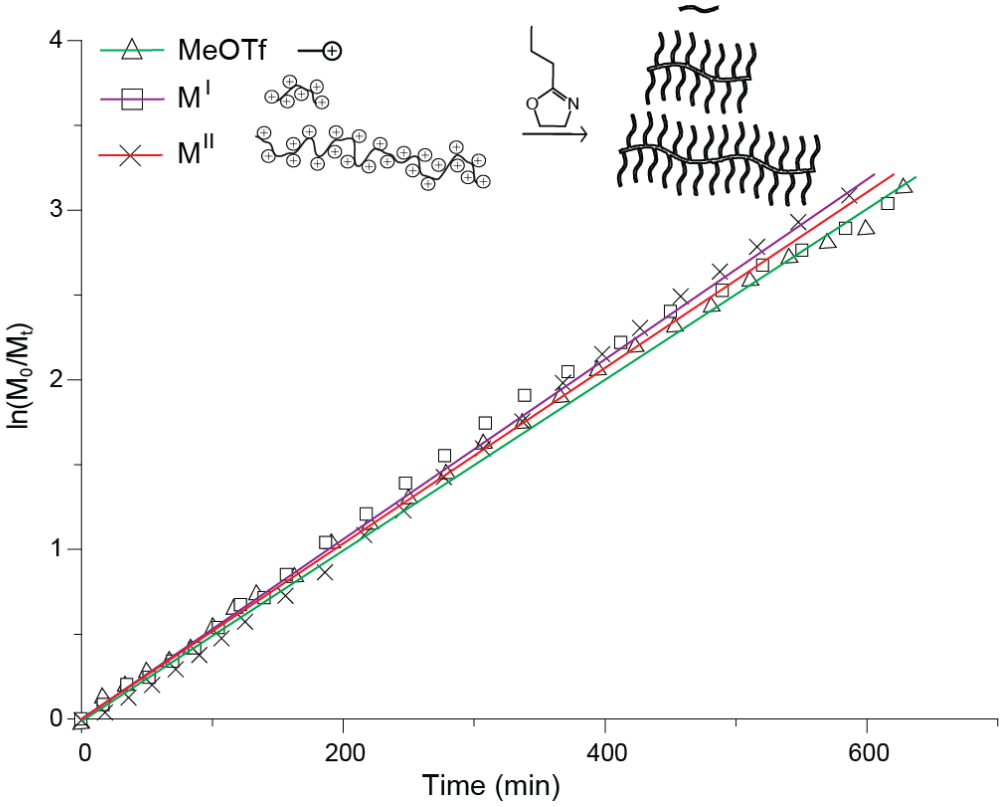

Figure 84. First order kinetic plots for the polymerization of *n*PrOx with MeOTf , M^{I} and M^{II}.

The resulting molecular brushes with homopolymer side chains e.g. poly(2-ethyl-2-oxazoline) (PEtOx), poly(2-isopropyl-2-oxazoline) (P*i*PrOx) and poly(2-*n*-propyl-2-oxazoline) (P*n*PrOx) showed thermo-responsive properties i.e. having defined cloud point in aqueous solution. Factors such as side chain length, backbone length (molar mass), side chain end groups and concentration were investigated in detail and have significant effect on the LCST. For example, as shown in **Figure 85**, the LCST values of P(IPOx-g-*n*PrOx) decreased from 24 ℃ (side chain degree of polymerization is 3) to a minimum of 18.2 ℃ (side chain degree of polymerization is 10). Further increase of the side chain length slightly increased the LCST because of the increase of free volume per side chain (the longer the side chains, the higher the mobility and the free volume the side chains).

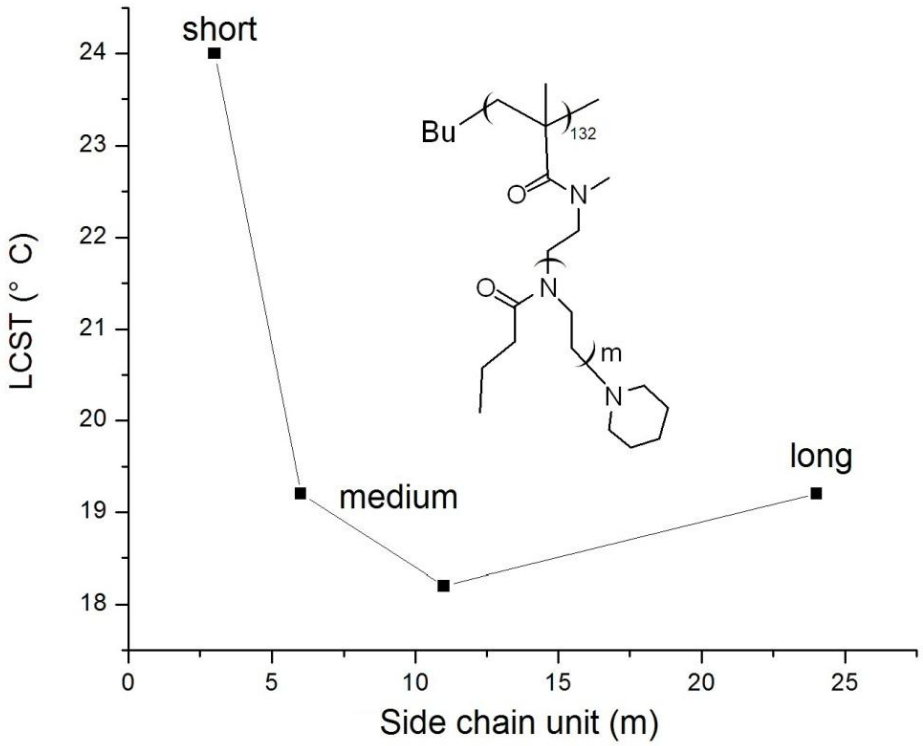

Figure 85. LCST of molecular brushes P(IPOx-g-nPrOx)^{A} as a function of side chain length. The LCST was determination by transmittance changes (10% decrease) for molecular brushes in 1.0 wt % of aqueous solution (heating curves).

As shown in **Figure 86**, the LCST of the molecular brushes decreased steadily with the increasing backbone length which is consistent with previous reports for linear poly(2-oxazoline)s. As for the concentration effect, the LCST of P(IPOx-g-*n*PrOx)^{A} decreased from 24 ℃ to 19.1 ℃ as the concentration increased from 0.1 % to 1.0 % but further increase of the concentration has only little effect on the LCST decrease (**Figure 87**).

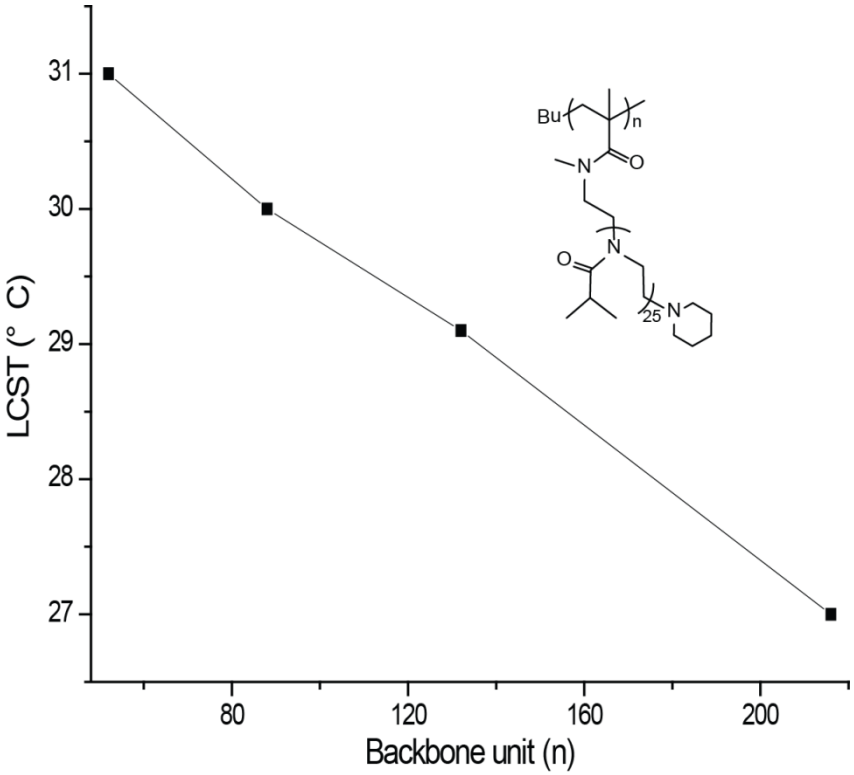

Figure 86. Cloud point of molecular brush P(IPOx-g-iPrOx)^{A} as a function of the PIPOx backbone unit (all the molecular brushes with a side chain DP =25, determined from heating curves).

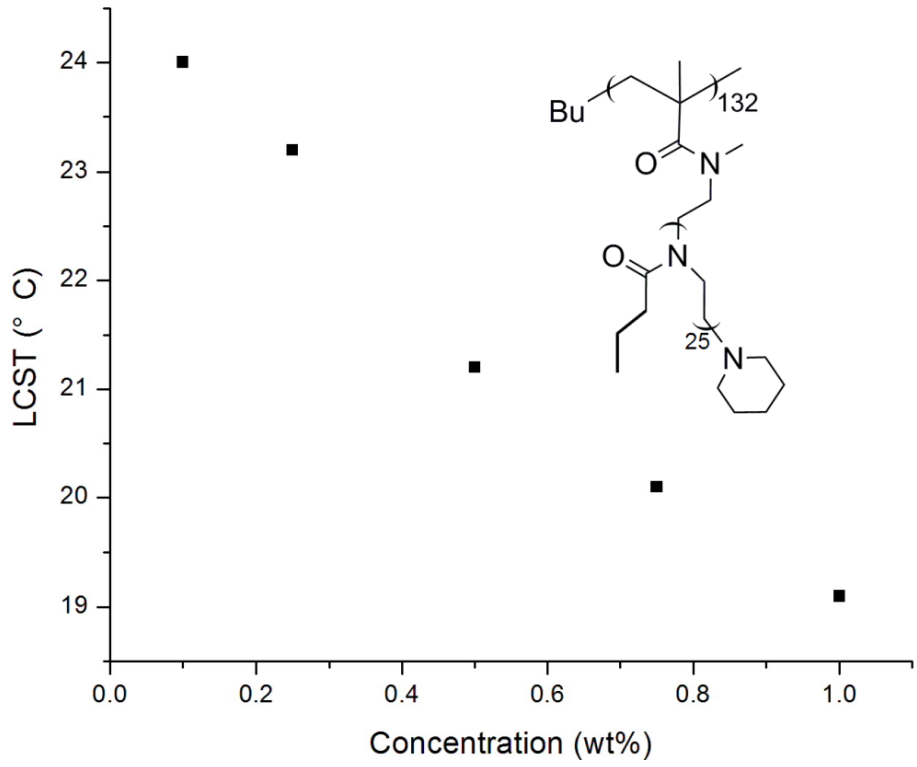

Figure 87. Cloud point of molecular brush P(IPOx-g-*n*PrOx)^{A} as a function of the concentration. (side chain DP = 25, determined from heating curves).

Molecular brushes with random/ gradient copolymer i.e. poly(*n*PrOx-co-MeOx) side chains were also prepared. It was found that the clould point could be tuned in the range of 19-81 ℃ by variation of the content of hydrophilic MeOx monomer (**Figure 88**). The cloud points as a function of the percentage of MeOx in the molecular brushes are shown in **Figure 89**. Furthermore, we prepared molecular brushes with block copolymer side chain and investigated their thermo-responsiveness. Molecular brushes with a hydrophilic core of PMeOx and a hydrophobic shell of P*n*PrOx resulted in a higher LCST compared to brushes with a hydrophobic brush core and a hydrophilic shell.

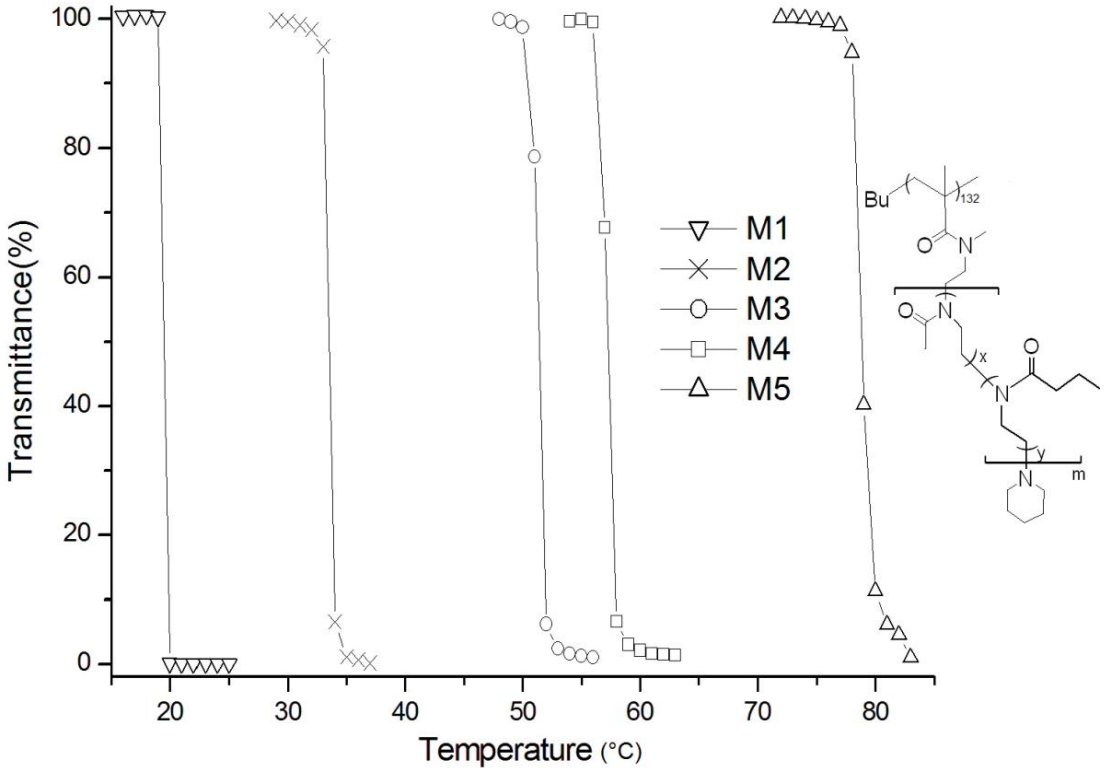

Figure 88. Determination of cloud points of molecular brushes with random copolymer side chains.

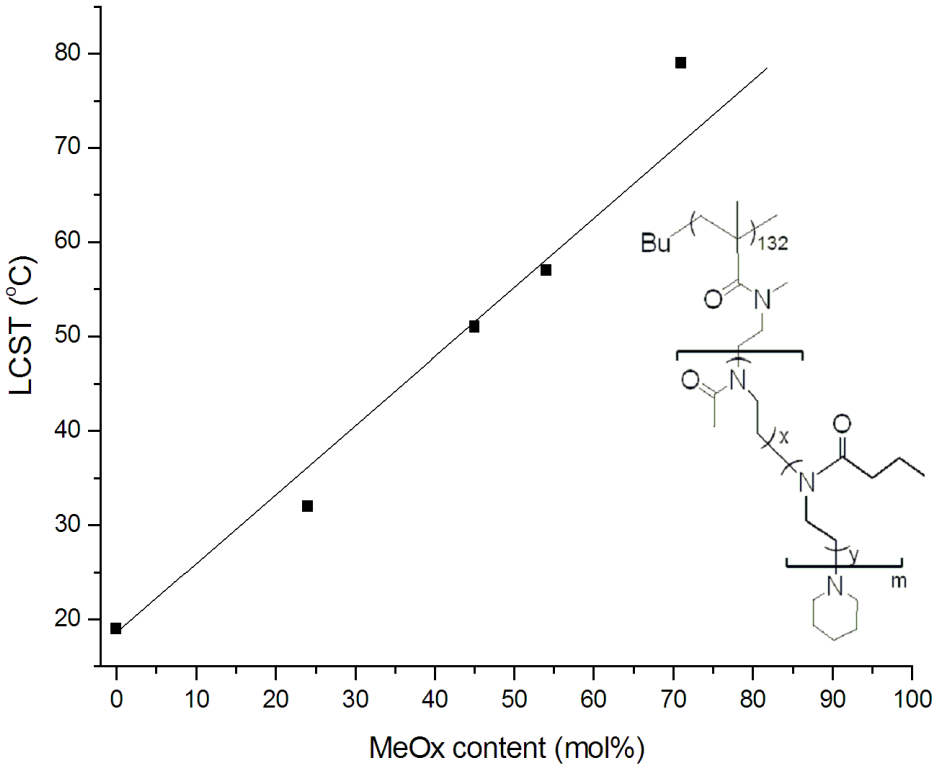

Figure 89. LCST values versus MeOx molar content of the side chain of molecular brushes.

The self-initiated photografting and photopolymerization (SIPGP) of 2-isopropenyl-2-oxazoline on glassy carbon and aminosilane modified oxidized silicon resulted in homogeneous and stable poly(2-isopropenyl-2-oxazoline) (PIPOx) brushes. The pendant oxazoline ring of the PIPOx brushes allowed the conversion to macroinitiator brushes and a successive living cationic ring-opening polymerization (LCROP) with different substituted 2-oxazoline monomers, which resulted in the so-called bottle-brush brushes (BBBs). Moreover, we demonstrated the possibility to functionalize the BBB side chain termini with specific sterically demanding molecules. The reactions are summarized in **Figure 90**. The ease of chemical modification allows for a precise fabrication of a broad variety of functional surfaces for the design of a soft interlayer between solids and e.g. biological systems.

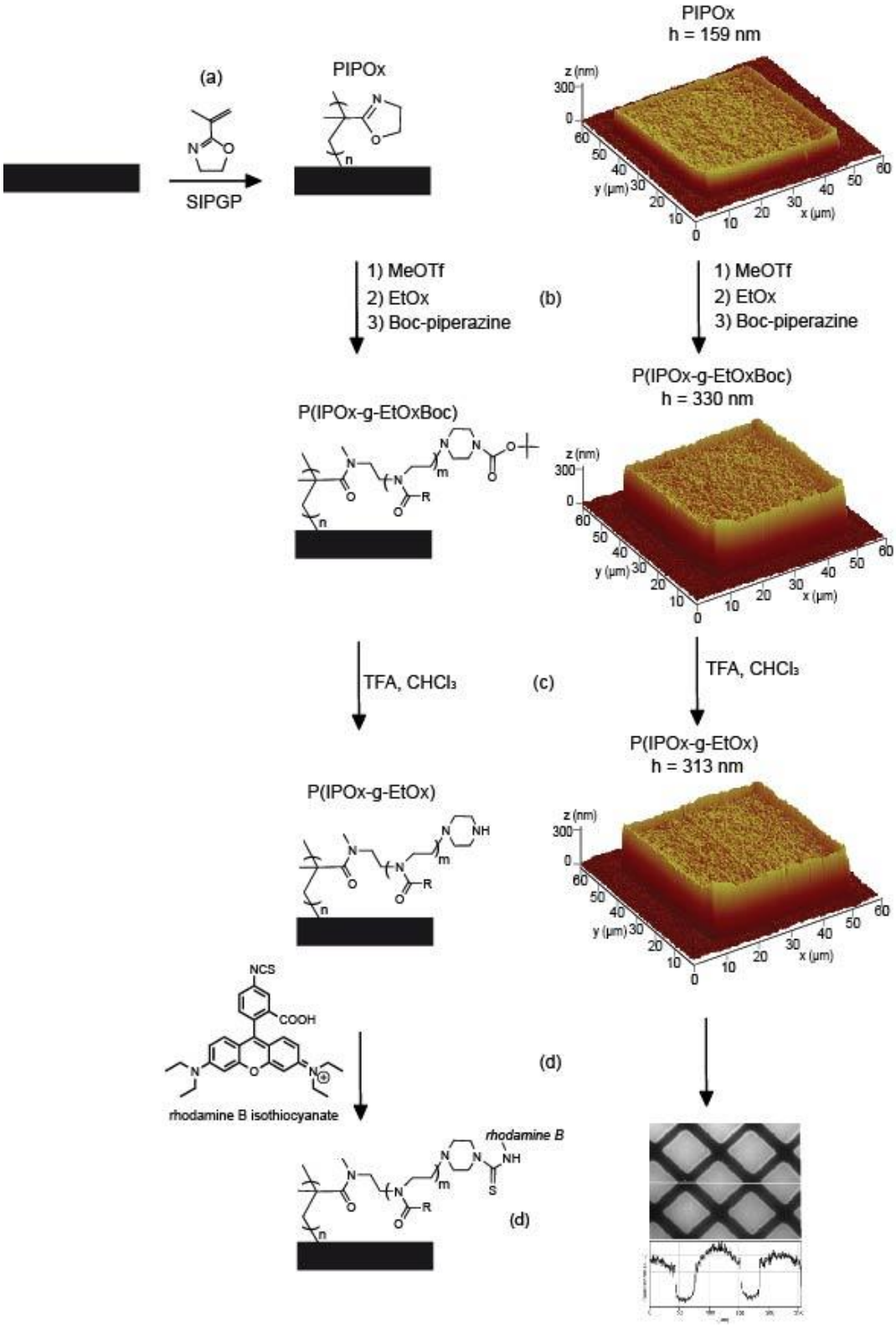

Figure 90. Left: Reaction scheme of the preparation of well-defined bottle-brush brushes on glassy carbon; and Right: Corresponding AFM 3D and fluorescent images of the polymer brushes structure on glassy carbon. (a) The self-initiated photografting and photopolymerization (SIPGP) of 2-isopropenyl-2-oxazoline (IPOx) for 40h through a stencil mask results in structured PIPOx brushes with a thickness of 159 ± 8 nm. (b) The living

cationic ring-opening polymerization (LCROP) of EtOx and termination with N-Boc-piperazine results in 330 ± 10 nm thick P(IPOx-g-EtOxBoc) BBBs. (c) Deprotection of the side chain terminal Boc group results in a 313 nm thick P(IPOx-g-EtOx). (d) The side chain end of BBB was further labelled by Rhodamine B and its fluorescent image (right).

Finally, we investigated the protein adsorption of fibronectin on BBBs of poly(2-oxazoline)s (POx) on oxidized silicon substrates. Quantification of adsorbed protein reveals that, the manipulation of polymer composition and architecture can greatly influence the bioadsorption properties of the resulting BBBs surfaces. Specifically, (1) BBBs with PMeOx and PEtOx side chains due to the strong hydrophilicity, show very much reduced protein adsorption as compared to BBBs with P*n*PrOx side chains (**Figure 91 a**), (2) Given the same side chain composition, a stronger protein resistance is observed for BBBs with longer hydrophilic side chains, which is also ascribed to the increased surface wettability of BBBs (**Figure 91 b**). (3) Side chain end groups influences the bioadsorption properties as well, however, the influence is rather limited. The further cell adhesion experiments revealed the amount of adhered cells on protein layers, which nicely supported the quantification results of protein adsorption (**Figure 92**). The obtained results rearding the thermoresponsiveness of poly(2-oxazoline) brushes and their interactions with biomolecules may open up the possibility for broadening the choice of protein resistant surfaces in the future.

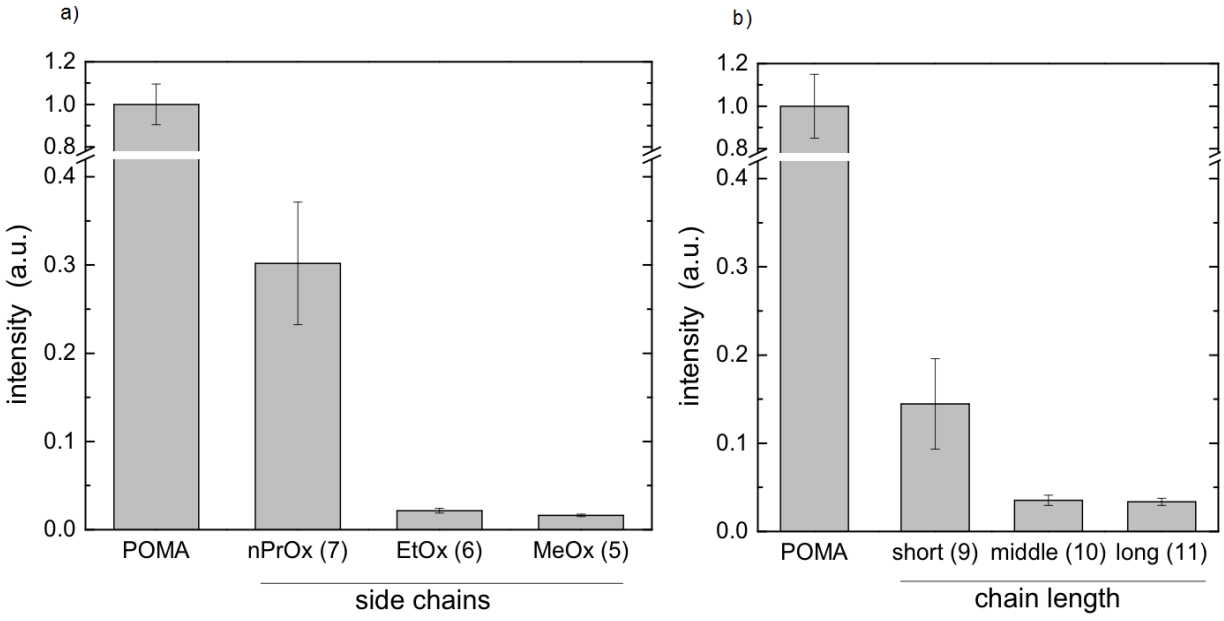

Figure 91. Protein adsorption as a function of side chain compositon and side chain length on the BBBs of poly(2-oxazoline)s. a) BBBs with a variation of side chain composition. b) BBBs with a variation of side chain length.

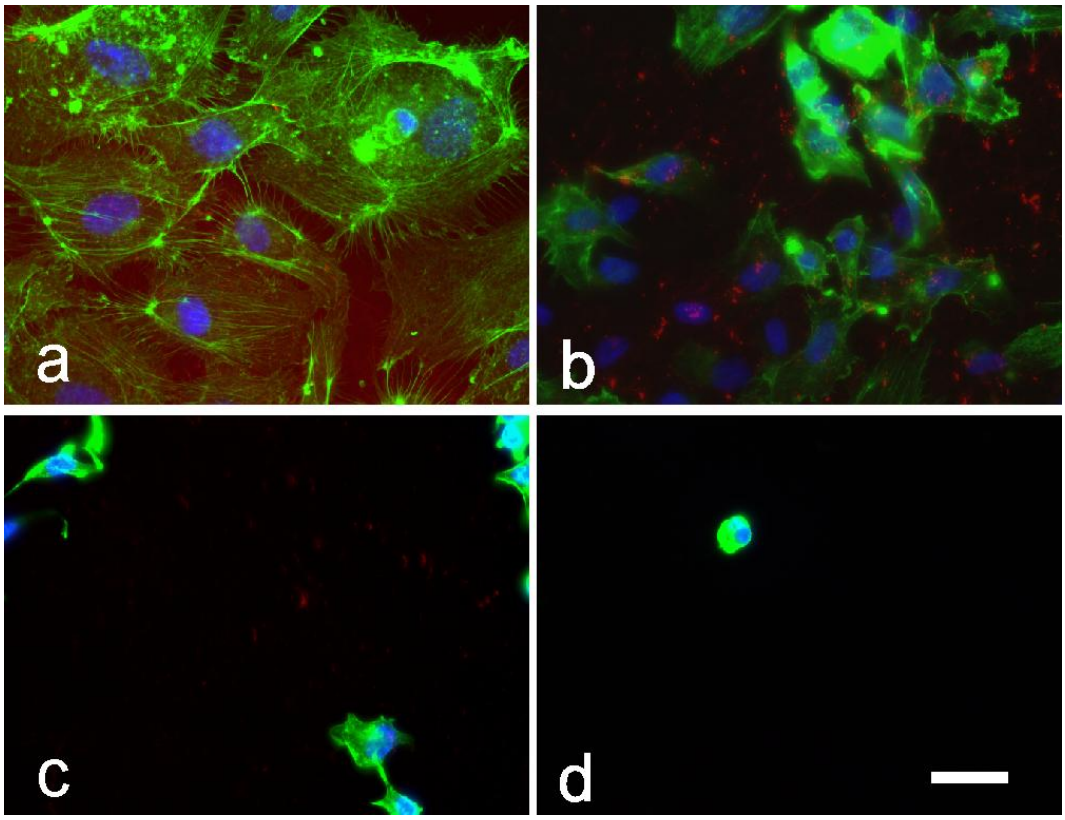

Figure 92. Fluorescence images of cell adhesion on different fibronectin-adsorbed BBBs of POx. In correlation to the amount of adsorbed fibronectin, different degrees of cell adhesion can be observed on POx BBBs surfaces: (a) very good cell adhesion with highly spread cells on BBB with P*n*PrOx side chains of medium length and piperidine end group, (b) good cell adhesion with spread cells on BBB with PMeOx side chains of medium length and Boc end groups, (c) not good cell adhesion with few and almost unspread cells on BBB with PMeOx side chains of medium length and OH end groups, (d) no cell adhesion on BBB with PMeOx side chain of medium length and piperidine end group. [fibronectin (red), actin (green), and nuclei (blue). Scale bar: 50 µm.]

Zusammenfassung

Diese Arbeit beschäftigte sich erstmals mit der Synthese wohldefinierter molekularer Bürsten auf Basis von Poly(2-oxazolin)en. Sämtliche hier beschriebenen molekularen Bürsten wurden durch Kombination aus freier radikalischer, sowie lebender anionischer Polymerisation von 2-iso-Propenyl-2-oxazolin (IPOx) (zur Herstellung des Polymerrückgrates) und einer lebenden kationischen Ringöffnungspolymerisation von 2-Oxazolinen (zur Herstellung der Seitenketten) nach dem "*grafting from*" Ansatz synthetisiert (**Abbildung 93**). Die Bürstenpolymere, deren Rückgrat / Polymerhauptkette über freie radikalische Polymerisation hergestellt wurde, haben aufgrund des verhältnismäßig unkontrollierten Polymerisationsmechanismus einen relativ hohen Polydispersitätsindex (PDI). Wenn das Polymerrückgrat über anionische Polymerisation hergestellt wird, kann jedoch sowohl in der Hauptkette, als auch in den Seitenketten ein niedriger PDI erzielt werden.

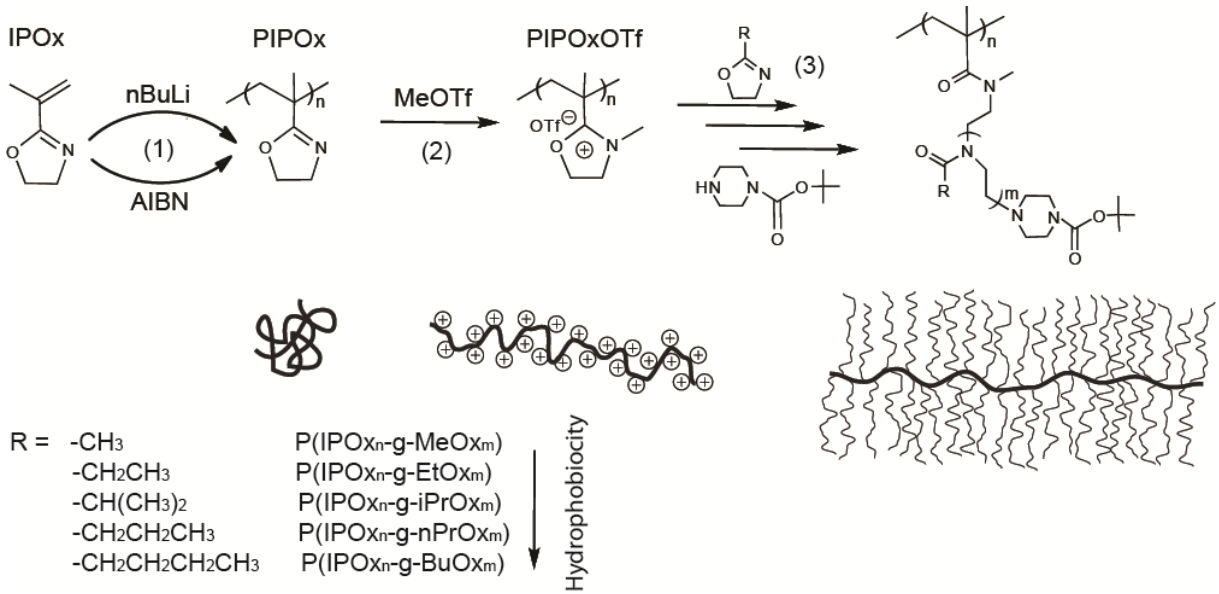

Abbildung 93. Herstellung von Poly(2-oxazolin) Bürstenpolymeren über freie radikalische oder anionische Polymerisation (zur Synthese der Hauptkette), anschließende Umsetzung mit MeOTf unter Bildung des Makroinitiators und der Aufbau der Seitenketten über eine lebende kationische Ringöffnungspolymerisation mit 2-Oxazolinen.

Ausgehend von einem Makroinitiator erfolgt die „*grafting from*" Polymerisation von 2-Oxazolinen, wie zum Beispiel 2-n-Propyl-2-oxazolin (*n*PrOx) und 2-iso-Propyl-2-oxazolin (*i*PrOx), einer Reaktionskinetik erster Ordnung und die Molmasse des entstehenden Polymers steigt mit dem Monomerumsatz. Es konnte gezeigt werden, dass alle Initiatorgruppen gleiche

Reaktivität besitzen und die scheinbare Polymerisationsrate unabhängig von der Größe des Makroinitiators ist. Infolgedessen entstehen wohldefinierte molekulare Bürsten mit hohen Propfungsdichten der Seitenketten (**Abbildung 94**).

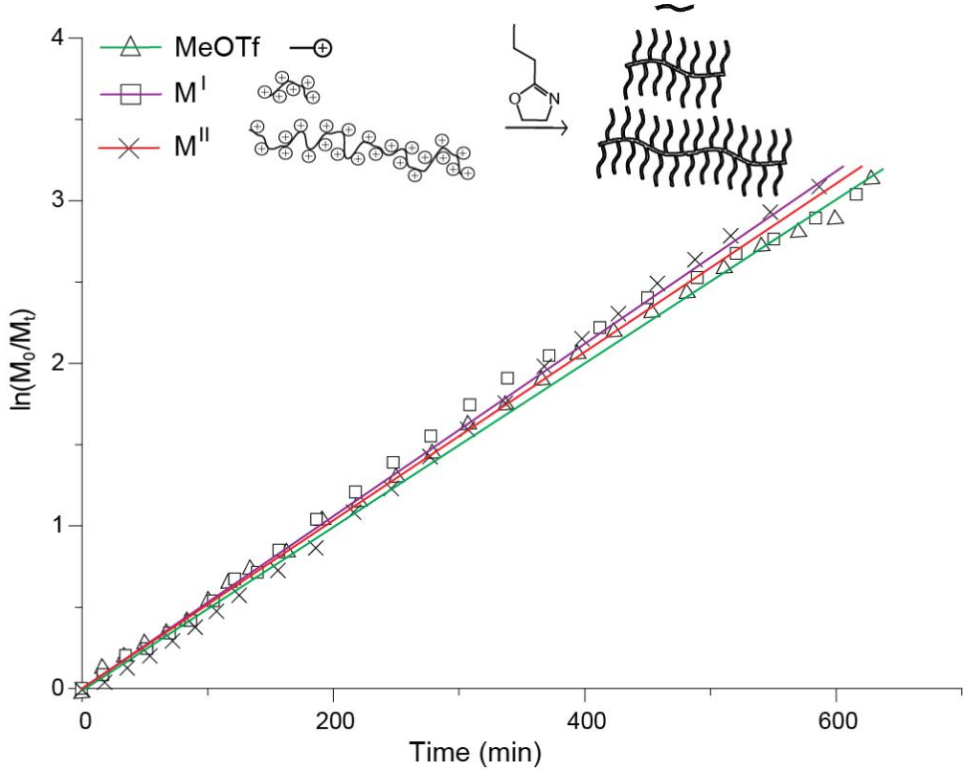

Abbildung 94. Auftragung der Reaktion erster Ordnung für die Polymerisation von *n*PrOx mit MeOTf , M^{I} und M^{II}.

Bürstenpolymere mit Homopolymer-Seitenketten, wie z.B. Poly(2-ethyl-2-oxazolin), Poly(2-isopropyl-2-oxazolin) (P*i*PrOx) und Poly(2-n-propyl-2-oxazolin) (P*n*PrOx), zeigen temperatursensitives Verhalten, d.h. einen *cloud point* oder auch Trübungspunkt in wässriger Lösung. Verschiedene Parameter wie die Länge der Seitenketten, Länge der Polymerhauptkette (Molmasse), funktionelle Endgruppen an den Seitenketten und die Konzentration wurden ausführlich untersucht, wobei jeweils ein großer Einfluss auf die *lower critical solution temperature* (LCST) beobachtet wurde. In **Abbildung 95** wird am Beispiel von P(IPOx-g-*n*PrOx) gezeigt, dass die LCST von 24 °C (bei einem Polymerisationsgrad der Seitenketten von 3) auf ein Minimum von 18.2 °C (bei einem Polymerisationsgrad der Seitenketten von 10) abfällt. Im Falle von noch längeren Seitenketten steigen die LCST Werte wiederum, nachdem mehr freies Volumen pro Seitenkette vorhanden und somit eine höherer Kettenbeweglichkeit möglich ist.

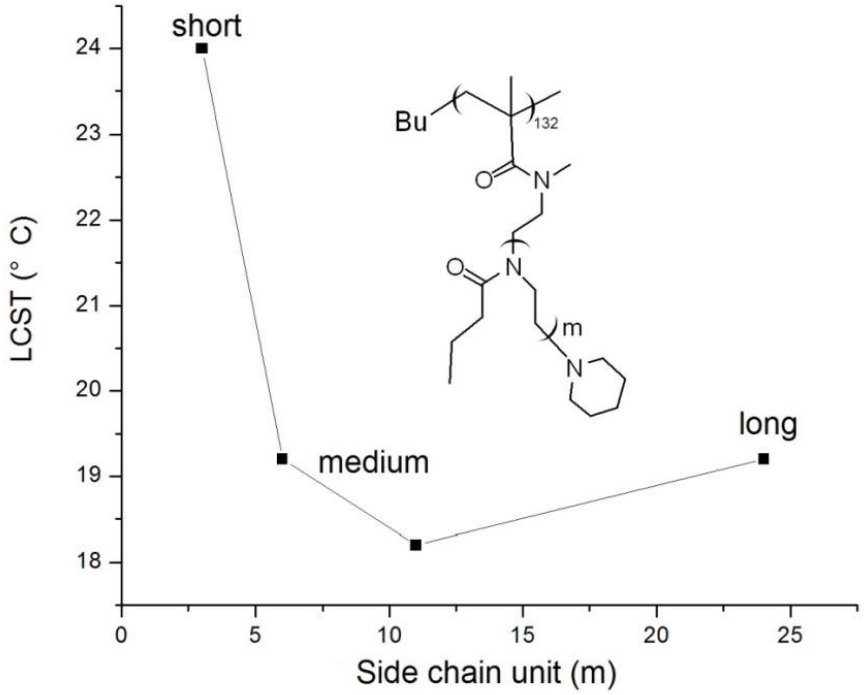

Abbildung 95. LCST von P(IPOx-g-nPrOx)^{A} Bürstenpolymeren als Funktion der Seitenkettenlänge. Die LCST wurde über die Transmissionsänderung (10% Abnahme) einer wässrigen Polymerlösung (1.0 gew.) bestimmt (Aufnahme einer Heizkurve).

In **Abbildung 96** wird deutlich, dass die LCST der Bürstenpolymere mit wachsender Länge der Hauptkette ansteigt. Dies ist in guter Übereinstimmung mit Ergebnissen aus Experimenten mit linearen Poly(oxazolin)en. Was den Konzentrationseffekt betrifft, so sinkt die LCST von P(IPOx-g-*n*PrOx)^{A} von 24 °C auf 19.1 °C ab, wenn die Konzentration von 0.1% auf 1.0% erhöht wird, wobei eine weitere Konzentrationserhöhung nur noch sehr geringen Einfluss aufzeigt (**Abbildung 97**).

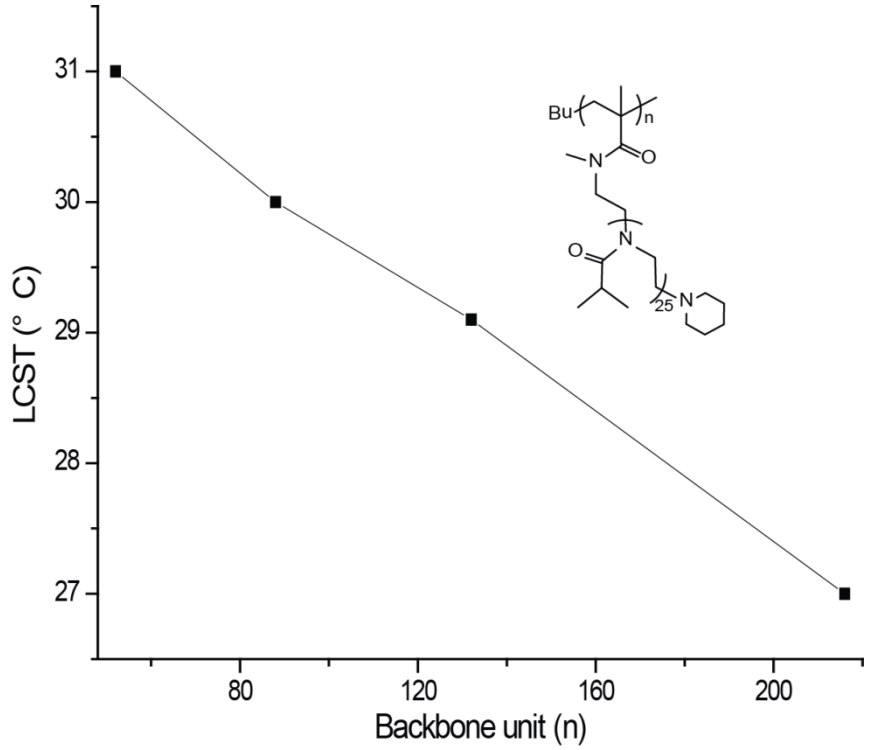

Abbildung 96. Der *Cloud point* von P(IPOx-g-iPrOx)^{A} Bürsten als Funktion der Anzahl an IPOx Einheiten in der Hauptkette (Polymerisationsgrad der Seitenketten von jeweils 25 - Aufnahme einer Heizkurve)

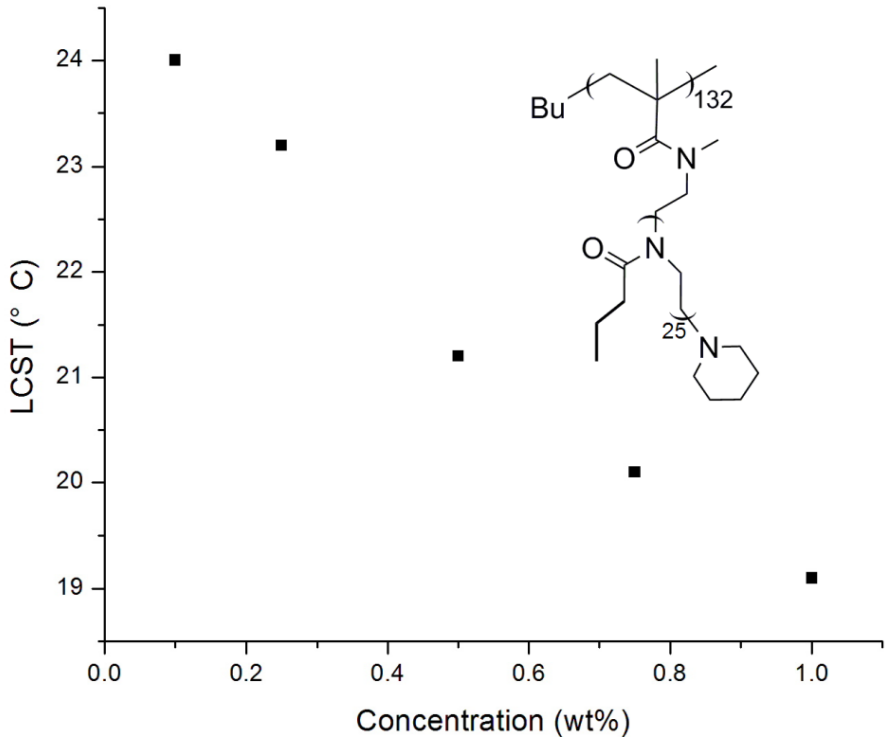

Abbildung 97. Der *Cloud point* von P(IPOx-g-*n*PrOx)^{A} als Funktion der Konzentration (Polymerisationsgrad der Seitenketten = 25, Aufnahme einer Heizkurve).

Im weiteren Verlauf der Arbeit wurden Bürstenpolymere mit statistisch verteilten oder Gradientcopolymer- Seitenketten synthetisiert, z.B. Poly(*n*PrOx-co-MeOx). Durch Variation des Monomeranteils an hydrophilem MeOx konnte der *cloud point* im Bereich zwischen 19 °C und 81 °C definiert eingestellt werden kann. (**Abbildung 98**). Der *cloud point* als Funktion des MeOx Anteils ist in **Abbildung 99** dargestellt. Des Weiteren wurden Bürsten mit Blockcopolymer Seitenketten hergestellt und ebenfalls deren Temperaturverhalten untersucht. Polymere mit hydrophilem Kern aus PMeOx Bürsten und einer hydrophoberen P*n*PrOx Schale besitzen eine höhere LCST als diejenigen mit umgekehrtem Aufbau.

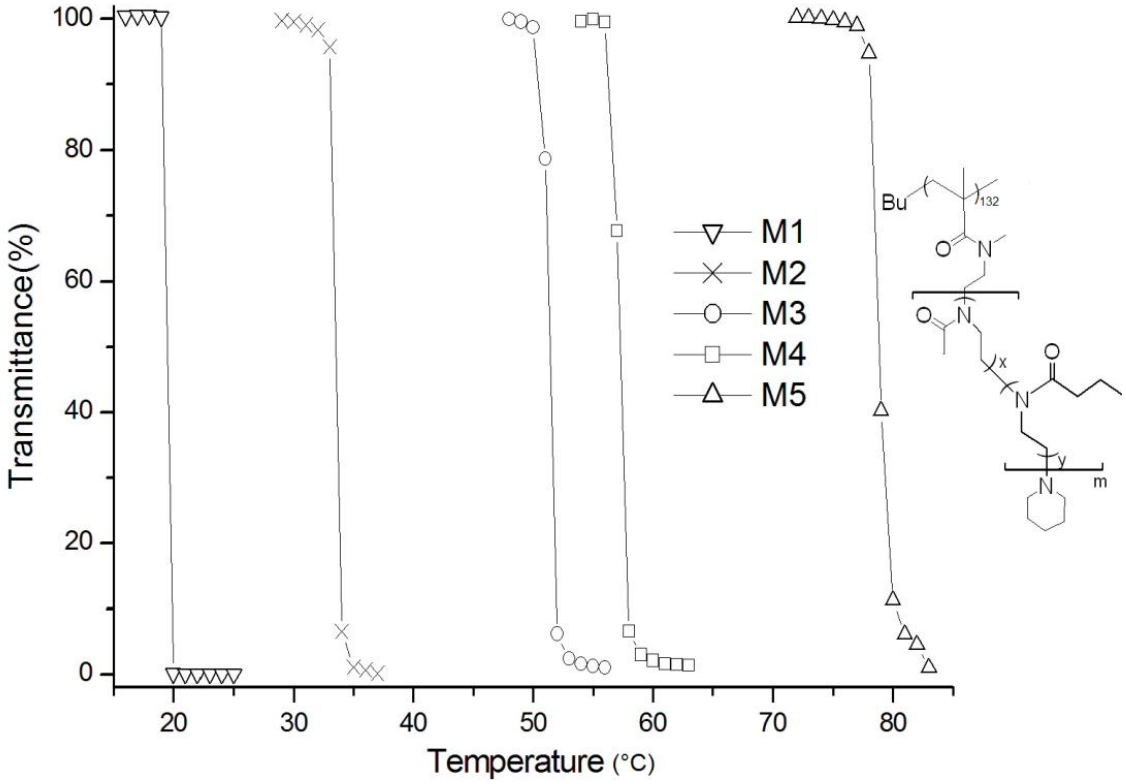

Abbildung 98. Bestimmung des *clound point* von Bürstenpolymeren mit unterschiedlicher, statistischer Monomerzusammensetzung in den Seitenketten.

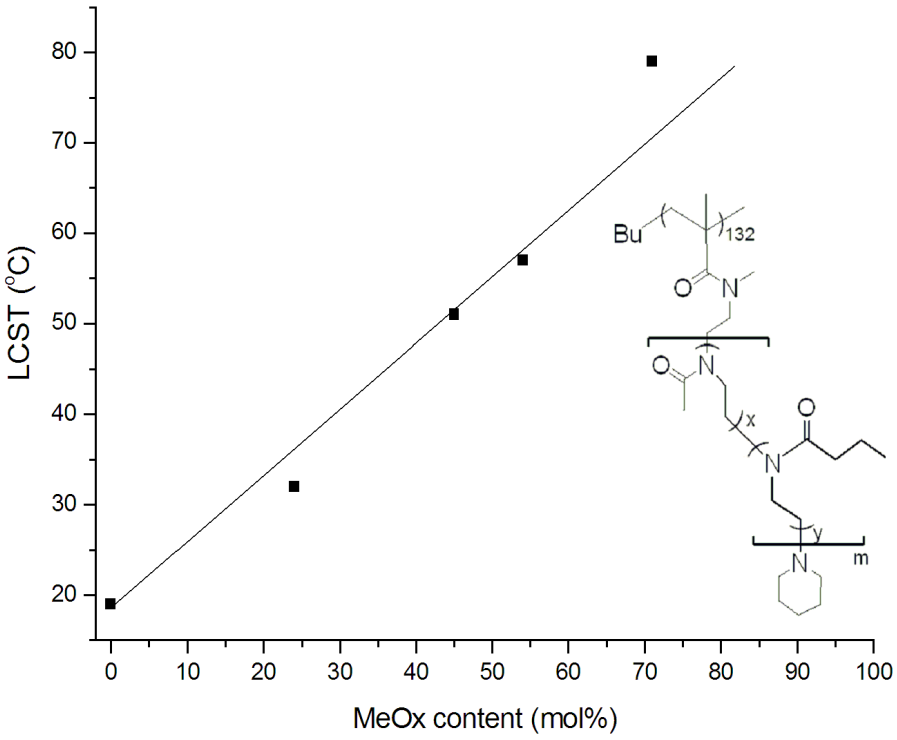

Abbildung 99. Der *Cloud point* der Bürstenpolymere als Funktion der Anzahl an MeOx Einheiten pro P(MeOx-co-*n*PrOx) Seitenkette.

Durch so genannte *self-initiated photografting and photopolymerization* (SIPGP) von 2-iso-Propenyl-2-oxazolin auf glasartigem Kohlenstoff und Aminosilan-modifiziertem SiO_x und Biphenylthiol modifizierten Goldsubstraten wurden homogene und stabile Poly(2-isopropenyl-2-oxazolin) Polymerbürsten hergestellt. Über die Oxazolingruppen der Poly(2-isopropenyl-2-oxazolin) Bürsten konnte nach Initiierung mit MeOTf eine zweite lebende kationische Ringöffnungspolymerisation (engl.: „*living cationic ring-opening polymerization*“ LCROP) mit verschieden substituierten 2-Oxazolin Monomeren erfolgen. Dieser Reaktionsschritt führte zur Ausbildung von pfeifenputzerförmigen Polymerbürsten (engl.: „*bottle-brush brushes*“ (BBB)). Außerdem konnte gezeigt werden, dass es möglich ist die Endgruppen der Seitenketten dieser BBBs mit sterisch anspruchsvollen Molekülen zu funktionalisieren. Das entsprechende Reaktionsschema ist in **Abbildung 100** dargestellt. Aufgrund der vergleichsweise unkomplizierten chemischen Modifizierungsmöglichkeiten kann eine Vielzahl an unterschiedlich funktionalisierten Oberflächen als Grenzfläche zwischen Festkörpern und z.B. biologischen Systemen hergestellt werden.

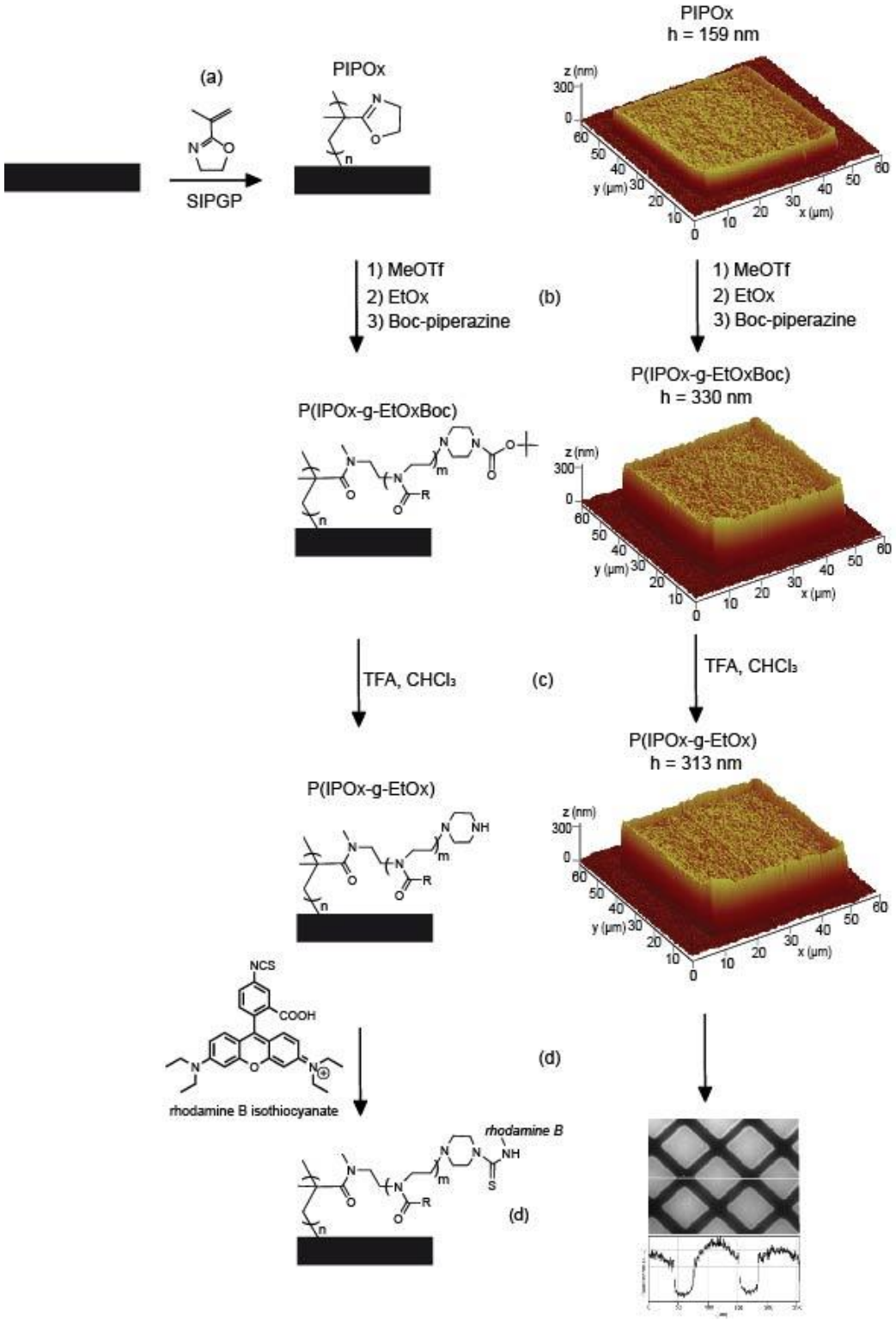

Abbildung 100. Links: Reaktionsschema für die Synthese von *bottle-brush brushes* (BBBs) auf glasartigem Kohlenstoff; Rechts: entsprechendes 3D AFM- oder Fluoreszenzbild von strukturierten Polymerbürsten auf glasartigem Kohlenstoff. (a) Durch so genannte *self-initiated photografting and photopolymerization* (SIPGP) von 2-iso-Propenyl-2-oxazolin (IPOx) bei 40 h UV Bestrahlung durch eine Maske entstehen strukturierte PIPOx Bürsten mit einer Schichtdicke von 159 ± 8 nm. (b) Eine lebende kationische Ringöffnungspolymerisation

(engl.: „*living cationic ring-opening polymerization*“ LCROP) von EtOx und anschließender Kettenabbruch mit N-Boc-Piperazin ergab 330 ± 10 nm dicke P(IPOx-g-EtOxBoc) BBBs. (c) Die Entschützen der terminalen Boc-Schutzgruppen in der Seitenketten liefert 313 nm dicke P(IPOx-g-EtOx) BBBs. (d) Die freien Aminogruppen der BBB-Seitenketten wurde in einem weiteren Schritt mit Rhodamin B fluoreszenzmarkiert (rechts: Fluoreszenzbild).

Schließlich wurde das Adsorptionsverhalten von Fibronektin auf POx BBBs auf SiO_x Substraten untersucht. Die Anzahl an adsorbiertem Protein lässt einen deutlichen Zusammenhang zwischen der Polymerzusammensetzung und -architektur und dem Adsorptionsverhalten von Biomolekülen auf den entsprechenden BBB-modifizierten Oberflächen erkennen. Folgende Punkte konnten in dem Zusammenhang besonders festgehalten werden: (1) BBBs mit PMeOx und PEtOx Seitenketten weisen aufgrund ihrer Hydrophilie im Gegensatz zu BBBs mit P*n*PrOx Seitenketten eine geringere Proteinadsorption auf (**Abbildung 101 a**). (2) Im Falle von gleicher chemischer Zusammensetzung der Seitenketten zeichnen dich diejenigen mit längeren hydrophilen Seitenketten durch eine stärkere Proteinresistenz aus, was ebenfalls auf eine höhere Benetzbarkeit der Oberfläche zurückzuführen ist (**Abbildung 101 b**). (3) Unterschiedliche Seitenkettenendgruppen haben ebenfalls, wenn auch in geringem Maße, Einfluss auf die Proteinadsorption. Anschließende Zelladsorptionsexperimente auf den Protein-modifizierten BBBs sind in guter Übereinstimmung mit den vorangegangenen Ergebnissen aus der Untersuchung der Proteinadsorption (**Abbildung 102**). Die, in dieser Arbeit gewonnen Ergebnisse im Bereich Temperaturverhalten von Poly(2-oxazolin) basierten Bürstenpolymeren und deren Wechselwirkung mit Biomolekülen liefern wichtige Erkenntnisse, um das Spektrum an proteinresistenten Polymeren zu erweitern.

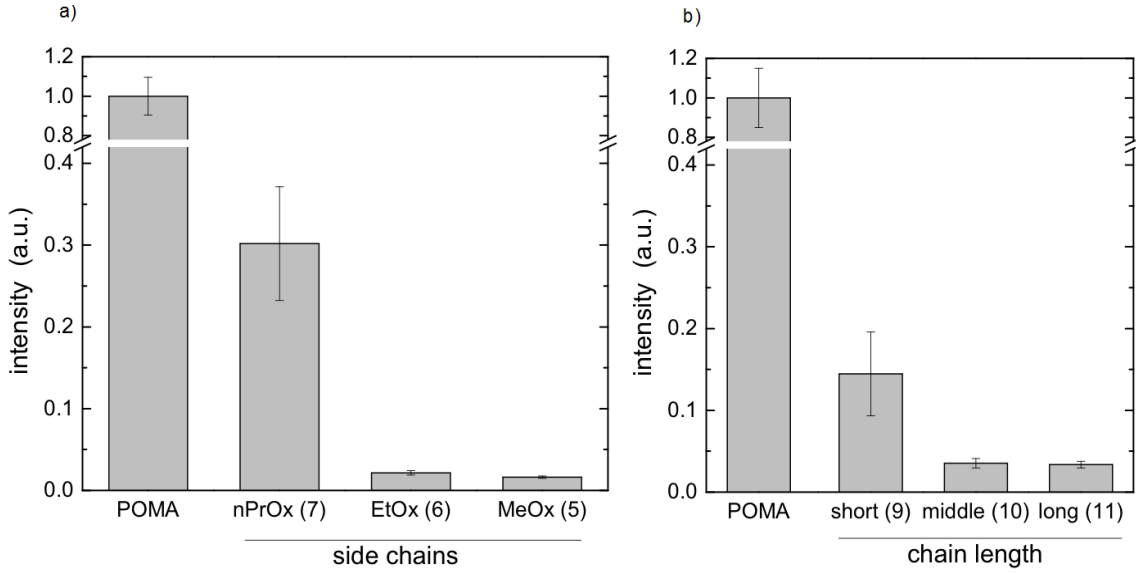

Abbildung 101. Proteinadsorption an Poly(2-oxazolin) BBBs als Funktion der Seitenkettenzusammensetzung und der Seitenkettenlänge a) BBBs mit unterschiedlichen Zusammensetzungen der Seitenketten. b) BBBs mit unterschiedlicher Seitenkettenlänge.

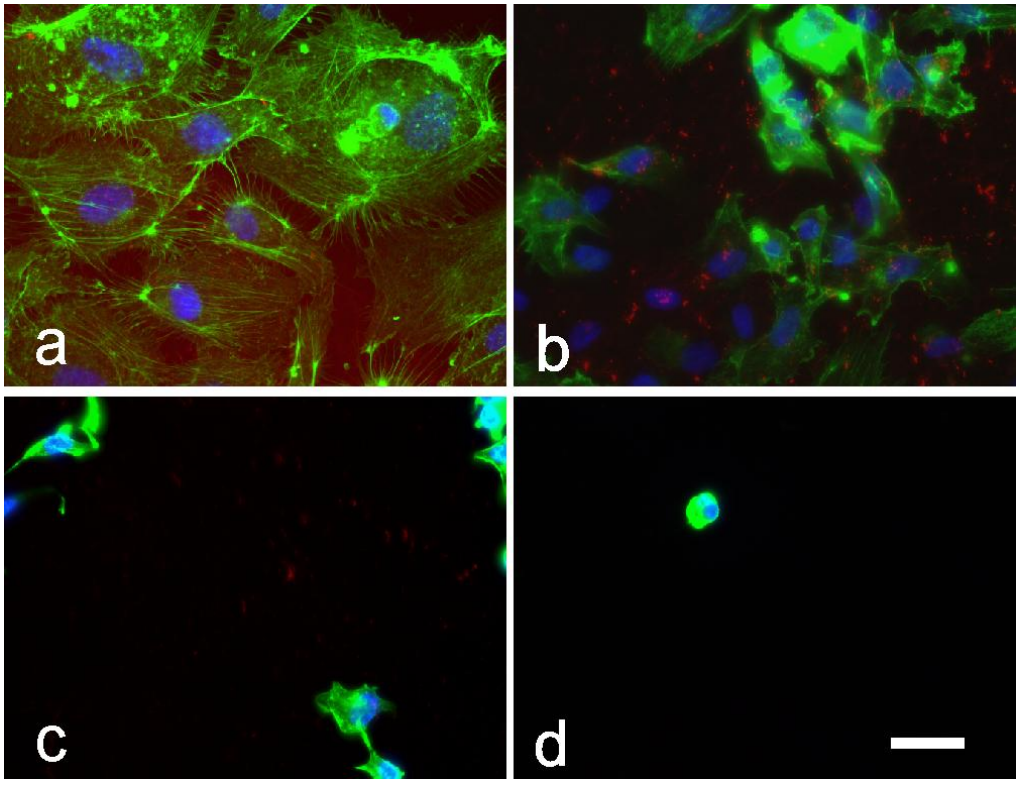

Abbildung 102. Fluoreszenzbilder der Zelladsorption auf Fibronektin modifizierten POx BBBs. In Abhängigkeit der Menge an adsorbiertem Fibronektin werden unterschiedlich starke Zelladhäsionen auf POx BBB Oberflächen beobachtet: (a) Sehr gute und weit verbreitete Zelladhäsion auf BBBs mit P*n*PrOx Seitenketten, (b) gute und leicht verteilte Zelladhäsion auf BBBs mit mittellangen PMeOx Seitenketten und Boc-geschützten Endgruppen, (c)

geringe Zelladhäsion und geringe Verbreitung auf BBBs mit mittellangen PMeOx Seitenketten und Hydroxy-Endgruppen, (d) Keine Zelladhäsion auf BBBs mit mittellangen PMeOx Seitenketten und Piperidin Endgruppen. [Die Fluoreszenzbilder der Zelladhäsion zeigen Fibronektin (rot), Aktin (grün) und Zellkerne (blau). Die Größenordnung beträgt 50 µm]

Chapter 6 Experimental

6.1 Instruments

Atomic force microscopy (AFM)

Fa. Digital Instruments, MMAFM-2

Scanner: 5298 J and 5308 E

AFM tips: Veeco, MPP-11100

All AFM measurements were performed in tapping mode. The AFM measurements were analyzed and visualized using the Nanoscope III-software (version 5.12r3, Digital Instruments).

Gel permeation chromatography (GPC)

GPC was performed on a Waters system (pump mod. 510, RI-detector mod. 410) using Resi Pore Guard (50 × 7.5 mm) and 2× Resi Pore (300 × 7.5 mm) columns as the stationary and dimethyl acetamide (DMAc) (75 mmol/L LiBr, T = 80 °C, 1 mL/min) as the mobile phase. The calculation of the average molar mass was performed using a calibration with poly(methyl methacrylate) (PMMA) standards from PSS (Mainz, Germany). Prior to the measurements, the polymer samples were dissolved in DMAc and filtered through 0.2 µm PTFE filters.

Lower critical solution temperature (LCST)

Turbidity measurements were carried out on a Cary 3 UV-vis spectrophotometer from Varian. The cloud point was determined by spectrophotometric detection of the changes in transmittance at λ= 500 nm of the aqueous polymer solutions (1.0 wt %). The heating/cooling

rate was 0.5 K min^{-1} followed by a 10 min period of constant temperature to ensure equilibration. Given values for the cloud point were determined as the temperature corresponding to a 10 % decrease in optical transmittance.

Nuclear magnetic resonance (NMR)

^{1}H NMR spectra were recorded on a Bruker ARX 300 at 292 K. The spectra were calibrated using the solvent signals ($CDCl_3$ 7.26 ppm, CD_3CN 1.94 ppm).

Fourier transform infrared spectroscopy (FTIR)

IR spectra were obtained on a Bruker IFS 55s spectrometer with a MCT detector and a single bounce SplitPea-ATR sampling accessory from Harrick with a diamond crystal sampling unit at a spectral resolution of 4 cm^{-1}. For diffuse reflectance Fourier transform infrared (DRIFT), for each spectrum, 500 scans were accumulated with a spectral resolution of 4 cm^{-1}. Background spectra were recorded on corresponding bare substrate samples.

Gas chromatography (GC)

GC was performed on a Varian CP 3380 equipped with a CombiPal robot arm and with a Nordion NB-54 column (25 m, 0.20 mm, 0.25 mm) and FID detector (helium carrier gas). For the kinetic measurements, the polymerization mixture was prepared and sealed in a glove-box under an inert and dry atmosphere. The agitator was preheated to the indicated temperature. The CombiPal was programmed for 2 syringe wash cycles (ACN) prior and after sampling. The sealed reaction container was introduced to the agitator immediately (≈1 s) before the first sampling, in order to obtain a zero-time value. Per injection, 2 µL of the reaction mixture were taken. The monomer consumption was followed by the change of the ratio of the integrals of the monomer and the internal standard (chlorobenzene).

Dynamic light scattering (DLS)

DLS experiments were performed on a Malvern Zetasizer Nano ZS. A He-Ne laser with a wavelength of 632.8 nm was applied as the light source. Measurements were taken at 2.0 ℃ intervals.

Fluorescence microscopy

Fluorescence microscopy images were obtained with an Axiovert 200M Zeiss AG microscope equipped with an ORCA-ER camera (Hamamatsu Photonics Japan). The sample was irradiated using a 00 filter set (530-585 nm). The cross section analysis was obtained by pixel analysis of the 256 bit black and white fluorescence image using the *Image J* software package.

Microwave (MW)

Microwave-assisted synthesis was performed using a CEM Discover LabMate system.

Contact angle (CA)

The water contact angles were determined with a full automated Krüss DSA 10 Mk2 contact angle goniometer. The data were obtained with the aid of the Krüss Drop Shape Analysis v3 software package.

6.2 Methods

Micro-structuring of the substrates by electron beam lithography

The electron beam lithography was performed in the research group of Prof. Grunze. The electron beam lithography of the ω-functionalized biphenylthiol SAMs and the preparation of the electron beam induced carbon deposits (EBCDs) were performed under identical irradiation conditions. No precursor molecules were introduced into the vacuum chamber during the EBCD process.

A flood gun (Specs Flood Gun 15/40, electron energy: 50 eV) was used to irradiate the samples through a stencil mask (Quantifoil Micro Tools, Jena, hole radius: 1 µm, center-to-center distance: 4 µm).

Direct writing with a focused e-beam was performed with a LEO 1530 scanning electron microscope with a Raith Elphy Plus Pattern Generator System (REPGS) software. The electron beam energy was set at 3 keV, vacuum pressure ~ 5 x 10^{-6} mbar.

Cytotoxicity assay, MTT

MCF 7/ADR cells, a human breast MDR cancer cell line, were seeded in 96 well plates (10^4 cells per well) and were allowed to reattach for 24h. Treatment solutions were prepared from a 1 mg/mL polymer stock solution in assay buffer (containing 122 mM NaCl, 25 mM $NaHCO_3$, 10 mM glucose, 10 mM 4-(2-hydroxyethyl)-1-piperazineethanesulfonic acid (HEPES), 3 mM KCl, 1.2 mM $MgSO_4$, 1.4 mM $CaCl_2$, and 0.4 mM K_2HPO_4, pH 7.4) by appropriate dilution with media (Dulbecco's Modified Eagle's Medium) (DMEM), supplemented with 10% FBS, 25 mM HEPES and penicillin/streptomycin) for 2 h incubation. For 72 h incubation, 1 mg/mL stock solutions where prepared in full media. The cells were incubated for 72 h with $P(IPOx\text{-}g\text{-}MeOx)^R$ in 200 µL of treatment solution. After discarding the treatment solution, cells were washed thrice with PBS. FBS-free DMEM (100 µL/well) as well as 25 µL of a 5 mg/mL solution of 3-(4,5-dimethylthiazol-2-yl)-2,5-diphenyltetrazolium bromide (MTT, Invitrogen, Eugene, OR, USA) in PBS were added and the cells incubated at 37 °C for 2 hours. The media was discarded subsequently and replaced with 100 µL of solvent (25% v/v DMF, 20% w/v SDS in H_2O). The purple formazan product was allowed to dissolve over night and the absorbance at 570 nm was obtained using a plate reader (SpectraMax M5, Molecular Devices). Positive controls were cells treated with media alone; negative controls were wells without cells. Each concentration was repeated in four wells, results are expressed as mean ± standard error of the mean(SEM).

Protein adsorption and cell adhesion

Protein adsorption and cell culture was performed similarly to procedures described recently [213]. Briefly, samples were immersed in 70% ethanol/water to provide sterile conditions for cell culture. Thereafter polymer surfaces were immersed in a 50 µg/mL fibronectin (purified from human plasma) solution in phosphate buffered saline (PBS) (Sigma)

at pH 7.4 and 37 ℃ for 1 h. Carboxytetramethylrhodamine FluoReporter (Invitrogen, Karlsruhe, Germany) was used to label fibronectin prior to the experiments.

Human endothelial cells from the umbilical cord vein (HUVECs) were seeded in endothelial cell growth medium ECGM (Promocell, Heidelberg, Germany) containing 2 % fetal calf serum at density of 1×10^5 cells per cm^2 on the fibronectin-coated substrates. After 1 h of cell culture samples were fixed with 4% paraformaldehyde for 10 min and stained with DAPI (Sigma) and phalloidin-Alexa488 (Invitrogen) to visualize nuclei and actin cytoskeleton, respectively, in fluorescence microscopy. The microscopic analysis was performed on inverse epi-fluorescence microscope (DMIRE2, Leica Microsystems, Germany) with a 40x oil immersion objective using Openlab software (Perkin Elmer). The protein amounts remaining on the substrate surface were quantified in terms of fluorescence intensities using Openlab software. Reference intensities were collected from fibronectin-coated poly(octadecen-*alt*-maleic anhydride) surfaces and uncoated surfaces.

6.3 Materials

All chemicals were purchased from Aldrich, or Acros (American chemical society purity or higher). Solvents of lower grade were purified and dried prior to use. The 2-oxazoline monomers were dried with CaH_2 and purified by fractionation distillation at reduced pressure. THF was dried by refluxing over sodium and benzophenone. Dry THF was collected until the mixture turn to blue/purple. The 2-isopropenyl-2-oxazoline was stored at -25 ℃ and degassed by at least 4 freeze-thaw cycles before SIPGP.

Gold substrate pretreatment

Thin gold film (around 50 nm thick) on p-doped silicon substrates were obtained from Albert Coatings, Heidelberg.[214] Before use, the substrates were cleaned by exposing the surfaces for 2 hours in UV-light (253 nm) under inert atmosphere. The surfaces were then washed with dimethylformamide and ethanol and dried by a jet of nitrogen.

Glass substrates:

Mechanically polished borosilicate glass (Borofloat® 33) was obtained from Schott GmbH, Mainz. Before use, the samples were cleaned by ultrasound in toluene, ethyl acetate and ethanol, 2 min each and dried by a jet of nitrogen.

Glassy carbon substrates:

Mechanically polished glassy carbon substrates (Sigradur®) were purchased from HTW Hochtemperatur-Werkstoffe GmbH, Thierhaupten. Before use, the samples were cleaned by ultrasound in toluene, ethyl acetate and ethanol, 2 min each and dried by a jet of nitrogen.

Silicon substrates:

P-doped Si(100) wafers were obtained from Wacker Chemie AG, Munich, Germany. Before use, the samples were sonificated for 2 minutes in toluene, ethyl acetate and ethanol, dried by a jet of nitrogen and cleaned in a piranha solution, rinsed with water and dried again.

6.4 Monomer synthesis

2-*n*-Propyl-2-oxazoline (*n*PrOx)

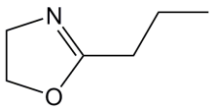

In a Schlenk flask, 15 g (0.21 mol) of *n*-butyronitrile, 18 g (0.26 mol, 1.2 eq) aminoethanol and 0.9g (3.2 mmol) cadmium acetate dihydrat were stirred and heated to 130 °C. After 12 h, the reaction was cooled to room temperature. The red raw product was purified by vacuum distillation (boiling point (bp), 57 °C at 11 mbar) and then stored under a dry nitrogen atmosphere prior to use (yield, 16.5 g, 68%).

^{1}H NMR (250 MHz, $CDCl_3$): δ=4.27 (t, 2H), δ=3.81 (t, 2H), δ=2.23 (t, 2H), δ=1.69 (st, 2H), δ=0.95 (t, 3H).

2-*n*-Butyl-2-oxazoline and 2-*iso*-propyl-2-oxazoline were synthesized accordingly.

2-*n*-Butyl-2-oxazoline (BuOx)

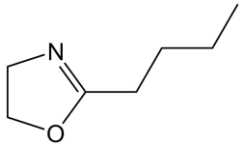

^{1}H NMR (250 MHz, $CDCl_3$): δ=4.17 (t, , 2H), δ=3.77 (t, 2H), δ=2.23 (t, 2H), δ=1.60 (q, 2H), δ=1.38 (sp, 2H), δ=0.88 (t, 3H).

2-*iso*-Propyl-2-oxazoline (*i*PrOx)

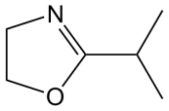

^{1}H NMR (250 MHz, $CDCl_3$): δ=4.23 (t, 2H), δ=3.78 (t, 2H), δ=2.62 (sp, 3H), δ= 1.18 (d, 6H).

2-Isopropenyl-oxazoline (IPOx)

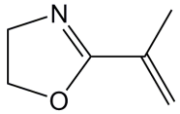

IPOx was synthesized according to the procedure reported before.[135] 2-ethyl-oxazoline reacted with 1 equivalent of paraformaldehyde in the presence of catalytic amounts of triethylamine to form the hydroxyethyl derivative. Water can be eliminated readily at elevated temperatures when alkali metal alkoxide is used as catalysts. Finally, 2-isopropenyl-oxazoline is distilled under reduced pressure before use.

^{1}H NMR (250 MHz, $CDCl_3$): δ=5.78 (s, 1H), δ=5.41 (s, 1H), δ=4.27 (t, 2H), δ= 3.93 (t, 2H),δ= 2.00 (t, 3H).

6.5 Synthesis of molecular brushes

6.5.1 Free radical and anionic polymerizations

Free radical polymerization: poly(2-isopropenyl-2-oxazoline); PIPOx^R

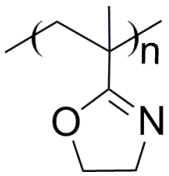

Under a dry nitrogen 2-isopropenyl-2-oxazoline (IPOx) (1.00 g, 9.00 mmol) and AIBN (14.8 mg, 0.09 mmol) was heated to 60 ℃ for 8 h. Afterwards, the reaction mixture was equilibrated to room temperature, diluted with chloroform (approx. 15 mL), and precipitated into dry diethyl ether. The product was reprecipitated twice using chloroform and ether. After filtration and freeze drying from water, a colorless powder was obtained (0.5 g, yield = 50 %). The obtained yield is typical for the free radical polymerization of IPOx as reported earlier by Fréchet et al.[215]

^{1}H NMR ($CDCl_3$): δ (ppm) 4.16 (br, 2H), 3.76 (br, 2H), 1.98–1.76 (br, 2H) and 1.24–1.12 (br, 3H).

IR (ATR, film): 2941 (C-H str) (m), 1654 (C=N str) (vs), 1118 (C-O) (vs) (unconjugated), 986, 951(vs) (ring skeletal vibration) cm^{-1}. Analysis of the ratio of α-methyl proton signals calculated to a tacticity ratio of syndiotactic(*S*):heterotactic(*H*):isotactic(*I*) of 57.0:37.2:5.8 .

GPC: PDI = 2.12, M_n = 9800 g/mol.

Living anionic polymerization: poly(2-isopropenyl-2-oxazoline); PIPOx^A

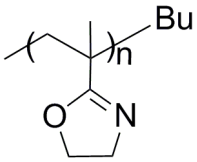

Adapting an early procedure of Tomalia et al.,[216] 3 mL dry THF and 0.1 mL of a 2.5 M *n*-butyl lithium solution in hexane (0.236 mmol, 1 equiv) were cooled under a dry argon atmosphere, to approx. -50 ℃ (acetone/dry ice). Over a period of 30 min, 1 mL (9.45 mmol, 40 equiv) IPOx was added dropwise. After stirring the mixture for another 30 min at -50 ℃, the mixture was equilibrated to room temperature and stirred again for 30 min. The polymer was endcapped by addition of 1 mL methanol. The mixture was then precipitated using diethyl ether. After freeze-drying (water), 1.07 g (95 % yield) of PIPOx^A was obtained as a colorless powder.

^{1}H NMR ($CDCl_3$): δ (ppm) 4.16 (br, 2H), 3.76 (br, 2H), 1.86–1.75 (br, 2H), 1.24–1.14 (br, 3H) and 0.85(br, C_4H_9).

IR (ATR, film): 2941 (C-H str) (m), 1654 (C=N str) (vs), 1118 (C-O) (vs) (unconjugated), 986, 951(vs) (ring skeletal vibration) cm^{-1}. Analysis of the ratio of α-methyl proton signals calculated to a tacticity ratio of syndiotactic(*S*):heterotactic(*H*):isotactic(*I*) of 73.0:24.8:2.2 (Figure 1).

GPC: PDI =1.20, M_n = 24350 g/mol.

6.5.2 Macroinitiator

Macroinitiator salt: poly(2-isopropenyl-2-oxazolium triflate); PIPOxOTf

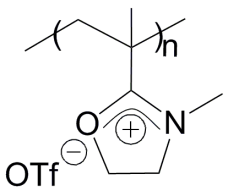

Under dry and inert conditions, PIPOx (222 mg, 1.0 equiv of oxazoline unit) and 394 mg (2.4 mmol, 1.2 equiv) of MeOTf were added to 5 mL dry acetonitrile at approx. -35 ℃. After stirring for 5 h at 0 ℃, the mixture was poured into cold and dry diethyl ether to precipitate the oxazolinium salt. The colorless precipitate was washed twice with cold ether to yield 529 mg (1.92 mmol, 96 %).

^{1}H NMR (CD_3CN): δ (ppm) 5.08 (br, 2H, =N-CH_2-CH_2-O-), 4.54 (br, 2H, =N-CH_2-CH_2-O-), 3.70 (s, 3H, CH_3-N), 2.49 (2H, -C-CH_2-), 1.36 (br, 3H, -C-CH_3)

6.5.3 Living cationic ring-opening polymerization

Poly(2-isopropenyl-2-oxazoline-g-2-methyl-2-oxazoline); P(IPOx-g-MeOxboc)^R

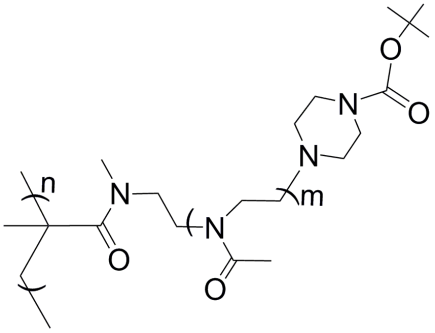

At 0 ℃, PIPOxOTf^R (110 mg, 0.4 mmol, 1.0 equiv) was dissolved in 10 mL of acetonitrile and 850 mg of 2-methyl-2-oxazoline (MeOx) (10 mmol, 25 equiv) was added. The polymerization solution was heated by a prepared oil bath to 85 ℃ and stirred for 20 h. The mixture was cooled to 0 ℃, and 298 mg (1.6 mmol, 4 equiv) of *N-tert*-butyloxycarbonylpiperazine (N-Boc-pip) was added. After stirring the reaction mixture for 4 h at room temperature, an excess of finely grounded potassium carbonate (~60 mg) was added and the mixture was allowed to stir overnight. The solvent was removed under reduced pressure and the residual dissolved in approx. 15 mL chloroform and then precipitated three times into dry diethyl ether. The product was freeze-dried (water) to yield a colorless powder (860 mg, 80 % yield). Additionally, the product was purified by column chromatography using Sephadex G100 to quantitatively separate the product from minor portions of homopolymer side products.

^{1}H NMR (CD_3Cl): δ (ppm) 3.44 (br, 82H, -N-CH_2-CH_2-N-)，2.13/2.07 (m, 57H, -CO-CH_3), 1.98/1.92 (br, 2H, CH_2-C)，1.46/1.44 (br, 12H, CH_3^{Boc} and CH_3-C).

IR (ATR, film): 2939 (C-H str) (m), 1696 (C=O str, ester), 1629 (C=O str, amide I) (vs), 1419 δ(CH_2-CO) (s), 731 cm^{-1} r(CH_2) (w).

GPC: PDI =1.69, M_n= 69500 g/mol.

Poly(2-isopropenyl-2-oxazoline-g-2-ethyl-2oxazoline); P(IPOx-g-EtOxboc)^{R}

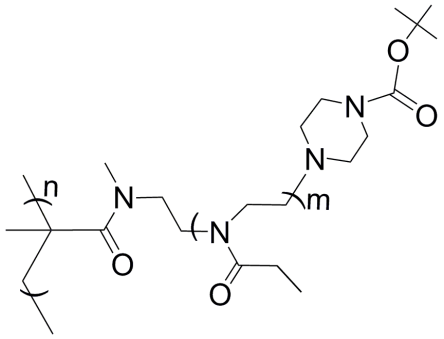

As described above, P(IPOx-g-EtOx)^{R} was obtained using 110 mg of PIPOxOTf^{R}, 990 mg 2-ethyl-2-oxazoline (EtOx) and 298 mg N-Boc-pip. The polymerization time was 30h. After column chromatography and freeze drying, a colorless powder was obtained (940 mg, 76 % yield).

^{1}H NMR (CD_3Cl): δ (ppm) 3.44 (br, 86H, -N-C*H*$_2$-C*H*$_2$-N-)， 2.39(br, 41H, -CO-C*H*$_2$CH$_3$), 1.98/1.92 (br, 2H, -C*H*$_2$-C), 1.46/1.44 (br, 12H, C*H*$_3^{Boc}$ and C*H*$_3$-C), 1.10(br, 62H, -CO-CH$_2$C*H*$_3$).

IR (ATR, film) 2937 (C-H str) (m), 1699 (C=O str, ester), 1629 (C=O str, amide I) (vs), 1428 δ(CH_2-CO) (s), 731 cm^{-1} r(CH_2) (w).

GPC: PDI =1.75, M_n = 77500 g/mol.

Poly(2-isopropenyl-2-oxazoline-g-2-isopropyl-2-oxazoline); P(IPOx-g-*i*PrOxboc)^{R}

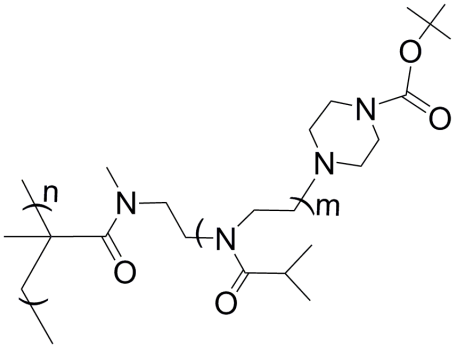

Following the procedure described above, P(IPOx-g-iPrOx)^{R} was obtained using 110 mg PIPOxOTf^{R}, 1.13 g *i*PrOx and 298 mg N-Boc-pip. The polymerization time was 40 h. After freeze drying (water), a colorless powder was obtained (630 mg, 50 % yield). In this case, no homopolymer side product could be detected.

^{1}H NMR (CD_3Cl): δ (ppm) 3.45 (br, 72H, -N-C*H*$_2$-C*H*$_2$-N-)， 2.88 (br, 22H, -CO-C*H*$(CH_3)_2$), 1.98/1.92 (br, 2H, C*H*$_2$-C), 1.46/1.45 (br, 12H, C*H*$_3^{Boc}$ and C*H*$_3$-C), 1.09 (br, 105H, -CH$(CH_3)_2$).

IR (ATR, film): 2937 (C-H str) (m), 1698 (C=O str, ester)，1637 (C=O str, amide I) (vs), 1419 δ(CH_2-CO) (s), 731 cm^{-1} r(CH_2) (w).

GPC: PDI =1.58, M_n = 53200 g/mol.

Poly(2-isopropenyl-2-oxazoline-g-2-*iso*propyl-2-oxazoline) (P(IPOx-g-*i*PrOx))^R

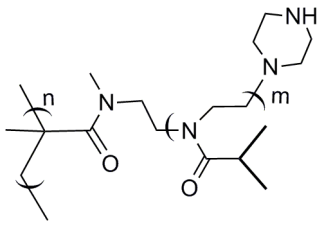

200 mg P(IPOx-g-*i*PrOxboc)^R was dissolved in a solution of 1 mL trifluoroacetic acid (TFA) and 1mL of chloroform. The mixture was stirred at RT for 2 h. Then, the mixture was dried and redissolved in chloroform and precipitate twice in diethyl ether. After freeze drying (water), a colorless powder was obtained (150 mg, 78% yield).

^{1}H NMR (CD_3Cl): δ (ppm) 3.45 (br, 42H, -N-CH_2-CH_2-N-)，2.88 (br, 18H, -CO-CH(CH_3)$_2$), 1.09 (br, 67H, -CH(CH_3)$_2$).

GPC: PDI = 1.45, M_n = 50000 g/mol

Poly(2-isopropenyl-2-oxazoline-g-2-isopropyl-2-oxazoline); P(IPOx-g-iPrOx)^A

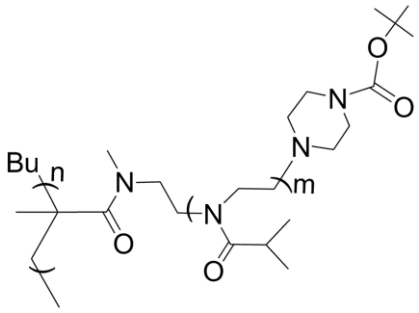

Following the procedure described above, P(IPOx-g-iPrOx)^A was obtained accordingly (49 % yield). Also in this case, no homopolymer side product could be detected.

^{1}H NMR (CD_3Cl): δ (ppm) 3.45 (br, 76H, -N-CH_2-CH_2-N-)，2.88(br, 23H, -CO-CH(CH_3)$_2$), 1.98/1.92 (br, 2H, CH_2-C), 1.46/1.45 (br, 12H, CH_3^{Boc} and CH_3-C), 1.09 (br, 110H, -CH(CH_3)$_2$).

IR (ATR, film): 2937 (C-H str) (m), 1698 (C=O str, ester)，1637 (C=O str, amide I) (vs), 1419 δ(CH_2-CO) (s), 731 cm^{-1} r(CH_2) (w).

GPC: PDI =1.33, M_n = 125000 g/mol.

Poly(2-isopropenyl-2-oxazoline-g-2-*n*propyl-2-oxazoline) (M-I1~M-I3 and M-II1~M-II4) gas chromatography (GC) measurement

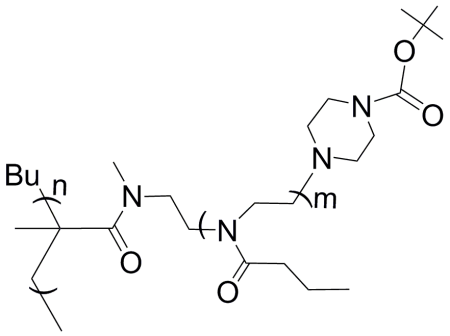

At 0 ℃, M^{I}/M^{II} (44 mg, 0.16 mmol, 1.0 equiv) was dissolved in 4 mL of acetonitrile and 452 mg of *n*PrOx (4.0 mmol, 25 equiv) was added. The polymerization solution was performed at 80 ℃. Samples were withdrawn periodically for monomer conversion (GC) and molecular weight (GPC) measurement. The polymerization was stopped by adding excess of piperidine. After stirring the reaction mixture for 8 h at room temperature, an excess of finely grounded potassium carbonate (~60 mg) was added and the mixture was allowed to stir overnight. The solvent was removed under reduced pressure and the residual dissolved in chloroform and then precipitated three times into dry diethyl ether. The product was freeze-dried (water) to yield a colorless powder. Additionally, the product was purified by column chromatography using Sephadex G100 to quantitatively separate the product from minor portions of homopolymer side products.

^{1}H NMR ($CDCl_3$): δ=3.44 (s, br, 93 H, N-(CH_2)$_2$-N); δ=2.33/2.20 (m, 48 H, CO-CH_2-CH_2-CH_3); δ=1.62 (s, br, 51 H, CO-CH_2-CH_2-CH_3); δ=0.94 (s, br, 75 H, CO-CH_2-CH_2-*CH_3*).

Poly(2-isopropenyl-2-oxazoline-g-2-*iso*propyl-2-oxazoline) (M-II5~M-II7) were synthesized according to the above procedure.

^{1}H NMR ($CDCl_3$): δ (ppm) 3.45 (br, 76H, -N-CH_2-CH_2-N-) 2.88(br, 23H, -CO-CH(CH_3)$_2$), 1.98/1.92 (br, 2H, CH_2-C), 1.45 (br, 3H, CH_3-C), 1.09 (br, 110H, -CH(CH_3)$_2$).

6.6 Preparation of bottle-brush brushes

6.6.1 Bottle-brush brushes on glassy carbon

Self-initiated photopolymerization and photografting (SIPGP) of IPOx on glassy carbon.

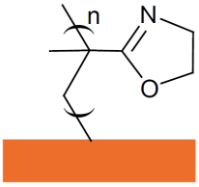

Polished glassy carbon substrates (or other surfaces) were cleaned by sequential ultrasonification in ethanol, ethyl acetate and toluene before use. The glassy carbon substrates were clamped with a square mesh grids (square size: 50×50 μm^2) and subsequently submerged in approximately 2 mL of freshly distilled and degassed IPOx in a glass vial. Polymerization was allowed to complete in 2 to 40 h under constant irradiation with UV light (λ_{max} = 350 nm) at room temperature (RT). After photopolymerization, the samples were immediately cleaned by sequential ultrasonification in ethanol, ethyl acetate and toluene (all HPLC grade) for five minute each.

IR (DRIFT): 1648 cm^{-1} (C=N stretching), 1128 cm^{-1} (C-O stretching), 987^{-1} and 951^{-1}(oxazoline skeletal viberation).

Poly(2-isopropenyl-2-oxazolium triflate) on glassy carbon; PIPOxOTf

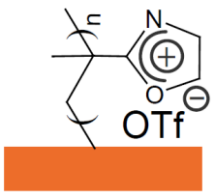

The poly(2-isopropenyl-2-oxazoline) (PIPOx) modified glassy carbon substrates were submerged in a solution of 2 mL acetonitrile (ACN) with an excess amount of methyl trifluoromethane sulfonate (MeOTf) (0.1 g) at approximately -35 ℃ under nitrogen atmosphere. After stirring for 6 h at 0-5 ℃, the mixture was allowed to equilibrate to RT and was stirred for another 2 h.

Surface initiated living cationic ring-opening polymerization (SI-LCROP).

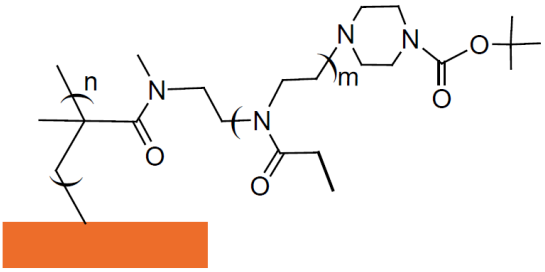

Without washing, the glassy carbon substrate coated with PIPOxOTf was taken to a microwave reaction vial filled with a solution of 1 g 2-alkyl-2-oxazoline (alkyl = methyl, ethyl, propyl or butyl) and several drops of MeOTf in 3mL ACN at 0 ℃. Catalytic amounts of MeOTf were added to consume the minor impurities in the liquid phase. The reaction solution was irradiated by microwaves for 20 min with a temperature setting of 130 ℃. The solution was cooled to 0 ℃, and 150 mg of *N*-*tert*butoxycarbonylpiperazine (*N*-Boc-piperazine) dissolved in 1 mL of ACN was added. Successively, the solution was stirred for 16 h at room temperature. After this, an excess of potassium carbonate (70 mg) was added to the solution and stirred overnight. The substrate was then removed from the solution and cleaned by sequential ultrasonication in deionized water, ethanol, ethyl acetate and toluene for 1 minute each.

IR (DRIFT) (side chain = PEtOx): 2932 cm^{-1} (CH_x stretching), 1627 cm^{-1} (carbonyl stretching of the amide), 1421cm^{-1} (CH_x deformation).

Deprotection of poly(2-isopropenyl-2-oxazoline-g-2-ethyl-2oxazoline-Boc) (P(IPOx-g-EtOx)).

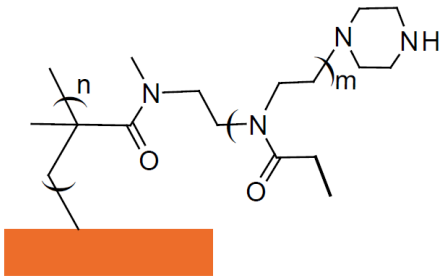

The P(IPOx-g-EtOxBoc) coated glassy carbon substrates were submerged in a solution of 1 mL trifluoroacetic acid (TFA) and 1 mL chloroform. The mixture was stirred at RT for 3 h. Then, the glassy carbon substrate was neutralized in a 5 % $NaHCO_3$ aqueous solution for 2 h. Finally, the polymer coated glassy carbon substrate was thoroughly cleaned by ultrasonification in water, ethanol, ethyl acetate and toluene.

Fluorescent labeling of P(IPOx-g-EtOx) grafts

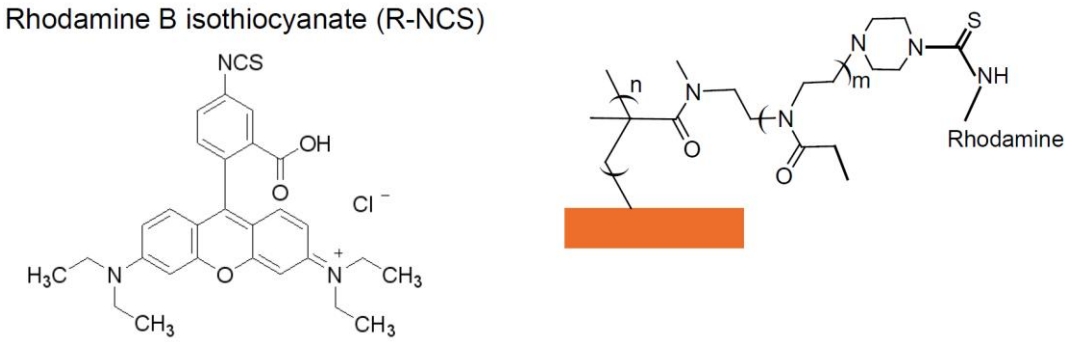

A P(IPOx-g-EtOx) modified glassy carbon substrate was submerged in a 15 mM rhodamine B isothiocyanate solution in methanol for 3 days at RT. Finally, the functionalized glassy carbon substrate was cleaned by ultrasonification in ethanol.

6.6.2 Bottle-brush brushes on SAM of 3-aminopropyltrimethoxysilane on oxidized silicon substrate

Aminopropyltrimethoxysilane SAM

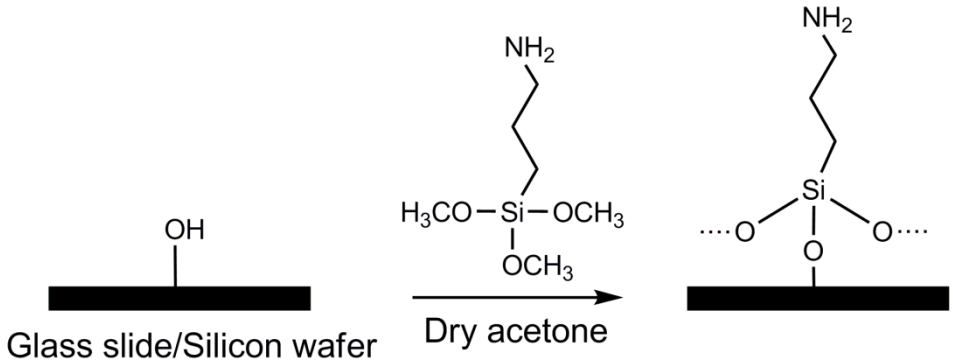

The glass slides were covered with a 5% v/v 3-aminopropyltrimethoxysilane solution in dry acetone and left in ultrasonication for 30 minutes at room temperature under nitrogen. After the reaction was completed, the slides were washed with acetone, and then dried under vacuum. (Water contact angle: 55 ±3 °)

Self-initiated photopolymerization and photografting (SIPGP) of IPOx on aminopropyltrimethoxysilane SAM

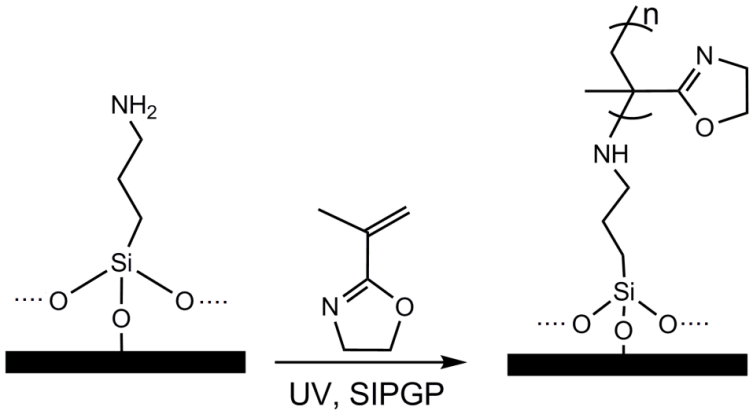

Adapt the procedure for preparation of SIPGP of IPOx on glassy carbon, PIPOx brushes on aminopropyltrimethoxysilane monolayer modified glass slide were prepared analogously.
DRIFT-IR: 1656 cm^{-1} (C=N stretching), 1130 cm^{-1} (C-O stretching), 990^{-1} and 953^{-1}(oxazoline skeletal viberation).

Surface-initiated Living Cationic Ring-Opening Polymerization (SI-LCROP)

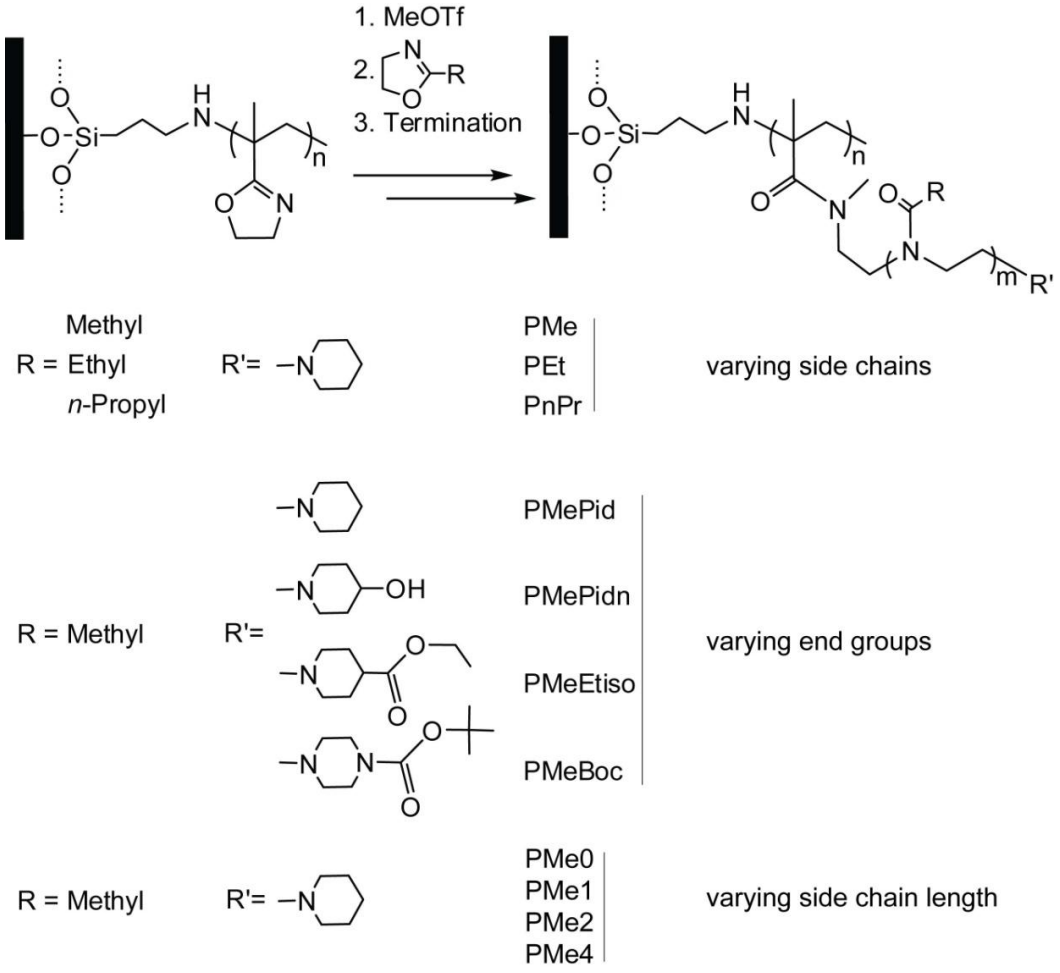

Poly(2-isopropenyl-2-oxazoline-g-2-methyl-2-oxazoline) (P(IPOx-g-MeOx)), Poly(2-isopropenyl-2-oxazoline-g-2-ethyl-2-oxazoline) (P(IPOx-g-EtOx)) and Poly(2-isopropenyl-2-oxazoline-g-2-propyl-2-oxazoline) (P(IPOx-g-*n*PrOx)) were prepared according the procedure for the preparation of Bottle-brush brushes on glassy carbon substrates. Moreover, P(IPOx-g-MeOx) brushes with different side chain length and termini were also prepared analogously.
DRIFT-IR(side chain = PMeOx, end group = piperidine): 2958 cm^{-1} (CH_x stretching), 1639 cm^{-1} (carbonyl stretching of the amide), 1431cm^{-1} (CH_x deformation).

6.6.3 Bottle-brush brushes on SAM of biphenyl on gold

Preparation of ω-functionalized biphenylthiol SAMs on gold

The synthesis of 4-mercapto-1,1'-biphenyl (BT), 4'-methyl-1,1'-biphenyl-4-thiol (MBT), 4'-hydroxy-1,1'-biphenyl-4-thiol (HBT) and 4'-nitro-1,1'-biphenyl-4-thiol (NBT) and the preparation of the SAMs was performed in the research group of Prof. Grunze. The SAMs were prepared by immerging the gold substrate in a 15 mmol solution of the respective ω-functionalized biphenylthiols in ethanol for three days. The substrates were cleaned by sonification for 5 minutes in air and dried.

PIPOx brushes & bottle-brush brushes on SAMs on gold

PIPOx brush as well as successive LCROP of 2-oxazoline on biphenylthiol modified gold surface was prepared according to the procedure for preparation of bottle-brush brushes on glassy carbon.

References

[1] Zhang, M.; Müller, A. H. E. *J. Polym. Sci. Part A: Polym. Chem.* **2005**, *43*, 3461-3481.

[2] Xu, H.; Sun, F. C.; Shirvanyants, D. G.; Rubinstein, M.; Shabratov, D.; Beers, K. L.; Matyjaszewski, K.; Sheiko, S. S. *Adv. Mater.* **2007**, *19*, 2930-2934.

[3] Pakula, T.; Zhang, Y.; Matyjaszewski , K.; Lee, H.; Boerner, H.; Qin, S.; Berry, G. C. *Polymer* **2006**, *47*, 7198-7206.

[4] Djalali, R.; Li, S. Y.; Schmidt, M. *Macromolecules* **2002,** *35*, 4282-4288.

[5] Neugebauer, D.; Zhang, Y.; Pakula, T.; Sheiko, S. S.; Matyjaszewski, K. *Macromolecules* **2003**, *36*, 6746-6755.

[6] Bourret, R. B.; Borkovich, K. A.; Simon, M. I. *Annu. Rev. Biochem.* **1991**, *60*, 401-441.

[7] http://en.wikipedia.org/wiki/Callistemon

[8] Seog, J.; Dean, D.; Plaas, A. H. K.; Weng-Palms, S.; Grodzinsky, A. J.; Ortiz, C. *Macromolecules* **2002**, *35*, 5601-5615.

[9] Sheiko, S. S.; Sumerlin, B. S.; Matyjaszewski, K. *Prog. Polym. Sci.* **2008**, *33*, 759-785.

[10] Kato, M.; Kamigaito, M.; Sawamoto, M.; Higashimura, T. *Macromolecules* **1995**, *28*, 1721-1723.

[11] Wang, J.; Matyjaszewski, K. *J. Am. Chem. Soc.* **1995**, *117*, 5614-5615.

[12] Cowie, J. M. G.; Arrighi, V. *Polymers: Chemistry and Physics of Modern Materials; CRC Press Taylor and Francis Group: Boca Raton, Fl, 3rd Ed.* **2008**, 82-84.

[13] Sumerlin, B. S.; Neugebauer, D.; Matyjaszewski, K. *Macromolecules* **2005**, *38*, 702-708.

[14] Neugebauer, D.; Sumerlin, B. S.; Matyjaszewski, K.; Goodhart, B.; Sheiko, S. S. *Polymer* **2004**, *45*, 8173-8179.

[15] Stuart, M. A. C.; Huck, W. T. S.; Genzer, J.; Müller, M.; Ober, C.; Stamm, M.; Sukhorukov, G. B.; Szleifer, I.; Tsukruk, V. V.; Urban, M.; Winnik, F.; Zauscher, S.; Luzinov, I.; Minko, S. *Nature Materials* **2010**, *9*, 101-113.

[16] Jeong, B.; Gutowska, A. *Trends Biotechnol.* **2002**, *20*, 305-311.

[17] Kikuchi, A.; Okano, T. *Prog. Polym. Sci.* **2002**, *27*,1165-1193.

[18] Hoffman, A. S. et al. *J. Biomed. Mater. Res.* **2000**, *52*, 577-586.

[19] Galaev, I. Y.; Mattiasson, B. *Trends Biotechnol.* **1999**, *17*, 335-340.

[20] Qiu, Y.; Park, K. *Adv. Drug Deliv. Rev.* **2001**, *53*, 321-339.

[21] Sershen, S.; West, J. *Adv. Drug Deliv. Rev.* **2002**, *54*, 1225-1235.

[22] Yokoyama, M. *Drug Discov. Today* **2002**, *7*, 426-432.

[23] Chilkoti, A.; Dreher, M.R.; Meyer, D. E.; Raucher, D. *Adv. Drug. Deliv. Rev.* **2002**, *54*, 613-630.

[24] Bromberg, L. E.; Ron, E. S. *Adv. Drug Deliv. Rev.* **1998**, *31*, 197-221.

[25] Weidner, J. *Drug Discov. Today* **2001**, *6*, 1239-1248.

[26] Pinkrah, V. T.; Snowden, M. J.; Mitchell, J. C.; Seidel, J.; Chowdhry, B. Z.; Fern, G. R. *Langmuir* **2003**, *19*, 585-590.

[27] Peng, T.; Cheng, Y. L. *Polymer* **2001**, *41*, 2091-2100.

[28] Bignotti, F.; Penco, M.; Sartore, L.; Peroni, I.; Mendichi, R.; Casolaro, M.; D'Amore, A. *Polymer* **2000**, *41*, 8247-8256.

[29] Gan, L. H.; Gan, Y. Y.; Deen, G. R. *Macromolecules* **2000**, *33*, 7893-7897.

[30] Huber, S. Doctor thesis, TU München, **2007**.

[31] Otake. K.; Inomata, H.; Konno, M.; Saito, S. *Macromolecules* **1990**, *23*, 283-289.

[32] Furyk, S.; Zhang, Y.; Ortiz-Acosta, D.; Cremer, P. S.; Bergbreiter, D. E. *J. Polym. Sci. Part A: Polym. Chem.* **2006**, *44*, 1492-1501.

[33] Huber, S.; Hutter, N.; Jordan, R. *Colloid Polym. Sci.* **2008**, *286*, 1653-1661.

[34] Satokawa, Y.; Shikata, T.; Tanaka, F.; Qiu, X.; Winnik, F. M. *Macromolecules* **2009**, *42*, 1400-1403.

[35] Lee, H.; Pietrasik , J.; Sheiko, S. S.; Matyjaszewski, K. *Prog. Polym. Sci.* **2010**, *35*, 24-44.

[36] Li, C.; Gunari, N.; Fischer, K.; Janshoff, A.; Schmidt, M. *Angew. Chem., Int. Ed.* **2004**, *43*, 1101-1104.

[37] Yamamoto, S.; Pietrasik, J.; Matyjaszewski, K. *Macromolecules* **2008**, *41*, 7013-7020.

[38] Pietrasik, J.; Sumerlin, B. S.; Lee, R. Y.; Matyjaszewski, K. *Macromol. Chem. Phys.* **2007**, *208*, 30-36.

[39] Lutz, J. F.; Akdemir, O.; Hoth, A. *J. Am. Chem. Soc.* **2006**, *128*, 13046-13047.

[40] Yamamoto, S.; Pietrasik, J.; Matyjaszewski, K. *Macromolecules* **2007**, *40*, 9348-9353.

[41] Lutz, J. F.; Hoth, A. *Macromolecules* **2006**, *39*, 893-896.

[42] Lutz, J. F.; Weichenhan, K.; Akdemir, Ö.; Hoth, A. *Macromolecules* **2007**, *40*, 2503-2508.

[43] Fournier, D.; Hoogenboom, R.; Thijs, H. M. L.; Paulus, R. M.; Schubert, U. S. *Macromolecules* **2007**, *40*, 915-920.

[44] Balamurugan, S. S.; Bantchev, G. B.; Yang, Y.; McCarley, R. L. *Angew. Chem. Int. Ed.*

2005, *44*, 4872-4876.

[45] Lutz, J. F. *J. Polym. Sci. Part A: Polym. Chem.* **2008**, *46*, 3459-3470.

[46] Sheiko, S. S.; Möller, M. *Chem. Rev.* **2001**, *101*, 4099-4124.

[47] Xu, H.; Shirvaniants, D.; Beers, K.; Matyjaszewski, K.; Rubinstein, M.; Sheiko, S. S. *Phys. Rev. Lett.* **2004**, *93*, 206103/1-206103/4.

[48] Sheiko, S. S.; Silva, M. D.; Shirvaniants, D.; LaRue, I.; Prokhorova, S.; Möller, M.; Beers, K.; Matyjaszewski, K. *J. Am. Chem. Soc.*, **2003**, *125* , 6725-6728.

[49] Sheiko, S. S.; Sun, F. C.; Randall, A.; Shirvanyants, D.; Rubinstein, M.; Lee, H.; Matyjaszewski, K. *Nature*, **2006**, *440*, 191-194.

[50] Lebedeva, N. V.; Sun, F. C.; Lee, H. I.; Matyjaszewski, K.; Sheiko, S. S. *J. Am. Chem. Soc.* **2008**, *130*, 4228-4229.

[51] Raynor, J. E.; Capadona, J. R.; Collard, D. M. *Biointerphases* **2009**, *4*, FA3-FA16.

[52] Yan, L.; Zhao, X. M.; Whitesides, G. M. *J. Am. Chem. Soc.* **1998**,*120*, 6179-6180.

[53] Purrucker, O.; Förtig, A.; Jordan, R.; Tanaka, M. *Chem. Phys. Chem.* **2004**, *5*, 327-335.

[54] Jordan, R; Ulman, A. *J. Am. Chem. Soc.* **1998**, *120*, 243-247.

[55] Rehfeldt, F.; Tanaka, M.; Pagnoni, L.; Jordan, R. *Langmuir* **2002**, *18*, 4908-4914.

[56] Förtig, A.; Jordan, R.; Graf, K.; Schiavon, G.; Purrucker, O.; Tanaka, M. *Macromol. Symp.* **2004**, *210*, 329-338.

[57] Wang, A.; Tang, H.; Cao, T.; Salley, S. O.; Simon Ng, K. Y. *J. Colloid Interface Sci.* **2005**, *291*, 438-447.

[58] Hernando, J.; Pourrostami, T.; Garrido, J. A.; Williams, O. A; Gruen, D. M.; Kromka, A.; Steinmüller, D.; Stutzmann, M. *Diamond Relat. Mater.* **2007**, *16*, 138-143.

[59] Schlenoff, J. B.; Li, M.; Ly, H. *J. Am. Chem. Soc.* **1995**, *117*, 12528-12536.

[60] Brewer, N. J.; Janusz, S.; Critchley, K.; Evans, S. D.; Leggett, G. J. *J. Phys. Chem. B* **2005**, *109*, 11247-11256.

[61] Yang, W.; Rånby, B. *J. Appl. Polym. Sci.* **1996**, *62*, 533-543.

[62] Deng, J. P.; Yang, W. T.; Rånby, B. *Macromol. Rapid Commun.* **2001**, *22*, 535-538.

[63] Wang, H. L.; Brown, H. R. *Macromol. Rapid Commun.* **2004**, *25*, 1095-1099.

[64] Li, S. J.; Li, C. G.; Li, T.; Cheng, J. J.; *"Polymer Photochemistry Principles and Applications", 1st edition, Fudan University Press, Shanghai.* **1993**, 110.

[65] Fang, W. H.; Liu, R. Z. *J. Am. Chem. Soc.* **2000**, *122*, 10886-10894.

[66] Steenackers, M. Doctor thesis, TU München, **2007**.

[67] Steenackers, M.; Lud, S. Q.; Niedermeier, M.; Bruno, P.; Gruen, D. M.; Feulner, P.;

Stutzmann, M.; Garrido, J. A.; Jordan, R. *J. Am. Chem. Soc.* **2007**, *129*, 15655-15661.

[68] Steenackers, M.; Jordan, R.; Küller, A.; Grunze, M. *Adv. Mater.* **2009**, *21*, 2921-2925.

[69] Steenackers, M.; Küller, A.; Stoycheva, S.; Grunze, M.; Jordan, R. *Langmuir* **2009**, *25*, 2225-2231.

[70] Kim, J. B.; Bruening, M. L.; Baker, G. L. *J. Am. Chem. Soc.* **2000**, *122*, 7616-7617.

[71] Kim, J. B.; Huang, W. X.; Miller, M. D.; Baker, G. L.; Bruening, M. L. *J. Polym. Sci., Part A: Polym. Chem.* **2003**, *41*, 386-394.

[72] Xiao, D. Q.; Wirth, M. J. *Macromolecules* **2002**, *35*, 2919-2925.

[73] Yang, Q.; Tian, J.; Hu, M. X.; Xu, Z. K. *Langmuir* **2007**, *23*, 6684-6690.

[74] Lee, H. J.; Nakayama, Y.; Matsuda, T. *Macromolecules* **1999**, *32*, 6989-6995.

[75] Ma, H.; Li, D.; Sheng, X.; Zhao, B.; Chilkoti, A. *Langmuir* **2006**, *22*, 3751-3756.

[76] Advincula, R. C.; Brittain, W. J.; Caster, K. C.; Rühe, J. *Polymer Brushes: Synthesis, Characterization, Applications; Wiley-VCH: Weinheim*, Germany.

[77] Dwek, R. A. *Chem. Rev.* **1996**, *96*, 683-720.

[78] Prime, K. L.; Whitesides, G. M. *J. Am. Chem. Soc.* **1993**, *115*, 10714-10721.

[79] Sigal, G. B.; Mrksich, M.; Whitesides, G. M. *J. Am. Chem. Soc.* **1998**, *120*, 3464-3473.

[80] Krishnan, S.; Weinman, C. J.; Ober, C. K. *J. Mater. Chem.*, **2008**, *18*, 3405-3413.

[81] Hucknall, A.; Rangarajan, S.; Chilkoti, A. *Adv. Mater.* **2009**, *21*, 2441-2446.

[82] Herrwerth, S.; Rosendahl, T.; Feng, C.; Fick, J.; Eck, W.; Himmelhaus, M.; Dahint, R.; Grunze, M. *Langmuir* **2003**, *19*, 1880-1887.

[83] Murthy, N.; Campbell, J.; Fausto, N.; Hoffman, A. S.; Stayton, P. S. *J. Controlled Release* **2003**, *89*, 365-374.

[84] Werner, C.; Maitz, M. F.; Sperling, C. *J. Mater. Chem.* **2007**, *17*, 3376-3384.

[85] Nath, N.; Hyun, J.; Ma, H.; Chilkoti, A. *Surf. Sci,* **2004**, *570*, 98-110.

[86] Mrksich, M.; Whitesides, G. M. *Annu. Rev. Biophys. Biomol Struct.* **1996**, *25*, 55-78.

[87] http://www.bootschoon.com/antifouling.htm

[88] Herrwerth, S.; Eck, W.; Reinhardt, S.; Grunze, M. *J. Am. Chem. Soc.* **2003**, *125*, 9359-9366.

[89] Lasseter, T. L.; Clare, B. H.; Abbott, N. L.; Hamers, R. J. *J. Am. Chem. Soc.* **2004**, *126*, 10220-10221.

[90] Tanaka, M.; Mochizuki, A.; Shiroya, T.; Motomura, T.; Shimura, K.; Onishi, M.; Okahata, Y. *Colloids Surf., A* **2002**, *203*, 195-204.

[91] Cho, W. K.; Kong, B.; Choi, I. S. *Langmuir* **2007**, *23*, 5678-5682.

[92] Ladd, J.; Zhang, Z.; Chen, S.; Hower, J. C.; Jiang, S. *Biomacromolecules*, **2008**, *9*, 1357-1361.

[93] Statz, A. R.; Meagher, R. J.; Barron, A. E.; Messersmith, P. B. *J. Am. Chem. Soc.* **2005**, *127*, 7972-7973.

[94] Holland, N. B.; Qiu, Y.; Ruegsegger, M.; Marchant, R. E. *Nature* **1998**, *392*, 799-801.

[95] Zhu, J.; Marchant, R. E. *Biomacromolecules* **2006**, *7*, 1036-1041.

[96] Raynor, J. E.; Petrie, T. A.; Fears, K. P.; Latour, R. A.; Garc á A. J.; Collard, D. M. *Biomacromolecules* **2009**, *10*, 748-755.

[97] Harris, J. M. *Poly(Ethylene Glycol) Chemistry: Biotechnical and Biomedical Applications (Ed: J. M. Harris), Plenum, New York* **1992**, p. 1.

[98] Herold, D. A.; Keil, K.; Bruns, D. E. *Biochem. Pharmacol.* **1989**, *38*, 73-76.

[99] Shen, M.; Martinson, L.; Wagner, M. S.; Castner, D. G.; Ratner, B. D.; Horbett, T. A. *J. Biomater. Sci., Polym. Ed.* **2002**, *13*, 367-390.

[100] Li, L.; Chen, S.; Jiang, S. *J. Biomater. Sci., Polym. Ed.* **2007**, *18*, 1415-1427.

[101] Hansen, C. B.; Kao, G. Y.; Moase, E. H.; Zalipsky, S.; Allen, T. M.; *Biochim. Biophys. Acta-Biomembranes* **1995**, *1239*, 133-144.

[102] Hayward, J. A.; Chapman, D. *Biomaterials* 1984, *5*, 135-142.

[103] Zhang, Z.; Chao, T.; Chen, S.; Jiang, S. *Langmuir*, **2006**, *22*, 10072-10077.

[104] Kagiya, T.; Narisawa, S.; Maeda, T.; Fukui, K. *J. Polym. Sci., Polym. Lett. Ed.* **1966**, *4*, 441-445.

[105] Saegusa, T.; Kobayashi, S. *Encyclopedia of Polymer Science and Technology, John Wiley and Sons, New York* , **1976**.

[106] Kobayashi, S. *Prog. Polym. Sci.* **1990**, *15*, 751-823.

[107] Chujo, Y.; Saegusa, T. *Ring-Opening Polymerization, Hanser, Munich*, **1993**.

[108] Aoi, K.; Okada, M. *Prog. Polym. Sci.* **1996**, *21*, 151-208.

[109] Hoogenboom, R.; Fijten, M. W. M.; Schubert, U. S. *J. Polym. Sci. Polym. Chem.* **2004**, *42*, 1830-1840.

[110] Hoogenboom, R.; Paulus, R. M.; Fijten, M. W. M.; Schubert, U. S. *J. Polym. Sci. Polym. Chem.* **2005**, *43*, 1487-1497.

[111] Litt, M.; Levy, A.; Herz, J. *J. Macromol. Sci. Chem.* **1975**, *5*, 703-727.

[112] Kobayashi, S.; Uyama, H. *Polym. News* **1991**, *16*, 70 -76.

[113] Gaertner, F. C.; Luxenhofer, R.; Blechert, B.; Jordan, R.; Essler, M. *J. Contr. Release* **2007**, *119*, 291-300.

[114] Woodle, M. C.; Engbers, C. M.; Zalipsky, S. *Bioconjugate Chem.* **1994**, *5*, 493-496.

[115] Zalipsky, S.; Hansen, C. B.; Oaks, J. M.; Allen, T. M. *J. Pharm. Sci.* **1996**, *85*, 133-137.

[116] Adams, N.; Schubert, U. S. *Adv. Drug Delivery Rev.* **2007**, *59*, 1504-1520.

[117] Hoogenboom, R. *Angew. Chem., Int. Ed.* **2009**, *48*, 7978-7994.

[118] Lin, P.; Clash, C.; Pearce, E. M.; Kwei, T. K.; Aponte, M. A. J. *Polym. Sci. Part B* **1988**, *26*, 603-619.

[119] Huber, S.; Jordan, R. *Colloid Polym. Sci.* **2008**, *286*, 395-402.

[120] Diehl, C.; Schlaad, H. *Macromol. Biosci.***2009**, *9*, 157-161.

[121] Kim, C.; Lee, S. C.; Kang, S.W.; Kwon, I. C.; Jeong, S. Y. *J. Polym. Sci. Part B* **2000**, *38*, 2400-2408.

[122] Hoogenboom, R.; Thijs, H. M. L.; Wouters, D.; Hoeppener, S.; Schubert, U. S. *Soft Matter* **2008**, *4*, 103-107.

[123] Schlaad, H.; Diehl, C.; Gress, A.; Meyer, M.; Demirel, A. L.; Nur, Y.; Bertin, A. *Macromol. Rapid Commun.* **2010**, *31*, 511-525.

[124] Goddard, P.; Hutchinson, L. E.; Brown, J.; Brookman, L. J. *J. Controlled Release* **1989**, *10*, 5-16.

[125] Park, Y. S.; Kang, Y. S.; Chung, D. J. *e-Polym.* **2002**, no. 016.

[126] Miyamoto, M.; Naka, K.; Shiozaki, M.; Chujo, Y.; Saegusa, T. *Macromolecules* **1990**, *23*, 3201-3205.

[127] Mero, A.; Pasut, G.; Via, L. D.; Fijten, M. W. M.; Schubert, U. S.; Hoogenboom, R.; Veronese, F. M. *J. Controlled Release* **2008**, *125*, 87-95.

[128] Meyers, A. I.; Mihelich, E. D. *Angew. Chem. Int. Ed.* **1976**, *15*, 270-281.

[129] Gabriel, S.; Eschenbach, G. *Chem. Ber.* **1897**, *23*, 2494-2497.

[130] Zarka, M. T.; Nuyken, O.; Weberskirch, R. *Chem. Eur. J.* **2003**, *9*, 3228-3234.

[131] Cesana, S.; Auernheimer, J.; Jordan, R.; Kessler, H.; Nuyken, O. Macromol. *Chem. Phys.* **2006**, *207*, 183-192.

[132] Witte, H.; Seeliger, *W. Liebigs Ann. Chem.* **1974**, *6*, 996-1009.

[133] Persigehl, P.; Jordan, R.; Nuyken, O. *Macromolecules* **2000**, *33*, 6977-6981.

[134] Taubmann, C.; Luxenhofer, R.; Cesana, S.; Jordan, R. *Macromol. Biosci.* **2005**, *5*, 603-612.

[135] Seeliger, W.; Aufderhaar, E.; Diepers, W.; Feinauer, R.; Nehring, R.; Thier, W.; Hellman, H. *Angew. Chem. Int. Ed.* **1966**, *5*, 875-888.

[136] Miyamoto, M.; Sano, Y.; Kimura, Y.; Saegusa, T. *Macromolecules*, **1985**, *18*, 1641-1648.

[137] Groß, A.; Maier, G.; Nuyken, O. *Macromol. Chem. Phys* **1996,** *197*, 2811-2826.

[138] Uyama, H.; Honda, Y.; Kobayashi, S. *J. Polym. Sci., Part A: Polym. Chem.* **1993,** *31*, 123-128.

[139] Shoda, S. I.; Masuda, E.; Furukawa, M.; Kobayashi, S. *J. Polym. Sci., Part A: Polym. Chem.* **1992,** *30*, 1489-1494.

[140] Kobayashi, S.; Kaku, M.; Sawada, S.; Saegusa, T. *Polym. Bull.* **1985**, *13*, 447-451.

[141] Jordan, R.; West, N.; Ulman, A.; Chou, Y. M.; Nuyken, O., *Macromolecules* **2001,** *34*, 1606-1611.

[142] Kobayashi, S.; Shimano, Y.; Saegusa, T. *Polym. J.* **1991,** *23*, 1307-1315.

[143] Nuyken, O.; Rueda-Sanchez, J.; Voit, B. *Macromol. Rapid Commun.* **1997,** *18*, 125-131.

[144] Grasmüller, M.; Rueda-Sanchez, J.; Voit, B.; Nuyken, O. *Macromol. Symp.* **1998,** *127*, 109-114.

[145] Nuyken, O.; Rueda-Sanchez, J.; Voit, B. *Polym. Bull.* **1997,** *38*, 657-664.

[146] Weberskirch, R.; Hettich, R.; Nuyken, O.; Schmaljohann, D.; Voit, B. *Macromol. Chem. Phys* **1999**, *200*, 863-873.

[147] Kagiya, T.; Matsuda, T.; Zushi, K. *J. Macromol. Sci. Chem.* **1972,** *6*, 1349-1372.

[148] Kagiya, T.; Matsuda, T.; Nakato, M.; Hirata, R. *J. Macromol. Sci. Chem.* **1972,** *6*, 1631-1652.

[149] Dibona, D. M.; Fibiger, R. F.; Gurnee, E. F.; Shuetz, J. E. *J. Appl. Polym. Sci.* **1986,** *31*, 1509-1514.

[150] Nuyken, O.; Maier, G.; Gross, A.; Fischer, H. *Macromol. Chem. Phys.* **1996,** *197*, 83-95.

[151] Luxenhofer, R.; Jordan, R. *Macromolecules* **2006,** *39*, 3509-3516.

[152] Bovey, F. A.; Tiers, G. V. D., *J. Polym. Sci.* **1960,** *44*, 173-182.

[153] Bonne, T. B.; Lüdtke, K.; Jordan, R.; Stepanek, P.; Papadakis, C. M. *Colloid Polym. Sci.* **2004,** *282*, 833-843.

[154] Bonne, T. B.; Papadakis, C. M.; Lüdtke, K.; Jordan, R. *Colloid Polym. Sci.* **2007,** *285*, 491-497.

[155] Ivanova, R.; Komenda, T.; Bonne, T. B.; Lüdtke, K.; Mortensen, K.; Pranzas, P. K.; Jordan, R.; Papadakis, C. M. *Macromol. Chem. Phys.* **2008,** *209*, 2248-2258.

[156] Purrucker, O.; Förtig, A.; Lüdtke, K.; Jordan, R.; Tanaka, M. *J. Am. Chem. Soc.* **2005,** *127*, 1258-1264.

[157] Foreman, M. B.; Coffman, J. P.; Murcia, M. J.; Cesana, S.; Jordan, R.; Smith, G. S.; Naumann, C. A. *Langmuir* **2003,** *19*, 326-332.

[158] Gil, E. S.; Hudson, S. M. *Prog Polym. Sci*. **2004**, *29*, 1173-1222.

[159] Diab, C.; Akiyama, Y.; Kataoka, K.; Winnik, F. M. *Macromolecules* **2004**, *37*, 2556-2562.

[160] Christova, D.; Velichkova, R.; Loos, W.; Goethals, E. J.; du Prez, F. *Polymer* **2003**, *44*, 2255-2261.

[161] Uyama, H.; Kobayashi, S. *Chem. Lett.* **1992,** *9*, 1643-1646.

[162] Tang, C.; Dufour, B.; Kowalewski, T.; Matyjaszewski, K. *Macromolecules* **2007**, *40*, 6199-6205.

[163] Rihova, B. *Adv Drug Deliv. Rev.* **1996**, *21*, 157-176.

[164] Mosmann, T. *J. Immunol Meth.* **1983**, *65*, 55-63.

[165] http://en.wikipedia.org/wiki/MTT_assay

[166] Arest, Y.; A. A.; Litvesenko, G. I. *Prog. Polym. Sci.* **1996**, *21*, 335-398.

[167] Park, J. S.; Kataoka, K. *Macromolecules* **2007**, *40*, 3599-3609.

[168] Hoogenboom, R.; Thijs, H. M. L.; Jochems, M. J. H. C.; van Lankvelt, B. M.; Fijten, M.W. M.; Schubert, U. *Chem. Commun.* **2008**, 5758-5760.

[169] Zhang, B.; Gröhn, F.; Pedersen, J. S.; Fischer, K.; Schmidt, M. *Macromolecules* 2006, *39*, 8440-8450.

[170] Saariaho, M.; Subbotin, A.; Ikkala1, O.; Brinke, G. *Macromol. Rapid Commun.* **2000**, *21*, 110-115.

[171] Park, J. S.; Kataoka, K. *Macromolecules* **2006**, *39*, 6622-6630.

[172] Nie, Z.; Kumacheva, E. *Nat. Mater.* **2008**, *4*, 277-290.

[173] Bailey, R. C.; Hupp, J. T. *Anal. Chem.* **2003**, *75*, 2392-2398.

[174] Stoykovich, M. P.; Cao, H. B.; Yoshimoto, K.; Ocola, L. E.; Nealey, P. F. *Adv. Mater.* **2003**, *15*, 1180- 1184.

[175] Nath, N.; Chilkoti, A. *Adv. Mater.* **2002**, *14*, 1243-1247.

[176] Cowlard, F. C.; Lewis, J. C. *J. Mater. Sci.* **1967**, *2*, 507-512.

[177] http://en.wikipedia.org/wiki/Glassy_carbon

[178] Harris, P. J. F. *Philos. Mag.* **2004**, *84*, 3159-3167.

[179] Rice, R. J.; McCreery, R. L. *Anal. Chem.* **1989**, *61*, 1637-1641.

[180] Mehandru, S. P.; Anderson, A. B.; Angus, J. C. *J. Phys. Chem.* **1992**, *96*, 10978-10982.

[181] Ray III, K. G.; McCreery, R. L. *J. Electroanal. Chem*. **1999**, 469, 150-158.

[182] Collier, W. G.; Tougas, T. P. *Anal. Chem.* **1987**, *59*, 396-399.

[183] Wright, J. S.; Carpenter, D. J.; McKay, D. J.; Ingold, K. U. *J. Am. Chem. Soc.* **1997**, *119*,4245-4252.

[184] Steenackers, M.; Küller, A.; Ballav, N.; Zharnikov, M.; Grunze, M.; Jordan R. *Small* **2007**, *3*, 1764-1773.

[185] Hoogenboom, R.; Wiesbrock, F.; Huang, H.; Leenen, M. A. M.; Thijs, H. M. L.; van Nispen, S. F. G. M.; van der Loop, M.; Fustin, C.; Jonas, A. M.; Gohy, J.; Schubert, U. S. *Macromolecules* **2006**, *39*, 4719-4725.

[186] Ulman, A. *Chem. Rev.* **1996**, *96*, 1533-1554.

[187] Balachander, N.; Sukenik, C.N. *Langmuir* **1990**, *6* ,1621-1627.

[188] Naciri, J.; Fang, J. Y.; Moore, M.; Shenoy, D.; Dulcey, C. S.; Shashidhar, R. *Chem. Mater.* **2000**, *12*, 3288-3295.

[189] Heiney, P. A.; Grüneberg, K.; Fang, J.; Dulcey, C.; Shashidhar, R. *Langmuir* **2000**, *16*, 2651-2657.

[190] Sugimura, H.; Hozumi, A.; Kameyama, T.; Takai, O. *Surf. Interface Anal.* **2002**, *34*, 550-554.

[191] Heise, A.; Menzel, H.; Yim, H.; Foster, M. D.; Wieringa, R. H.; Schouten, A. J.; Erb, V.; Stamm, M. *Langmuir* **1997**, *13*, 723-728.

[192] Gribov, L. A.; Novakov, I. A.; Pavlyuchko, A. I.; Korolkov, V. V.; Orlinson, B. S. *J. Struct. Chem.* **2004**, *45*, 951-959.

[193] Eck, W.; Gölzhäuser, A.; Zharnikov, M.; Stadler, V.; Geyer, W.; Grunze M. PCT/DE00/03264, **1999**.

[194] Gölzhäuser, A.; Eck, W.; Geyer, W.; Stadler, V.; Weimann, T.; Hinze, P.; Grunze, M. *Adv. Mater.* **2001**, *13*, 806-809.

[195] Jia, X.; Jiang, X.; Liu, R.; Yin, J. *Macromol. Chem. Phys.***2009**, *210*, 1876-1882.

[196] Takei, Y. G.; Aoki, T.; Sanui, K.; Ogata, N.; Sakurai, Y.; Okano, T. *Macromolecules* **1994**, *27*, 6163-6166.

[197] Boxshall, K.; Wu, M.; Cui, Z.; Cui, Z.; Watts, J. F.; Baker, M. A. *Surf. Interface Anal.* **2006**, *38*, 198-201.

[198] Chen, S.; Jiang, S. *Adv. Mater.* **2008**, *20*, 335-338.

[199] Johnston, E.; Ratner, B. D. *Immobilized Biomolecules in Analysis, Oxford Press,* **1998**.

[200] Ratner, B. D.; Hoffman, A. S.; Schoen, F. J.; Lemons, J. E. *Biomaterials science: an introduction to materials in* medicine,Academic Press, **2004**.

[201] Harris, J. M. *Poly(Ethylene Glycol) Chemistry: Biotechnical and Biomedical Applications, Plenum,* **1992**.

[202] Rampal, J. B. *Microarrays*, 2nd Edition, Humana press, Volume 1, 2007.

[203] Woodle, M. C.; Lasic, D. D. *Biochim. Biophys. Acta* **1992**, *1113*, 171-199.

[204] Konradi, R.; Pidhatika, B.; Mühlebach, A.; Textor, M. *Langmuir* **2008**, *24*, 613-616.

[205] Pidhatikaa, B.; Möllerb, J.; Vogelb, V.; Konradi, R. *CHIMIA* **2008**, *62*, 264-269.

[206] Lüdtke, K.; Jordan, R.; Hommes, P.; Nuyken, O.; Naumann, C. A. *Macromol. Biosci.* **2005**, *5*, 384-393.

[207] Kobayashi, S.; Uyama, H. *J. Polym. Sci., Part A: Polym. Chem.* **2002**, *40*, 192-209.

[208] Hoogenboom, R.; Wiesbrock, F.; Leenen, M. A. M.; Thijs, H. M. L.; Huang, H. Y.; Fustin, C. A.; Guillet, P.; Gohy, J. F.; Schubert, U. S. *Macromolecules* **2007**, *40*, 2837-2843.

[209] Fijten, M. W. M.; Kranenburg, J. M.; Thijs, H. M. L.; Paulus, R. M.; van Lankvelt, B. M.; de Hullu, J.; Springintveld, M.; Thielen, D. J. G.; Tweedie, C. A.; Hoogenboom, R.; Van Vliet, K. J.; Schubert, U. S. *Macromolecules* **2007**, *40*, 5879-5886.

[210] Fijten, M. W. M.; Haensch, C.; van Lankvelt, B. M.; Hoogenboom, R.; Schubert, U. S. *Macromol. Chem. Phys.* **2008**, *209*, 1887-1895.

[211] Luxenhofer, R.; Bezen, M.; Jordan, R. *Macromol. Rapid Commun.* **2008**, *29*, 1509-1513.

[212] Jordan, R.; Martin, K.; Räder, H. J.; Unger, K. K. *Macromolecules* **2001**, *34*, 8858-8865.

[213] Herlotz, M.; Werner, C.; Pompe, T. *Biomaterials* **2009**, *30*, 395-402.

[214] Georg Albert PVD-Coatings, Heidelberg, Germany.

[215] Havard, J. M.; Yoshida, M.; Pasini, D.; Vladimirov, N.; Frechet, J. M. J.; Medeiros, D. R.; Patterson, K.; Yamada, S.; Willson, C. G.; Byers, J. D. *J. Polym. Sci. Part A: Polym. Chem.* **1999**, *37*, 1225-1236.

[216] Tomalia, D. A.; Thill, B. P.; Fazio, M. J. *Polym. J.* **1980**, *12*, 661-675.